BULGARIAN ACADEMY OF
SCIENCES

INSTITUTE OF ASTRONOMY
AND
NATIONAL ASTRONOMICAL
OBSERVATORY

A study of eruptive activity of symbiotic stars

A dissertation submitted for the degree of
Doctor of Sciences
presented by Nikolai Aleksandrov Tomov

Sofia, 2015

Contents

Chapter 1

Introduction

Symbiotic stars are long-period interacting binaries consisting of a cool visual primary and a hot compact secondary component accreting matter from the atmosphere of its companion. Their photometric and spectral variability is determined on one hand from the orbital motion, eclipses and heating/reflection effects and on the other hand from the outburst events of the hot component. The outburst are often accompanied by intensive loss of mass in the form of optically thick shells, stellar wind outflow and bipolar collimated jets.

1.1 Observed properties

Multiple criteria and quantitative requirements for classification of the symbiotic stars were appeared through the history of their observations (Boyarchuk 1969; Allen 1979; Nussbaumer 1982; Kenyon 1986). Because of the variety of their behaviour (Kenyon 1986) writes that "every known symbiotic star has, at one time or another, violated all the classification criteria invented in the past 50 years". The last classification criteria are of Belczynski et al. (2000). According to these authors the observed properties of the symbiotic stars can be summarized as:

1. The presence of absorption features of a late-type giant; in practice, these include (among others) TiO, H_2O, CO, and VO bands, as well as CaI, CaII, FeI and NaI absorption lines.

2. The presence of strong emission lines of HI and HeI and either

- emission lines of ions with an ionization potential of at least 35 eV (e.g. [OIII]), or

- an A- or F-type continuum with additional shell absorption lines from HI, HeI and singly ionized metals.

The latter corresponds to the appearance of a symbiotic star in outburst.

3. The presence of the λ 6825 Å emission feature, even if no features of the cool star (e.g. TiO bands) are found.

1.2 Symbiotic stars as binary systems

Symbiotic stars are commonly accepted as binary systems, in which a red giant star transfers material to its hotter companion. The binarity has been proved in four different ways. The first one is based on optical photometric data, which showed eclipses in some systems like AR Pav (Mayall 1937) and CI Cyg (Hofleit 1968; Belyakina 1991). By now about 30 symbiotics have known orbital periods and > 50 per cent of them are eclipsing systems (Mikolajewska 1997; Belczynski et al. 2000). The second way is related to obtaining the elements of the spectroscopic orbit. The orbital periods are of several hundred days of the vast majority of the symbiotics. For the rest of them they are of several thousands days. In most cases the cool giant is the more massive component having mass of $\sim 1 - 3$ $M_{\odot}$ and the mass of its compact companion in the most systems is $\sim 0.3 - 0.7$ $M_{\odot}$. The separations of the most systems are of $1 \div 3$ AU, but there are, also, some groups of objects whose separations are close to 10 AU or more. About 20 systems have spectroscopic orbits (Belczynski et al. 2000).

Very important argument in favour of binarity of the symbiotics is the availability of the orbital parameters of few systems obtained by means of spectropolarimetric observations of the Raman scattered $\lambda\lambda$ 6825, 7082 ÅÅ emission lines. One result is that the orbital period of 80 years and inclination of about 60° of V1016 Cyg were obtained which is the first direct estimate for orbital parameters of symbiotic Mira (Schild & Schmid 1996).

The presence of a hot secondary component in the symbiotic binaries was directly established for the first time by the IUE satellite. Its data revealed a strong UV continuum in practically every observed star.

1.3 Cool component, infrared properties and space distribution

Symbiotic systems divide into two major types, **s**- and **d**-type, according to the infrared spectrum, emitted by their cool components (Webster & Allen 1975). Belczynski et al. (2000) composed a catalogue of 188 objects. This catalogue contains objects divided into three types: **s**-, **d**- and **d′**-types. The majority of the systems (132) are related to **s**-type, 30 systems are related to **d**-type, 7 of them – to **d′**-type and 36 objects have no IR classification.

S-type systems have near-IR colours consistent with those ones of the normal cool giants, or with a stellar photosphere with a temperature of about 3000 – 4000 K. The IR continuum of these systems is emitted by their cool components and is practically invariable.

The near-IR colours of **d**-type systems are greater than of normal late-type stars and indicate a presence of warm dust shells with $T_d \sim 1000$ K. Moreover, IR photometric data show that **d**-type systems contain long-period, $P \sim 300^d - 600^d$, Mira variables (Whitelock 1987; Belczynski et al. 2000).

The systems of **d′**-type in the catalogue of Mürset & Schmid (1999) have several special characteristics. One of the most important is the presence of a F, G or K giant instead of a cooler star. The systems containing cool components of these spectral types are included in the small group of yellow symbiotics. These yellow symbiotics divide into **s**- and **d′**-type systems.

As far as the orbital periods of the **d**-type systems R Aqr and V1016 Cyg are known only and these periods are long – about $10\,000^d$ and $29\,000^d$ respectively (Schild & Schmid 1996) – it is supposed that all **d**-type systems have long orbital periods. On this basis the symbiotics are divided into two classes:

- Short period **s**-type systems ($P_{orb} \sim 500 \div 1000^d$)
- Long period **d**-type systems ($P_{orb} \sim 10\,000^d$).

According to Whitelock (1987) and Kenyon et al. (1988) the mass-loss rate of **s**-type systems is of $\sim 10^{-7}$ $M_\odot$ yr^{-1} and of **d**-type systems – of $\sim 10^{-5}$ $M_\odot$ yr^{-1}.

Most galactic symbiotics belong to the intermediate or old disk population (Allen 1980). From the other hand most **s**-type yellow systems belong to the old metal-poor (halo) population.

1.4 Hot component

1.4.1 Classification, based on the intrinsic variability

The UV/optical light of many symbiotic stars shows that their basic characteristics is the alteration of quiescent periods and active phases. The light curve during the active phases is determined by the intrinsic variability of the hot component. Kenyon (1986) supposes that symbiotic systems are naturally divided into three distinct groups on the basis of the number and the duration of their outbursts during the active phases:

1. *Recurrent novae (SyRNe).* This group has prototypes T CrB and RS Oph.

2. *Classical symbiotic stars (ClSS).* The prototypes of this group are CI Cyg and Z And.

3. *Symbiotic novae (SyNe),* with a prototype AG Peg.

The recurrent novae undergo eruptions of several magnitudes with recurrence time of tens of years. The active phases of the classical symbiotic stars are realized on time scale of a few years when they undergo occasional 1 – 3 mag eruptions. The time between active phases is 15 – 20 years. The symbiotic novae undergo a single slow outburst of several magnitudes and duration of one or several decades.

According to Kenyon (1986) the symbiotic novae are divided into two subgroups depending on the appearance of their spectrum at maximum visual light:

(a) systems, whose spectrum reminds A – F supergiant;

(b) systems, whose spectrum reminds planetary nebula.

There are seven known symbiotic novae. AG Peg (the beginning of the outburst was around 1850), RT Ser (1909), RR Tel (1944) and PU Vul (1978) are from the first type. V1329 Cyg (1964), V1016 Cyg (1964) and HM Sge (1975) are from the second type. After the initial increase of the light all symbiotic novae evolve at roughly constant luminosity (L $\sim 10^3 \div 10^4$ $L_\odot$) towards very high temperatures of about 10^5 K. The spectroscopic data show that the hot components of all of them experienced a wind mass-loss, observed in some lines of HI, HeI, HeII, CIV, NIV and NV at phase after the maximum visual light. However, there is a marked difference in the wind velocities υ_∞ between type (a) (with giant phase) and type (b) (without giant phase) symbiotic novae. The lines of the stars of type (a) show velocities of $\upsilon_\infty \sim 500 \div 1000\,\mathrm{km\,s^{-1}}$ whereas these ones of the type (b) show much greater velocities $\upsilon_\infty \sim 2000 \div 3000\,\mathrm{km\,s^{-1}}$ (Schmid 2000). The AG Peg system is the brightest one and the literature provides many wind line observations. It has been concluded that its hot component has ejected $\sim (1-2) \times 10^{-4}$ $M_\odot$ throughout the eruption (Kenyon et al. 1993).

During the outbursts of some classical symbiotic stars (Z And or FG Ser type) an early-type spectrum develops and progressively dominates over the TiO bands of the cool giant at longer wavelengths (Munari 1997). The high ionization permitted lines progressively decrease in integrated absolute flux. These are indications of expanding of the hot component whose continuum contributes to the UV and visual region. The expanding in this way leads to both an increase of the bolometric luminosity and continuum energy redistribution. Expanding shells and mass outflow are often observed.

There is, also, another type of behaviour of the classical symbiotic stars (YY Her type, Munari 1997) during the active phase. In this case an increase of the integrated absolute flux of the high-ionization and forbidden lines during the rise to maximum is observed. Moreover, a blue continuum develops. These characteristics are not indication of a cooling of the outbursting star.

The optical light curve of the recurrent novae has two (type T CrB) or one (type RS Oph) peaks. When the curve is double-peaked the first brightening is of a greater amplitude and the whole active phase lasts less than one year. Hachisu & Kato (1999) have reproduced theoretically the second peak of the T CrB outbursts with a radiation induced instability of an accretion disc around the white dwarf in the system. Such an instability develops if the condition

$$\frac{\dot{M}_{acc}}{3\times10^{-8}\,\mathrm{M}_\odot\,\mathrm{yr}^{-1}} \leq \left(\frac{R_{\rm disc}}{\mathrm{R}_\odot}\right)^{1/2}\left(\frac{L_{\rm bol}}{2\times10^{38}\,\mathrm{erg\,s}^{-1}}\right)\left(\frac{R_{wd}}{0.004\,\mathrm{R}_\odot}\right)^{1/2}\left(\frac{M_{wd}}{1.35\,\mathrm{M}_\odot}\right)^{-1/2} \tag{1.1}$$

is satisfied (Southwell et al. 1997). If this condition is not satisfied, the second peak is absent – the case of RS Oph. In this case the decline of the optical light after its maximum is explained with decrease of the emission of the outbursting white dwarf and irradiation of the accretion disc and the red giant in the system (Hachisu & Kato 2000).

The recurrent novae have rapid decline (~ 0.3 mag day^{-1}) after the maximum and high initial ejection velocities > 4000 km s^{-1} (Bode 2010).

1.4.2 Mechanisms of increase of the accretion rate

The eruptive activity of the compact object is induced by accretion or a change of the accretion rate. A mechanism of an increase of the accretion rate in the symbiotic binary systems was proposed by Bisikalo et al. (2002) and Mitsumoto et al. (2005). These authors have modeled the evolution of the gas flow in the vicinity of the hot component which accretes matter of the wind of the cool giant. They have considered the dependence of the accretion rate from the wind velocity. According to these considerations an accretion disc surrounding the compact component exists when the velocity takes some lower values. When the velocity takes higher, but close values, the disc is destroyed and some part of its mass accretes in a typical time less than 0.1 of the orbital period after the epoch of the velocity increase. This results in a growth of the accretion rate.

1.4.3 Mechanisms of outburst

Thermonuclear outbursts

Most models for symbiotic eruptions are related to hydrogen burning of material accreted by a white dwarf – compact companion in one symbiotic binary. An accreting white dwarf has three possible configurations (regimes), depending on the mass accretion rate $\dot{M}_{acc}$ (Kenyon 1988; Mikolajewska & Kenyon 1992). For a small range of $\dot{M}_{acc}$ hydrogen burns in a steady state in a shell at the surface of a white dwarf when physical conditions in this shell have become appropriate for its ignition. In this range the accretion rate is equal to the burning rate and material burns completely as it is accreted and does not accumulate on the surface of the white dwarf (Paczynski & Zytkow 1978; Fujimoto 1982). According to Iben (1982) the minimum accretion rate for steady burning (the lower limit of this range) is

$$\dot{M}_{steady,min} \approx 1.32 \times 10^{-7}\,\mathrm{M_\odot\,yr^{-1}}\,{M_{wd}}^{3.57}\ , \tag{1.2}$$

where M_{wd} is the white dwarf mass in $\mathrm{M_\odot}$. The luminosity of the white dwarf (the minimum luminosity) is

$$L_{steady,min} \approx 10^4\,\mathrm{L_\odot}\,{M_{wd}}^{3.57} . \tag{1.3}$$

According to Paczynski (1970) and Üüs (1970) the maximum accretion rate for steady burning (the upper limit of the range) is

$$\dot{M}_{steady,max} \approx 8 \times 10^{-7}\,\mathrm{M_\odot\,yr^{-1}}\,(M_{wd} - 0.522\,\mathrm{M_\odot}) . \tag{1.4}$$

The luminosity corresponding to this accretion rate (the maximum luminosity) is given by the core mass-luminosity relation (Paczynski 1970; Üüs 1970):

$$L_{plateau} \approx 59.250\,\mathrm{L_\odot}\,(M_{wd} - 0.52\,\mathrm{M_\odot}) . \tag{1.5}$$

A white dwarf burning hydrogen in this range of accretion rates has a large luminosity of $\sim (1-50) \times 10^3\,\mathrm{L_\odot}$ and a very high effective temperature of $\sim (1-2) \times 10^5$ K. It is supposed that the members of the group of classical symbiotic stars with a very high temperature and luminosity in their quiescent state are in regime of steady burning of hydrogen at the surface of an accreting white dwarf.

If the accretion rate exceeds the maximum rate $\dot{M}_{acc} > \dot{M}_{steady,max}$, the accreting material accumulates above the burning shell. The unburnt material forms an extended envelope which can have dimensions of a red giant (Kenyon 1988; Mikolajewska & Kenyon 1992). Since the burning regime at the base of the envelope is not changed, such an object evolves at constant bolometric luminosity. The effective temperature of the expanding object decreases from $\sim (1-2) \times 10^5$ K to $\sim 10^4$ K which leades to strong continuum energy redistribution and an increase of the optical flux. According to the theory the optical eruption occurs on a thermal time scale

$$\tau_{th} \sim 0.1\,\mathrm{yr} \left(\frac{M_{\mathrm{env}}}{10^{-4}\,\mathrm{M}_{\odot}} \right) \left(\frac{L}{10^4\,\mathrm{L}_{\odot}} \right)^{-1} , \tag{1.6}$$

where L is the total luminosity and M_{env} is the mass of the accreted envelope (Paczynski & Rudak 1980; Fujimoto 1982; Iben 1982). Both L and M_{env} depend on the mass of the white dwarf: M_{env} decreases when the mass of the white dwarf increases, and L increases with the mass of the white dwarf. $\tau_{th} \leq 1$ yr for $M_{wd} > 1$ $\mathrm{M}_{\odot}$ (Mikolajewska & Kenyon 1992), which means that an increase in $\dot{M}_{acc}$ above the upper limit of steady burning can cause eruption only in systems with massive white dwarfs.

There is the next relation between the velocity of the expansion and the accretion rate

$$\frac{dR}{dt} = 8\,\mathrm{m\,s^{-1}} \left(\frac{\dot{M}_{acc} - \dot{M}_{steady,max}}{10^{-6}\,\mathrm{M}_{\odot}\,\mathrm{yr}^{-1}} \right) \left(\frac{M_{\mathrm{env}}}{10^{-5}\,\mathrm{M}_{\odot}} \right)^{-1} . \tag{1.7}$$

Observations, however, show that in a number of cases photometric and spectral characteristics of the outbursting classical symbiotic stars do not follow the theoretical prediction. Some systems do not evolve at constant bolometric luminosity during their active phases but the luminosity increases (Gonzalez-Riestra et al. 1999; Tomov et al. 2003a; Skopal et al. 2006; Sokoloski et al. 2006; Skopal et al. 2009a,b) and, moreover, the expansion of the outbursting compact object is accompanied by spectral indication of loss of mass (stellar wind), which means that it is due not to accumulation of mass resulted from an increase of the accretion rate, but rather to mass outflow (Skopal et al. 2006; Sitko et al. 2006; Iijima 2006; Tomov et al. 2008, 2010b; Mc Keever et al. 2011; Skopal, Tomov et al. 2013). That is why a combined model was proposed to explain the eruptive activity of the prototype of the classical symbiotic stars Z And where different mechanisms operate at different stages of the increase of the optical light (Sokoloski et al. 2006; Bisikalo et al. 2006). In the framework of this model the increased accretion rate leads not to accumulation of mass not included in the burning, but to change of regime of hydrogen burning. This model provides possibility to interpret both the increase of the bolometric luminosity and the mass outflow from the outbursting compact object.

According to some more recent hydrodynamic simulations of accretion of solar material onto white dwarfs steady burning regime does not occur (Starrfield et al. 2012).

If the accretion rate falls below its minimal value $\dot{M}_{acc} < \dot{M}_{steady,min}$, hydrogen burning exhausts the envelope faster than accretion can restore it. The absence of material in the envelope leads to cessation of the burning. Accretion, however, leads to accumulation of material on the surface of the white dwarf again and the next configuration originates: CO or ON white dwarf and hydrogen rich envelope onto it with a mass of $\sim 10^{-5} \div 10^{-4}$ $M_\odot$ (Kenyon & Truran 1983; Mikolajewska & Kenyon 1992; Starrfield et al. 2012). Because of gravitation the density and temperature at the base of the envelope increase. The pressure at the base of the envelope is

$$P_{\rm ss} = \frac{G M_{wd} \dot{M}_{acc}\, t}{4\pi R_{wd}^4}\,, \tag{1.8}$$

where R_{wd} is the radius of the white dwarf and t – the time of accretion between the outbursts. When the temperature and the pressure at the base of the envelope reach some critical values of $T \sim 10^7$ K and $p \sim 10^{19}$ dyn cm^{-2} hydrogen burning begins and a shell source of energy forms. Initially energy is generated solely by p-p reactions, but after some time CNO reactions realize too.

Depending on the accretion rate $\dot{M}_{acc}$, luminosity L and mass of the white dwarf M_{wd} the next possibilities can be realized:

– degenerate outburst (thermonuclear runaway, TNR), when $\dot{M}_{acc}$ is fairly low, $\dot{M}_{acc} \sim 10^{-10} \div 10^{-9}$ $M_\odot$ yr^{-1} or

– non-degenerate outburst, when $\dot{M}_{acc} \sim 10^{-8}$ $_\odot$ yr^{-1}.

When the accretion rate and the luminosity of the white dwarf are low ($L \leq 0.1$ $L_\odot$) the accreting material can cools efficiently and forms degenerate envelope (Kenyon 1988). In this envelope the accreted hydrogen is compressed up to degenerate conditions, thus leading to thermonuclear burning without control (explosive burning) (Hernanz & José 2000). The hydrogen burning in the framework of CNO reactions cycle produces some β^+ unstable nuclei of relatively short timescales (^{13}N, ^{14}O, ^{15}O and ^{17}F), which are transported by convection to the outer parts of the envelope, where they are preserved from destruction until they decay. Their subsequent decay leads to large liberation of energy, which provokes expansion of the envelope, increase in luminosity and mass ejection – processes observed in classical novae, symbiotic novae and recurrent novae.

When $\dot{M}_{acc} > 10^{-9}\,\mathrm{M_\odot\,yr^{-1}}$ the accreting material is not cooling before falling in the white dwarf atmosphere. This causes heating of the white dwarf by newly arrived hydrogen-rich material and leads to appearance of non-degenerate envelope. The hydrogen outburst in this case is relatively weak (Kenyon 1988).

When during one degenerate outburst the temperature and the pressure at the base of the envelope have reached their critical values of $T \sim 10^7$ K and $p \sim 10^{19}\,\mathrm{dyn\,cm^{-2}}$, CNO reactions are actually the source of energy and convection and electron conductivity are the basic mechanisms of energy transfer from the shell source through the envelope to its surface. The outburst itself is realised at two stages: rapid increase in bolometric luminosity at nearly constant radius followed by a slow expansion at constant bolometric luminosity.

At the first of these stages when the energy generation rate ϵ_{nuc} (the energy released by unit mass in the burning material per unit time) and the temperature at the base of the envelope reach values of $\sim 10^7 - 10^9\,\mathrm{erg\,g^{-1}\,s^{-1}}$ and $\sim 3\times10^7$ K a small convective zone appears above the shell source, which zone feeds fresh ^{12}C nuclei into it (Kenyon & Truran 1983). This accelerates the burning (runaway), ϵ_{nuc} and T increase more and reach their maximal values of $\sim 10^{13} - 10^{14}\,\mathrm{erg\,g^{-1}\,s^{-1}}$ and $\sim 1.3 \times 10^8$ K and the envelope becomes fully convective. Soon after, the large energy flux generated by the shell source reaches the surface and the luminosity increases rapidly. Convection, however, is not able to transport the energy generated by the shell source and since the material is degenerate (i.e. pressure does not increase together with the temperature and the envelope does not expand), such object explodes. The velocity of the ejected particles is greater than the escape velocity of the white dwarf, so one gravitationally not connected shell appears, which gradually dissipates in the interstellar medium. The energy released from decay of the β^+ unstable nuclei of ^{13}N, ^{14}O, ^{15}O and ^{17}F play an essential role in the expansion of the envelope. The explosion causes rapid ejection of the outer envelope and the top of the convective zone begins to return to the surface of the white dwarf. So the convective zone shrinks, which leads ϵ_{nuc} and T to decrease rapidly to approximately constant values of $\sim 10^9\,\mathrm{erg\,g^{-1}\,s^{-1}}$ and $\sim 5\times10^7$ K. When ϵ_{nuc} and T reach their maximum, the luminosity increases very rapidly – the bolometric magnitude decreases from $+11^{\rm m}$ to $-5^{\rm m}$ for about $100^{\rm s}$.

Maximum luminosity of $\sim 10^4$ L$_\odot$ occurs from $\sim$ 1 hour to $\sim$ 1 month depending on the parameters of the model.

When $\epsilon_{nuc} \sim 10^9$ erg g^{-1} s^{-1} and $T \sim 5 \times 10^7$ K the bolometric luminosity and magnitude have reached their maximal values and the second stage of the outburst – expansion at constant luminosity begins. As a result of the expansion the effective temperature of the outbursting object decreases, which, from its side, leads to strong continuum energy redistribution and an increase of the optical flux (optical flux can begin to increase during the previous stage, that of growth of the bolometric luminosity, too). After the ejection of the envelope, some part of it remains unejected and the nuclear reactions in the underlying shell source continue to act. The effective temperature of such an object is $\sim (1-2) \times 10^5$ K. It begins to decrease when the energy generation rate begins to decrease or when the nuclear reactions stop.

During the stage of constant bolometric luminosity the star loses mass at two phases. The first one is that of ejection of the envelope. The mean mass-loss rate during this phase reaches $\dot{M} \sim 10^{-4}\,{\rm M}_\odot\,{\rm yr}^{-1}$ (Shara et al. 1993). During the second phase the star loses mass via stellar wind. The loss of mass stops when $M_{\rm env}$ becomes too small to support its own pressure, a period of dynamical contraction follows. The bolometric luminosity and the energy generation rate ϵ_{nuc} decrease.

According to some models, the total mass lost during both phases is of $3.75 \times 10^{-4}\,{\rm M}_\odot$, a little more than the total mass accreted of about $3.7 \times 10^{-4}\,{\rm M}_\odot$. The difference is related to small amount of core material of the white dwarf, which has been mixed in the envelope. The white dwarf loses some amount of its mass in every outburst cycle (accretion – burning – explosion) (Shara et al. 1993). According to some other models, the mass of the evolving white dwarf increases with every outburst cycle. If the mass of this white dwarf (component of a symbiotic system) is close to Chandrasekhar limit, such system is regarded as progenitor of supernova of Type I (Bode 2010 and references therein; Starrfield et al. 2012). The scenario of the non-degenerate outburst is similar. Symbiotic systems, whose white dwarf component experiences strong, degenerate outburst, have spectral features of A–F supergiant at the time of the optical maximum and thus resemble classical novae. The spectrum of the symbiotic systems, whose white dwarf component experiences weak, non-degenerate outburst, resembles spectrum of planetary nebula at the time of the optical maximum (Paczynski & Rudak 1980; Iben 1982; Kenyon & Truran 1983).

The evolutionary cycle and the recurrence time scale of the eruptions in regime of TNR depend on the mass of the white dwarf, the mass of the accreted envelope, the accretion rate and the luminosity at maximum L. The evolutionary cycle is determined from the time spent at quiescence $\Delta t_{\rm off}$ and the upper limit of the time spent in eruption $\Delta t_{\rm on}$ (Kenyon 1988):

$$\Delta t_{\rm off} \approx 10^4\,{\rm yr}\left(\frac{M_{\rm env}}{10^{-5}\,{\rm M}_\odot}\right)\left(\frac{10^{-9}\,{\rm M}_\odot\,{\rm yr}^{-1}}{\dot{M}_{acc}}\right) \tag{1.9}$$

and

$$\Delta t_{\rm on} \sim 40\,{\rm yr}\left(\frac{M_{\rm env}}{10^{-5}\,{\rm M}_\odot}\right)\left(\frac{2\times10^4\,{\rm L}_\odot}{L}\right)\,. \tag{1.10}$$

Short recurrence time scales are possible for massive white dwarfs accreting matter at very high rates (low mass white dwarfs can be in regime of TNR only at comparatively low accretion rates). According to Kovetz & Prialnik (1994) a CO 1.4 $\rm M_\odot$ white dwarf accreting at a rate of 10^{-8} $\rm M_\odot\,yr^{-1}$ undergoes outbursts typical of recurrent novae: the recurrence time is less than 20 yr, velocities are $\sim$ 1500 $\rm km\,s^{-1}$, and the ejected mass – larger than the accreted mass, of about 2×10^{-7} $\rm M_\odot$.

Accretion powered outbursts

An other mechanism which is used to explain the eruptive activity of symbiotic stars is related to accretion powered outbursts. Accretion is source of energy in this case and luminosity variations result from changes in the accretion rate.

Disc instability is a physical mechanism which can change the accretion rate through an accretion disc. Disc instability appears as a result of liberation of angular momentum in the disc and its transport outward. It can be happened, for example, when the mass transfer rate into the disc is larger than the mass flow rate through the disc (Duschl 1986a,b; and references therein). Disc instability appears as a result of thermal instability in the disc too (Abramowicz et al. 1995). The liberation of angular momentum, on its side, contributes to the growth of the density in the disc. When the density grows, the surface density in the disc grows too and the efficiency of liberation of angular momentum increases. This leads to sharp increase of the accretion rate and growth of the luminosity of the disc.

Accretion powered outbursts can be distinguished observationally from thermonuclear events by an increase in the emitted flux at all wavelengths, rather, than the continuum flux redistribution (Mikolajewska & Kenyon 1992).

Ionization eruptions

An other mechanism suggested to explain the activity of the symbiotic stars is that known as "ionization eruptions" (Nussbaumer & Vogel 1987, 1988). It is supposed to act in a detashed system consisting of a red giant and an accreting very luminous white dwarf which ionizes the gas in the wind of the giant to form a density bounded nebula in the quiescent state of the system. One optical eruption begins when the mass-loss rate of the giant increases, leading to growth of the nebular emission and consequently to growth of the optical flux of the whole system. The components of this model system are as follows: a hot compact object with a radius of 9×10^8 cm radiates as a blackbody with temperature 1.5×10^5 K and ionizes the wind of a giant with a radius of 50 $R_\odot$, mass-loss rate of $\leq 10^{-7}$ $M_\odot\,yr^{-1}$ and velocity of its wind of 80 $km\,s^{-1}$. The components separation is 5×10^{13} cm. An increase of the mass-loss rate of the giant to $\sim 10^{-5}$ $M_\odot\,yr^{-1}$ causes a growth of the optical flux of the system of several magnitudes for a typical time of about one year – a time, need one wind particle to travel the distance between the components.

1.4.4 Collimated ejection

Symbiotic stars have observational indication of collimated outflows which appear in most cases during phase of activity. There are five systems with optical indication related to additional high velocity satellite emission/absorption components of the spectral lines (Tomov T. et al. 1990, 2000; Munari et al. 2001; Tomov et al. 2007; Skopal, Tomov et al. 2013). Some other symbiotic systems have radio indication of jets (Burgarella & Paresce 1992; Taylor et al. 1986, 1989; Sokoloski et al. 2008; Leedjarv 2004). The origin and nature of the collimated ejection are controversial. According to Sokoloski et al. (2008) the proposed mechanisms for its generating include (1) intrinsically asymmetric explosions, (2) ejecta that move into an inhomogeneous environment, and (3) mechanisms providing high degree of collimation. The third group is related to action of magnetic field. The view that presence of magnetized accretion disc surrounding the compact object is the most probable reason for the collimated ejection by symbiotic stars and the magnetic field is responsible for the acceleration and collimation of the ejected material is widely accepted. The magnetic field extracts energy and angular momentum from the accretion disc and transfers them to the outflow which is magneto-centrifugally accelerated.

According to Livio (2011; and references therein) the basic idea is that the lines of the magnetic field are open and form some angle with the disc surface.

These lines are corotating with their foot points in the disc and disc material is accelerated by the centrifugal force. The acceleration in this model can occur for an inclination larger than 30°. In the magneto-centrifugal model the acceleration stops at the Alfven surface, where the kinetic energy density is comparable to the magnetic energy density. The collimation, however, occurs outside the Alfven surface too. Outside the Alfven surface the field generates loops which are carried by the outflow to form a spiral field. This spiral field can collimate the ejected material. According to this theory collimated outflows in the symbiotic stars should be observed during both of their states – the quiescent and active ones. Observations, however, show that in most of these stars indication of collimated outflow appears only during their active phase when is accompanied by indication of noncollimated one. That is why an other model was suggested to interpret their line profiles – the model of collimated stellar wind (Tomov et al. 2014).

1.5 Nebula

The symbiotic nebula appears as a result of the loss of mass of both stellar components. It gives rise to the emission spectrum which is characterized by the simultaneous presence of lines requiring different excitation conditions. However the symbiotic nebulae distinguish themselves from the planetary nebulae by higher densities resulting in appearance of very prominent permitted and intercombination (HI, HeI, HeII, OIII], CIV, NV) emission lines and relatively weak forbidden lines ([OIII], [NeIII]). The data for the emission line fluxes are used to obtain physical conditions within the nebula. These data indicate densities of $n_{\mathrm{e}} \sim 10^{8} \div 10^{10}$ cm^{-3} in **s**-type and much lower $n_{\mathrm{e}} \sim 10^{6}$ cm^{-3} in **d**-type symbiotics (Kenyon 1986). The more detailed study of the nebula in some systems (e.g. Kenyon et al. 1993; Mikolajewska et al. 1995; Skopal 2005) showed that the electron temperature is 15 000 – 40 000 K. This means that radiation and not collisions are in general responsible for its ionization. The symbiotic nebulae can be also radio sources (Seaquist & Taylor 1990). Free-free radio continuum has been detected from about 25 per cent of all symbiotic systems. The radio emission is correlated with the IR properties. This correlation is expressed essentially in the fact that all **d**-type systems are radio sources. Moreover, the systems with the greatest mass-loss have the greatest radio luminosity.

The symbiotic nebula gives rise to the emission features at $\lambda\lambda$ 6825 Å and 7082 Å which appear as a result of Raman scattering of the photons with wavelengths $\lambda\lambda$ 1032 Å and 1038 Å of the OVI resonance transitions (Schmid 1997). In symbiotic systems the OVI emission appears near the hot component and is converted by neutral hydrogen into Raman photons in the extended atmosphere and wind of the cool giant. In this process an OVI photon excites atomic hydrogen from its ground state $1s^2S$ to an exited state, followed by the emission of a photon leaving the atom in the lower $2s^2S$ state and the emission of a Ly photon. Between the wavelengths of these photons exists the next relation $1/\lambda_{\mathrm{Raman}} = 1/\lambda_{\mathrm{OVI}} - 1/\lambda_{\mathrm{Ly}\alpha}$. It can be derived the scattering efficiency $N_{\mathrm{Raman}}/N_{\mathrm{OVI}}$ from the measured fluxes of the OVI lines and the Raman lines if there are simultaneous UV and optical spectral data. That parameter provides information about the extent of the scattering region with respect to the region emitting the OVI lines.

In a number of cases the symbiotic nebulae are X-ray sources as well. Some of these cases are related to the eruptive phases of the symbiotics when their hot stellar components generate a wind outflow with a high velocity. This wind interacts with the wind of the cool giant, modifying significantly the structure of the nebula and creating a shock region which gives rise to X-ray emission of $\sim 1\ L_{\odot}$ (Wilson et al. 1984; Nussbaumer & Walder 1993).

1.6 Main aims of the investigation

As a result of accretion onto the compact object processes of heating and eruption develop, observed as optical outbursts and often accompanied by intensive loss of mass. Heating and ejection of mass lead to change of the bolometric luminosity and continuum energy redistribution of the outbursting object and have thus pronounced photometric manifestation. Accretion and ejection of mass manifest themselves in change of the spectrum when line profiles with a complex morphology form.

Investigation of the components interaction is of fundamental importance to study the nature and evolution of the interacting binary stars. The basic factor determining the interaction of the components is the loss of mass. In symbiotic stars the cool component (donor) loses mass all the time and during phase of activity the hot compact object (accretor) loses mass too.The combination of different rates of loss of mass with the other parameters of the system leads to possibility a great diversity of regimes of interaction and observational behaviour to appear. The existing accretion structures contribute to this diversity too. That is why the view the behaviour of every particular system during active phase is unique is widely accepted among the investigators of symbiotic stars and the approach every system to be studied individually and a specific model to interpret its light and spectrum to be searched for is applied for this reason. In this way the next question arises: are symbiotic stars such class of objects where the behaviour of each of them requires one particular model or their behaviour can be explained in the framework of more common models, since the diversity from object to object is due only to difference of some individual parameters? This question determines the main aims of the present investigation. We treated several symbiotic systems during their active phases. These are the systems EG And, AG Peg, AG Dra, Z And, Hen 3-1341, StHα 190 and BF Cyg. EG And is of interest to us because of the fact that on one hand optical eruptions were not observed up to now in this system and of the other one the lines C IV 1548 – 1550 had profiles of the type P Cyg indicating stellar wind. AG Peg is a prototype of the class "symbiotic novae" and underwent the most prolonged outburst among symbiotics ever recorded. The eruptive activity of AG Dra is of type Z And, but in contrast to it, AG Dra has never had indication of collimated ejection. It is no accident that the system Z And is included in this group. On one hand it is a prototype of the classical symbiotic stars and whole class of symbiotics. On the other hand it has a complicated line spectrum indicating an unusual variety of physical conditions: densities, temperatures and velocity regimes. Moreover, only five of more than 200 known symbiotic systems have optical indication of bipolar ejection and Z And is one of them. Other three systems of this group are Hen 3-1341, StHα 190 and BF Cyg. They showed simultaneous presence of spectral indication of bipolar ejection and stellar wind like Z And.

The main aims of our research are as follows:

1. To suggest:
   - a model to interpret the behaviour of the optical light;
   - a model to interpret the behaviour of the line spectrum.
2. To investigate the process of loss of mass and to obtain quantitative estimate of the mass-loss rate of the outbursting compact object.

1.7 Structure of the dissertation

The dissertation contains six chapters and conclusion.

The **first chapter** contains an introduction to the topic of symbiotic stars, a treatment of their observed properties, some of the basic items of theory of their eruptive activity, motivation of the study, undertaken by us, and its main aims. The orbital variability of the line spectrum of the system EG And is considered in the **second chapter**, where a model for its interpretation is suggested. The **third chapter** is devoted to the prototype of the symbiotic novae AG Peg where its photometric and spectral behaviour at the final stage of the outburst is considered. A model for interpretation of its light curve is suggested. The **fourth chapter** is devoted to the yellow symbiotic AG Dra during its 1994–1998 active phase and in some time of quiescence before it. Some of the basic parameters of the system are determined. A scenario for interpretation of the growth of the optical light is suggested. The prototype of the classical symbiotic stars and the whole class of symbiotics Z And during its last and most prolonged 2000–2013 active phase is investigated in the **fifth chapter**. A mechanism of increase of the optical light and a model for interpretation of the line spectrum are suggested. All symbiotic systems with spectral indication of bipolar ejection and stellar wind are considered in the **sixth chapter**. The line profiles of all of them are interpreted in the framework of the model of collimated stellar wind. The light curve of one of them, BF Cyg, during its last 2006–2015 outburst is interpreted in the framework of this model. The **conclusion** contains the basic results of the investigation. A **list of author's papers** used in this dissertation is presented at its end.

Chapter 2

The symbiotic binary EG And

2.1 Introduction

The symbiotic binary EG And (HD 4174, SAO 36618, Boss 880, BD +39°167) consists of a normal M3 giant (Mürset & Schmid 1999) and a hot compact object with a low luminosity (Mürset et al. 1991). The variability of its line spectrum and its interpretation is considered in the works of Tomov (1995) and Tomov & Tomova (1995a,b). For the need of this consideration the spectroscopic elements of Munari et al. (1988), JD$= 2439251 + 481.2 \times E$ are used, where zero phase corresponds to the epoch of ascending node.

Smith (1980) has investigated the variations in the profile, radial velocity and equivalent width of the Ha emission line during the orbital period. The variations in the radial velocity and equivalent width are close to sinusoidal, and are opposite in phase. The profile is also variable. It is single at the time of maximum equivalent width, and double at the time of minimum equivalent width. A pronounced asymmetry is observed when single. The line variations have been compared with the visual brightness, which probably varies with the same period. The line is most intense at maximum light and least intense at minimum. The variations of the H_α equivalent width and the light of the star (Hric et al. 1991, 1993; Skopal et al. 1995; Tomov & Tomova 1996) as well as the correlation of these parameters with the profile variations, are highly reminiscent of the situation in another symbiotic system, AG Peg (Boyarchuk 1966, 1967a; Hutchings & Redman 1972; Hatchings et al. 1975; Boyarchuk et al. 1987; Tomov & Tomova 1992).

IUE spectra, taken in the 1150–3200 Å region (Stencel 1984), show flux variations in some emission lines, as well as continuum flux variations near to these lines. The fluxes decrease remarkably near phase 0.72, where there is a minimum in the Ha equivalent width according to Smith (1980). The

He II 1640 line disappears entirely at phase 0.64. The continuum flux at wavelengths less than 1630 Å also decreases to zero at the same phase. It has been concluded that the sharp decrease in flux is an indication of an eclipse.

Oliversen et al. (1985) have determined the orbit of the cool component from their Reticon spectra, taken in the H_α region. According to them, the orbit is circular and the barycentric velocity is equal to -94.8 km s^{-1}. In view of the result of Kenyon's (1983) diagnostics – the secondary in this system is a hot subdwarf, similar to the central star of a planetary nebula – Oliversen et al. supposed its mass to be of the order of 0.7 $M_\odot$. Assuming a mass ratio of ~ 3.5, they obtained a primary mass of ~ 2.5 $M_\odot$, and a separation of ~ 1.7 au. For the radius of the primary Roche lobe, they obtained about 180 $R_\odot$. On the other hand, Oliversen et al. supposed the radius of the primary to be about 100 $R_\odot$, in agreement with Kenyon & Gallagher (1983). They therefore came to the conclusion that the cool component does not fill its Roche lobe, and consequently an outflow via the inner Lagrangian point L_1, is not possible.

Oliversen et al. (1985) also considered the profiles, fluxes and radial velocity data of some emission lines in the 1150–2000 Å region from two IUE spectra. The first of these was taken at phase 0.72 and the second one at phase 0.00. In general, the emission-line fluxes are weaker at phase 0.72 than at phase 0.00, and the lines of O I and O IV, as well as He II 1640, at phase 0.72 disappear entirely. This observational result was interpreted as being due to an eclipse. The profiles of the C IV resonance lines $\lambda\lambda$ 1548, 1550 Å at phase 0.00 are P Cygni in form, which indicates the existence of a hot wind in the system. The difference between the barycentric velocity and the central reversal velocity is equal to the wind velocity, and amounts to 74 km s^{-1}. As the P Cyg profile disappears during the time of the eclipse, Oliversen et al. (1985) associated this wind with the hot component.

The He II 1640 emission line at phase 0.00 consists of a central narrow component with FWHM equal to 180 km s^{-1}, and a broad component with FWZI (full width at zero intensity) equal to 960 km s^{-1}. Oliversen et al. (1985) supposed that the broad component originates in a rapidly rotating disc surrounding the hot component of the system. The emission profile suggests that it is optically thin. In well separated symbiotic systems such a disc is formed as a result of wind accretion from the giant.

The existence of an accretion disc surrounding the hot component is also assumed by Pesce et al. (1987). According to them, mass transfer in the system is helped by the expansion of the red giant atmosphere. This expansion is caused by the radiative heating by the companion star. The cool component of the EG And system is unlikely to be heated, however, as it would then behave observationally like its counterpart in the AG Peg system (Boyarchuk 1966, 1967a; Hatchings et al. 1975; Tomov & Tomova 1992).

The C IV $\lambda\lambda$ 1548, 1550 Å profiles of the EG And system have also been examined by Sion & Ready (1992). In their opinion, the profiles are P Cygni in form, and the absorption components are perhaps the most pronounced seen in any symbiotic system. According to Sion & Ready, the wind observed in these lines belongs to the secondary, since the profiles do not reveal asymmetry in their blue wings; asymmetry implies a gradual increase in velocity, which is typical of the profiles of cataclysmic variable disc winds.

The wind velocity measured by Sion & Ready (1992) is 124 km s^{-1}. The average of this value and the one obtained by Oliversen et al. (1985) is about 100 km s^{-1}, considerably lower than the hot wind velocity in symbiotic novae, which is of the order of 1000 km s^{-1}. Sion & Ready (1992) have also discussed a sequence of models describing the outburst behaviour of an accreting low-mass white dwarf – a component of a binary symbiotic system. An essential fact is that the absorption velocity of the C IV 1548–1550 P Cyg profiles is 240 km s^{-1} (Sion & Ready 1992), i.e. very close to the C IV outflow velocity of the EG And system. Sion & Ready (1992) considered their low-mass white dwarf accretion model to be probably applicable to both BF Cyg and EG And, as well as to any symbiotic system that has features attributable to a hot moderate-velocity wind.

The C IV $\lambda\lambda$ 1548, 1550 Å profiles of EG And were examined by Vogel (1993) too. This author used four IUE spectra with identification numbers SWP 20269, 23692, 26268 and 46021. The first three of them, however, are those used by Oliversen et al. (1985) and Pesce et al. (1987). The last one was taken on 20 Oct. 1992 (JD 2448915.5) at orbital phase 0.08, which shows the same P Cyg profile and velocity of the wind.

The complex H_α profile of EG And, displaying features of self-absorption, argues for gaseous structure with complicated geometry and various physical conditions. It was not explained in the framework of any of the models proposed for this system. Model in which both components have a stellar wind have been considered in some theoretical works (Girard & Willson 1987; Luo et al. 1990). According to it, gaseous structures possessing density and temperature inhomogeneities arise as a result of colliding winds. The line radiation from these structures in many cases is influenced by self-absorption. We believe that, in carrying out a treatment of the observational data of EG And in the light of this model, we will be successful in both resolving the difficulties of the accretion disc model and explaining the H_α profile variations. The basic aim of our research is to suggest a model for explanation of the line spectrum of the system during the orbital cycle.

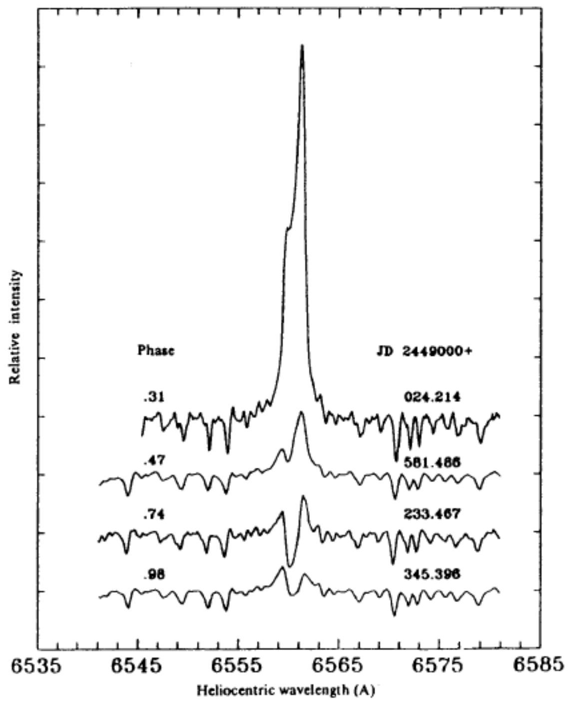

Figure 2.1: H_α profile variations during the orbital period. The average continuum level is one ordinate unit above zero intensity. The phases are according to Munari et al. (1988).

2.2 Observations

Four spectra in the H_α region have been taken between February 1993 and August 1994 by means of ISTA CCD array, mounted at the Coudé focus of the 2m RCC telescope of the National Astronomical Observatory Rozhen (Fig 2.1). The spectral resolution at orbital phases 0.47 and 0.98 is equal to 0.2 Å px^{-1} , and at phases 0.31 and 0.74 – 0.1 Å px^{-1} The material derived was processed by means of the pcIPS program (Smirnov et al. 1992). The ReWiA package was used for obtaining dispersion curve (Borkowsky 1988).

2.3 Model

The most plausible supposition is the observed low-velocity P Cyg wind (Oliversen et al. 1985; Sion & Ready 1992) to be associated with the secondary component, which according to Kenyon (1983, 1986) is a hot, compact object similar to the central star of a planetary nebula.

Girard & Willson (1987) have developed a theoretical model of a nebular region, formed as a result of a collisional shock between the winds of the two components in a symbiotic system. This region is in the shape of a shell. The authors distinguish two parts of the shell: a conical part and a spherical one. The conical part surrounds the area behind the cool component, and the apex of the cone is between the two components. The geometry of the conical part, as well as its mass distribution and velocity profile, depends on the wind parameters – the mass-loss rate $\dot{M}$ and the velocity υ. Possible mechanisms for line excitation in this region include shocks and photoionization.

For a consideration of the available data on the EG And system within the framework of such a model, estimates of the wind parameters of its components are need. We adopt the value of 10^{-7} $\mathrm{M_\odot\,yr^{-1}}$ for the mass-loss rate of the cool component, which is an average value for the cool components of S-type symbiotics (Kenyon et al. 1988; Mürset et al. 1991). According to Hagen (1978), typical wind velocities of M giants are in the range 5–10 $\mathrm{km\,s^{-1}}$. For the purpose of our investigation we will use a value of 10 $\mathrm{km\,s^{-1}}$.

Mass-loss rate estimates for the hot components of symbiotic systems are considerably more uncertain. The central stars of planetary nebulae have mass-loss rates of 10^{-10} to 10^{-7} $\mathrm{M_\odot\,yr^{-1}}$ (Pottasch 1984). The absence of a mass-loss indication in the line profiles in the visual region (Smith 1980; Oliversen et al. 1985), the availability of mass-loss evidence only in the C IV resonance line profiles in the UV region, and the low wind velocity measured from these lines (Oliversen et al. 1985; Sion & Ready 1992) all imply that the mass-loss rate of the hot component in the EG And system is comparatively low. We assume that it is about 10^{-9} $\mathrm{M_\odot\,yr^{-1}}$, which is less than average for the central stars of planetary nebulae.

To summarize, the adopted parameters for the cool component wind (cool wind) are approximately $\dot{M}_0 \sim 10^{-7}$ $\mathrm{M_\odot\,yr^{-1}}$ and $\upsilon_0 \sim 10$ $\mathrm{km\,s^{-1}}$ and those of the hot component wind (hot wind) – $\dot{M}_i \sim 10^{-9}$ $\mathrm{M_\odot\,yr^{-1}}$ and $\upsilon_i \sim 100$ $\mathrm{km\,s^{-1}}$. Then the product of the wind parameters, lw (Girard & Willson 1987), where $l = \dot{M}_i/\dot{M}_0$ and $w = \upsilon_i/\upsilon_0$ is equal to 0.1. This product gives information about the wind momentum ratio and determines in a simple way the asymptotic cone angle and the cone position with respect to the centres of the components. The fact that $lw < 1$ means that the cool wind predominates over the hot wind and the conical surface envelops the area behind the hot component. Following on from the assumptions on which the dynamical shell model is based (Girard & Willson 1987), we conclude that the spherical part of that shell will not be formed in the case of the EG And system, and we therefore consider only the nebular conical region. For the asymptotic cone half-angle, according to the steady-state region model, we obtain a value of $\sim 52°$. In reality, however, because of the orbital motion,

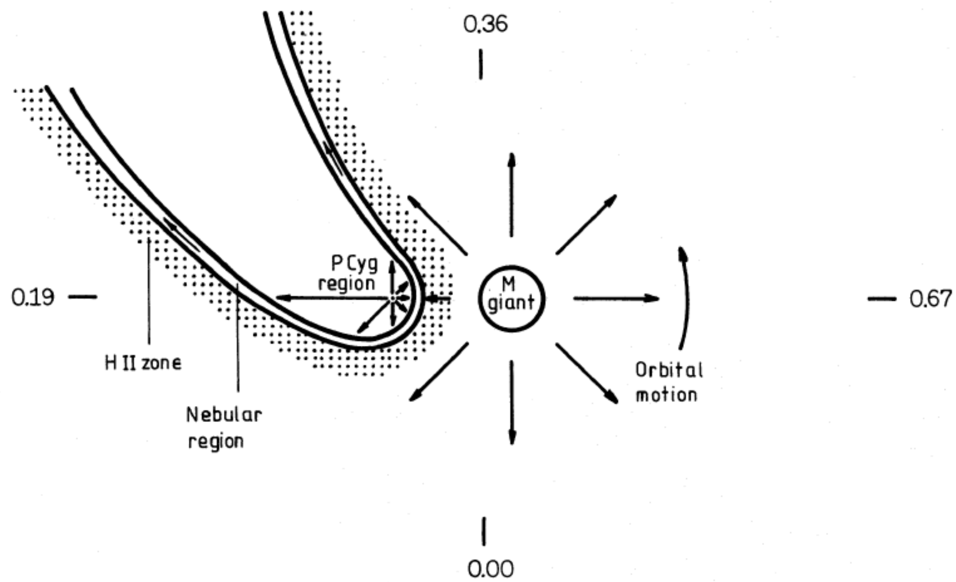

Figure 2.2: A schematic diagram of the EG And system in the orbital plane. The phases of quadratures and spectral conjunctions are marked. The phases have been calculated by means of the elements of Munari et al. (1988).

the value will be smaller according to the dynamical shell model. For the distance between the nebular region and the centre of the hot component, normalized with respect to the binary separation, we obtain $r_1 = 0.24$, which for a separation of ~ 1.7 au is equal to 0.41 au or 88 $R_\odot$ (Fig. 2.2).

The emission-line spectrum of the EG And system can be understood if, together with the nebular region formed as a result of the wind interaction, we take into account all regions in the system where ionization of the gas is possible. Such regions probably include a portion of the wind of the giant. A function, defining the form and the specific size of the ionized portion of this wind (the H II zone) for the case of a system without a hot wind, has been derived by Taylor & Seaquist (1984). The boundary of the H II zone is determined by the recombination-ionization balance and the flow of neutral hydrogen atoms across the boundary surface. Since the recombination time is a small fraction (10^{-3}) of the orbital period, the orbital motion is ignored in the treatment of this zone. An H II zone, calculated for the case of the EG And system [$X \sim 0.10$, where X is the ionization parameter (Taylor & Seaquist 1984)] assuming the absence of a hot wind, is shown in Fig. 2.3. A value of 10 $L_\odot$ has been used for the hot-component luminosity – approximately an arithmetical mean of the luminosities derived by Boyarchuk (1985) and Mürset et al. (1991). In reality, however, a hot wind is observed in this

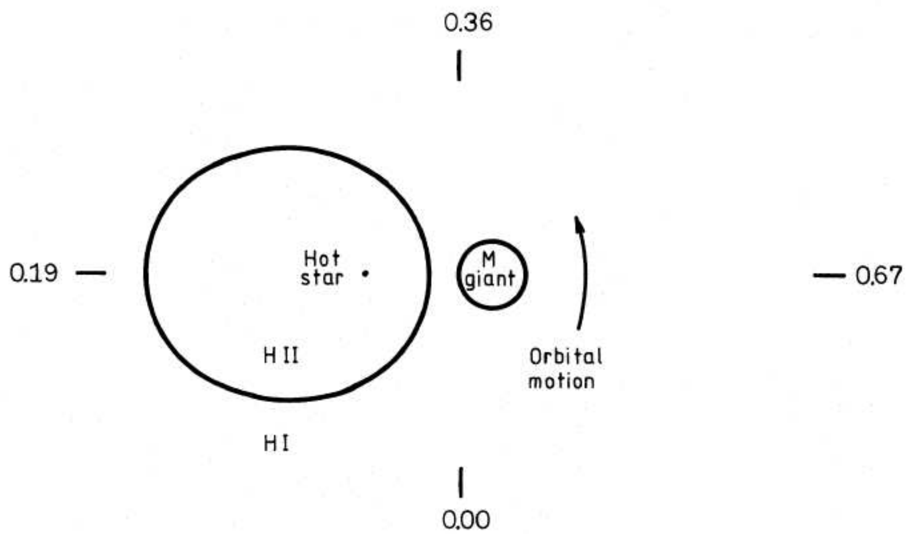

Figure 2.3: The neutral and ionized portions of the giant's wind in the EG And system, calculated assuming absence of a wind from the hot component. The phases marked are the same as in Fig. 2.2.

system. Its absorption beyond the limit of the Lyman series(i.e. wavelengths less than 912 Å) is negligible in comparison with that by the giant's wind, as a result of the lower density, and for this reason an H II zone will probably form in the giant's wind. The method of Taylor & Seaquist (1984) cannot be used to calculate the size of this zone, as their approach does not consider the case when a hot wind is present in addition to the hot secondary. In this case, the form and the specific size of the H II zone will depend on the position of the conical nebular region with respect to the components. Its calculation is a problem of a theoretical nature, and needs to be considered in detail. The aim of the present work is to carry out a qualitative interpretation of the observational data on the EG And system, which is why we confine ourselves to the intuitive supposition that the H II zone will surround the conical nebular region.

According to Schwank et al. (1997) the maximal optical depth in the Balmer lines of the symbiotic stars is at orbital phases close to the inferior conjunction of the giant component and is determined by the increasing density in the transition region between the H II and H I zones.

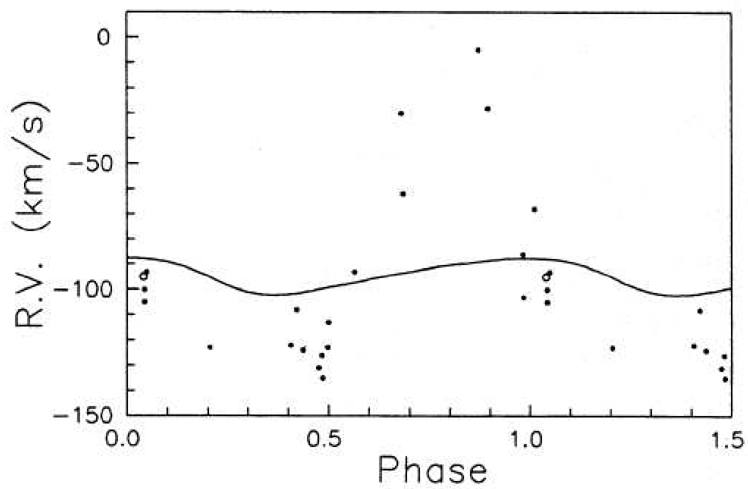

Figure 2.4: A radial velocity curve for the EG And cool component (Munari et al. 1988) and H_α radial velocity data, taken from Smith (1980, dots). The mean velocities of the Balmer members, from the same work, are marked with circles.

2.4 H_α line

The primary radial velocity curve, derived by Munari et al. (1988), is shown in Fig. 2.4. The elements of the orbit are listed in Table 2.1. The H_α radial velocity variations from Smith's (1980) observations are also shown in Fig. 2.4. It can be seen that the radial velocity variations in the H_α emission line are not in phase with those of the cool component, implying that the motion of the emitting gas differs from the stellar orbital motion. We suppose that the H_α radial velocity is related to the gas flowing in the nebular region from the innermost area to the outer parts. As the orbit is an ellipse and the orbital velocity varies with the phase, the angle between the cone axis and the direction of the orbital motion varies too. The H_α radial velocity variations appear not to be sinusoidal, and they have been assumed to have a steep slope between phases 0.8 and 1.1 (Smith 1980). Using these incomplete data, it is difficult to derive a definite phase shift between the curves, but, estimating the approximate shifts between the maxima and the minima respectively, we obtain 0.10–0.15 for the average value. This phase shift depends upon the average angle between the cone axis and the direction of the orbital motion shown in Fig. 2.2.

Figure 2.5 shows the H_α profile variations from the observations of Oliversen et al. (1985). When the line is purely in emission, its FWHM is about

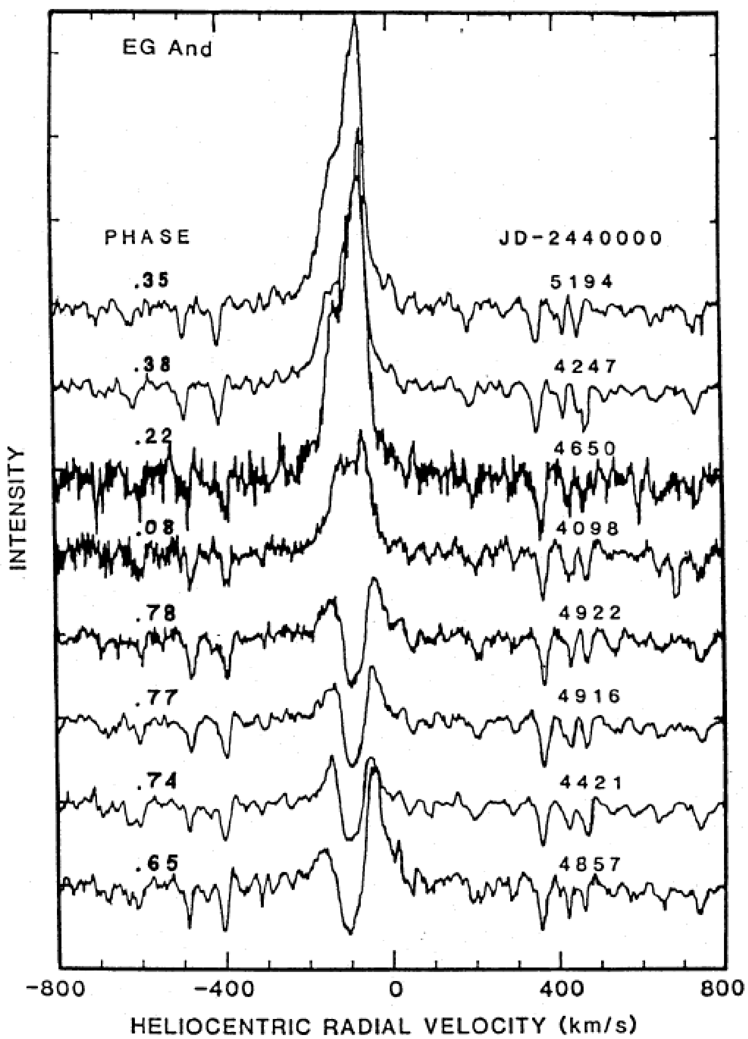

Figure 2.5: H_α profile variations during the orbital period, taken from Oliversen et al. (1985). The average continuum level is one ordinate unit above zero intensity. The phases are according to Munari et al. (1988).

Table 2.1: Orbital elements of EG And (Munari et al. 1988).

Period		=	$481.2 \pm 0.7\,\mathrm{d}$
Periastron passage	T_0	=	JD 2 439 367 ± 31
Eccentricity	e	=	0.24 ± 0.15
Periastron angle	ω	=	$112° \pm 27°$
$a\,\sin i$		=	$(47 \pm 6)\times 10^6\,\mathrm{km}$
Semi-amplitude	K	=	$7 \pm 1\,\mathrm{km\,s^{-1}}$
Barycentric velocity	V_0	=	$-94 \pm 1\,\mathrm{km\,s^{-1}}$
Mass function	$f(m)$	=	$0.018 \pm 0.005\,\mathrm{M_\odot}$
Standard deviation from the curve		=	$\pm\,3\,\mathrm{km\,s^{-1}}$

100 km s^{-1}. This width is caused first of all by significant gas turbulence, which is due (Girard & Willson 1987) to the large velocity gradients perpendicular to the mean flow in the nebular region. The line also has wings with an average full width to zero intensity (FWZI) of 300 km s^{-1}. It is seen that its central part varies, whereas the intensity in the wings remains practically constant. The H_α profile of the AG Peg system, as published by Boyarchuk et al. (1987), is similar. In analysing their data these authors come to the conclusion that the intensity in the wings is determined by radiation damping. In our opinion, the same factor determines the wing behaviour of this line in the EG And spectrum also.

In the phase interval 0.65–0.78, the profile consists of two weak emission components both blueward and redward of an absorption line going below the continuum. At other phases, an emission profile only is observed, with pronounced asymmetry. The Balmer line profiles of many symbiotics have a similar structure (Kenyon 1986). Obviously, the profile variations are determined by variations of absorption of neutral hydrogen (self-absorption) with orbital phase, as is also concluded by (Stencel 1984).

ln accordance with the radial velocity curve of the giant (Fig. 2.4), the spectral conjunctions are at phases 0.19 and 0.67, and the epochs of spectral quadratures are at phases 0.0 and 0.36 respectively. These phases are marked in Fig. 2.2. At phases 0.74, 0.77 and 0.78 the density in all regions of ionization increases towards the observer. For these reason, maximum absorption is observed (Fig. 2.5). The line intensity is minimal around phase 0.75, as can be seen in Fig.6 2.7, where the equivalent width variations as a function of phase are shown. The absorption line observed in the profile, however, goes considerably below the continuum. In our opinion, the reason for this is as follows. Since the direction of gas flow in the nebular region differs slightly from the direction of the giant's orbital motion, and the velocity of the flow (Girard & Willson 1987) is not much greater than the orbital velocity, the photospheric absorption is superimposed on the emission. As the emission is greatly weakened by self-absorption, it is particularly influenced by the absorption line. The profile observed at phases 0.74, 0.77 and 0.78 (Fig. 2.5) is therefore formed.

At phases 0.35 and 0.38 when the nebular region is observed through the inside of the cone, the line is completely in emission with minimal self-absorption. At these phases the density in all regions of ionization decreases towards the observer. At the other phases, for example 0.08, a borderline case is observed.

On considering line profiles at phases 0.74, 0.77 and 0.78 we noted that the velocity in the nebular region is of the order of the orbital velocity of the giant. In the area of excitation of the Balmer lines, the gas flow velocity probably varies (Girard & Willson 1987), and an effective value will be observed. It is possible to show that it is close to the giant's orbital velocity. Figure 2.4 shows that the amplitude of the H_α radial velocity is comparatively large: 7 or 8 times that of the stellar velocities. At the time of maximum H_α radial velocity according to Smith (1980) the line profile is double, and the velocity data have been derived by measuring the redward component. If the whole of the profile was measured, the corresponding points would be shifted and the amplitude would be decreased considerably. The curve would be situated more symmetrically about the barycentric velocity.

The H_α data obtained by us (Fig 2.1) can be interpreted in the same way.

Figure 2.6 shows variations of the H_α profile of EG And with the orbital phase based on the observations of Burmeister (2010). These data show that in the period 2001 – 2006 the line has had the same behaviour like in 1979 – 1982 (Oliversen et al. 1985) and 1993 – 1994 (Tomov & Tomova 1995a,b). Based on these data we conclude that this behaviour has not changed in a long time of 26 – 27 years and can be interpreted in the framework of the model of colliding winds, suggested by us.

The interpretation of the H_α line variability, however, will be better if the observed flux is found to be comparable with the calculated one emitted by the areas of ionization in the system. The total H_α flux will consist of two parts: one determined by shock excitation of the nebular region, and the other by radiative excitation of the nebular region together with the H II zone of the giant's wind.

On shock heating the emitted energy is taken from the wind kinetic energy. The sum of kinetic energies of the two winds is calculated to be 6.3×10^{30} erg s^{-1} or 1.7×10^{-3} L$_\odot$. This is an upper limit, since the wind velocity components normal to the nebular region surface are less than the

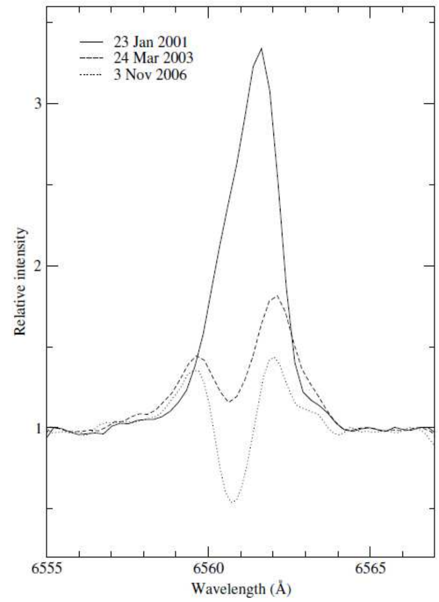

Figure 2.6: H_α profile variation during the orbital period, taken from Burmeister (2010).

velocities themselves. The distance to the EG And system is 320 pc (Vogel 1991) and the flux at that distance is calculated to be 5.2×10^{-13} erg cm^{-2} s^{-1}.

The line flux emitted by a spherical hydrogen nebula with a high degree of ionization is given by

$$F = \frac{zAh\nu}{d^2}\int n^2 r^2 \mathrm{d}r\,, \tag{2.1}$$

where n is the gas number density, r is the nebular radius, d is the distance and A is the spontaneous transition probability. This formula, however, does not account for self-absorption. On comparing the calculated flux with the observed one, the data at phases where the self-absorption is minimal will be used. Moreover, the shape of the gas component emitting as a result of radiative heating differs greatly from spherical, and is not known. With the aim of reducing the error, the flux will be divided by a factor of 2, i.e. it will be considered as being emitted by a hemisphere with the same radius.

Our interpretation of the H_α radial velocity is related to the flow in the nebular region. The nebular region can exist at a distance from the system of up to

$$b = P\upsilon_{\mathrm{neb}}/2\,, \tag{2.2}$$

where P is the orbital period and υ_{neb} is the gas flow velocity (Zamanov,

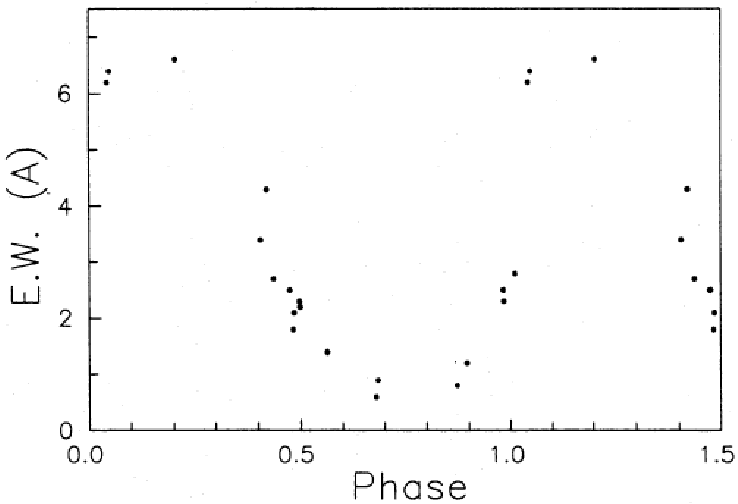

Figure 2.7: The equivalent width of H_α as a function of phase from Smith's (1980) observations.

private communication). This distance only sometimes exceeds the separation D. Moreover, the process of self-absorption is realized at high densities ($n > 10^6$ cm^{-3}). For these reasons we have integrated the H_α flux analytically over the r^{-2} density distribution from an inner radius of $D/2$ to an outer one of 10 au. The temperature is assumed to be 20 000 K. Then, in the Menzel case B the parameter z is calculated to be 1.34×10^{-21} cm^3 (Sobolev 1975). Using these data for half of the flux we obtain a value of 6×10^{-10} erg cm^{-2} s^{-1}. The real flux is probably smaller, as the emitting volume is less than that of the hemisphere adopted, it can be considered to be about 10^{-10} erg cm^{-2} s^{-1}. For the flux emitted via shock heating of the nebular region we obtained an upper limit of 5.2×10^{-13} erg cm^{-2} s^{-1} and will accept the value $\sim 10^{-13}$ erg cm^{-2} s^{-1}. Then it is negligible compared with the flux from radiative heating.

The observed flux can be obtained by means of multicolour photometry. The monochromatic continuum flux at the position of H_α is equal to the R photometric flux. We do not however have R photometric data for the star EG And, leaving us with one possible course of action: extrapolation of B and V data. The error from this method will not be greater than 50 per cent.

Unfortunately, there are no UBV data at the time of a maximum H_α intensity among the observations of Oliversen et al. (1985). According to the data from the work of Luthardt (1990) no trend of the optical light in the interval JD 2 446 000 − 2 448 000 is seen. A phase plot of the UBV observations taken in the same interval is displayed by Hric et al. (1991). Their values at maximum are in good agreement with our unpublished measurements, $B = 8\overset{\mathrm{m}}{.}69$ and $V = 7\overset{\mathrm{m}}{.}07$. Our observations were carried out on JD 2 448 582.35 at phase 0.39. Using these values to calculate the monochromatic continuum flux at the position of H_α, we obtained 9.1×10^{-12} erg cm^{-2} s^{-1} Å^{-1}. The H_α equivalent widths at phases 0.35 and 0.38 (Oliversen et al. 1985) are equal to 6.35 and 5.24 Å. Multiplying these equivalent widths by the monochromatic continuum flux, for the observed H_α fluxes at phases 0.35 and 0.38 we obtained 5.8×10^{-11} and 4.8×10^{-11} erg cm^{-2} s^{-1}, or about 5×10^{-11} erg cm^{-2} s^{-1}. It is seen that the calculated H_α flux of the gas component of the system is consistent with this result and the difference is due primarily to self-absorption.

2.5 UV lines

The fluxes and radial velocity data for the ultraviolet lines, obtained with the IUE, are unfortunately insufficient for plotting velocity curves. These data are poorly sampled with respect to phase, and will be considered together with the profiles.

2.5.1 C IV lines

The resonance lines of C IV $\lambda\lambda$ 1548, 1550 Å have a P Cyg profile at some phases (Oliversen et al. 1985; Vogel 1993) and the blueshifted absorption component is observed only when a broad component of the line is present. When the broad component is weak, the absorption is also weak and does not go below the continuum. This is the case at phase 0.53 (spectrum SWP 26268 from the work of Pesce et al. (1987). The observation on 1982 October 29 (Stencel 1984) shows that the continuum is not eclipsed at this phase, which does not remove the possibility an absorption feature to appear. This means that the broad component and the absorption are probably connected, indicating the same wind, and this wind has natural variability.

The C IV lines are shown in Fig. 2.8, taken from the work of Oliversen et al. (1985). If the narrow component of these lines was related to the hot compact secondary, as a result of the orbital motion, the velocity difference of this component at quadratures would be several times greater than the radial velocity amplitude of the giant. The observations at phases 0.00, 0.72 (Oliversen et al. 1985), 0.53 and 0.88 (Pesce et al. 1987) show that this difference is too small. These data propose that the broad component and the blueshifted P Cyg absorption are related to stellar wind which belongs most

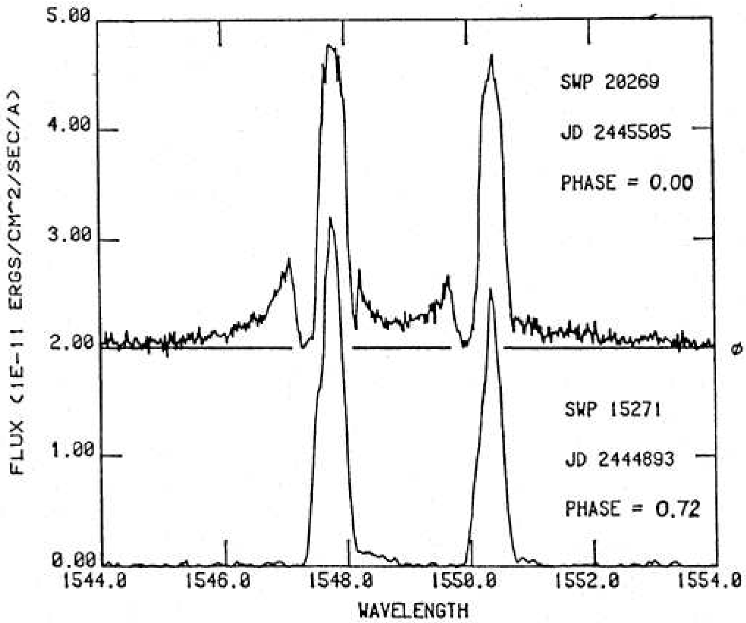

Figure 2.8: The C IV line profiles taken from Oliversen et al. (1985). The phases are according to Munari et al. (1988).

probably to the hot compact secondary. The narrow emission component is probably emitted in an area unconnected gravitationally with the secondary. A similar view is expressed by Penston & Allen (1985) about the profiles of these lines in the spectrum of the AG Peg system.

According to Oliversen et al. (1985) the broad component is evidence of an accretion disc surrounding the hot compact object. In our view, the broad component is radiated in the wind region, which is eclipsed by the cool component of the system. As the orbit is elliptical, the eclipse precedes the spectral conjunction and is at phase 0.65. (This is not seen clearly enough in Fig. 2.2, where the spectral conjunction phases are indicated). Consequently, an absence of the broad component should be observed at the phases near to 0.65. This is seen in the lower part of Fig. 2.8, at phase 0.72. At this phase, the blue wing is entirely absent, and the red one has been greatly weakened. The reason can be of a geometrical nature, as will be demonstrated in the following argument. The wind region between the hot component and the observer, where the blue wing forms, is small and entirely eclipsed by the cool component. The wind region behind the hot component, where the red wing forms, is not bounded by the nebular region, and some portion remains uneclipsed. The supposition of eclipse of the C IV broad component is also confirmed by observations at phase 0.53 described by Pesce et al.

(1987). The profile at phase 0.88 from the same work, however, does not support the conclusion of an eclipse. The broad component at phase 0.88 is considerably weaker than at phase 0.00, but the eclipse should not be observed with adopted radius of the giant. This fact, however, has little influence on the plausibility of the interpretation of EG And in the framework of the colliding-winds model, as the P Cyg C IV profile is clearly seen.

The narrow emission component is probably radiated in both the nebular region and the H II zone of the giant's wind. This component is, however, saturated in nearly all observations. For this reason, it is difficult to conclude whether its flux varies during the orbital period. Since an evidence of an eclipse, such as that observed in the He II λ 1640 line, is definitely absent, it seems that the area of this emission is large compared with the size of the giant. Figure 2.8 shows that the wavelength positions of the C IVnarrow components at both phases are almost the same, which means that their velocities are practically the same. The velocities at phases 0.53 and 0.88 (Pesce et al. 1987) are close to these values too. This means that the possible radial velocity amplitude of the lines is less than the typical velocity in the nebular region. The reason can be that both the nebular region and the H II zone of the giant wind contribute to the radiation.

2.5.2 He II λ 1640 line

In contrast to the C IV lines, this line varies greatly in intensity during the orbital cycle and its flux decreases to zero at some phases, which is clearly seen in Fig. 2.9, taken from the work of Oliversen et al. (1985). The view that this observational fact is an indication of an eclipse is commonly accepted.

The line flux has been obtained at different phases in the interval 0.5–1.0 by Stencel & Sahade (1980); Stencel (1984); Oliversen et al. (1985); Pesce et al. (1987) and Mürset et al. (1991). It has been calculated for the whole line, however, without separating the two components, which are comparable in intensity. The search for the location of their appearance would be helped to a great extent if their fluxes were available separately. The distinction between their profiles unambiguously shows that they appear in different parts of the system, as is also supposed by Oliversen et al. (1985) and Pesce et al. (1987). The FWHM of the broad component is in the interval 600–700 $\mathrm{km\,s^{-1}}$. If its profile is assumed to be determined by electron scattering in the vicinity of the hot component of the system, at a temperature of 10^4 K the width must be equal to 900 $\mathrm{km\,s^{-1}}$. It is difficult now for us to find a more acceptable idea for the explanation of the process determining the profile and the width of this line. The narrow component probably forms in the nebular region, comparatively near to the apex of the cone, rather than in the H II zone of

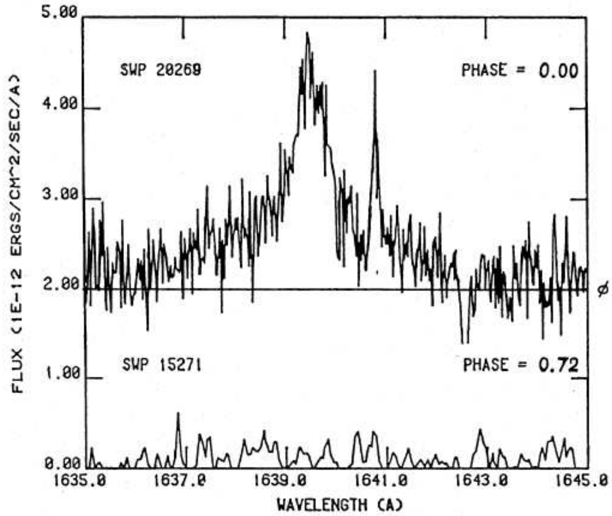

Figure 2.9: The He II λ 1640 line profile, taken from Oliversen et al. (1985). The phases are according to Munari et al. (1988). The emission feature on the long-wavelength wing is probably [OI] λ 1641 (Oliversen et al. 1985).

the giant's wind. The absence of the line at phase 0.72 (Fig. 2.9) shows that its area is eclipsed entirely.

2.5.3 O IV λ 1401, Si IV λ 1403 and O IV λ 1405 lines

The O IV lines disappear entirely at phase 0.72 like the He II λ 1640 line, which is seen in Fig. 2.10, taken from the work of Oliversen et al. (1985). They probably form in the same area which is eclipsed by the giant. Another aspect of the behaviour is shown by the line Si IV λ 1403. Figure 2.10 shows that it is present at both phases.

Pesce et al. (1987) compared the radial velocities of the lines at phases near to the orbital quadratures and came to the conclusion that the area of their excitation has approximately the same sign and amplitude of the velocity as those of the red giant primary. This conclusion can be understood in the light of the suggested model (Fig. 2.2).

Oliversen et al. (1985) have obtained the electron density in the region where the O IV lines are excited by using their intensity ratio. It amounts to 1.6×10^9 cm^{-3}. The electron density is of the same order according to the work of Stencel & Sahade (1980) also, in which different ultraviolet lines of the elements O III, O IV, C III, N IV, Si III and Si IV were used. We suppose that the density obtained is related to the areas located comparatively close to the apex of the cone.

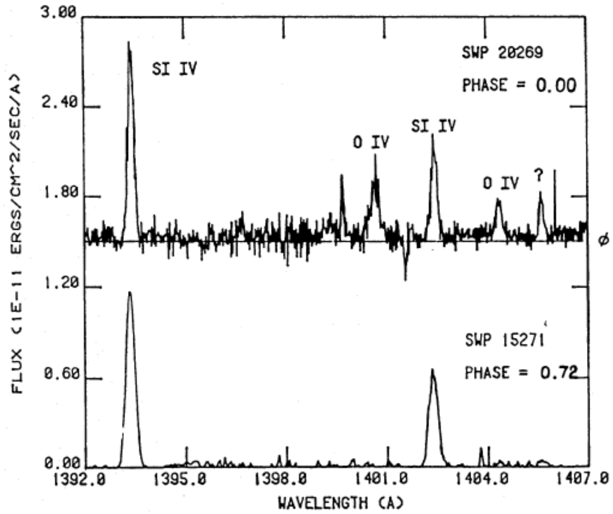

Figure 2.10: The O IV and Si IV line profiles, taken from Oliversen et al. (1985). The phases are according to Munari et al. (1988).

2.6 Conclusion

A P Cyg wind was observed in the C IV resonance lines of the EG And symbiotic system which was associated with the hot compact component (Oliversen et al. 1985; Sion & Ready 1992). We suggest that the spectral variability of this system can be explained in the light of the colliding winds model (Girard & Willson 1987). A nebular region, having the form of a cone, occurs on the collision boundary between the two winds. As the hot wind has low velocity and mass-loss rate, its momentum is smaller than that of the cool wind, and the conical surface surrounds the area behind the hot component. As a consequence of the orbital motion, the cone axis probably deviates from the straight line, determined via the centres of the two components, in a direction opposite to the motion. Beyond the nebular region, the hot component also ionizes a portion of the giant's wind. We suppose that the electron density amounts to $n_e \sim 10^9$ cm^{-3} in the areas comparatively close to the apex of the cone. This value was derived by Stencel & Sahade (1980) as well as by Oliversen et al. (1985), using some ultraviolet emission lines.

On the basis of the elements of the orbit, as well as profiles, fluxes and radial velocities of H_α and ultraviolet lines, we conclude that some of these lines are radiated in the ionization areas under consideration.

We have not succeeded in providing a sufficiently plausible interpretation of the He II λ 1640 broad component. On one hand, the radiation in the atmosphere of hot objects like the secondary in this system is influenced by electron scattering. On the other hand, the line is not broad enough to be explained by this mechanism.

Chapter 3

The symbiotic novae prototype AG Peg

3.1 Introduction

The symbiotic system AG Peg (HD 207 757) is the oldest known symbiotic nova. It has undergone a single outburst (Lundmark 1921; Boyarchuk 1967a), which is the most prolonged one among the outbursts of symbiotics. Its visual light was 9^{m} before the middle of the 19-th century. Between the years 1841 and 1855 it has begun to increase, reaching a maximum of approximately 6^{m} around 1885. Then it has gradually decreased and now it is practically equal to its value before the outburst.

The symbiotic system AG Peg consists of a normal cool giant of spectral type M 3–4 (Kenyon & Fernandez-Castro 1987; Mürset & Schmid 1999), a hot compact object with a temperature of about 90 000 K (Mürset et al. 1991; Kenyon et al. 1993; Altamore & Cassatella 1997) and a circumbinary nebula, partly photoionized by the compact object. The visual light shows two kinds of variation. It gradually fades, which is caused by the decreasing emission of the nebula. Moreover the visual light displays also an 800^{d} periodicity whose amplitude increases to shorter wavelengths (Belyakina 1992). This periodicity is related to the orbital motion as confirmed by the radial velocity curves of different elements (Hutchings et al. 1975). The V and B orbital variations are explained mainly with a heating of this hemisphere of the cool giant which faces the hot companion. The spectrum in the U band is mainly emitted by the circumbinary nebula whose continuum becomes more important at shorter wavelengths. The amplitude of the U orbital modulation changes, but is always close to about one magnitude (Belyakina 1992; Belyakina & Prokofieva 1992; Skopal et al. 2004, 2007, 2012). It was proposed (Kenyon et al. 1993) that the UV and the radio continua, which vary in phase with the optical light, are emitted mainly by a bright area located close to the photosphere of the giant. Its occultation determines the variations of these continua during the orbital cycle.

The analysis of the spectral observations carried out in different ranges during the past years, imply one and the same model of this system – a stage of colliding winds. For the first time this model was proposed by Penston & Allen (1985) on the basis of three IUE high resolution spectra, where a high velocity P Cyg wind was detected in the lines of N V, N IV, C IV and He II. Since the cool giant also loses mass through a stellar wind, it was concluded that the two winds probably interact.

Later the UV spectrum of AG Peg was studied by Kenyon et al. (1993); Vogel & Nussbaumer (1994) and Altamore & Cassatella (1997). Each of these analyses showed that a hot high velocity wind is observed in the lines of N V, C IV and He II and in every one of them a conclusion about colliding winds was made.

A model of winds in collision was proposed also by Tomov (1993b) on the basis of profiles, fluxes and radial velocities, derived from homogeneous high dispersion spectral observations in the visual during two consecutive orbital cycles (Tomov & Tomova 1992; Tomov 1993a). The broad components of the first Balmer lines and the line He II 4686 were caused by radial flow of gas with high velocity.

Supposing a regime of colliding winds in the AG Peg system Vogel & Nussbaumer (1994) theoretically calculated the radio image of its nebula being in good agreement with the observed one. A proof for existence of a shock region of the winds was obtained on the basis of ROSAT data by Mürset et al. (1995). They created a hydrodynamical model whose X-ray energy distribution was in agreement with the observations.

There are also observational data showing that some parameters of the wind of the hot companion are changed. According to both UV (Kenyon et al. 1993; Vogel & Nussbaumer 1994; Altamore & Cassatella 1997) and visual (Hutchings & Redman 1972; Ilmas 1987; Tomov & Tomova 1992) observations, the lines, appearing in this wind, began to weaken after the year 1978. The decrease of their intensities is determined by decreasing mass-loss rate (Kenyon et al. 1993; Vogel & Nussbaumer 1994; Altamore & Cassatella 1997). Having in mind their behaviour Zamanov & Tomov (1995) prognosticated that in the near future the change of the mass-loss at the observed rates will cause its decreasing below a given minimal value. At that time the momentum of the hot wind will not be sufficient to realize a collision and the system will move to a regime of a wind accretion. This transformation will be the final stage of the outburst begun in the first half of the last century.

The change of the mass-loss rate of the hot companion causes changes in the dynamics and the physical parameters of the nebular envelope and consequently of its spectrum.

The basic aims of our research are as follows:

1. To suggest a model for explanation of the U orbital variation and the fading of the U light on a long timescale of decades;

2. To investigate the process of loss of mass and to obtain quantitative estimate of the mass-loss rate of the outbursting compact object.

For our consideration we adopted a distance to the system $d = 650$ pc, which is mostly used in the current analyses (Mürset et al. 1991; Vogel & Nussbaumer 1994; Mürset et al. 1995; Altamore & Cassatella 1997).

3.2 Photometric investigation

3.2.1 Observations

The photometric behaviour of AG Peg was described and interpreted in the works of Tomov & Tomova (1998) and Tomov & Tomova (2001). Most of the observational data used are from the literature. One part of them (190) was obtained by Belyakina (1992) in the period JD 2 444 514 – 2 447 825 (October 1980 – October 1989). These data range over four orbital cycles. An other part of the data was obtained by Skopal et al. (2004, 2007, 2012) in the period 2001 – 2011. They range over four orbital cycles too and are actually the best sample of photoelectric U data of the system AG Peg. The last part of the data includes 33 U estimates obtained by us in an extensive UBV observational campaign during JD 2 449 974 – 2 451 557 (September 1995 – January 2000) with the photoelectric photometer, mounted at the Cassegrain focus of the 0.6 m telescope of the National Astronomical Observatory Rozhen. The star BD +11°4681 having $\mathrm{V} = 8\overset{\mathrm{m}}{.}18$, $\mathrm{B} - \mathrm{V} = 1\overset{\mathrm{m}}{.}03$ and $\mathrm{U} - \mathrm{B} = 0\overset{\mathrm{m}}{.}81$ (Belyakina 1992) was used as a comparison star. The m.s. errors are not larger than $0\overset{\mathrm{m}}{.}01$ in V and B, and $0\overset{\mathrm{m}}{.}02$ in U.

3.2.2 Description and analysis of the data

The eclipsing binaries have typical light curves, where the eclipses cover small phase intervals. The system AG Peg is not an eclipsing binary. We suppose that the decrease of its U light during the orbital period is caused by an

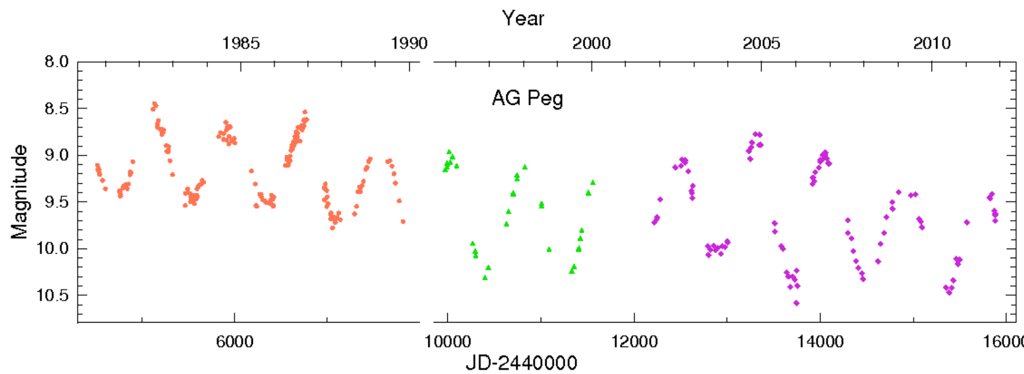

Figure 3.1: Photoelectric U observations of AG Peg. The data taken in 1980 – 1989 are of Belyakina (1992), the data taken in 1995 – 2000 are from our works (Tomov & Tomova 1998, 2001) and the data taken in 2001 – 2011 are of Skopal et al. (2004, 2007, 2012).

occultation of a bright nebular region by the giant in the system (Fig. 3.1). From its side this means that the region is not partially occulted at the time of the orbital maximum only. Then there is only possibility the bright region to be located around this hemisphere of the giant, which faces the hot companion.

Figure 3.1 shows that besides the gradual fading, other characteristics of the light of AG Peg are seen as well. Some of them are related to irregular variations of the minimum flux from cycle to cycle together with data scattering. These characteristics indicate variations of the number of the recombinating ions which from its side can be due to dynamical motions in the ionized region where different masses of gas appear from behind the stellar disk of the giant.

We considered the U flux of AG Peg at the epoch JD 2 450 059 of the orbital maximum of its light, obtained with the elements of the light of Fernie (1985) and at the epoch of the next minimum (Fig. 3.1) because the photometric data at the time of the last orbital minimum are not complete due to the visibility of the star. We used the U magnitudes of $9^{\mathrm{m}}.02$ and $10^{\mathrm{m}}.32$ taken at the epochs JD 2 450 049 and JD 2 450 398 which are close to the times of the orbital maximum and minimum. They were transformed into continuum fluxes without correcting for the emission lines included in the region of the U photometric system as we were not provided with spectral data during the time of the photometric observations. The fluxes were corrected for the energy distribution of AG Peg in the U spectral region and the interstellar reddening. The first of these corrections was made by means of the spectrum in Fig. 1 of Kenyon et al. (1993). The continuum on the long wavelengths-side of the position 3660 Å is weaker which causes reducing the real flux at this position by 50 %. This amount was added to the observed flux. The second correction was made using the value E(B − V) = 0.12 (Penston & Allen 1985) and the extinction law by Seaton (1979). The corrected fluxes are equal to 2.737×10^{-12} erg cm^{-2} s^{-1} Å^{-1} and 0.826×10^{-12} erg cm^{-2} s^{-1} Å^{-1}. Their difference of 1.911×10^{-12} erg cm^{-2} s^{-1} Å^{-1} corresponds to the orbital amplitude.

Having the orbital amplitude, which actually is the emitted flux by the occulted region we can calculate its mean density if its volume is available. The giant occults a region with a shape of a cylinder. The light curve indicates, however, that the effective emission of this region appears in a place close to the giant which is not occulted at the epoch of the orbital maximum only. If this emission appeared in the whole volume of the cylinder, the form of the light curve would be different. The form of the light curve meets its explanation in the framework of the colliding-winds model, which is currently accepted for the AG Peg system (Penston & Allen 1985; Kenyon et al. 1993; Tomov 1993b; Vogel & Nussbaumer 1994; Mürset et al. 1995; Altamore & Cassatella 1997; Contini 1997). As the mass-loss rate of the hot companion gradually decreases (Vogel & Nussbaumer 1994; Altamore & Cassatella 1997), we will consider the geometry of the stellar winds at the time close to the epoch of the light maximum under consideration. We will use a binary separation of 505 $R_\odot$ obtained from the orbital period of Fernie (1985) and the masses of the stellar components based on the orbital solution of Fekel et al. (2000). The wind of the giant is supposed not to be variable (Kenyon et al. 1993). For its mass-loss rate we will adopt an arithmetical mean of 1.5×10^{-7} $M_\odot$ yr^{-1} of the values of Vogel & Nussbaumer (1994) and Proga et al. (1998) and for the velocity of the wind 20 km s^{-1} (Vogel & Nussbaumer 1994). For the mass-loss rate of the hot companion we will adopt 8.75×10^{-8} $M_\odot$ yr^{-1}, which is an arithmetical mean of the data of Vogel & Nussbaumer (1994) and Altamore & Cassatella (1997). This amount was calculated using the value of Vogel & Nussbaumer for the year 1993, whose middle epoch was at JD 2 449 169, as the observations of these authors were up to this year. The wind velocity of the companion does not change and we will use a value of 1000 km s^{-1} (Tomov et al. 1998). In this case basing of the supposition that the collision region of the two winds has zero thickness (Girard & Willson 1987) we derived its distance to the center of the giant on the line joining the two stars of 80 $R_\odot$. Kenyon et al. (1993) propose a radius of the giant of 85 $R_\odot$ supposing a distance to the system AG Peg of 800 pc. We adopted a distance of 650 pc. The radius in this case is reduced to about 70 $R_\odot$ and the distance between the collision region and the photosphere is obtained to be 10 $R_\odot$. According to the simplified approximation of Girard

& Willson (1987) the collision region is a thin shell. In that case we will consider the wind of the hot companion extends to about 10 $R_\odot$ from the giant's photosphere. The emission of the occulted part of this wind can be regarded as negligible, since the flux of the whole wind is $\sim 2\,\%$ from the observed U flux of the system (Tomov & Tomova 1998). Consequently the emission of the occulted part of the nebula of AG Peg, equal to the orbital amplitude, originates in a thin shell around the photosphere of the giant, including some parts of the collision region and the giant's wind. If the radius of the giant is about 70 $R_\odot$, the thin shell will probably have a typical thickness of $10-20$ $R_\odot$.

The volume of this shell is probably close to the volume of a hemispherical layer around the giant. Taking a flux, equal to the orbital amplitude we calculated its mean density. The emitted flux depends on the state of ionization of helium. The ratio of the helium quantities in the different states of its ionization can be obtained as a ratio of the emission measures. We derived the emission measure of He^o, allowing that its lines are pure recombination lines as the electron temperature was proposed to be 15 000 K (Kenyon et al. 1993). We used visual line fluxes of He^o and the flux of the He II 4686 line from the paper of Tomov et al. (1998) at time, close to the epoch of the light maximum under consideration. Only the flux of the narrow component of the line He II 4686 was used as its broad component appears in the wind of the hot companion. We obtained a ratio He^{++}/He^{+} of about 0.1. This result shows that the singly ionized helium is dominant in the nebula and we assume that its flux is formed mostly by the continuum emission from H^o and He^o. For the flux of its occulted part we have

$$F^{\rm occ} = \frac{1 + a({\rm He})}{4\pi d^2}\,[\gamma_\nu({\rm H^o}, T_{\rm e}) + a({\rm He})\gamma_\nu({\rm He^o}, T_{\rm e})]\, n^2 V \times \frac{c}{\lambda^2} 10^{-8}\ , \qquad (3.1)$$

where n is the mean density, V is the volume and d – the distance to the star. The quantities γ_ν are related to the emission coefficients of hydrogen and neutral helium and are determined by recombinations and free-free transitions. The value of $\gamma_\nu({\rm H^o}, T_{\rm e})$ was adopted in the next way. The position of the U photometric system is close to the Balmer limit. The blending of the Balmer lines with high numbers of AG Peg (Tomov et al. 1998) causes absence of Balmer discontinuity, i.e. it produces an apparent continuum which on the long wavelengths-side of the Balmer limit in the range $3650-3660$ Å has the same flux as on the short wavelengths-side. That is why we used the value of this emission coefficient on the short wavelengths-side (Osterbrock 1974; Pottasch 1984). We adopted also helium abundance of $a({\rm He}) = 0.1$ (Vogel & Nussbaumer 1994). Realizing our calculations we obtained a mean density of the occulted region of $(2-4)\times10^{10}$ cm^{-3}.

The same geometry of the occulted region of the system AG Peg was concluded by Kenyon et al. (1993) considering the optical depth of its circumbinary nebula at 60 μm in the radio continuum. They stated the emission measure required to produce this optical depth cannot be related to the wind of the hot companion because of its low density and can be supported only by the red giant's wind at small distances outside the photosphere where the density of this wind is high enough. According to the same authors the dominant part of the UV and radio continuum emission as well as the narrow permitted lines of low ionization appear just in this region.

The photometric data, however, indicate also pronounced irregular variations of the flux in the orbital maximum (see Fig. 3.1). In our view an idea for interpretation of this observational characteristic can be given in the framework of the colliding-winds model. The ionized part of the whole nebula is seen at the phase of the orbital maximum. Consequently the flux variations at this phase are determined from variations of the density. In our opinion these variations are rather due to motions of the nebular environment than to variations of the mass-loss rate of the giant. It can be possible for example, if a winds interaction zone with a higher density than that of the giant's wind exists in the system. This interaction zone is warping in a direction, opposite to the orbital motion (Girard & Willson 1987; Walder & Folini 2000). Being dynamically unstable (Walder & Folini 2000) it probably changes its geometry, leading to veiling different masses of gas by the stellar disk of the giant. The emission of the nebula in the orbital maximum decreases when more dense parts of the interaction zone are veiled.

3.2.3 Discussion

The system AG Peg has undergone a single outburst, which has led to mass outflow of its hot component. The bolometric luminosity of this star has been constant from the time of the visual maximum around 1885 to about 1980 (Kenyon et al. 1993) and after that it has begun to decrease in step with its mass-loss rate (Vogel & Nussbaumer 1994; Altamore & Cassatella 1997). The wind of the companion will exist while its local momentum is equal to this one of the giant's wind and is able to prevent accretion (Zamanov & Tomov 1995). The observational data in both spectral regions the UV (Kenyon et al. 1993; Vogel & Nussbaumer 1994; Altamore & Cassatella 1997) and the visual one (Boyarchuk 1966; Tomov & Tomova 1992; Tomov et al. 1998) show that the velocity of this wind is invariable. Then according to the approach of Zamanov (1993) the accretion in this system will be restored again, when the decreasing mass-loss rate of its hot component reaches some limit. Our calculations led to a value of 5×10^{-10} $M_\odot$ yr^{-1}. When this limit is reached only the wind of the giant should exist in the system and the bright shell created by the winds interaction will disappear. The nebular U orbital variation, however, will probably not disappear, since the decreasing Lyman photon luminosity of the companion produces decrease of the H II region in the system (Nussbaumer & Vogel 1987), which, from its side, leads only to decrease of the orbital amplitude.

3.3 Spectral investigation

3.3.1 Observations and reduction

The spectral behaviour of AG Peg was described and interpreted in the work of Tomov et al. (1998). This work is based on two spectrograms, taken with the Coudé spectrograph of the 2m RCC telescope of the National Astronomical Observatory Rozhen (NAO) on September 8, 1995 (JD 2 449 969.38) and September 13, 1995 (JD 2 449 974.38). The observations were performed in the region from 3600 Å to 5000 Å on ORWO ZU emulsion, with a resolution of 0.5 Å. (The reciprocal linear dispersion was 18 Å mm^{-1}.) Both exposures were comparatively deep, each of 240 minutes, in order to bring out the wings of the bright emission lines and to detect the fainter features. The spectra were digitized with the Joyce Loeble microdensitometer of NAO and ReWiA package was used for wavelength and density calibration as well as for calculation of the radial velocities and the equivalent widths. Sections of the spectrum taken on JD 2 449 969.38 are displayed in Fig. 3.2 where the lines with measured radial velocities have been marked. As the strongest lines are not seen in this figure, the profile of one of them is displayed separately in Fig. 3.3. The profiles of the others are similar. The radial velocity of each group of lines is listed in Table 3.1.

We obtained the line fluxes using only the spectrogram of JD 2 449 969.38 as it turned out that the sensitivity of the other one was decreased in the long wavelengths region. Only fluxes of comparatively stronger lines were measured such that their equivalent width errors should be less than 30%. We consider the intensities of the same emission lines investigated in the work of Tomov (1993a) to have possibility for comparison. Some of these lines are the members of Pickering series of He II having wavelengths $\lambda\lambda$ 4200 and 4542 Å. They are unresolved blends. At the phases of our observations the line He II 4542 is blending with the line Fe II 4542, but the latter of them has considerably lower intensity. The line He II 4200 is blending with the line N III 4200 which has also lower intensity. In our opinion the blending of these

Table 3.1: Radial velocities in units of $\mathrm{km\,s^{-1}}$

Elem.	JD 2 449 000$^{\mathrm{d}}$+		Elem.	JD 2 449 000$^{\mathrm{d}}$+	
	969$^{\mathrm{d}}$.38	974$^{\mathrm{d}}$.38		969$^{\mathrm{d}}$.38	974$^{\mathrm{d}}$.38
Abs. lines	-18.1 ± 2.9	-19.5 ± 1.8	He II, N III, C III	-20.8 ± 2.4	-20.3 ± 0.9
H I	-22.2 ± 1.0	-20.1 ± 1.4	He II 4686 (N)	-13.7	-6.5
He^1 I	-14.2 ± 1.0	-14.4 ± 1.8	[O III] 4363	-16.1	-18.7
He^3 I	-14.1 ± 1.6	-17.0 ± 0.3	Fe II, Ti II	-18.7 ± 0.6	-18.2 ± 0.5

Table 3.2: Emission line fluxes in units of $10^{-11}\ \mathrm{erg\,cm^{-2}\,s^{-1}}$

Line	1986	1995	Line	1986	1995	Line	1986	1995
N III 4097	0.43	0.19	Fe II 4296	0.06	0.03	Fe II 4584	0.14	0.14
Hδ 4103	4.95	1.52	H$_\gamma$ 4340 (N)	8.07	2.00	Fe II 4629	0.15	0.10
He^3 I 4121	0.32	0.16	[O III] 4363	0.34	0.07	N III 4634	0.19	0.15
He^1 I 4144	0.49	0.17	He^1 I 4388	0.59	0.36	N III 4640	0.35	0.21
Fe II 4173	0.11	0.07	He^3 I 4471	0.71	0.38	He II 4686 (N)	5.20	1.74
Fe II 4179	0.12	0.09	Fe II 4508	0.09	0.04	He^3 I 4713	0.53	0.29
He II 4200	0.10	0.08	Fe II 4520	0.09		H$_\beta$ 4861 (N)	14.71	6.02
Fe II 4233	0.23	0.11	He II 4542	0.12	0.12	He^1 I 4922	1.18	0.65

lines works unessentially on the measurement of their equivalent widths.

The line fluxes have been obtained by means of our unpublished B= 9$^{\mathrm{m}}$.76 and V= 8$^{\mathrm{m}}$.56 photometric estimates, taken on JD 2 449 974.34. The monochromatic continuum fluxes at the positions of emission lines considered were calculated via linear interpolation of the fluxes at the positions of the sensitivity maxima of the B and V photometric systems. The error of the monochromatic continuum fluxes, obtained in this way, is due first of all to the presence of the bands of titanium oxide. This error is approximately equal to the error of the level of the local continuum (∼10%), as titanium oxide bands of the AG Peg system are shallow because of an overwhelming by the hot continuum (Boyarchuk 1966; Tomov & Tomova 1992). The line fluxes were corrected for interstellar reddening as described above and are listed in Table 3.2.

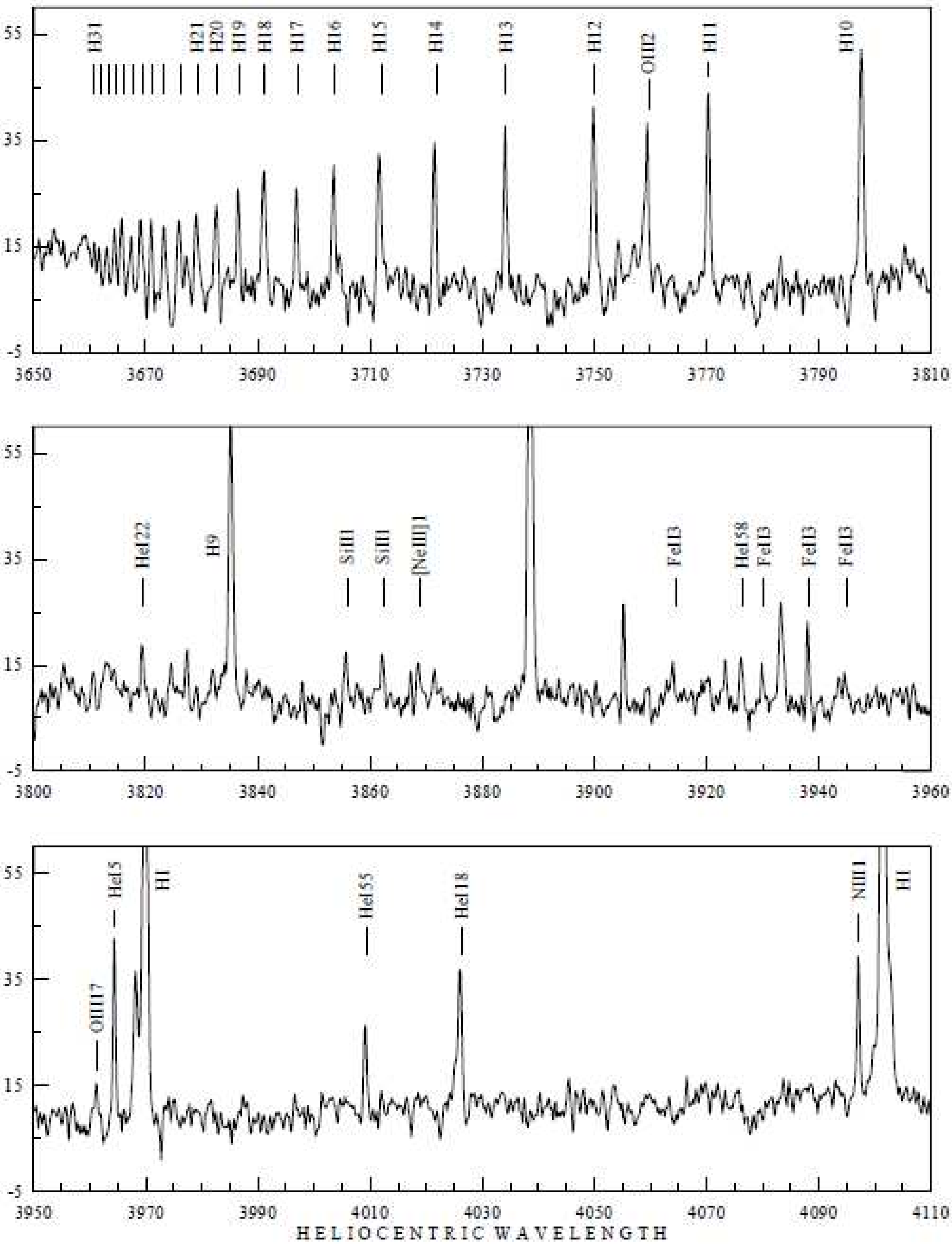

Figure 3.2: Sections of the spectrum, taken on JD 2 449 969.38. The ordinate scale is in arbitrary units.

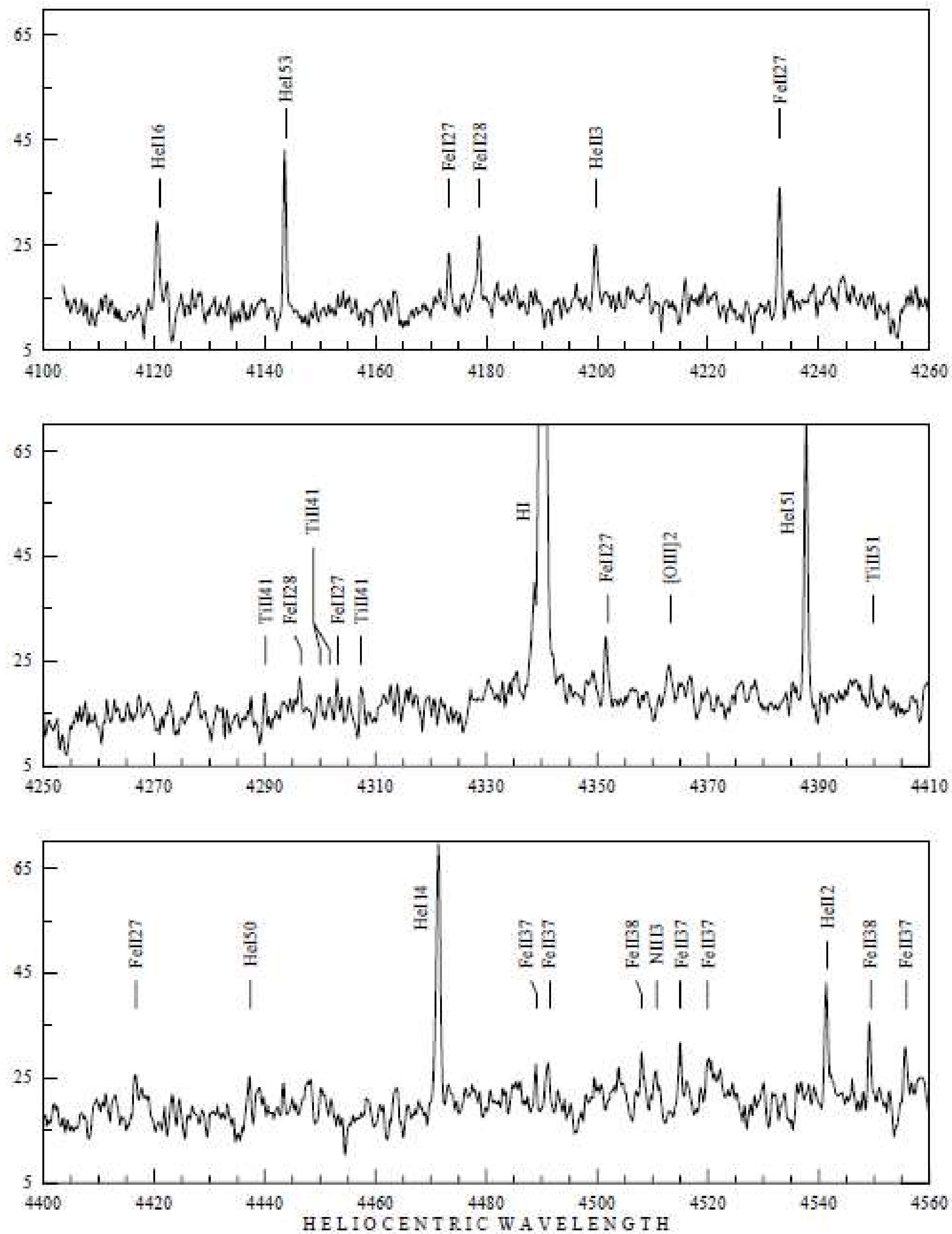

Figure 3.2: *continued*

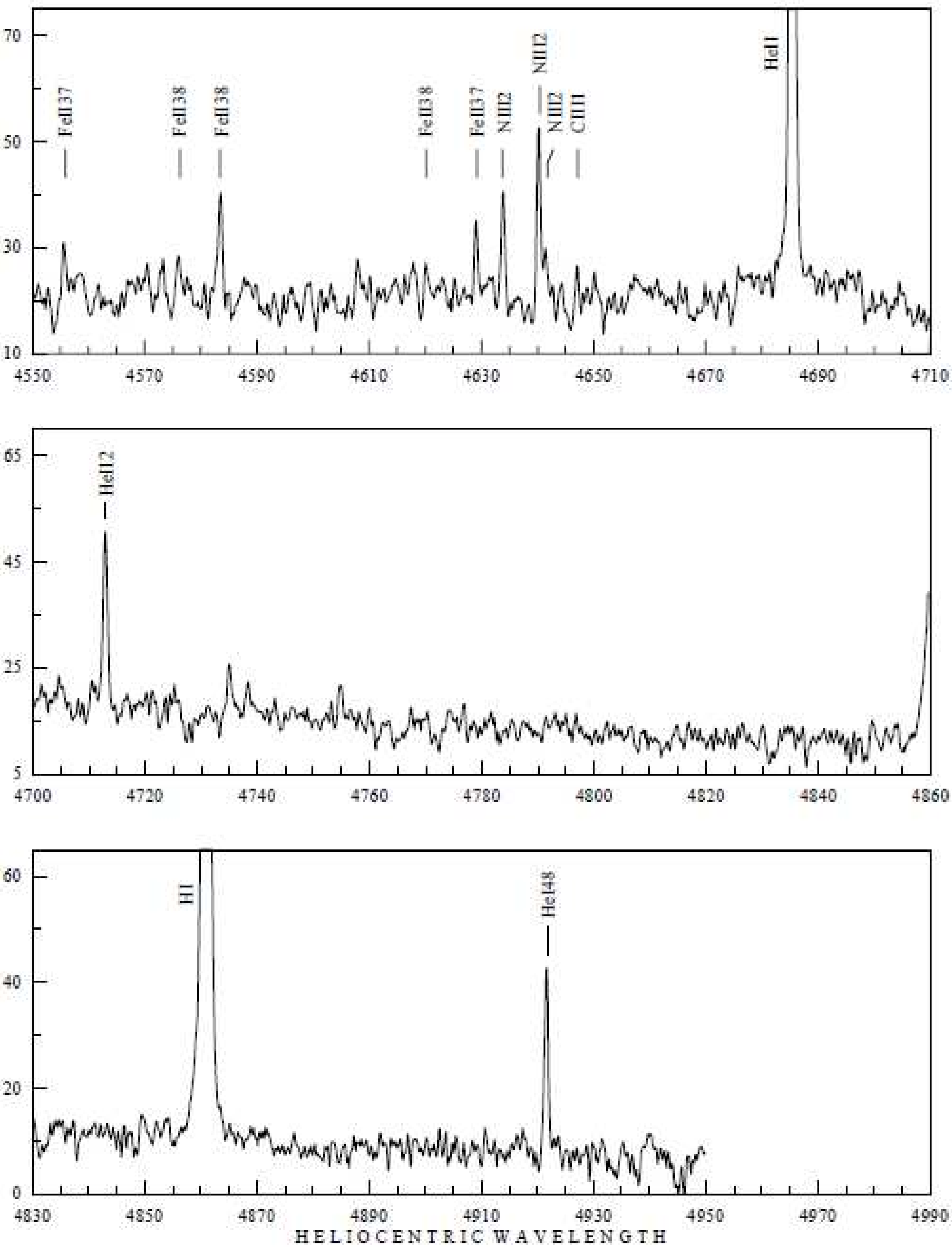

Figure 3.2: *continued*

Table 3.3: Radial velocity data of AG Peg in units of $km\,s^{-1}$ (Tomov & Tomova 1992)

JD$_\odot$ 2 446 000+	Phase	Abs.lines	He II 4686 (B)	H I	He^1 I	He II, N III, O III, C III	He II 4686 (N)	[O III] 4363
221.50	0.300	-19.8 ± 0.7	-0.6	-9.2 ± 2.0	-12.4 ± 0.9	-12.6 ± 2.3	-6.8	-21.1
244.55	0.329	-21.0 ± 2.0		-20.2 ± 1.0	-17.4 ± 1.1	-23.5 ± 2.0	-22.3	-31.4
252.52	0.338	-18.3 ± 1.4		-17.0 ± 0.2	-14.4 ± 0.3	-14.6 ± 2.2	-11.8	-29.5
252.57	0.339	-22.0 ± 3.4	-6.7	-14.2 ± 0.4	-13.7 ± 1.5	-20.2 ± 1.3	-21.7	-29.9
273.52	0.364	-18.7 ± 1.0	3.0	-31.2 ± 1.6	-19.3 ± 0.4	-21.7 ± 1.6	-25.3	-36.6
277.40	0.369	-22.0 ± 1.8		-35.6 ± 1.6	-19.1 ± 0.9	-23.4 ± 1.8	-19.5	-33.7
301.39	0.398	-21.3 ± 1.7		-38.4 ± 2.4	-20.0 ± 1.5	-29.0 ± 4.1	-29.3	-35.0
330.23	0.434	-16.7 ± 0.7	-35.8	-41.0 ± 6.8	-29.1 ± 2.7	-32.7 ± 0.1	-34.6	-40.2
370.30	0.483	-19.1 ± 1.3	-32.7	-53.6 ± 5.6	-30.4 ± 0.6	-35.4 ± 0.9	-43.1	-42.3
452.21	0.583			-64.9 ± 1.4	-31.1 ± 0.4	-41.9 ± 2.9	-53.9	-45.5
603.53	0.768	-12.8 ± 1.7	-36.8	-20.5 ± 1.2	-19.4 ± 1.9	-20.0 ± 1.7	-26.3	-25.7
603.57	0.768	-14.9 ± 0.9	-47.4	-16.5 ± 1.2	-21.3	-16.6 ± 1.6	-22.6	-30.1
605.49	0.771	-16.5 ± 0.7		-24.2 ± 1.1	-19.1 ± 0.5	-19.9 ± 1.4	-27.8	-20.2
627.53	0.798	-12.7 ± 1.4	-41.7	-16.4 ± 0.7	-15.4 ± 0.5	-17.4 ± 0.3	-24.1	-22.7
630.19	0.801	-12.8 ± 0.9	-50.4	-17.3 ± 1.2	-14.1 ± 0.4	-16.3 ± 0.5	-20.2	-16.2
638.49	0.811	-13.8 ± 1.2	-43.3	-14.2 ± 0.3	-16.2 ± 0.8	-19.3 ± 2.3	-25.0	-19.8
638.59	0.811	-16.3 ± 1.1		-16.9 ± 0.6	-17.6 ± 1.3	-15.6 ± 0.5	-16.7	-17.7
660.53	0.838	-14.8 ± 1.0		-15.8 ± 0.6	-14.4 ± 1.2	-15.9 ± 1.8	-21.0	-14.1
752.18	0.950	-21.1 ± 0.9		-2.9 ± 0.4	-11.1 ± 0.4	-7.8 ± 1.0	0.9	7.6
755.27	0.954	-19.2 ± 1.0	-30.9	-7.8 ± 0.3	-14.7 ± 0.5	-8.4 ± 1.4	-2.8	2.1
775.15	0.979	-19.2 ± 1.9	-28.6	-11.0 ± 0.8	-8.6 ± 0.4	-6.6 ± 1.0	5.8	14.8
928.50	0.166	-26.2 ± 1.4	32.3	-7.8 ± 3.7	-15.5 ± 0.4	-8.4 ± 0.9	-3.1	-4.0
990.52	0.242	-22.0 ± 1.2	10.5	-14.0 ± 0.7	-20.2 ± 1.2	-15.3 ± 2.4	2.8	-37.6
991.51	0.244	-24.2 ± 1.3		-13.1 ± 1.8	-18.1 ± 1.0	-15.7 ± 0.4	-9.4	-31.7
1023.53	0.283	-22.7 ± 2.0		-18.8 ± 0.9	-16.4 ± 0.8	-13.6 ± 0.4	-14.0	-33.3
1025.48	0.285	-21.6 ± 1.1		-17.0 ± 1.0	-15.8 ± 1.1	-14.8 ± 0.6	-22.3	-33.2
1047.26	0.312	-22.0 ± 1.9	13.8	-15.5 ± 0.3	-14.2 ± 0.7	-15.5 ± 0.4	-16.7	-34.9
1346.50	0.678			-34.6 ± 3.6	-18.1 ± 0.2	-26.3 ± 2.0	-40.7	-31.8

For the aims of our consideration the ephemeris of Fernie (1985)

$$\mathrm{Max(V) = JD}\ 2\,442\,710.1 + 816.5 \times \mathrm{E}$$

will be used. The epoch of the photometric maximum when the hot companion is before the giant is used as a start epoch. In this case our observations are at phases 0.891 and 0.897.

The data obtained will be compared with the results of our previous observations (Tomov & Tomova 1992) and that is why some of these results are listed in Table 3.3 and displayed in Fig. 3.4 as well. These are radial velocities data derived also on the basis of photographic observations in the blue spectral region. 40% of these spectrograms were taken with the Coudé spectrograph of the 6m telescope of the Special Astrophysical Observatory of Russian Academy of Sciences and have dispersion of 9 $\mathrm{Å\,mm^{-1}}$ and the rest – with the Coudé spectrograph of the 2m RCC telescope of NAO, with dispersion of 18 $\mathrm{Å\,mm^{-1}}$. All these spectrograms were processed with the oscilloscopic comparator of NAO, whose positioning error is equal to 0.5 μm.

The radial velocity curves of all groups of emission lines (Fig. 3.4) were plotted by means of the same program, used for obtaining the orbital solution. The lines in this figure plot the best-fitting circular orbits for the data in Table 3.3. The phase shift of each curve with respect to the absorption lines velocity curve, determined by the orbital motion of the cool component, is presented in the second column of Table 3.4. The parameters corresponding to the baricentric velocity V_0 and the semiamplitude K for each curve are presented in the third and fourth columns of this table. The standard deviation s is in the last column.

3.3.2 Description and analysis of the emission line spectrum

Balmer lines

The lines of Balmer series are visible as far as H 31. The profiles of the first of them consist of two components: a central narrow component with FWHM equal to about 95 $\mathrm{km\,s^{-1}}$ and a broad component, indicating stellar wind and having FWZI (full width of zero intensity) of about 2000 $\mathrm{km\,s^{-1}}$. Only the broad component of H_β is confidently seen. The profiles of the rest of the Balmer members consist of one component, i.e. they are ordinary nebular lines. Some of the Balmer profiles have asimmetry.

The line H 8 is badly blending with the line He I 3889 and is inappropriate for investigation.

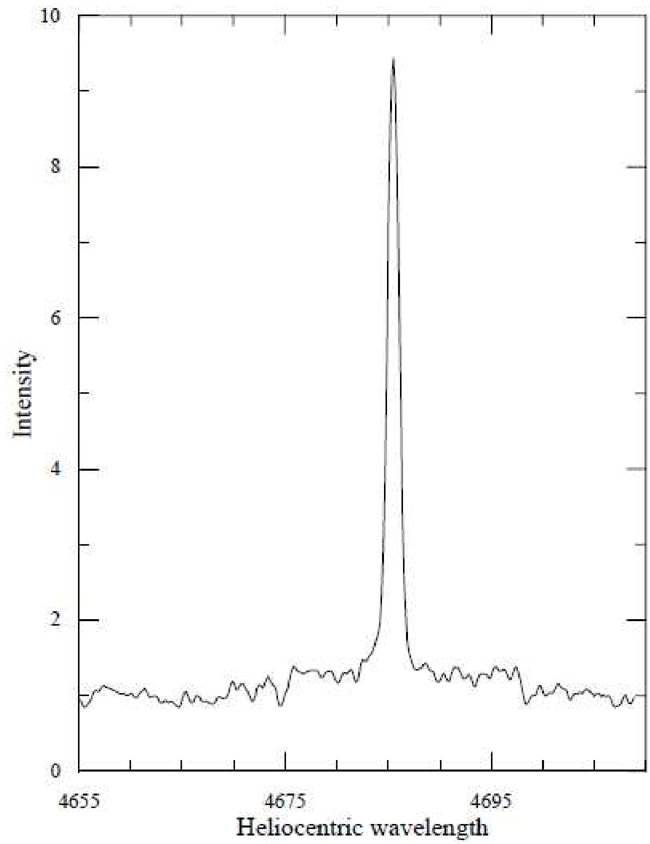

Figure 3.3: The profile of the He II 4686 line, observed on JD 2 449 969.38 and normalized with respect to the local continuum. It consists of two components – a narrow and a broad one.

We obtained radial velocities, measuring only the narrow components (Table 3.1). The radial velocities of all lines were the same within the range of the error, i.e. we didn't ascertain the existence of Balmer progression. The velocities of both spectra differ appreciably from the values of the radial velocity curve of the hydrogen lines at our phases in Fig. 3.4. These differences exceed the level of our error and that is why we consider they are due to a change of dynamics of the nebula.

The line fluxes (Table 3.2) obtained at the present time are compared with the fluxes obtained in 1986 (Tomov 1993a). Each of the latter of them is an arithmetical mean of three spectra taken at the moments JD 2 446 660.53, 2 446 752.18 and 2 446 755.27, which are at phases 0.838, 0.950 and 0.954. We compare spectra taken approximately at the same phases since the intensity of most of the emission lines vary during the orbital cycle. The line fluxes

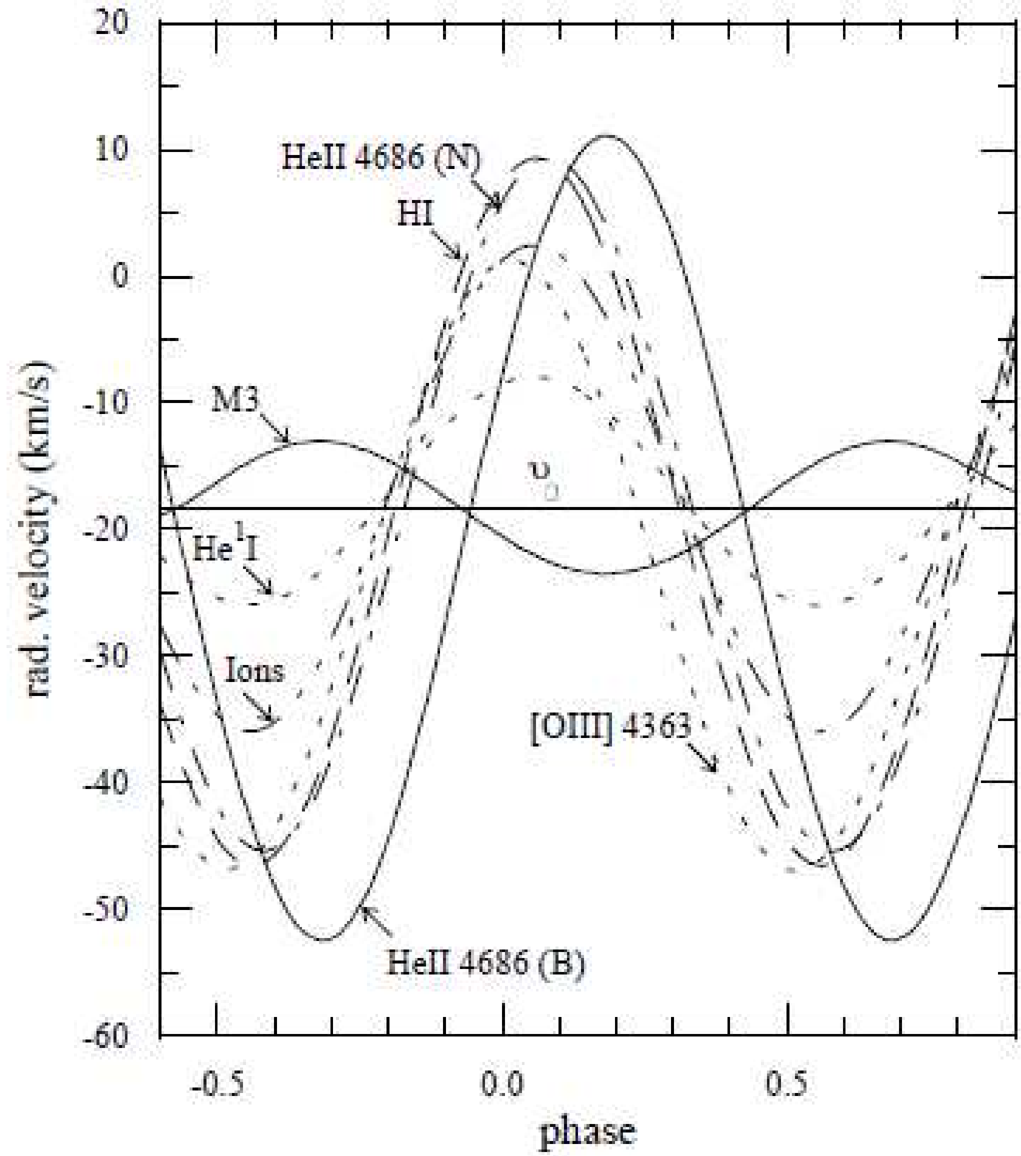

Figure 3.4: The orbital radial velocity curves of the visual lines of AG Peg from the work of Tomov & Tomova (1992). The elements of each curve as well as the designation of the M 3 giant and the barycentric velocity have been marked.

Table 3.4: Parameters of the radial velocities curves of AG Peg

Group of lines	Phase shift	V_0 ($\mathrm{km\,s^{-1}}$)	K ($\mathrm{km\,s^{-1}}$)	s ($\mathrm{km\,s^{-1}}$)
Abs. lines		−18.37	5.22	1.60
He II 4686 (B)	0.50	−20.69	31.77	9.88
H I	0.38	−18.56	27.94	6.88
He^1 I	0.38	−16.96	9.01	3.91
He II, N III, O III, C III	0.38	−16.74	19.18	3.14
He II 4686 (N)	0.40	−18.00	27.36	5.12
[O III] 4363	0.34	−22.81	24.08	6.83

in the work of Tomov (1993a) have been systematically reduced by a factor of about 1.5. The data used in the present work have been improved and then deredened in the way described in the last section. The data from the table show that the fluxes of the Balmer lines have decreased on average by a factor of 3.2.

Helium lines

The FWHM of the singlets is 45 − 50 $\mathrm{km\,s^{-1}}$ and those of the triplets – about 60 $\mathrm{km\,s^{-1}}$. Some of the lines of both groups have asymmetry in their profiles. The two groups have the same velocity (Table 3.1) practically equal to the value at our phases of the radial velocity curve of the helium lines in Fig. 3.4. The line fluxes of the singlets have decreased on average by a factor of 2.1 and those ones of the triplets – by a factor of 1.9 (Table 3.2).

Lines of elements of high degree of ionization

Lines of different highly ionized elements namely He II, N III, O III and C III are present in the blue region of the spectrum of AG Peg.

Like the Balmer lines the line of He II 4686 consist of two components: a central nebular component with FWHM equal to 80 $\mathrm{km\,s^{-1}}$ and a broad component, indicating stellar wind. The profile of the broad component, observed at the moment JD 2 446 755.27 when the line was more intensive is compared with the one, observed at JD 2 449 969.38 in Fig. 3.5. The error of the local continuum in the first case is equal to ±5% as Kodak IIaO emulsion having a lower noise was used. This error in the second case is about ±10%. The observed spectrum in the region of the He II 4686 broad component was corrected through removing the strongest absorption lines of the red giant

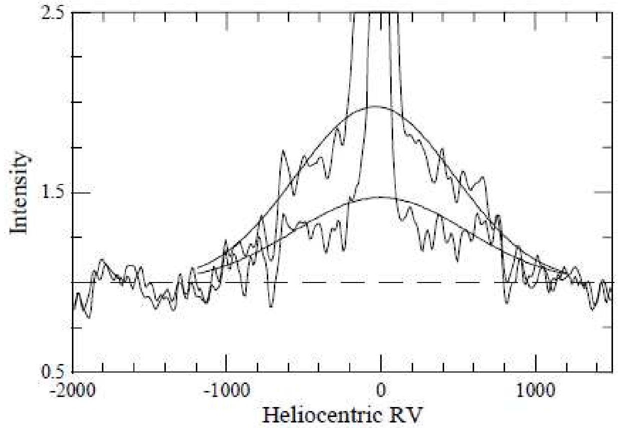

Figure 3.5: The broad component of the He II 4686 line, observed at the moments JD 2 446 755.27 (more intensive one) and JD 2 449 969.38. The level of the local continuum is marked with a dashed line. The radial velocities are in units km s^{-1}.

spectrum. Then the individual profiles were analysed by fitting with a sum of two gaussian components. The FWHM of the broad component in the first case is equal to 1210 ± 50 km s^{-1} and in the second one – 1310 ± 200 km s^{-1}. Taking into account the observational errors we have no reason to suppose that the line width has changed. This procedure allows us to obtain the equivalent width and the line flux with errors equal to about 30% in the first case, and about 50% in the second one. These errors are due first of all to the errors of the local continuum. If we take a velocity of the wind at a distance 2σ from the center of the line this velocity is obtained to be 1030 km s^{-1} and 1110 km s^{-1} in the two cases. We are inclined to adopt the first one of these values made up to 1000 km s^{-1}, as it is based on emulsion with better quality.

The velocity of the narrow component of He II 4686 (Table 3.1) is in agreement with the radial velocity curve of this line in Fig. 3.4. In a period of nine years its flux has decreased by a factor of 3.0 (Table 3.2).

We considered only the lines He II 4200 and He II 4542 of the Pickering series as the rest of them are badly blended with Balmer lines. The profiles of the lines He II 4200 and He II 4542 are asymmetric and their FWHM are equal to 55 km s^{-1} and 48 km s^{-1} respectively. The FWHM of the N III lines are about 45 – 50 km s^{-1}.

Since there was a great difference between the velocities of the O III lines of the two spectrograms, their values were excluded from further consideration. The lines of the rest of the elements have practically the same velocities whose arithmetical mean is shown in Table 3.1. However, they differ from the values of the radial velocity curve of the ionized elements at the some phases in Fig. 3.4.

The fluxes of the Pickering lines of He II have decreased on average by a factor of 1.1 and those of N III – by a factor of 1.7.

Forbidden lines

Only the lines of the elements [O III] and [Ne III] are included in this group. In contrast to the middle of eighties (Tomov & Tomova 1992), now the lines of [O III] $\lambda\lambda$ 4959 and 5007 have disappeared entirely and [O III] 4363 has considerably weakened – its flux has been reduced by a factor of 4.9 (Table 3.2). Its FWHM is equal to 73 $\mathrm{km\,s^{-1}}$.

There was a great difference between the [Ne III] 3868 line radial velocities in the two spectrograms and that is why they were excluded from further consideration. Like H I, He II, N III and C IV lines, the velocity of the [O III] 4363 line (Table 3.1) differs considerably from the one obtained previously at the same phases (Fig. 3.4).

Lines of ionized metals

Besides all groups of lines examined up to now, emission lines of singly ionized and neutral metals as Fe II, Ti II, Si II, Ca II, Cr II, Mg II, V II, Ni II, Al II, Fe I, Si I, Ca I and [Fe II] present in the visual spectrum of AG Peg. Only the Fe II and Ti II lines are intensive enough to make investigation possible. Their FWHM is equal to 45 $\mathrm{km\,s^{-1}}$. The K and H lines of Ca II are inappropriate for investigation because of blending with the lines N III 3934 and He II 3968, [Ne III] 3968 respectively.

The radial velocity of the Fe II and Ti II lines (Table 3.1) was obtained to be equal to the velocity of the lines of the singly ionized metals (Tomov & Tomova 1992) which doesn't vary with the orbital phase and is equal to -18.1 $\mathrm{km\,s^{-1}}$. These facts are probably due to the following reason: in contrast to the rest of nebular lines the lines of the singly ionized metals are excited in a part of the giant chromosphere, which faces the hot companion (Boyarchuk 1966; Kenyon et al. 1993) and is located very close to the mass center of the system, whose velocity is derived in the interval 16–18 $\mathrm{km\,s^{-1}}$ (Hutchings et al. 1975; Tomov & Tomova 1992; Kenyon et al. 1993).

The line fluxes of Fe II have decreased on average by a factor of 1.7 (Table 3.2).

3.3.3 Broad components and mass-loss rate

The evolution of the hot component of the AG Peg system has been considered by Mürset et al. (1991); Kenyon et al. (1993); Vogel & Nussbaumer (1994) and Altamore & Cassatella (1997). Their analyses show that after the year 1978 the radius, the luminosity and the mass-loss rate of this star have been decreased at nearly constant temperature. We will examine if the variations of the line intensities, observed by us, are in line with the variations of these parameters. Only the broad components of the lines H_β , H_γ and He II 4686 will be considered since only they appear in the wind of the hot companion (see Sect. 5) and depend solely on its parameters. The fluxes of these lines will be calculated and compared with the observed ones.

The mass-loss rate has been derived by Vogel & Nussbaumer (1994) and Altamore & Cassatella (1997) with the same methods using UV spectra obtained during approximately one and the same period of time. The first of these methods is based on the dependence of the equivalent width of the He II 1640 line on the mass-loss rate of the Wolf-Rayet stars (Schmutz et al. 1989) and is related to the case when the line is optically thick. This dependence has been extrapolated to the atmosphere of the hot companion of AG Peg. The second method is based on the relation between the energy emitted in the He II 1640 line and the mass-loss rate when the wind has spherical symmetry and a constant velocity. It is related to the case when the line is optically thin. The results obtained with the two methods are in good agreement.

In our study we will consider the hot wind in the nebular approach, i.e. we will follow the second of these methods and that is why the value of the mass-loss rate, derived in this case will be used. The arithmetical means of the data of Vogel & Nussbaumer (1994) and Altamore & Cassatella (1997) for the years 1986 and 1995 are 1.55×10^{-7} $M_\odot\,yr^{-1}$ and 8.75×10^{-8} $M_\odot\,yr^{-1}$ respectively. The second of them was calculated using the value of Vogel & Nussbaumer for the year 1993, as their observations were up to this moment.

The line flux determined by recombinations is given by

$$F = \frac{h\nu}{4\pi d^2} \int_V n_{\rm ion} n_{\rm e} \alpha_{\rm eff}(T_{\rm e}, n_{\rm e})\, {\rm d}V, \tag{3.2}$$

where $n_{\rm ion}$ is the density of the ion treated; $n_{\rm e}$, the electron density; $\alpha_{\rm eff}(T_{\rm e}, n_{\rm e})$, the effective recombination coefficient of this line and V, the emitting volume. If helium is ionized twice in this volume, the electron density will be $n_{\rm e} = (1 + 2a({\rm He}))n$ and the density of the given ion $n_{\rm ion} = a(X)n$, where $a(X)$ is the abundance by number of the element X relative to hydrogen. Then for the line flux we obtain

Table 3.5: The line fluxes of the broad components in units of 10^{-11} $\mathrm{erg\,cm^{-2}\,s^{-1}}$

Line	1986		1995	
	F_{calc}	F_{obs}	F_{calc}	F_{obs}
H_β (B)	2.86	2.43	1.12	1.61
H_γ (B)	1.36	1.95	0.53	<0.70
He II 4686 (B)	3.12	4.35	1.22	1.65

$$F = \frac{h\nu a(X)\,(1+2a(\mathrm{He}))\,\overline{\alpha_{\mathrm{eff}}}}{4\pi d^2} \int_V n^2\,\mathrm{d}V\,. \tag{3.3}$$

The abundance by number of He relative to H, $a(\mathrm{He})$, is adopted to be 0.1 (Vogel 1993; Vogel & Nussbaumer 1994). The recombination coefficient $\overline{\alpha_{\mathrm{eff}}}$ corresponds to an electron temperature of $T_{\mathrm{e}} = 20\,000$ K (Pottasch 1984). The density in the hot wind is a function of the distance to the center and can be expressed via the continuity equation

$$n(r) = \frac{\dot{M}}{4\pi r^2 \mu m_{\mathrm{H}} \upsilon}\ , \tag{3.4}$$

where $\dot{M}$ is the mass-loss rate; υ, the wind velocity equal to 1000 $\mathrm{km\,s^{-1}}$ and μm_{H}, the mean molecular weight in the hot wind, $\mu = 1.4$ (Nussbaumer & Vogel 1987). Using Eq(s). 3.2 and 3.3 we can calculate the line flux emitted by a nebula formed by a wind with spherical symmetry and a constant velocity.

We will consider that the temperature of the hot companion of the AG Peg system in both moments has been equal to 90 000 K, which is approximately an average of the results of Mürset et al. (1991); Kenyon et al. (1993) and Altamore & Cassatella (1997). In this case the photon fluxes beyond the limits of the ground series of hydrogen and ionized helium (Nussbaumer & Vogel 1987) are fully sufficient for ionizing these elements in the hot wind to infinity.

It is necessary for the calculation of the line fluxes to determine the region of integration. We treat the wind in the nebular approach Vogel (1993); Vogel & Nussbaumer (1994) and that is why the inner radius is thought to be the radius of the star. We will use for its value the arithmetical means of Vogel & Nussbaumer (1994) and Altamore & Cassatella (1997), which are 0.11 $\mathrm{R}_\odot$ and 0.09 $\mathrm{R}_\odot$ in the two moments respectively. Let's consider the outer radius of integration. Since both components have stellar wind, for the outer radius we will use 300 $\mathrm{R}_\odot$, which is about a half of the binary separation.

The calculated fluxes are listed in Tabl. 3.5 where they are compared with the observed ones. It is seen that their difference ranges up to about 45%. One of the reasons for this difference is the equivalent width error, which is due to the error of the local continuum. The equivalent width error of the broad components reaches 50%.

3.3.4 Discussion

The analisis of the emission line spectrum showed that the intensity of all lines has decreased. The excitation mechanisms in the nebular region are photoionization and shock. Then the total flux of the emission lines appearing in this region will consist of two parts: one determined by recombination and the other – by shock excitation. Moreover the hot star is possible to ionize one additional region of the wind of the giant, which will contribute to the line flux too. The mass-loss rate of the giant and the velocity of its wind are considered to be constant having values 1.5×10^{-7} $\mathrm{M_{\odot}\,yr^{-1}}$ and 20 $\mathrm{km\,s^{-1}}$ (Vogel & Nussbaumer 1994; Proga et al. 1998). The wind parameters of the hot companion are presented in the last section. Then the sum of the kinetic energies of the winds in the two times considered by us is 4.91×10^{34} $\mathrm{erg\,s^{-1}}$ and 2.77×10^{34} $\mathrm{erg\,s^{-1}}$, which is of the order of 10 $L_{\odot}$ and is small compared to the luminosity of the circumbinary nebula. Moreover the sum of the kinetic energies is an upper limit of the luminosity determined by shock, since the wind velocity component normal to the surface of the winds interaction is less than the velocity itself. Then the shock excitation has small contribution in the line flux.

The bulk of the flux of the emission lines results from photoionization of the circumbinary nebula by the hot star and the decrease of the flux will depend mainly from the change of its Lyman luminosity. The ratio of the luminosities at the two times considered by us is 1.5 and the arithmetical mean of the decrease factor of the lines of different elements is 2.5. These quantities are in agreement, since the uncertainty of the luminosity is 50%.

3.4 Conclusion and results

We present results of photometric observations of the symbiotic binary AG Peg at the final stage of its outburst. Based on the shape of the light curve we propose that the orbital U variations of the symbiotic star AG Peg are determined from the visibility of a thin bright region located around this hemisphere of its cool giant which faces the hot companion. The bright region exists probably because the interaction zone of the stellar winds of the two components is situated very close to the cool giant. The irregular changes of the U flux in the orbital minima and maxima are most probably due to dynamical instability of the interaction zone. We suppose that clouds of gas having different densities appear from behind the disk of the giant in the orbital minima, and clouds with different densities of the winds interaction zone are veiled by it in the orbital maxima. A flux equal to the orbital amplitude between two particular photometric maximum and minimum leads to a mean density of the bright region of $(2-4)\times10^{10}\,\mathrm{cm}^{-3}$. This region will disappear when the decreasing mass-loss rate of the hot companion drops below a value of about 5×10^{-10} $\mathrm{M}_{\odot}\,\mathrm{yr}^{-1}$ and only the wind of the giant remains in the system. The U flux at the orbital phase of the photometric maximum decreased by a mean factor of 1.6 in the period 1986 – 1995, which is in good agreement with the decrease of the Lyman luminosity of the outbursted compact object.

Moreover we present results of observations of the blue range of the spectrum of the system AG Peg at the final stage of its outburst when the luminosity and the mass-loss rate of its hot component decrease. The radial velocity data and the line fluxes have been obtained.

The radial velocities of the emission lines are compared with the radial velocity curves of the same elements during the orbital cycle, based on earlier observations, realized nine years ago (Tomov & Tomova 1992). It turns out that some of them differ considerably from the corresponding values of the curves, which in our opinion, is determined by change of dynamics of the nebular environment. Balmer progression was not established.

The profile of the lines H_{β} , H_{γ} and He II 4686 consists of two components: a central narrow component and a broad component indicating stellar wind. The comparison with earlier spectra (Tomov & Tomova 1992) shows the width of the broad component has not changed, which means that the wind velocity has had a constant value. The line fluxes of the broad components have been calculated by means of the mass-loss rate, obtained on the basis of contemporaneous UV observations. They are in agreement with the observed fluxes which confirms this mass-loss rate and its decreasing by a factor of 1.8 during this period of nine years.

The line fluxes of the more intensive among the narrow lines have also been obtained. A decrease of these fluxes by a mean factor of about 2 for all elements has been derived during this period.

Chapter 4

Investigation of the symbiotic binary AG Dra during quiescence and its phase of activity in 1994 – 1998

4.1 Introduction

The star AG Dra is a known symbiotic system with a low metal abundance, large barycentric velocity ($\gamma = -148\ \mathrm{km\,s^{-1}}$) and high galactic latitude ($b = 41°$) belonging thus to the old halo population (Smith et al. 1996). It belongs to the group of yellow symbiotics and consists of a cool primary of the spectral type K, probably more luminous than a normal class III giant (Huang et al. 1994; Mikolajewska et al. 1995; Greiner et al. 1997), a hot compact object with a high luminosity and temperature of $1.0 \times 10^5 - 1.7 \times 10^5$ K (Mikolajewska et al. 1995; Greiner et al. 1997) and an ionized circumbinary nebula. Its photometric period is about 550^d (Meinunger 1979; Skopal 1994). The consistency of this period with the orbital period of the binary is confirmed by radial velocity variations of the cool primary component, measured by Garcia & Kenyon (1988); Mikolajewska et al. (1995); Smith et al. (1996) and Fekel et al. (2000) as well as by polarization variations as measured by Schmid & Schild (1997). AG Dra binary is enriched in the heavy s-process elements and situated in the galactic halo (Smith et al. 1996).

The quiescent B and V light variations of AG Dra with a period of about 360^{d} and an amplitude of $0\overset{\mathrm{m}}{.}10 \div 0\overset{\mathrm{m}}{.}15$ are probably caused by an intrinsic variability of the cool giant, whose radiation becomes more important at longer wavelengths (Bastian 1998; Friedjung et al. 1998). The continuum of the giant also contributes to the U flux, but its variations at the time of the orbital maximum are determined primarily by changes of the emissivity of the nebula, since they are significantly larger than $0\overset{m}{.}15$ up to about $0\overset{m}{.}30$.

AG Dra belongs to the group of symbiotics that show "classical" or Z And type outburst. It has undergone several active phases (after 1936, 1951, 1966, 1980, 1994 and 2001), characterised by one or more light maxima. The reason for this activity is probably related to the nature of its cool component, which drives the eruptions of the hot companion (Friedjung 1997; Greiner et al. 1997; Galis et al. 1999). These eruptions are induced by variations of the accretion rate which are due to variations of the mass-loss rate of the giant rather than to an elliptical motion, since its radial velocity curve shows no sign of a measurable eccentricity (Mikolajewska et al. 1995; Smith et al. 1996; Galis et al. 1999). Consequently the investigation of the reasons for the brightenings of AG Dra is related to the study of the nature of its cool component. One task is to estimate its absolute size, which from its side is related to obtaining the distance to the system.

In 1994 AG Dra entered new active phase characterized by several consecutive outbursts having intervals of about one year between the times of their light maxima and U amplitudes up to more than 3 mag. In this way AG Dra underwent five optical brightenings, the last of them being in 1998. Analysis of the photometric data (Montagni et al. 1996; Greiner et al. 1997; Skopal 1998; Petrik et al. 1998; Tomova & Tomov 1998; Tomov & Tomova 2000) showed that the growth of the visual light is due to the increased radiation of the circumbinary nebula. Different models about the outburst activity of AG Dra have been proposed.

Leibowitz & Formiggini (1992) supposed the 1980 – 1983 and 1985 – 1986 optical outbursts of AG Dra to be associated with the liberation of mechanical energy in the atmosphere of the giant. Mikolajewska et al. (1995) came to the conclusion that these outbursts are most probably due to thermonuclear events on the surface of a white dwarf. Greiner et al. (1997) assumed the 1994 and 1995 outbursts to be determined by an expansion and cooling of the compact secondary, since their ROSAT data anticorelate with the optical photometry. They proposed this star to be in a steady-state burning of hydrogen at its surface, which provides its high X-ray luminosity during the quiescent state of the system. The accretion rate increases during the outburst and causes accumulation of matter, which is not included in the burning process. As a result of the expanding and cooling, the star decreases its X-ray emission. One possibility for the expansion to be restricted, according to the authors, is the appearance of a high velocity wind from the hot photosphere. The cooling of the star in principle provides a possibility for growth of its optical continuum but the visual brightenings of the system are caused by variation of its nebular spectrum. That is why the authors are forced to search for an additional emission mechanism in the surrounding nebula.

Gonzalez-Riestra et al. (1999) identified cool and hot outbursts of the AG Dra system determining the Zanstra temperature of its hot component. During the cool 1980 – 1983 and 1994 – 1995 outbursts the temperature of this component decreased compared to its quiescent value and during the hot 1985 – 1986 outbursts it increased. Viotti et al. (2007) suggested that during all outbursts the system first passes through a hot phase and during only the strongest outbursts it evolves towards a cool phase.

Galis et al. (1999) proposed a mechanism for increase of the accretion rate related to resonance of the pulsations of the cool giant and its orientation to the companion. They supposed that the pulsations are probably nonradial, leading to an appearance of an asymmetric stellar wind. The ratio of the orbital to the pulsation period was found to be very close to 14/9. It is possible for the mass loss of the giant to reach its maximal value when the most dense part of the wind is orientated towards the companion. This would provide a great increase of the accretion rate causing the observed outbursts.

One approach to test any single outburst model is to investigate the possibility the behaviour of the nebular emission to be explained in its framework. We obtained indications of high-velocity stellar wind from the compact component of the system during several of the outbursts. On one hand the frequency of appearance of this wind and the mass-loss rate obtained by us cannot be explained in the framework of the thermonuclear model. On the other hand the mechanism proposed for the interpretation of the X-ray data (Greiner et al. 1997) meets difficulties with the increase of the nebular emission. We suppose that the hot companion has a luminosity high enough to ionize the greatest part of the nebula with the exception only of the region behind the cool giant. That is why it may be able to ionize additional amount of gas in the wind of the giant when its mass-loss rate increases during outburst phase. This would be a natural explanation of the growth of the nebular emission.

The basic aims of our research are as follows:

i) to suggest a mechanism providing a growth of the nebular emission and a scenario for interpretation of the light curve during active phases;

ii) to investigate the process of loss of mass and to obtain quantitative estimate of the mass-loss rate of the outbursting compact object.

We used the Skopal (1994) ephemeris $\mathrm{JD(U_{min})} = 2\,442\,514.4 + 552.4{\times}\mathrm{E}$ since its derivation is based on the greatest number of photometric data.

The zero epoch is that of the photometric minimum, when the system's cool component is in front of the hot component.

4.2 Luminosity and distance

4.2.1 Photometric data analysis

At the present time there is no good knowledge of some of the fundamental parameters of the system AG Dra like the distance, radius and luminosity of the cool component (Friedjung et al. 1998; Gonzalez-Riestra et al. 1999; Galis et al. 1999). To derive the radius and the distance we used the radiation at the wavelength of the U photometric system, as the continuum fluxes of the circumbinary nebula and the giant are close at this wavelength. We compose one system of two equations with two unknown quantities – the distance to the system and the radius of the cool giant using the nebular and the giant's emission (Tomov et al. 2000).

During quiescence the U light of AG Dra displays a 550^{d} periodicity with an amplitude of about one magnitude. This periodicity is related to the orbital motion of the binary as confirmed by the radial velocity curve of its cool component (Garcia & Kenyon 1988; Mikolajewska et al. 1995; Smith et al. 1996). Important characteristics of the U light curve are the changes in the phases and shapes of the orbital maxima as well as the variations by more than 20 % of their fluxes (Hric et al. 1993, 1994; Friedjung et al. 1998). The decrease of the flux at the time of the orbital minimum is supposed to be caused by an occultation of a bright region that surrounds the hot companion (Mikolajewska et al. 1995; Friedjung et al. 1998). It was proposed as well (Friedjung et al. 1998; Gonzalez-Riestra et al. 1999) that the flux variations of the orbital maxima are due to variation of the giant's wind.

For our investigation we used the photoelectric data obtained in the period JD 2 446 700 ÷ 2 449 200 after the time of activity of AG Dra in 1985–86, since these data actually are the best sample of U photometry, taken during quiescent state of the system. These data were obtained during four orbital cycles (Fig. 4.1) in the framework of the international campaign for symbiotic stars launched by Hric & Skopal (1989), and are presented in the papers of Hric et al. (1993, 1994). For our calculations we used the U magnitudes of $11\overset{\mathrm{m}}{.}1$ and $11\overset{\mathrm{m}}{.}9$ giving the mean value of the light at the times of the orbital maximum and minimum on JD 2 447 700 and JD 2 448 000. They were selected because the data set is complete around these times and can be used for a reasonable estimate of the maximum and minimum fluxes. The magnitudes were converted into continuum fluxes without correcting for

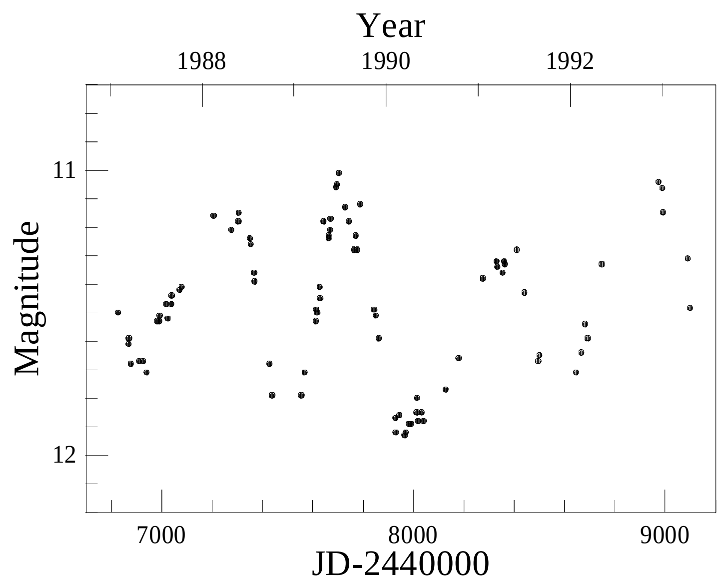

Figure 4.1: Photoelectric U observations of AG Dra during quiescent state.

the emission lines included in the wavelength region of the U photometric system as we were not provided with spectral data during the time of these photometric observations.

The fluxes were corrected for the energy distribution of AG Dra in the U spectral region. The continuum of this star on the long wavelengths-side of the Balmer jump is considerably weaker, which leads to a reduction of the flux at 3650 Å. The corrections were made by means of the spectrum in Fig. 3 of Mikolajewska et al. (1995). It turned out that the observed U flux is 20 % smaller than the real flux at 3650 Å. This amount was added to the observed flux.

Finally the fluxes were corrected for the interstellar reddening. We used the value $E(B-V) = 0.06$ (Mikolajewska et al. 1995; Greiner et al. 1997; Gonzalez-Riestra et al. 1999) and the extinction law by Seaton (1979). So the U magnitudes used by us led to dereddened continuum fluxes of 0.257×10^{-12} $\mathrm{erg\,cm^{-2}\,s^{-1}\,Å^{-1}}$ and 0.122×10^{-12} $\mathrm{erg\,cm^{-2}\,s^{-1}\,Å^{-1}}$ for the considered times of the orbital maximum and minimum, respectively. In this case the flux difference of 0.135×10^{-12} $\mathrm{erg\,cm^{-2}\,s^{-1}\,Å^{-1}}$ corresponds to the amplitude of the light variations.

The next step of our consideration is to estimate the contribution of the stellar components of the system. The flux of the hot companion was determined supposing that it radiates as a blackbody and using the ratio of the fluxes at 1340 Å and 3650 Å of a blackbody with the same temperature and the observed flux at wavelength $\lambda\,1340$ Å. Gonzalez-Riestra et al. (1999) have obtained a mean value of the dereddened quiescent flux at this wavelength of about 0.28×10^{-12} erg cm^{-2} s^{-1} Å^{-1} and Zanstra temperature of the companion of 110 000 K. On the basis of these data we derived an U band flux of $F^{\rm hot} = 0.007 \times 10^{-12}$ erg cm^{-2} s^{-1} Å^{-1}.

Let us consider the contribution of the cool component. The dereddened optical spectrum of AG Dra was fitted with that of a K giant and H$^{\rm o}$ continuum emission with electron temperature $T_{\rm e} = 15\,000$ K (Mikolajewska et al. 1995). We obtained the flux of this component supposing that it has the same continuum energy distribution like α Boo and the rest of the observed U flux is a nebular emission. We calculated the 3650 Å / 5500 Å flux ratio of α Boo and scaled it to the dereddened visual flux of AG Dra. Using the visual flux of AG Dra in its orbital minimum, when the nebular emission can be supposed to be negligible, we obtained for the flux of its cool component $F^{\rm cool} = 0.075 \times 10^{-12}$ erg cm^{-2} s^{-1} Å^{-1}.

After subtraction of the fluxes of the two stellar components from the observed flux at the orbital maximum the nebular continuum turned out to be $F^{\rm neb} = 0.175 \times 10^{-12}$ erg cm^{-2} s^{-1} Å^{-1}. The contribution of the nebula near orbital minimum is 0.040×10^{-12} erg cm^{-2} s^{-1} Å^{-1}, close to that of the red giant.

The shape of the U light curve indicates that the region emitting a flux, corresponding to the orbital amplitude is not occulted at the time of the orbital maximum only. This means that it is located close to the hemisphere of the giant facing the hot companion. The density of this small region is probably much higher than the mean density of the unocculted part of the nebula, since its radiation of 0.135×10^{-12} erg cm^{-2} s^{-1} Å^{-1} is by a factor of about 3 greater than the radiation of the unocculted part. One cause for the appearance of this small high density region was suggested by Galis et al. (1999), who assumed that the strong radiation pressure from the hot component tends to stop the matter of the giant's wind approaching the hot component and photoionization creates an ionized region with a higher density and emissivity.

4.2.2 Mass-loss rate

Besides the U photometric data, for our calculations the mass-loss rate of the giant is needed as well. The mass-loss rate of the cool components of the symbiotic stars is not an observed quantity and is difficult to determine. This quantity for AG Dra was estimated by Mikolajewska et al. (1995) using the radio flux at 4.9 GHz from Seaquist & Taylor (1990) and adopting a wind velocity of 30 km s^{-1}. This estimate, however, depends on their assumed system distance of 2.5 kpc, and cannot, therefore, be used for our purposes.

Van Winckel et al. (1993) suggested that the H_α emission profile of the symbiotic stars affected by self-absorption can be an indicator for the mass-loss rate of their cool components, whose atmospheres are ionized by a hot source. They created a classification system of the symbiotic stars, based on their H_α profiles. Later this idea was quantitatively considered by Schwank et al. (1997). They calculated a variety of models of an expanding atmosphere of a cool giant of **s**-type symbiotic system. The atmosphere of the giant is irradiated and ionized from the outside by the hot stellar component. Schwank et al. also calculated the H_α emission profile at phase when this component is in front of the giant, taking into account the optical depth of the atmosphere and supposing that the line is mainly due to recombination. The profile includes an absorption which moves from the center of the line to its short wavelength-side depending on the velocity of the absorbing particles. When the mass-loss rate of the giant increases, the ionized portion decreases and the transition zone between the ionized and the neutral volumes shifts outwards approaching the hot component. An outward shift of this zone in a region with higher velocity gradient leads to an increase of the difference between the velocity of the absorbing particles and that of the underlying recombination region, and, consequently, to a blue shift of the absorption. So the position of the absorption can be an indicator of the mass-loss rate.

Taking into account the relation between the H_α profile of the symbiotic stars and the mass-loss rate of their cool components we decided to search another star having Balmer emission characteristics close to that of AG Dra and a known mass-loss rate of its cool component.

A good comparison object seems to be AG Peg whose cool component loses mass at a rate of $(1-2)\times10^{-7}\ M_\odot\,\mathrm{yr}^{-1}$ (Vogel & Nussbaumer 1994; Mürset et al. 1995; Proga et al. 1998). Let us compare the Balmer emission spectrum of the two systems. The characteristics and the orbital variations of the H_α profile of AG Peg were studied by Boyarchuk et al. (1987), and those of AG Dra during its quiescent state – by Tomova & Tomov (1999). H_α profiles of these stars can be also found in other works (e.g. Ivison et al. 1994; Viotti et al. 1998). In both symbiotic systems the intensity of H_α emission varies with the orbital phase as a result of both changes of the optical depth and of the giant's occultation. The maximum intensity is around the phase of the light maximum, when the hot component is closer to the observer. The orbital variations of the profile of this line in the two systems are also similar, being due also to optical depth changes. At the phases of the maximal intensity it is single-peaked with a blue shifted absorption producing a small shoulder or a general asymmetry only.

The profiles of the two stars are shown in Fig. 4.2. They are different

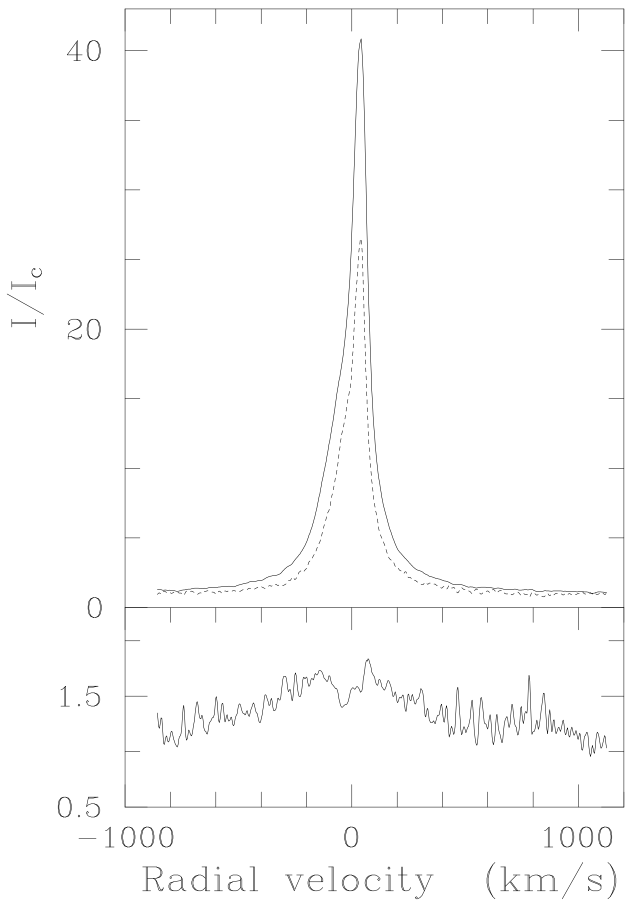

Figure 4.2: *Upper panel:* H_α profiles of AG Dra (solid line) taken on 2 February 1994 (Tomova & Tomov 1999), and of AG Peg of 30 June 1986 (from Ivison et al. 1994). *Lower panel:* AG Dra over AG Peg profile ratio.

from the theoretical profiles of Schwank et al. (1997), as the absorption is far away from the center of the line. This is due to the peculiar structure of the circumbinary nebulae of these stars. We used the H_α profile of AG Peg observed on 30 June 1986 before the photometric maximum, instead of that of 29 July 1991 which is nearer to the maximum but after it (Ivison et al. 1994). These data indicate that the H_α line reaches its maximum intensity probably a somewhat earlier than the light maximum, being more intense on 30 June 1986. The wings of the two lines in Fig. 4.2 are symmetric. As for comparison, we have divided the profiles of the two stars, as illustrated in the lower panel of the figure.

Let us now compare some other characteristics of the two systems in the light of the theoretical treatment of Schwank et al. (1997). These authors have shown that the H_α profile affected by the optical depth depends on the luminosity of the hot stellar component, the separation, the mass-loss rate of the cool giant and the velocity law of its wind. The AG Peg system (Boyarchuk 1966; Kenyon et al. 1993) as well as the AG Dra system (Mikolajewska et al. 1995; Greiner et al. 1997) have high luminosity hot companion, whose ionizing radiation probably reaches the innermost layers of the giant's wind where its density is the highest and where the bulk of the energy of the line is emitted. Then it will not be necessary to compare the companion's luminosities and the separations but only the velocity laws and the mass-loss rates. The velocity laws are different, but since the energy is emitted mostly from the layers near the giant's surface, the velocities and their gradients in these layers are low having probably close values. On the other hand there is similarity of the profiles morphology and according to the treatment of Schwank et al. (1997) the mass-loss rates must be probably close as well. Supposing that the mass-loss rate of the giant of AG Peg is $1 \div 2 \times 10^{-7}$ $M_\odot$ yr^{-1}, for its counterpart in the AG Dra system we adopt $2.0 \div 2.5 \times 10^{-7}$ $M_\odot$ yr^{-1}. As it will be shown in the next section, the mass-loss rates smaller than the lower limit lead to stellar radii below 28 $R_\odot$. So small values are probably not plausible, as the cool component of the AG Dra system is supposed not to be a normal giant, but K-type bright giant (Huang et al. 1994; Mikolajewska et al. 1995; Smith et al. 1996).

4.2.3 Method of calculation and results

Having the fluxes of the components of the binary AG Dra we can compose a system of two equations with two unknown quantities – its distance and the radius of its primary. The effective temperature of this component was estimated by Smith et al. (1996) and amounts to be 4300 K. The cool giant's continuum can be fitted with a function giving the energy distribution of α Boo, since, according to Griffin & Lynas-Gray (1999) the effective temperature of this star is 4290 ± 30 K the same as that of AG Dra. This function consists of two parts, the first part is related to the radiation of a blackbody with a temperature of 4300 K and the second one to the energy distribution of α Boo. At the wavelength of the U band the second part has a value of $C_\alpha = 0.788$. Then the first equation is:

$$F^{\rm cool} = \frac{2\pi hc^2 R^2}{d^2\lambda^5} \frac{1}{{\rm e}^{hc/\lambda kT} - 1} C_\alpha \times 10^{-8} \ , \qquad (4.1)$$

where R is the cool giant's radius and d – the distance.

Let us now consider the second equation. We suppose that the emitting circumbinary nebula is formed by a wind with spherical symmetry and a constant velocity and has an inner boundary the radius of the giant, as only a small portion occulted by it is not an ionized region (see below). To give an expression to the flux of the nebula the state of ionization of helium is need to be known. We calculated the ratio of the emission measures of the neutral and ionized helium, allowing that the lines of the He$^{\rm o}$ are pure recombination lines. That is really the case when the electron temperature is 15 000 K (Mikolajewska et al. 1995). We used visual line fluxes of He$^{\rm o}$ and the flux of the He II 4686 line from the paper of Gonzalez-Riestra et al. (1999) at a phase, close to the maximum light. Since these data are related to quiescence of the system, we used the sum of the fluxes of the narrow and broad emission components of the line He II 4686. In this way we obtained a ratio He^{++}/He^{+} of about 0.5. This result shows that the singly ionized helium is dominant in the nebula and we assume that the nebular emission mostly is continuum emission of hydrogen and neutral helium. For this flux we have

$$F^{\rm neb} = \frac{1+a({\rm He})}{4\pi d^2}\frac{c}{\lambda^2}\,10^{-8}\times \left[\int_V n^2\gamma_\nu({\rm H^o}, T_{\rm e})\,{\rm d}V + a({\rm He})\int_V n^2\gamma_\nu({\rm He^o}, T_{\rm e})\,{\rm d}V\right], \qquad (4.2)$$

where V is the volume of the nebula. We treate the nebula as spherical region whose center coincides with the center of the giant and suppose that the whole nebula is ionized. The ionizing radiation of the hot compact component penetrates close to the giant (see the previous section) and in this case according to Nussbaumer & Vogel (1987) the greater part of the nebula should be ionized region. The quantities γ_ν are related to the emission coefficients of hydrogen and neutral helium and are determined by recombinations and free-free transitions. The particle density in the giant's wind is a function of the distance to the center and can be expressed via the continuity equation

$$n(r) = \dot{M}/4\pi r^2 \mu m_{\rm H} \upsilon\,,$$

where $\dot{M}$ is the mass-loss rate, υ – the wind velocity, $\upsilon = 30$ km s^{-1} (Mikolajewska et al. 1995) and $\mu m_{\rm H}$ – the mean molecular weight, $\mu = 1.4$ (Nussbaumer & Vogel 1987). The inner boundary of the region of integration is the radius of the star and the outer one – infinity. It is also necessary to have the quantities γ_ν. The position of the U photometric system is close to the Balmer limit, and the spectral observations in this region of (Tomova & Tomov 1999) show another characteristic feature of the emission of AG Dra: the blending of the Balmer lines with high numbers produces an apparent continuum longward of the Balmer limit near 3650 – 3660 Å which has the same flux as the Balmer continuum excess shortward of 3650 Å. For this reason we used the values of the emission coefficients on the short wavelength side (Osterbrock 1974; Pottasch 1984). We adopt an electron temperature of 15 000 K as proposed by Mikolajewska et al. (1995) and helium abundance of 0.1 (Vogel & Nussbaumer 1994). Solving the system of equations, with the adopted values of the mass-loss rate the distance is obtained to be in the range 1560÷1810 pc, and the stellar radius – in the range 28÷32 $R_\odot$. This result shows that the size of the giant star is small compared with its Roche lobe.

Our estimates can be compared with the estimates, based on other methods. For example Smith et al. (1996) studying the IR absorption spectrum and performing an abundance analysis of the giant, concluded that its bolometric magnitude and radius are in the intervals $M_{\rm bol} \sim -1.1 \div -2.5$ and $R = 26 \div 50\ R_\odot$. Mikolajewska et al. (1995) came to the conclusion that the distance is ~ 2.5 kpc. On the other hand the observational data of *HIPPARCOS* satellite provided a lower limit to the distance of about 1 kpc (Viotti et al. 1997).

4.2.4 Discussion

The availability of an estimate of the radius of the primary of AG Dra gives us the chance to calculate some other parameters too. The abundance analysis of this star performed by Smith et al. (1996) provided an estimate of the surface gravity of $\log g = 1.6$. Using this estimate and a radius of $28{-}32\ R_\odot$ we derive a mass of $1.1{-}1.5\ M_\odot$ which is in agreement with the result of the analysis of this component by Mikolajewska et al. (1995). Having the radius and the effective temperature of the star, we found its bolometric luminosity, which turned out to be in the interval $242 \div 316\ L_\odot$.

The values for the distance to the system lead to the reduction of some of the parameters of its hot companion obtained by Greiner et al. (1997) which are based on a distance of 2.5 kpc. Since a very hot star was observed, these authors proposed that it is in a steady state hydrogen burning near its surface allowing its luminosity to be due only to nuclear processes. A steady state burning can be realized when the burning rate is equal to the accretion rate. Greiner et al. found that if the hot companion of the AG Dra system had such an accretion rate, it will be in the range of steady burning at the surface of a white dwarf with a mass of 0.3 $M_\odot$. This mass was calculated using the core mass–luminosity relation $L/L_\odot \approx 4.6 \times 10^4 (M_{\rm core}/M_\odot - 0.26)$ (Yungelson et al. 1996). Making corrections of their parameters we obtained that the bolometric luminosity and the accretion rate are in the intervals $967 \div 1302\ \mathrm{L}_\odot$ and $1.2 \div 1.7 \times 10^{-8}\ M_\odot\,\mathrm{yr}^{-1}$. The mass of the companion was calculated to be about 0.3 $M_\odot$, which leads to a minimum accretion rate for steady burning of 1.8×10^{-9} $M_\odot\,\mathrm{yr}^{-1}$. So it can be concluded that these new values are also in agreement with the model of a steady state burning at the surface of a white dwarf.

4.3 Photometric investigation

The photometric data of AG Dra taken by us during its 1994 – 1998 active phase were described and interpreted in the works of Montagni et al. (1996); Tomova & Tomov (1998) and Tomov & Tomova (2000).

4.3.1 Observations

Broad-band BVRI photometry of AG Dra was obtained during July 1994–January 1996 with the 30 cm, F/4.5 telescope at Greve (Firenze), and with the 50 cm, F/4.5 telescope at Vallinfreda (Roma). Both telescopes are equipped with a SBIG ST6 CCD detector. The photometric accuracy was excellent during most nights, the m.s. errors being of $0\overset{m}{.}03$ in B, $0\overset{m}{.}02$ in V, $0\overset{m}{.}03$ in R, and $0\overset{m}{.}02$ in I. As for the photometric sequence we have used the secondary standards listed in Table 4.1, whose photometric data were obtained using stars from the Landolt's (1992) catalogue.

Three colour UBV photometry was obtained during December 1993–February 1996, July 1996–October 1997 and January 1998–June 2000 with a single channel photoelectric photometer, mounted at the Cassegrain focus of the 60 cm, F/12.5 telescope of the National Astronomical Observatory "Rozhen". The star BD +67°925 having $V = 9\overset{m}{.}88$, $B - V = 0\overset{m}{.}56$ and $U - B = -0\overset{m}{.}04$ (Skopal & Chochol 1994) was used as a comparison star, checked by the star BD +67°926. We estimated the accuracy using the observational data of the check star. The m.s. errors are not larger than $0\overset{m}{.}02$ in U and B, and $0\overset{m}{.}01$ in V for the data taken during December 1993 – February 1996 and not larger than $0\overset{m}{.}01$ in all bands for the other data. The brightness data in the period JD 2 450 317÷2 450 324 were obtained with the similar telescope and equipment of the Astronomical Observatory Belogradtchik. The observational data are listed in Tables 4.2 and 4.3.

4.3.2 Analysis of the data

Figure 4.3 gives the five-colour light curve of AG Dra during its 1994–1995 active phase. The observations cover mainly the declining phases following

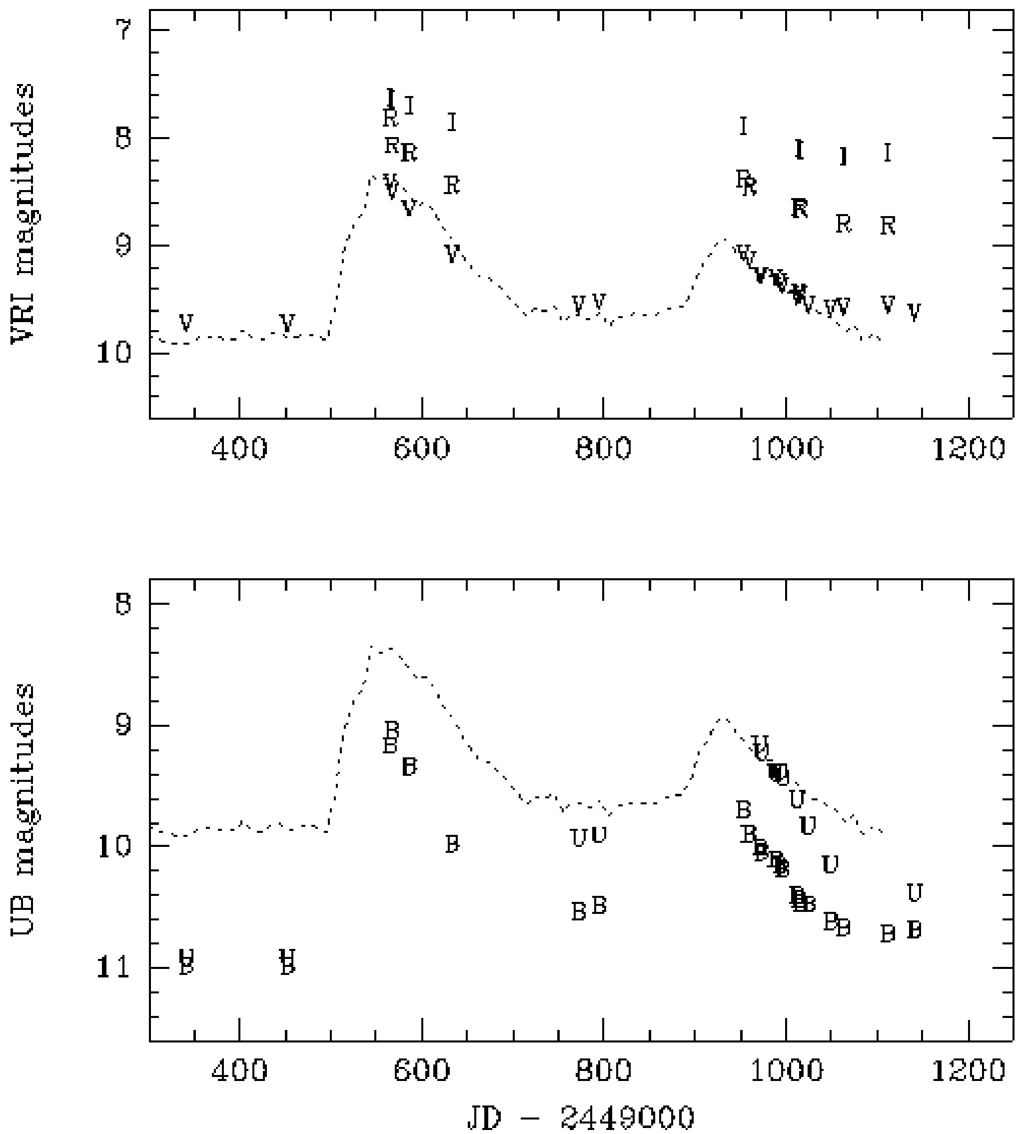

Figure 4.3: The five–colour light curve of AG Dra from December 1993 to February 1996. For comparison, the AAVSO visual light curve (10-day means, Mattei 1995) is shown as a dotted line.

Table 4.1: The BVRI photometric sequence

Star	$\alpha(2000)$ $^{h\ m\ s}$	$\delta(2000)$ $^{\circ\ \prime\ \prime\prime}$	B	σ	V	σ	R	σ	I	σ
a	16 03 25	+66 37 31	11.93	.02	11.13	.02	10.74	.03	10.34	.01
b	02 54	41 34	11.83	.02	11.12	.02	10.75	.03	10.37	.02
c	03 27	45 16	10.99	.02	10.43	.02	10.10	.03	9.82	.01
d	04 09	40 02	11.67	.03	11.04	.02	10.71	.03	10.39	.01
e	00 41	39 33	12.45	.03	12.00	.01	11.66	.03	11.39	.01
f	01 41	38 50	12.22	.02	11.72	.01	11.37	.03	11.05	.03
g	00 56	42 57	13.20	.09	12.27	.02	11.78	.03	11.32	.01

the primary (June 1994) and secondary (July 1995) light maxima. No U-band observations were obtained during the 1994 maximum, but that phase was also covered by the UBV observations of Skopal & Chochol (1994). The figure shows that AG Dra varied in all the colours, but the amplitude of the variation was larger (and the decline steeper) for the shorter wavelengths. This behaviour is opposite to that "typical" of symbiotic stars (and of some other types of variable stars) which are generally redder at maximum light. In particular, the variation of the U magnitude during the 1995 outburst – when compared to its value during quiescence – indicates an increase by a factor greater than 5 of the radiation near the Balmer jump. The variation was quite large also in B, with a flux increase (with respect to quiescence) of more than 2.1 and 1.3 magnitudes for the 1994 and 1995 outbursts, respectively. It should be noted that during the minimum phase in between the two light maxima, the U and B fluxes were well above their quiescent values. Finally, we remark that unexpectedly during the light maxima AG Dra significantly varied also in the I-band which is near the maximum of the energy spectrum of the cool stellar component.

These results can be interpreted in the light of a three spectral component model of AG Dra, in which the red–near IR is dominated by the cool star spectrum, while the blue–near UV radiation arises from the circumstellar nebula ionized by the radiation of the hot star (whose contribution to the near-UV is thought to be negligible).

In this model the optical outbursts should be associated with the increase of the size of the nebula, which from its side is the result of the increased flux of UV photons from the outbursting hot source. The U-band excess of AG Dra is therefore due to the nebular Balmer continuum, which has

Table 4.2: Photometric observations of AG Dra in 1993 – 1996

Date	JD-2400000	n	U	B	V	R	I
19 Dec 93	49341.2	3	10.92	10.99	9.73	—	—
10 Apr 94	49452.5	2	10.93	10.99	9.73	—	—
31 Jul 94	49565.4	1	—	9.17	8.41	7.82	7.63
2 Aug 94	49567.4	1	—	9.05	8.51	8.07	7.64
21 Aug 94	49586.4	1	—	9.34	8.67	8.14	7.70
7 Oct 94	49633.4	1	—	9.98	9.09	8.44	7.86
24 Feb 95	49772.6	2	9.94	10.54	9.56	—	—
18 Mar 95	49794.6	4	9.91	10.49	9.53	—	—
23 Aug 95	49953.4	1	—	9.70	9.08	8.39	7.89
29 Aug 95	49959.5	1	—	9.90	9.14	8.45	—
10 Sep 95	49971.3	2	9.16	10.01	9.28	—	—
12 Sep 95	49973.3	3	9.23	10.05	9.28	—	—
27 Sep 95	49988.4	2	9.40	10.11	9.30	—	—
2 Oct 95	49993.2	3	9.39	10.16	9.35	—	—
5 Oct 95	49996.4	3	9.44	10.19	9.38	—	—
21 Oct 95	50012.2	2	9.62	10.41	9.49	—	—
23 Oct 95	50014.3	2	—	10.44	9.44	8.64	8.10
24 Oct 95	50015.3	1	—	10.44	9.44	8.65	8.12
25 Oct 95	50016.3	4	—	10.47	9.46	8.66	8.11
2 Nov 95	50024.3	3	9.84	10.48	9.56	—	—
27 Nov 95	50049.3	2	10.16	10.62	9.59	—	—
11 Dec 95	50063.3	4	—	10.67	9.58	8.80	8.18
29 Jan 96	50112.3	1	—	10.72	9.56	8.81	8.14
27 Feb 96	50141.6	3	10.39	10.69	9.63	—	—

largely increased during the outbursts. The nebular emission appears also to contribute to the longer wavelengths, and the amplitude of the variation at different wavelengths can be used to determine the relative contribution of the nebular and cool star components. In this regard, it is of particular interest the fact that during the light maxima AG Dra largely varied also in the I-band (900 nm). This implies that at the light maximum the "nebular spectrum" should have contributed to at least 40% of the red/near-IR radiation of AG Dra. This contribution rises to more than 70% in V, and to more than $\sim$ 85% in B. We also argue that the contribution of the nebular emission to the red might possibly be not negligible also during the quiescent phase of

Table 4.3: Photometric observations of AG Dra in 1996 – 2000

JD-2450000	n	V	B	U	JD-2450000	n	V	B	U
267.3	3	9.24	10.12	9.15	739.2	5	9.65	10.78	10.46
268.3	3	9.26	10.14	9.21	741.2	2	9.71	10.83	10.60
293.6	2	9.48	10.46	9.73	742.2	3	9.69	10.83	10.58
294.6	3	9.43	10.37	9.60	828.7	2	9.79	11.18	11.57
295.4	3	9.41	10.35	9.47	865.7	3	9.71	11.10	11.43
296.4	3	9.38	10.32	9.45	866.6	3	9.71	11.09	11.43
297.3	3	9.41	10.31	9.42	867.6	4	9.73	11.10	11.42
303.4	2	9.34	10.27	9.36	877.6	3	9.72	11.09	11.40
317.3	3	9.48	10.50	9.47	1007.5	2	9.66	10.83	10.20
321.3	3	9.58	10.68	9.83	1015.4	3	9.62	10.68	10.02
322.3	3	9.60	10.68	9.84	1027.3	2	9.41	10.33	9.39
324.3	2	9.60	10.69	9.85	1087.2	2	9.64	10.76	10.18
390.2	2	9.77	11.05	11.08	1088.2	2	9.63	10.78	10.22
391.2	3	9.74	11.02	11.10	1226.6	3	9.75	11.15	11.40
398.2	3	9.69	10.98	11.06	1239.6	3	9.75	11.14	11.41
431.2	2	9.72	11.04	11.14	1293.4	3	9.82	11.22	11.51
466.3	2	9.72	11.01	—	1298.4	4	9.80	11.22	11.52
476.7	2	9.75	11.05	11.00	1332.4	3	9.79	11.19	11.53
477.7	2	9.76	11.04	11.00	1357.3	3	9.73	11.10	11.52
478.7	2	9.75	11.06	10.99	1401.3	3	9.70	11.09	11.46
504.6	3	9.72	11.01	10.96	1404.3	3	9.71	11.06	11.44
520.5	3	9.78	11.07	10.95	1408.3	2	9.72	11.10	11.47
628.5	3	9.17	9.99	8.96	1437.3	3	9.77	11.15	11.42
629.4	3	9.21	10.05	9.05	1509.2	1	9.71	11.10	11.34
643.5	2	9.14	10.00	8.92	1510.2	1	9.70	11.09	11.32
651.3	2	9.26	10.10	9.11	1581.6	3	9.76	11.12	11.11
652.3	2	9.25	10.08	9.07	1626.5	4	9.75	11.09	11.03
698.3	3	9.28	10.18	9.19	1627.5	4	9.74	11.09	11.01
699.3	4	9.32	10.18	9.25	1715.4	3	9.82	11.22	11.32
701.3	3	9.30	10.17	9.20	1716.5	2	9.83	11.24	11.34
702.3	3	9.28	10.17	9.19	1718.5	2	9.82	11.22	11.36
704.3	2	9.32	10.21	9.22	1721.4	3	9.83	11.24	11.38
729.2	3	9.64	10.70	10.17					

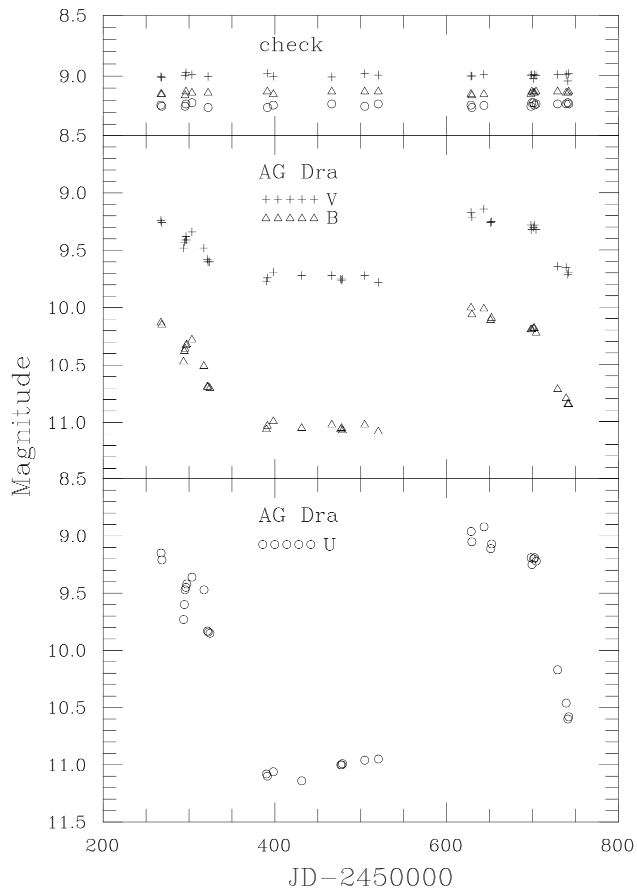

Figure 4.4: The UBV data of AG Dra during its 1996, 1997 outbursts

AG Dra. Therefore, some care should be taken when using the VRI colours (and the photospheric spectral line depth as well) for the determination of the red star's spectral type and luminosity class.

The three colour light curve of AG Dra during its 1996, 1997 outbursts is shown in Fig. 4.4. Our data cover mainly the declining phases and the quiescent period between the two outbursts. It can be noted the fact that the light monotonically increases in JD $\sim$ 2450290$\div$2450310, which is included in the first declining phase. The brightness of AG Dra varied in all the colours, but the amplitude of these variations was largest in U and decreased with the wavelength. In the time between the outbursts it reached the typical values of the quiescent state. The variation of the U magnitude indicates a mean increase for the two light maxima by a factor of about 5.3 of the continuum flux compared with the quiescent period before the 1994 outburst. The B and V increase factors are equal to 2.3 and 1.6. In our view the reason for

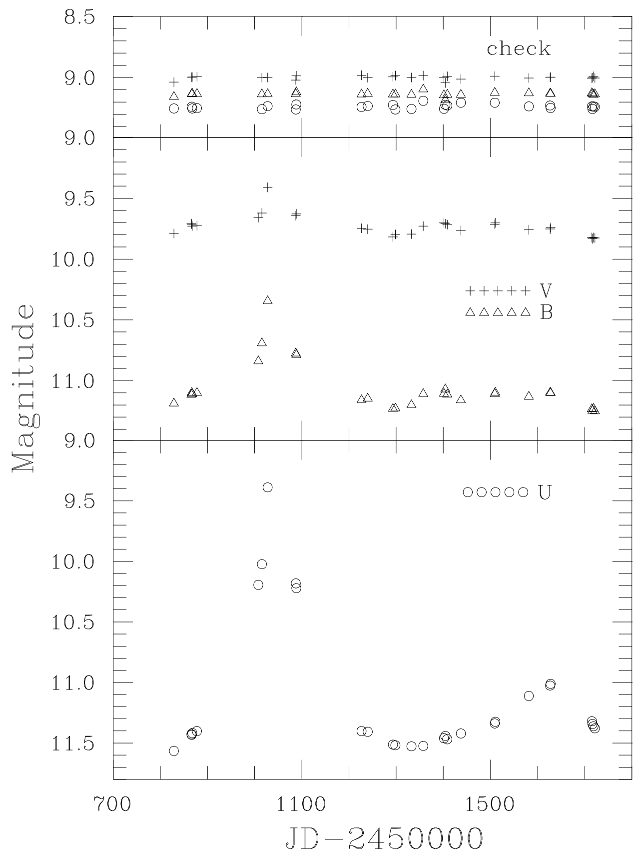

Figure 4.5: The UBV data of AG Dra during 1998 outburst

the visual brightening of AG Dra is the increased radiation of its nebula.

It is directly seen from the energy distribution of the star in the interval from IR to X-ray wavelengths, obtained during quiescence and outburst and displayed in the work of Greiner et al. (1997). According to these data the radiation of the hot component of the system in the visual U region is small compared with the observed magnitude. The spectrum in the optical/near-UV region is dominated by a nebular continuum which increases strongly during the outburst phase. That is why we conclude the growth of the UBV fluxes is determined by the increase of the size of the nebula, which from its side is due to the increased flux of Lyman photons from the outbursting hot companion. Then we can determine the lower limit of the contribution of the nebula for the maximal values of the B and V light on the basis of the approach used in the work of Montagni et al. (1996), using the amplitudes of the variation. It turns out this lower limit is about 55 % in B and 35 % in V.

Figure 4.5 gives the three-colour light curve of AG Dra during its 1998 outburst and after it. It is seen that the brightening of the star in 1998 is followed by a period of quiescence when the light in the B and V spectral regions reached its typical values during quiescent state. At that time the variations of the U light were probably determined by the orbital motion, since its smallest and greatest values are at the epochs of the orbital photometric minimum and maximum. Our data are not complete during the eruption, but they show that the light varied in all the colours and the amplitude of the variation was larger for the shorter wavelengths. The variation of the U magnitude indicates an increase by a factor of 4.8 of the light compared with the quiescent period before the 1994 – 1998 active phase. The B and V increase factors are 2.0 and 1.3.

4.3.3 Emission measure

The optical brightenings of AG Dra are caused by an increase in its nebular emission (Greiner et al. 1997) and in Sect. 4.6 we will consider the possibility to explain this behaviour. We will investigate the changes of the emission measure. Quantitative analysis of the emission measure can be carried out using the Balmer continuum emission, which can be derived from U-band photometric data. During the active phase a good sample of optical photometry (Fig. 4.6) was collected which gives us the possibility to calculate the emission measure at a number of typical epochs of variability of the light. We considered the emission measure at all epochs of maxima and minima of the light during 1994–1998 (Table 4.4). To compare these data with the quiescent ones we took the U fluxes of the circumbinary nebula at the orbital maximum and minimum $F^{\rm neb}_{\rm max} = 0.175 \times 10^{-12}$ erg cm^{-2} s^{-1} Å^{-1} and $F^{\rm neb}_{\rm min} = 0.040 \times 10^{-12}$ erg cm^{-2} s^{-1} Å^{-1}, obtained by Tomov et al. (2000).

The magnitudes were converted into continuum fluxes without correcting for the emission lines included in the wavelength region of the U photometric system as we were not provided with spectral data in this region. The fluxes were corrected for the energy distribution of AG Dra. The continuum of this star on the long wavelength-side of the Balmer jump is considerably weaker, which leads to a reduction of the flux at 3650 Å. The corrections were made as described in Sect. 4.2. The fluxes were also corrected for the interstellar reddening. Finally we obtained the U fluxes of the circumbinary nebula of AG Dra in its quiescent state subtracting the quiescent fluxes of the stellar components derived in Sect. 4.2. We made also approximate estimates of the fluxes of the hot component for the considered epochs of the active phase using the approach in the same section and data from the paper of Gonzalez-Riestra et al. (1999). These fluxes were also subtracted from the dereddened

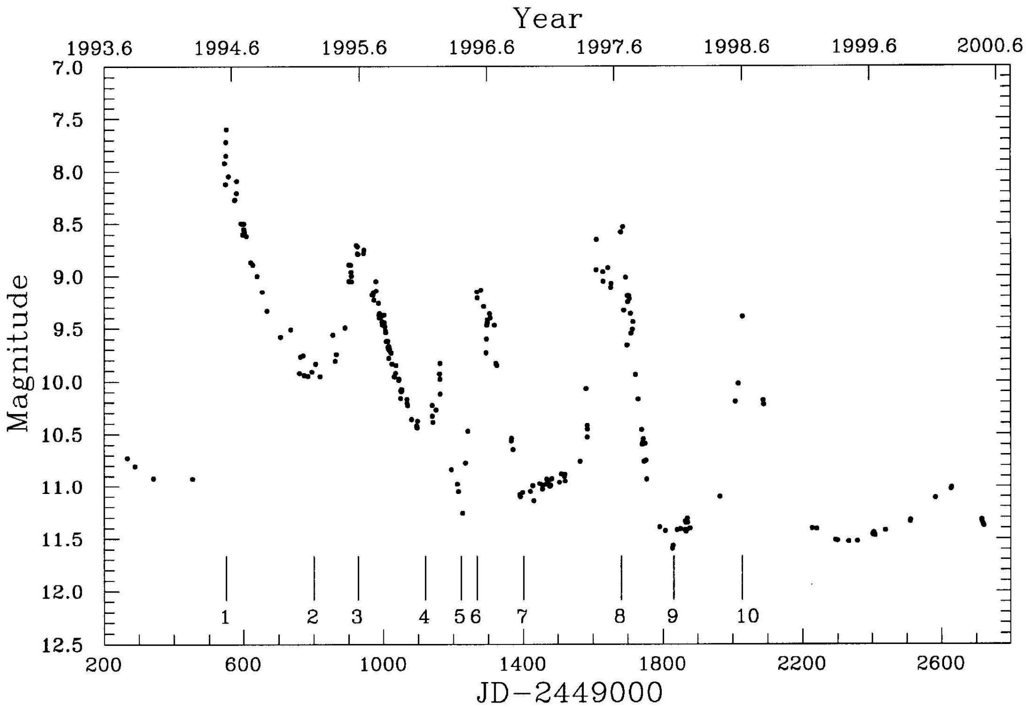

Figure 4.6: The U light curve of AG Dra during its active phase based on observations of (Skopal et al. 1995; Hric et al. 1996; Montagni et al. 1996; Skopal 1998; Petrik et al. 1998; Tomova & Tomov 1998; Tomov & Tomova 2000). The vertical lines indicate the local extrema under consideration, which are numbered from 1 to 10 and whose times are listed in Table 4.4.

fluxes of AG Dra.

To calculate the emission measure we need to know the state of ionization of helium. Mikolajewska et al. (1995) obtained an electron temperature for the nebula of AG Dra of about 15 000 K. In our calculations we assumed the same temperature in both the quiescent and the outburst states of the system. The helium ionization state in quiescence was determined in Sect. 4.2 by calculation of the ratio of the emission measures of the neutral and ionized helium. It was allowed that the lines of He^{o} are pure recombination lines since the same temperature of 15 000 K was adopted. A ratio He^{++}/He^{+} of about 0.5 was obtained, indicating that the singly ionized helium is dominant in the nebula.

During the 1994 – 1998 stage of activity we found data at the same epochs for some visual lines of He^{o} and the line He II 4686. These data were at orbital phases, close to the quiescent light maximum and were taken from the papers of Gonzalez-Riestra et al. (1999) and Tomova & Tomov (1999).

Only the flux of the narrow emission component of the line He II 4686 was used since its broad component indicates a high velocity stellar wind from the hot companion of the system (see Sect. 4.5). In this case we obtained a ratio He^{++}/He^{+} of about 0.4, which means that the singly ionized helium is dominant in the nebula during outburst too. Such a result was expected since the temperature of the companion was decreased. In our calculations we assumed that the nebular emission is mostly continuum emission of hydrogen and neutral helium. The quantities γ, related to the emission coefficients of these atoms and determined by recombinations and free-free transitions, were selected as explained in Sect. 4.2. A helium abundance of 0.1 (Vogel & Nussbaumer 1994) was also adopted.

The broad component of the He II 4686 line (Sect. 4.5) shows a region of high velocity stellar wind is present in the nebula of AG Dra during the active phase. The temperature of this region is probably higher than 15 000 K. Using the wind parameters and supposing an electron temperature of 20 000 K, we obtain the U continuum flux of this region to be 2.4×10^{-14} $\mathrm{erg\,cm^{-2}\,s^{-1}\,\AA^{-1}}$, which is negligible compared with the observed U flux (see below). Therefore the observed U flux is emitted practically by the rest of the ionized region(s) of the nebula and that is why we use the values of the emission coefficients of H and He II for an electron temperature of 15 000 K.

We adopted a distance of 1.7 kpc. So for the quiescent emission measures we derived $n_{\mathrm{e}}^2 V = 1.59 \times 10^{59} (\mathrm{d}/1.7\mathrm{kpc})^2\ \mathrm{cm}^{-3}$ at the orbital maximum and $n_{\mathrm{e}}^2 V = 0.36 \times 10^{59} (\mathrm{d}/1.7\mathrm{kpc})^2\ \mathrm{cm}^{-3}$ at the orbital minimum.

The results of the calculations of the data taken during the active phase are presented in Table 4.4. The observed U magnitude is listed in the fifth column, the flux of the nebula in the sixth column and its emission measure in the seventh column. The ratio m of the emission measure at some epoch during the active phase and the emission measure at the quiescent orbital maximum is listed in the eighth column. The data show that during the active phase the emission measure changes by factors from 0.5 to 36 compared to its maximal value at the quiescent state. The phase of the light minimum after the 1997 outburst is very close to the orbital minimum, but the emission measure is by a factor of about 2 greater than this one at the quiescent orbital minimum, indicating greater number of recombinating ions. In our opinion this is most probably a result of the increased loss of mass of the two stellar components during the outburst (see Sect. 4.6).

Table 4.4: The U flux and the emission measure of the circumbinary nebula.

No	Date	JD 2 449 000+	Phase	U mag	$F^{\mathrm{neb\,a}}$	EM^{b}	m
1	1994 Jul 16	550	0.736	7.60	6.319	57.56	36.2
2	1995 Mar 23	800	0.189	9.90	0.687	6.26	3.9
3	1995 Jul 22	921	0.408	8.70	2.249	20.49	12.9
4	1996 Feb 6	1120	0.768	10.40	0.406	3.70	2.3
5	1996 May 22	1226	0.960	11.26	0.139	1.27	0.8
6	1996 Jul 2	1267	0.034	9.15	1.455	13.26	8.3
7	1996 Nov 12	1400	0.275	11.10	0.175	1.59	1.0
8	1997 Aug 19	1680	0.782	8.55	2.595	23.64	14.9
9	1998 Jan 16	1830	0.054	11.56	0.086	0.78	0.5
10	1998 Aug 1	2027	0.410	9.39	1.148	10.45	6.6

[a] Continuum fluxes in units 10^{-12} erg cm^{-2} s^{-1} Å^{-1}.

[b] $EM = n_{\mathrm{e}}^2 V \times 10^{59} (\mathrm{d}/1.7\,\mathrm{kpc})^2$ cm^{-3}.

4.4 The line spectrum in quiescence and during the 1994 and 1995 outbursts

The line spectrum of AG Dra in quiescence and during its 1994 and 1995 brightenings was described and interpreted in the works of Tomov & Tomova (1997) and Tomova & Tomov (1999).

4.4.1 Observations and reduction

We acquired five photographic spectra in 1993 and 1995 with the Coudé spectrograph of the 2m RCC telescope of the National Astronomical Observatory Rozhen (Table 4.5). The observations were performed in the region from 3600 Å to 5000 Å, with a reciprocal linear dispersion of 18 Å mm^{-1}. The first two spectrograms were taken on Kodak IIaO emulsion sensitized with hydrogen with a resolution of 0.4 Å. The rest of the spectrograms are on ORWO ZU emulsion whose resolution is 0.5 Å. All exposures were comparatively deep but the continuum could be detected only in two cases when the star was the brightest and the atmospheric conditions were very good. The spectra were digitized with the Joyce Loeble microdensitometer and a ReWiA package was used for wavelength and density calibration, as well as

Table 4.5: List of the observations in the quiescent state of the system and during the 1994 – 1995 outbursts

Date	JD 2 449 000+	Phase	Detector; obs. region[a]	Exposure (minutes)	State of the system[b]
1993 Feb 6	024.51	0.785	CCD; H_α	60	Q
1993 Mar 16	062.51	0.854	Phot. IIaO	205	Q
1993 Apr 11	089.38	0.902	Phot. IIaO	255	Q
1994 Jan 2	354.59	0.383	CCD; H_α	2×20	Q
1994 Jan 24	376.60	0.422	CCD; H_α	30	Q
1994 Jan 24	376.64	0.422	CCD He II 4686	30	Q
1994 Feb 2	385.52	0.439	CCD; H_α	30	Q
1994 May 19	492.47	0.632	CCD; H_α	2×20	Q
1994 Jun 24	528.32	0.697	CCD; H_α	2×20	A
1994 Jun 24	528.38	0.697	CCD; H_β	20	A
1994 Jun 25	529.35	0.699	CCD; λ 4500 Å	10+20	A
1994 Jun 25	529.45	0.699	CCD; H_γ	10+20	A
1994 Aug 17	582.27	0.795	CCD; H_α	20	A
1994 Aug 17	582.29	0.795	CCD; H_β	20	A
1994 Aug 17	582.32	0.795	CCD; λ 4500 Å	2×20	A
1994 Aug 17	582.35	0.795	CCD; H_γ	20	A
1995 Oct 3	994.42	0.541	Phot. ZU	272	A
1995 Oct 4	995.36	0.543	Phot. ZU	360	A
1995 Nov 2	1024.33	0.595	Phot. ZU	345	A

[a] All photographic observations were made in the region λ 3600÷5000 Å.

[b] Q = quiescent, A = active

for calculation of the radial velocities and the equivalent widths. Sections of the spectrum taken on JD 2 449 995.36 where the fainter line features are most clearly seen are displayed in Fig. 4.7. The lines with measured radial velocities are marked. At this time the star was in a declining phase following the secondary (July 1995) light maximum. The strongest lines are not seen in this figure, but the upper part of their profiles is similar to those in Fig. 4.11.

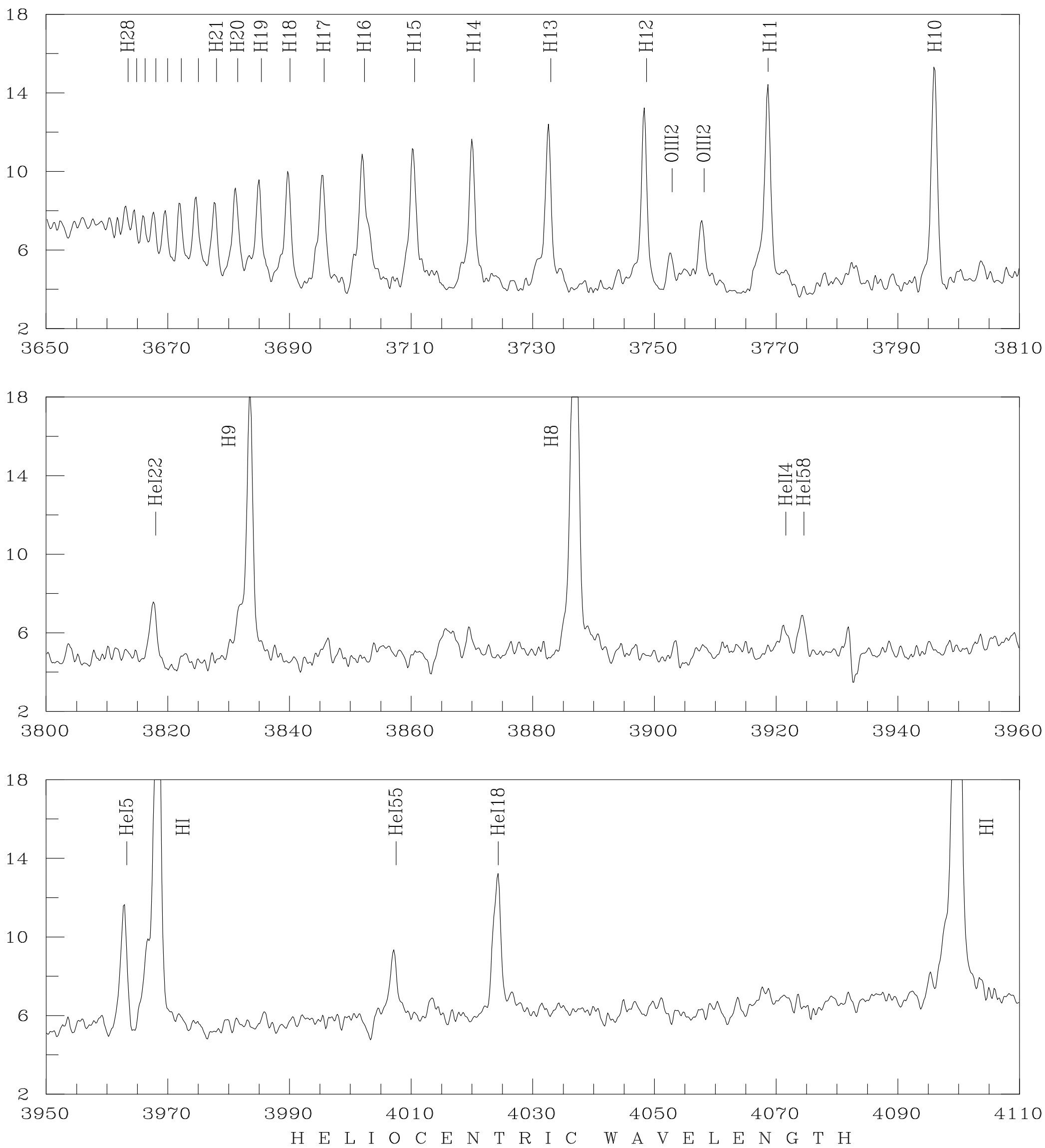

Figure 4.7: Sections of the spectrum, taken on JD 2 449 995.36. The ordinate scale is in arbitrary units.

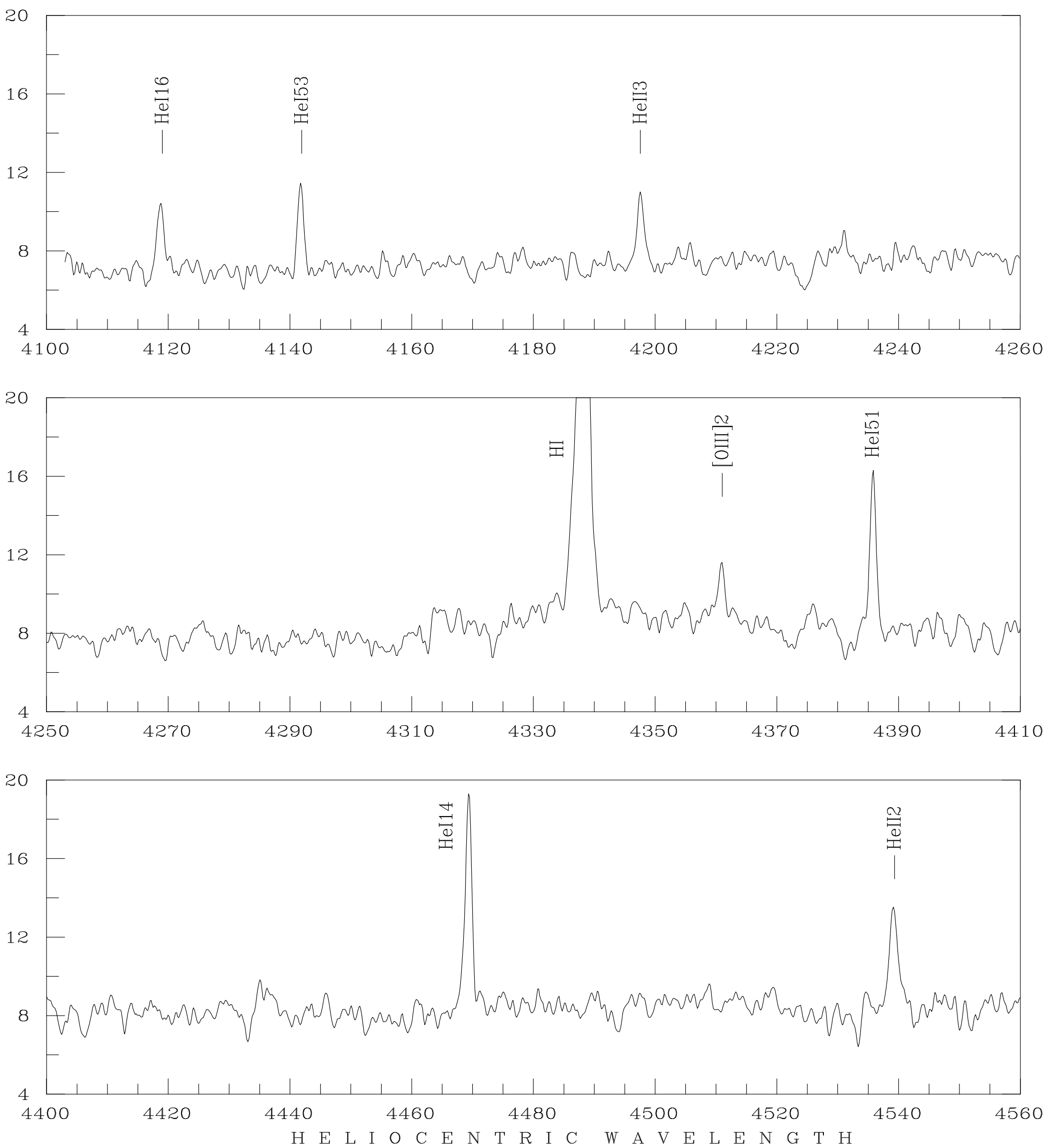

Figure 4.7: *continued*

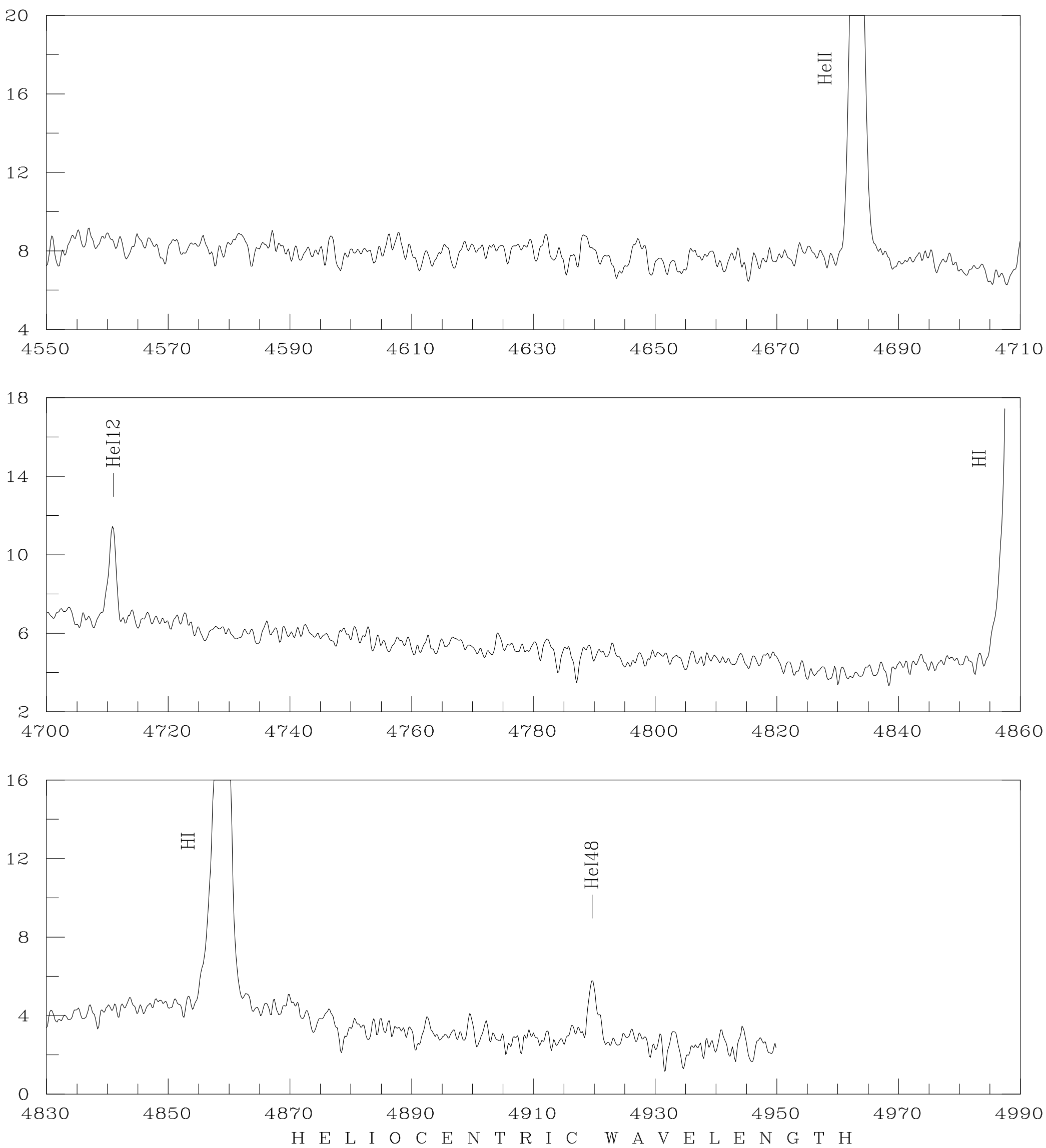

Figure 4.7: *continued*

Table 4.6: Radial velocity data in units of $\mathrm{km\,s^{-1}}$

JD 2 449 000+	Phase	H I All lines	H I H_α (core)	He^1 I	He^3 I	He II	O III	[O III] 4363	Abs. lines	State of the system[a]
024.51	0.785	−146.69	−106.45						−150.39 ±0.08	Q
062.51	0.854	−146.73 ±3.16		−144.30 ±1.88	−138.29 ±3.59	−144.51 ±1.56				Q
089.38	0.902	−149.07 ±1.45		−166.64 ±1.20	−145.09 ±1.48	−150.72 ±1.76				Q
354.59	0.383	−137.18	−98.75						−141.12 ±0.44	Q
376.6	0.422	−128.08	−86.81			−140.18			−138.62 ±0.50	Q
385.52	0.439	−137.18	−99.77						−144.79 ±0.50	Q
492.47	0.632	−146.28	−111.12						−152.71 ±0.52	Q
528.3	0.697	−151.14 ±4.13	−125.98						−153.00 ±0.97	A
529.4	0.699	−214.73		−188.22	−191.51	−169.32				A
582.3	0.795	−149.01 ±8.27	−110.23	−162.80	−176.27	−165.60			−151.25 ±0.95	A
994.42	0.541	−140.68 ±1.18		−150.52 ±2.68	−149.56 ±0.30	−156.68 ±0.25	−162.67	−174.01		A
995.36	0.543	−145.73 ±1.08		−149.61 ±3.77	−146.78 ±3.10	−160.40 ±1.59	−169.22 ±2.14	−157.64		A
1024.33	0.595	−137.69 ±0.33			−144.38 ±9.09	−149.00				A

[a] Q = quiescent, A = active

In our work we consider the intensity of the relatively strong lines whose equivalent width errors are not greater than 30%. Unfortunately it turned out that the spectrogram of JD 2 449 995.36 has had decreased sensitivity of its photographic emulsion in the wavelength region $\lambda > 4470$ Å and that is why the intensities only of these lines whose wavelengths are less than this limit were investigated. Among the other spectrograms only that of JD 2 449 994.42 was used for the intensity investigation, as the continuum in the other cases was not well detected. The error of the level of the local continuum for both of these spectrograms was not greater than 10%. The line fluxes were obtained by means of the B and V photometric estimates of Montagni et al. (1996) taken during this time. The monochromatic continuum fluxes at the positions of the emission lines considered were calculated via linear interpolation of the fluxes at the positions of the sensitivity maxima of the B and V photometric systems.

In addition some CCD frames were obtained with the same spectrograph mainly in the period January – August 1994. The H_α region was observed on almost all nights. The regions of the H_β, H_γ and He II 4686 and a region centered at 4500 Å and containing the He I 4471 and He II 4542 lines were observed on a few occasions. The spectral range of 110 Å gave us the possibility of observing the [O III] 4363 and He I 4388 lines together with H_γ. The resolving power was generally 15 000, and only for the spectra taken on JD 2 449 024.51 and JD 2 449 376.64 it was 30 000 (Table 4.5). The data were processed with the *pcIPS* program of Smirnov et al. (1992). As in the case of the photographic spectra, the ReWiA package was used for obtaining the dispersion curve and for calculating the radial velocities and the equivalent widths. Some absorption lines of the K star spectrum in the H_α region were used for measuring the radial velocity of the cool component (Table 4.6).

The line fluxes were obtained by means of the B, V and R photometric data of Hric et al. (1994); Skopal et al. (1995); Skopal (1996) and Montagni et al. (1996). Since there are no R data during the time when the initial five of our H_α spectra were obtained while the system was at the quiescent stage, we used the data of Montagni et al. (1996) taken at the end of 1995 and the beginning of 1996, when the visual light of the system had practically reached its value before the 1994 outburst (Mattei 1995). The H_α flux on August 17 was also obtained using the R photometry of Montagni et al. (1996). The spectrum on June 24 was taken during the time of increasing light, when R data are also absent in the literature, and only the equivalent width was obtained for this time.

The line fluxes were corrected for interstellar reddening. We used the value $E(B-V) = 0.06$ (Mikolajewska et al. 1995; Greiner et al. 1997) and the extinction law by Seaton (1979).

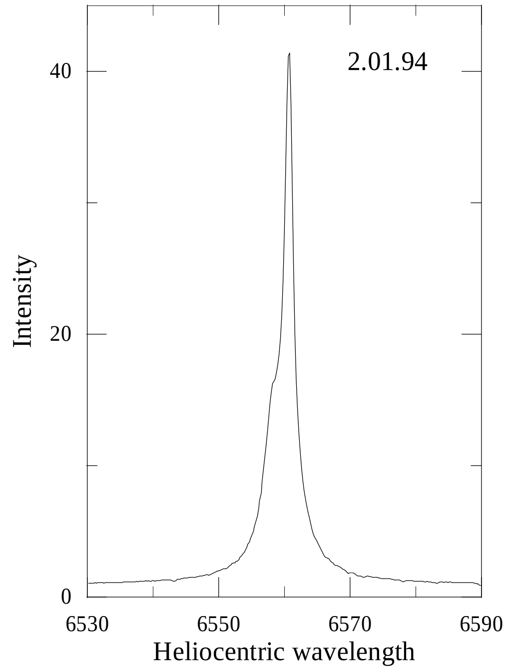

Figure 4.8: H_α profile of AG Dra normalized with respect to the local continuum.

Since we did not find systematic differences between the velocities of the lines of a given element in our observational data, the velocities of all elements have been obtained as arithmetical means of the velocities of all lines detected. The radial velocity data are listed in Table 4.6 and the line fluxes in Tables 4.7, 4.8 and 4.9.

4.4.2 Description and analysis of the emission line spectrum

Balmer lines

H_α line

In our spectra the H_α profile is single-peaked, with a shoulder on the short wavelengths-side at all phases (Fig. 4.8). In some cases this shoulder is highly pronounced and in the rest of them, where scarcely visible, it produces a general asymmetry only. In contrast to some other symbiotic systems like EG And and AG Peg (Oliversen & Anderson 1982; Oliversen et al. 1985; Boyarchuk et al. 1987) the H_α line of AG Dra during the period of our observations had unusually extended low intensity wings which practically

Table 4.7: Equivalent widths and fluxes of H_α

JD 2 449 000+	Phase	W_λ (Å)	$F\times10^{-12}$ $\mathrm{erg\,cm^{-2}\,s^{-1}}$	State of the system[a]
024.51	0.785	84	50.84	Q
354.59	0.383	174	106.04	Q
376.60	0.422	184	112.12	Q
385.52	0.439	159	96.86	Q
492.47	0.632	117	71.27	Q
528.32	0.697	98		A
582.27	0.795	104	130.94	A

[a] Q = quiescent, A = active

Table 4.8: Fluxes of the lines displaying two components – a narrow (N) and a broad (B) one in units of 10^{-12} $\mathrm{erg\,cm^{-2}\,s^{-1}}$

JD	Phase	H_β	H_γ		He II 4686	State of
2 449 000+		N	N	B	N	the system[a]
376.64	0.422				11.00	Q
528.38	0.697	44.56				A
529.45	0.699		37.54			A
582.32	0.795	31.92	18.13			A
994.42	0.541	33.08	10.08		17.50	A
995.36	0.543		7.51	2.38		A

[a] Q = quiescent, A = active

Table 4.9: Fluxes of one component lines during the active phase in units of 10^{-12} $\mathrm{erg\,cm^{-2}\,s^{-1}}$

JD 2 449 000+	Phase	He I 3965	He I 4009	He I 4026	$H\delta$ 4102	He I 4121	He I 4144	He II 4200	[O III] 4363	He I 4388	He I 4471	He II 4542	He I 4713
529.4	0.699									4.66	3.97	3.19	
582.3	0.795									2.24	2.56	0.92	
994.42	0.541	0.95	0.58	1.32	7.36	0.53	0.75	0.46	0.33	1.14	1.25	0.63	0.76
995.36	0.543	0.97	0.51	1.25	7.32	0.49	0.52	0.43	0.38	0.82	1.20		

reached the continuum level at about 2000 $km\,s^{-1}$ from the center of the line. It should be emphasized that the asymmetry was related to the upper part of the profile and the wings were always symmetrical.

Robinson et al. (1994) investigated double-peaked profiles of AG Dra and found an acceptable fit for an accretion disk with inner radius of 1.1×10^8 cm and outer radius of 1.3×10^{10} cm. If we suppose the existence of a disk having such a small size, it would have appeared most probably as a result of accretion of a stellar wind. But in this case, the wind of the giant will give rise to a circumbinary nebula, as well as the accretion disk. This nebula will also contribute to the emission lines, which will not due to the accretion disk alone.

The initial five of our H_α spectra (Table 4.5) are related to the quiescent stage and the spectra of June and August 1994 were taken immediately before and after the moment of the first light maximum (July 1994), when the V light increased by more than one magnitude (Skopal & Chochol 1994; Montagni et al. 1996). The width (FWHM) of the line was 90–100 $km\,s^{-1}$ during the quiescent stage and the shoulder was below the level of the half maximum. The intensity of the wings varied during this period (Fig. 4.9), which led us to suppose that different numbers of emitting hydrogen atoms were observed at different phases. The variation in the number of emitting atoms could be due to an occultation of a bright region around the hot component of the system, as was supposed by Mikolajewska et al. (1995).

The fact that the wings are symmetrical and the features leading to an asymmetry are located in the upper part of the profile give reason to suppose these features are a sign of self-absorption. Similar features are present in the H_α profile of the AG Peg system where they signal the same process. Our supposition is based also on the established fact that in both systems AG Peg (Boyarchuk 1967a) and AG Dra (Boyarchuk 1967b) the Balmer decrement differs greatly from the theoretical one because of self-absorption. In the final analysis we consider the profile variations are due to two factors during the period of our observations. The first of them is a variation in the emitting-atom number. It determines the intensity of the wings and is probably due to an occultation of the emitting region. The second one is a variation of the optical depth, which causes the changes of the upper part of the profile and is related to the orbital motion, too.

During the outburst the appearance of the profile remained the same, but the shoulder was above the level of the half maximum. The width of the line increased to about 150 $km\,s^{-1}$. The intensity of the wings also increased considerably (Fig. 4.9).

The behaviour of the flux at the phases of observation is displayed in Fig. 4.10. It decreased by a factor of 2.2 in the phase interval of 0.4. The

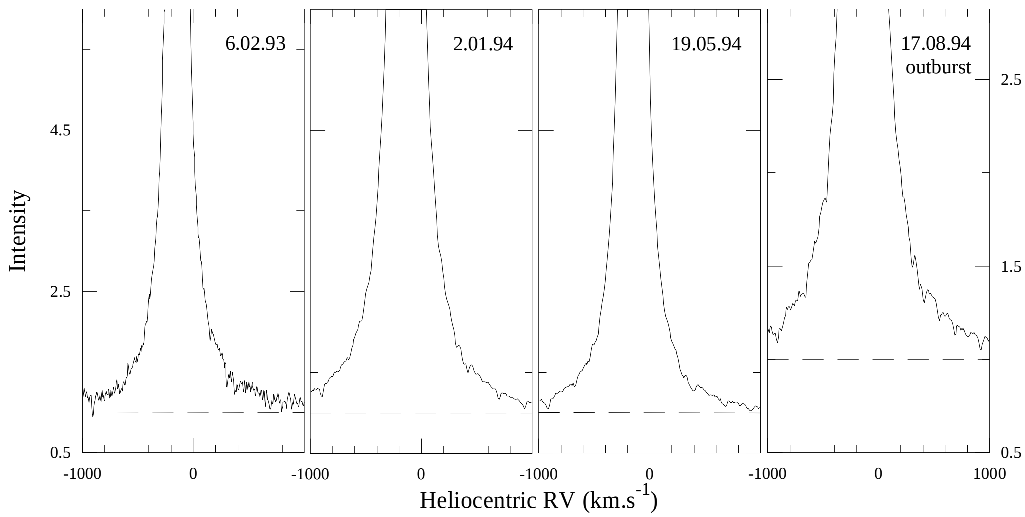

Figure 4.9: Variations of the wings intensity of the H_α line during quiescence and outburst. For a direct comparison of the intensities the ratio of the ordinate scales has been chosen to be equal to the ratio of the continuum fluxes at the position of H_α .

spectra taken on JD 2 449 024.51 and JD 2 449 582.27 are approximately at the same phase, one coming from the quiescent stage and the other from the outburst. Comparison of the fluxes in those moments indicates an increase by a factor of 2.5.

The wavelength position of H_α was measured at two places on its profile – in the upper part of the core of the line, where it is practically symmetrical, and in wing area. The radial velocity data of the core are scattered (Fig. 4.10), which is easily explained by assuming that this part of the line is influenced by self-absorption. The behaviour of the velocity of the wings is different and is identical to that of the other Balmer lines within the range of error. It turned out this velocity is very close to that of the mass center of the system at most phases of observation.

Table 4.6 shows that the lines of H I on JD 2 449 529.40 have a large negative radial velocity, which differs from the rest of the velocities, but is close to those of the lines of the other elements at this particular time. In our opinion the values of these velocities are not due to random error and seems to be emission observed from an area of the nebula whose movement is towards the observer, caused probably by an expanding envelope.

Let us compare our continuum emission measure with those calculated using our H_α data and assuming Menzel case B. At phases close to the photo-

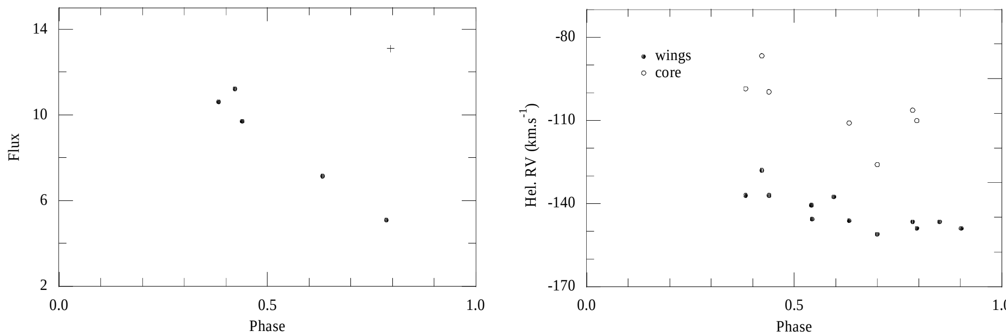

Figure 4.10: *Left:* H_α flux in units of 10^{-11} erg cm^{-2} s^{-1} as a function of phase. The flux during the outburst is marked with a cross. *Right:* Balmer radial velocities as a function of phase. The value of -214.73 km s^{-1} (Table 4.6) is not displayed in the figure.

metric maximum during quiescence, the values of the H_α flux produce values of the emission measure in the interval from 1.1×10^{59}(d/1.7kpc)^2 cm^{-3} to 1.2×10^{59}(d/1.7kpc)^2 cm^{-3}. The emission measure of the nebula increased during the outburst phase, as is seen from its quantity of $n_e^2 V = 1.4 \times 10^{59}$(d/1.7kpc)^2 cm^{-3}, determined by the H_α flux obtained on JD 2 449 582.27. These values were calculated with an effective recombination coefficient corresponding to an electron temperature of 15 000 K (Pottasch 1984).

Other hydrogen lines

On the spectra taken in 1993 when the AG Dra system was at the quiescent stage, the lines of Balmer series were visible as far as H 13, but the absence of those having higher numbers was probably due to the low density of the spectrograms. The profiles of many lines had asymmetry. Using a CCD camera in June and August 1994 we were only able to observe the lines H_β and H_γ (Fig. 4.11). All of these data revealed single peaked profiles of the Balmer members, i.e. they were ordinary nebular lines. On JD 2 449 529 the widths of H_β and H_γ were about 170 km s^{-1} and on JD 2 449 582 about 125 km s^{-1}. In October 1995, when the light of the star was decreasing after its second maximum (July 1995), the lines of Balmer series were visible as far as H 30 (Fig. 4.7). The profiles of H_β and H_γ consisted of two components: a central narrow component with width (FWHM) equal to about 100 km s^{-1} and a broad component, whose width was much greater (Fig. 4.11). The rest of the Balmer members had one component profile, which in most cases had asymmetry. Their width was approximately the same. The line H 8 is badly blended with the line He I 3889 and is inappropriate for investigation. The

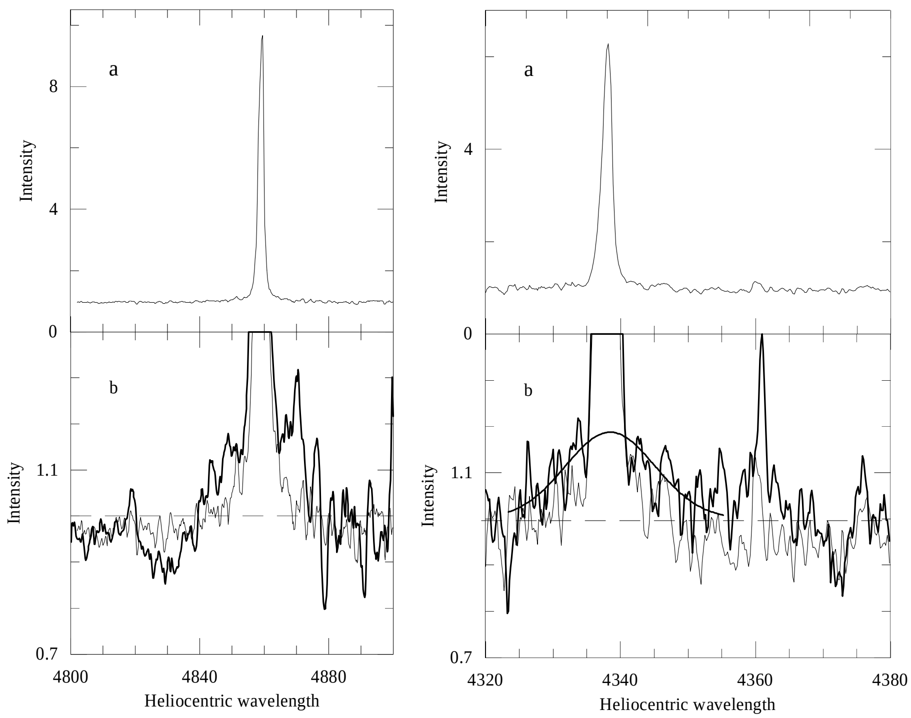

Figure 4.11: **a** The profile of H_β (left) and H_γ (right), based on photographic data on JD 2 449 995.36. **b** The area of the wings of these lines, compared with the case when a broad component is present (the thick line). The level of the local continuum is marked with a dashed line. The line [O III] 4363 is seen as well.

line $H\epsilon$ was also not investigated because of blending, most probably with the corresponding Pickering line and the H line of Ca II. Unfortunately it was not possible in this time to observe the line H_α, which in the other cases always had only one component. The line fluxes of H_β and H_γ are listed in Table 4.8.

The profile of the broad component of H_γ observed on JD 2 449 995.36 is displayed in Fig. 4.11, while the profile of H_β was not analysed because of the decreased sensitivity of the spectrogram in its region (see Sect. 4.4.1). Moreover we could not investigate the broad components of these lines using the spectrogram of JD 2 449 994.42 because of its higher noise. The error of the local continuum in the H_γ region of the spectrum taken on JD 2 449 995.36 is not greater than $\pm 5\%$. The observed spectrum in the region of the broad component was corrected through removing some weak emission lines of O II as well as the strongest absorption lines of the giant. Then it was analysed by fitting with a Gaussian function and its FWHM turned out to be equal to 1080±330 $\mathrm{km\,s^{-1}}$.This procedure allows us to obtain its equivalent width and the line flux with an error of about 60%, explained first of all by the error of the local continuum. In this way we consider the FWZI of the line to be determined from that distance from its center where the fit reaches the level of the noise – 780 $\mathrm{km\,s^{-1}}$. Taking into account the error of the local continuum again, we are inclined to increase this value to 800 $\mathrm{km\,s^{-1}}$.

There are different mechanisms of emission line broadening and one of them is the electron (Thomson) scattering. Let us consider the possibility that the broad components of the lines H_β and H_γ are determined by electron scattering. The H_γ total flux, which is a sum of the fluxes of the two components, is equal to 9.89×10^{-12} $\mathrm{erg\,cm^{-2}\,s^{-1}}$. With the parameters of the nebula adopted by us in Sect. 3.3 this yields an emission measure of $n_\mathrm{e}^2 V = 6.5 \times 10^{58} (\mathrm{d}/1.7\,\mathrm{kpc})^2$ $\mathrm{cm^{-3}}$. Assuming a constant electron density of 10^{10} $\mathrm{cm^{-3}}$ (Mikolajewska et al. 1995) we obtain a radius of 5.4×10^{12} cm of the spherical volume with this emission measure. If the broad component was produced by Thomson scattering it would appear in a region with an optical thickness of about 0.3. Using this optical thickness and an electron density of 10^{10} $\mathrm{cm^{-3}}$, we obtain 4.5×10^{13} cm for the radius of this region, which corresponds to an enormous emission measure of 3.8×10^{61} $\mathrm{cm^{-3}}$. Since this result is in disagreement with the previous one, we conclude that the broad component is probably not produced only by Thomson scattering. Thomson scattering, though, should have contribution in the broad component during phase of activity (see below). Another possible interpretation of this component will be given in Sect. 3.

Helium lines

During the time of our observations the lines of He I had one component profile (Fig. 4.7). In June and August 1994 using a CCD camera we observed only the lines with wavelengths $\lambda\lambda$ 4388 Å and 4471 Å. On JD 2 449 529.40 they were fairly broad and their widths were equal to 96 $\mathrm{km\,s^{-1}}$ and 130 $\mathrm{km\,s^{-1}}$. On JD 2 449 582.33 the widths were 74 $\mathrm{km\,s^{-1}}$ and 96 $\mathrm{km\,s^{-1}}$ respectively. In the beginning of October 1995 the arithmetical mean value of the singlets widths was about 85 $\mathrm{km\,s^{-1}}$ and of the triplets about 90 $\mathrm{km\,s^{-1}}$.

The fluxes of all of the helium lines observed by us are listed in Table 4.9. It is seen that those of He I 4388 and He I 4471 have decreased by a factor of about 2 during the period JD 2 449 529 – 2 449 582.

The radial velocity data of each group of the helium lines, both singlets and triplets, are listed in Table 4.6. The radial velocities are close to the velocity of the mass center of the system at most phases of observation.

Lines of elements of high degree of ionization

Only the lines of the elements He II and O III are included in this group, which are present in the spectrum of the star in both its quiescent and active phases.

The observation in the quiescent phase (see Table 4.5) revealed a single-peaked profile of the line He II 4686. Its width was equal to about 65 $\mathrm{km\,s^{-1}}$. Unfortunately it was missed in our observations during the 1994 outburst. In October 1995 a broad component was observed in the profile of this line, as for H_β and H_γ but more uncertainly. At this time its width was 115 $\mathrm{km\,s^{-1}}$. Data of the flux of the He II 4686 line are listed in Table 4.8. It increased by a factor of 1.6.

The spectrum on JD 2 449 376.64 is at phase 0.422, which is close to the maximal light phase. Then we can compare the emission measure derived from the He II 4686 line with this one of hydrogen based on Balmer continuum emission. The quiescent hydrogen emission measure is $n_\mathrm{e}^2V = 1.59\,10^{59}(\mathrm{d}/1.7\,\mathrm{kpc})^2\ \mathrm{cm}^{-3}$ at the phase of the photometric maximum. The photometric data of Montagni et al. (1996) on JD 2 449 994.42 provide a value of $n_\mathrm{e}^2V = 6.5 \times 10^{59}(\mathrm{d}/1.7\,\mathrm{kpc})^2\ \mathrm{cm}^{-3}$. The flux data of the He II 4686 line in Table 4.8 indicate $n_\mathrm{e}^2V = 2.9 \times 10^{58}(\mathrm{d}/1.7\,\mathrm{kpc})^2\ \mathrm{cm}^{-3}$ and $n_\mathrm{e}^2V = 4.6 \times 10^{58}(\mathrm{d}/1.7\,\mathrm{kpc})^2\ \mathrm{cm}^{-3}$ for He/H = 0.1. The comparison shows that the helium emission measure is in better agreement with the hydrogen one during outburst, as their ratio in this case is 0.07. In quiescence this ratio is 0.18.

Besides the line with wavelength $\lambda\lambda$ 4686 Å, the Pickering He II lines are also present in the emission spectrum of AG Dra (Fig. 4.7). We took data only for the lines with wavelengths $\lambda\lambda$ 4200 and 4542 Å of this series, as the rest of them are badly blended with Balmer lines. During the 1994 outburst we observed only the line He II 4542 with the CCD camera. On JD 2 449 529.35 its width was fairly broad of about 140 $\mathrm{km\,s^{-1}}$. After this time it decreased to 100 $\mathrm{km\,s^{-1}}$ on JD 2 449 582.32. In the beginning of October 1995 the width of this line was the same. Its flux decreased by a factor of 3.5 during the period JD 2 449 529 – 2 449 582 (Table 4.9).

All lines of He II investigated by us had the same velocities within the range of the error, which were close to the barycentric velocity at most of the observation phases (Table 4.6).

The lines of O III with wavelengths $\lambda\lambda$ 3755 Å and 3760 Å were so weak that their radial velocities could be measured only on the spectra taken in October 1995 (Table 4.6).

Forbidden lines

Among the visual forbidden lines we observed only [O III] 4363, which is present in the spectrum of AG Dra only during the outburst phase. In 1994 it was scarcely visible, so that radial velocity and flux data for it could be obtained using only the spectrograms taken in October 1995 (Tables 4.6 and 4.9). At that time it had a symmetric profile, and, like the other lines, its width was also appreciable – 80 $\mathrm{km\,s^{-1}}$.

4.4.3 Broad components and mass-loss rate

Emission lines similar to the broad components of the H_β, H_γ and He II 4686 lines can be radiated by a small accretion disk around the compact object, rotating with Keplerian velocity. Let us consider this possibility. For the radius of the secondary component we adopt a value of 0.10 $R_\odot$ (see below). The mass of this component is assumed by Mikolajewska et al. (1995) to be about 0.6 $M_\odot$ and by Greiner et al. (1997) to be no more than 0.6 $M_\odot$. We will perform our calculation for masses 0.3 – 0.6 $M_\odot$ (Gonzalez-Riestra et al. 1999). Using these data a Keplerian velocity of 760 – 1070 $\mathrm{km\,s^{-1}}$ is obtained. This velocity is comparable to the velocity of 800 $\mathrm{km\,s^{-1}}$, which corresponds to the HWZI of the broad component of H_γ and is related to a small disk located close to the hot secondary. Then our supposition for a disc origin of this component can not be thus rejected.

Another possibility is the broad component of the lines H_β, H_γ and He II 4686 to be emitted by a high-velocity stellar wind. According to Gonzalez-Riestra et al. (1999) the hot compact object in the AG Dra system expands during active phases and in this case we can expect the mass outflow to emit in spectral lines. Moreover the broad components are very similar to the components of the same lines of AG Peg which are emitted by high-velocity wind (Hutchings & Redman 1972; Ilmas 1987; Tomov et al. 1998). Then we should accept all three possibilities – notably that a scattering by free electrons as well as emission of Keplerian accretion disc and optically thin stellar wind give rise to a broad component.

From the flux of the broad component of H_γ we determined the upper limit of the mass-loss rate of the hot secondary during the 1995 outburst using one of the two methods described by Vogel (1993) and Vogel & Nussbaumer (1994). This method is based on the relation between the energy emitted in the He II 1640 line and the mass-loss rate when the wind has spherical symmetry and a constant velocity. The line is assumed to be dominated by recombination and to be optically thin. We performed our calculations assuming the broad component of H_γ to be an optically thin line. The particle density is a function of the distance to the center and is expressed via the continuity equation. In the last section the wind velocity was obtained to be 800 $\mathrm{km\,s^{-1}}$. The electron temperature was adopted to be $T_{\mathrm{e}} = 20\,000$ K and the state of helium ionization was supposed to be He III. We used a recombination coefficient of 1.233×10^{-14} $\mathrm{cm^3\,s}$ for case B, corresponding to this temperature and a density of 10^{13} $\mathrm{cm^{-3}}$ (Storey & Hummer 1995) and a parameter μ of 1.4 (Nussbaumer & Vogel 1987), determining the mean molecular weight μm_{H} in the hot wind. As the line flux is considered to be emitted by a spherical region, the radii of integration must be determined. Since we treat the wind in the nebular approach, the inner radius is thought to be the radius of the star. We used the value of this parameter based on the analysis of Greiner et al. (1997). An appearance of a stellar wind from the compact object is considered by these authors to be possible when its photosphere has expanded as a result of the increasing accretion rate. In this case the radius is assumed to be about 0.14 $\mathrm{R_\odot}$ at a distance to the system of 2.5 kpc. Since we used a distance of 1.7 kpc the radius was reduced to 0.10 $\mathrm{R_\odot}$. Let now determine the outer radius of integration. The numerical calculations of the evolution of the nebular environment in symbiotic systems (Nussbaumer & Walder 1993) show that six months after the appearance of the wind of the hot secondary its region has a size comparable with the binary separation. We could not determine this region during the last active phase of AG Dra as the variation of the mass-loss rate of its cool giant is not known. On the other hand it is easy to show that regions of high velocity wind far from its base have a negligible contribution. Thus, we will use an outer radius of integration equal to half of the binary separation, 166 $\mathrm{R_\odot}$. We obtain mass-loss rate of less than $0.97 \times 10^{-7}\,(\mathrm{d}/1.7\,\mathrm{kpc})^{3/2}$ $\mathrm{M_\odot\,yr^{-1}}$.

The secondary component of the AG Dra system is a hot compact star and the radiation in its atmosphere could be considerably influenced by electron scattering, which can be assessed by calculating the optical thickness of the hot wind for electron scattering. When the wind has spherical symmetry and a constant velocity, the optical thickness can be analytically integrated over the r^{-2} density distribution from the radius of the star to infinity, using the velocity of the wind and the mass-loss rate. The optical thickness obtained is about 0.5. Then the electron scattering affects the radiation of the hot component's atmosphere which means that the wind lines will also be broadened. This leads to overestimating the wind velocity from the line width at the level of the local continuum, so that the value of 800 $\mathrm{km\,s^{-1}}$, obtained by us, can be considered as an upper limit.

4.4.4 Discussion

Our study showed that the hot component of the AG Dra system does not produce a wind permanently, but only at times, most probably in its active periods. The cool component of this system is a late-type giant (Smith et al. 1996) with a stellar wind. Then during the period of this hot wind, the two winds should collide head-on as presented in the simplified approximation by Girard & Willson (1987). Supposing their collision region to have zero thickness, the location of the shock zone can be determined from the condition for equality of local momenta, which is $\dot{M}_{\rm hot}v_{\rm hot}/\dot{M}_{\rm cool}v_{\rm cool} = r^2_{\rm hot}/r^2_{\rm cool}$ on the line joining the two stars. The quantities $r_{\rm hot}$ and $r_{\rm cool}$ are the distances from the two components. The wind parameters of the hot companion are presented in the last subsection. For the mass-loss rate of the cool component we obtained a mean value of 2.2×10^{-7} $\rm M_\odot\,yr^{-1}$. We adopted a velocity of its wind of 30 $\rm km\,s^{-1}$ according to Mikolajewska et al. (1995). Using the orbital period of Skopal (1994) and a total mass of the system of 1.5 $\rm M_\odot$, based on our estimates of the masses of the components in the last section, and the estimates of Mikolajewska et al. (1995) and Schmid & Schild (1997) as well, for the separation we obtain 324 $\rm R_\odot$. Then the distance between the center of the giant and the collision region is derived to be 73 $\rm R_\odot$ i.e. the collision region is located very close to the giant.

The total kinetic energy of the winds is thus 5 $\rm L_\odot$, providing an order of magnitude estimate for the X-ray luminosity of the collision region.

Accretion is realized during the multiple quiescent periods of the AG Dra system. The wind of its hot component, observed by us during the 1995 outburst, has probably existed up to the time when its momentum has decreased to some lower limit being no longer able to prevent accretion. (Our unpublished spectral data of April 1996 do not show a presence of broad emission components.) If we suppose the wind velocity has been invariable, follow Zamanov's approach (1993) and adopting a circular orbit (Mikolajewska et al. 1995), we will obtain the next result: when the mass-loss rate of the hot component decreases to about 2×10^{-9} $\rm M_\odot\,yr^{-1}$, the accretion regime will be restored. In this case it would be useful to roughly evaluate the total mass lost by this component. We know neither the duration of the hot wind with good accuracy nor its possible variations. If we suppose that the hot component had a mass-loss rate of $0.97\times10^{-7}(\rm d/1.7\,kpc)^{3/2}$ $\rm M_\odot\,yr^{-1}$ for a typical time of about $100^{\rm d}\div\,200^{\rm d}$, the total mass lost amounts to about $2.6\times10^{-8}\div5.3\times10^{-8}$ $\rm M_\odot$.

4.5 The line spectrum during the 1996 and 1997 outbursts

The line spectrum of AG Dra during its 1996 and 1997 brightenings was described and discussed in the work of Tomov & Tomova (2002).

4.5.1 Observations and reduction

Nineteen CCD frames were acquired on sixteen nights during 1996 and 1997 with the Coudé spectrograph of the 2-m RCC telescope of the National Astronomical Observatory Rozhen. Two spectral regions were detected: one near H_α and the other near the He II 4686 line (Table 4.10). The spectral window of 110 Å gave us the possibility of observing the He I 4713 line together with He II 4686. The resolving power was 15 000. The IRAF package was used for data reduction as well as for obtaining the dispersion curve and calculating the radial velocities and the equivalent widths. The fluxes of the He I 4713 and He II 4686 lines were obtained by means of the equivalent widths and the monochromatic continuum fluxes at their positions. The continuum fluxes were calculated via linear interpolation of the fluxes at the positions of the sensitivity maxima of the B and V photometric systems. The flux of the line H_α can be obtained in the same way using V and R photometric data. However we did not have R photometric data and determined the monochromatic continuum flux at its position as follows.

Two components of the AG Dra system have contributions to its continuum at the position of H_α – the cool giant and the circumbinary nebula. We obtained the flux of the cool giant supposing that it has the same continuum energy distribution as α Boo, since the temperatures of these stars are equal, amounting to 4300 K (Smith et al. 1996; Griffin & Lynas-Gray 1999). We calculated the 6563 Å/5500 Å flux ratio of α Boo and scaled it to the dereddened visual flux of AG Dra taken in its quiescent orbital minimum, when the nebular emission can be supposed to be negligible.

Both groups of variations of the optical continuum of AG Dra, the quiescent and the active ones, are caused by the nebular emission (Montagni et al. 1996; Greiner et al. 1997; Tomova & Tomov 1998; Tomov et al. 2000). That is why the contribution of the circumbinary nebula at the wavelength position λ 6563 Å must be found at each epoch of H alpha observation. We calculated the fluxes at λ 5500 Å and λ 6563 Å of a continuum of gas emitted by recombinations and free-free transitions taking into account the temperature in the nebula of AG Dra and found that the flux at λ 5500 Å is greater by 8% than at λ 6563 Å. It was also supposed that the singly ionized

Table 4.10: List of the observations during the 1996 – 1997 outbursts

Date	JD 2 450 000+	Phase	Spectral region
1996 Jul. 28	293.321	0.082	H_α
1996 Jul. 28	293.394	0.082	He II 4686
1996 Jul. 30	295.489	0.086	H_α
1996 Aug. 2	298.396	0.091	H_α
1996 Aug. 25	321.383	0.133	H_α
1996 Aug. 26	322.282	0.134	He II 4686
1997 Jan. 27	475.523	0.412	H_α
1997 Mar. 28	536.333	0.522	H_α
1997 Apr. 26	565.383	0.574	H_α
1997 Jun. 18	618.419	0.670	H_α
1997 Jun. 19	619.369	0.672	He II 4686
1997 Jul. 12	641.515	0.712	H_α
1997 Aug. 13	674.340	0.772	H_α
1997 Aug. 16	677.283	0.777	He II 4686
1997 Sep. 11	703.243	0.824	H_α
1997 Sep. 11	703.307	0.824	He II 4686
1997 Sep. 13	705.332	0.828	H_α
1997 Oct. 10	732.274	0.877	He II 4686
1997 Oct. 10	732.356	0.877	H_α

helium is dominant. A spherical nebula with a density distribution of $1/r^2$ in the region $10^6 - 10^{10}$ cm^{-3}, typical of the densities of the symbiotic nebulae, was considered. Carrying out this calculation, we used the mean values for the radius of the cool giant and its mass-loss rate of 30 $R_\odot$ and 2.3 10^{-7} M/yr according to the paper of Tomov et al. (2000) and a wind velocity of 30 km s^{-1}(Mikolajewska et al. 1995).

Having the ratio of the fluxes of the nebula at λ 5500 Å and λ 6563 Å, we subtracted from the observed V flux at the epochs of the H_α data the contribution of the giant. The difference is a nebular continuum, which was decreased by 8% and added to the flux of the giant at λ 6563 A. In this way we obtained the continuum flux of the AG Dra system at this wavelength. For calculation of all line fluxes the photometric data of Skopal (1998); Petrik et al. (1998) and Tomova & Tomov (1998) were used.

All the fluxes were corrected for an interstellar extinction of $E(B-V) =$ 0.06 (Mikolajewska et al. 1995; Greiner et al. 1997; Gonzalez-Riestra et al.

1999) using the extinction law of Seaton (1979).

4.5.2 Description and analysis of the emission line spectrum

H_α line

We continue our analysis of the line H_α using data derived during the 1996 and 1997 brightenings and the lower state of the light between them (Table 4.10). All of our data reveal a single-peaked profile (Fig. 4.12) with unusually extended low intensity wings, reaching the level of the local continuum at a distance not less than 2000 $\mathrm{km\,s^{-1}}$ from the center of the line during all the time of observation. The wings were always symmetrical but an asymmetry in the upper part of the line was present. This asymmetric part was confined by a small shoulder that was hardly visible and located below the level of the half maximum on the short wavelengthside. Since the wings were symmetrical and the feature causing asymmetry was at the upper part of the line, as in our previous analysis (Tomova & Tomov 1999), we conclude that this feature is probably due to absorption of some part of the H_α photons. The profile varied during the time of our observations, which, in this case, is due to change of the optical depth.

The intensity of the wings also correlated with the optical light (Fig. 4.6). It was higher at the times of the two brightenings compared with its value in the lower state of the light between them (Fig. 4.13). This behaviour shows that greater number of emitting atoms was observed at the times of the increased light. We suppose (Sect. 4.6) that the increased number of emitting H_α line atoms in the circumbinary nebula of AG Dra during its active 1994 − 1998 phase is probably determined by an increase of both the mass-loss rate of its cool giant and Lyman photon luminosity of the hot companion.

The changes of the width (FWHM) of the line correlated with the light too. During the time of the increased light it was greater, reaching values of about 160 $\mathrm{km\,s^{-1}}$ at the 1996 maximum and about 140 − 150 $\mathrm{km\,s^{-1}}$ at the 1997 one. During the lower state of the light it was about 110 $\mathrm{km\,s^{-1}}$. These data indicate a more pronounced turbulence in the nebula during the times of increased light.

The behaviour of the H_α flux is shown in Fig. 4.14 and its data are listed in Table 4.11. It varied with the light too. The wavelength position of the line was measured in the area of the wings as its other part was influenced by selfabsorption (Table 4.11). Its radial velocity shows pronounced variation with the orbital phase during this stage of activity (Fig. 4.14). In our view

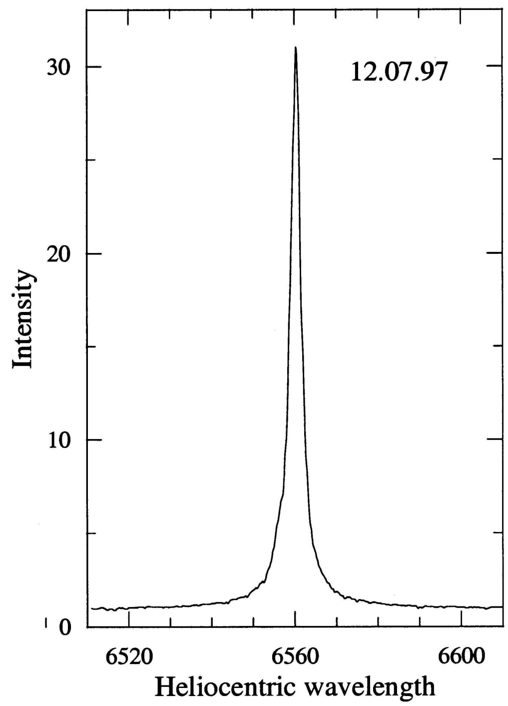

Figure 4.12: H_α profile of AG Dra normalized with respect to the local continuum.

Table 4.11: The H_α line data

JD 2 450 000+	Phase	RV $\mathrm{km\,s^{-1}}$	$F \times 10^{-12}$ $\mathrm{erg\,cm^{-2}\,s^{-1}}$
293.321	0.082	−129.41	136.203
295.489	0.086	−125.98	148.174
298.396	0.091	−125.22	146.124
321.383	0.133	−150.06	126.058
475.523	0.412	−153.90	83.090
536.333	0.522	−142.80	85.192
565.383	0.574	−138.32	82.028
618.419	0.670	−136.49	137.474
641.515	0.712	−138.91	154.769
674.340	0.772	−146.27	175.268
703.243	0.824	−142.20	202.230
705.332	0.828	−142.62	204.238
732.356	0.877	−151.37	173.298

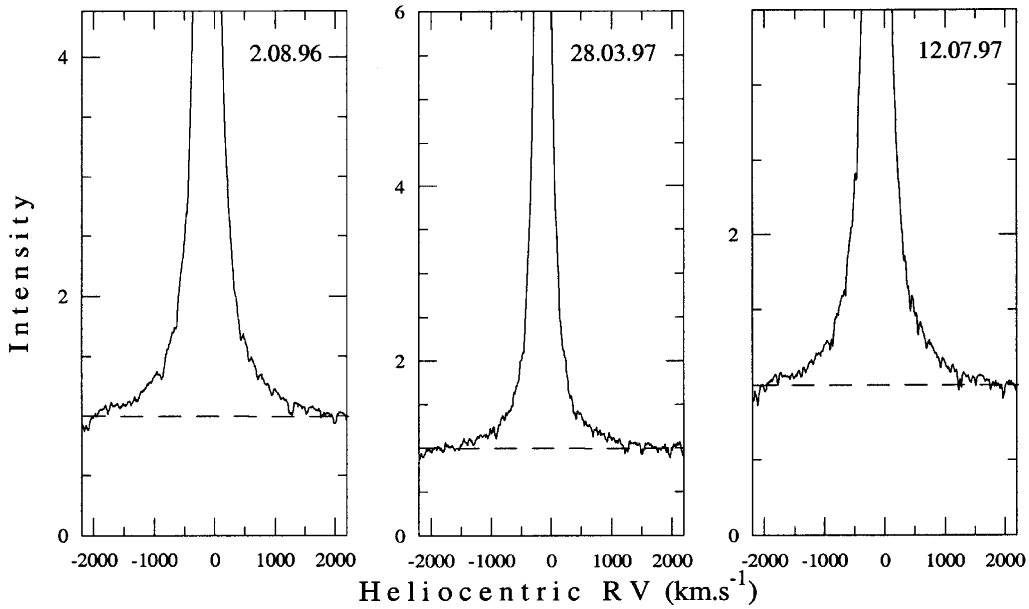

Figure 4.13: Variations of the wings intensity of the H_α line. For a direct comparison the ratio of the ordinate scales was chosen to be equal to the ratio of the continuum fluxes at the position of H_α.

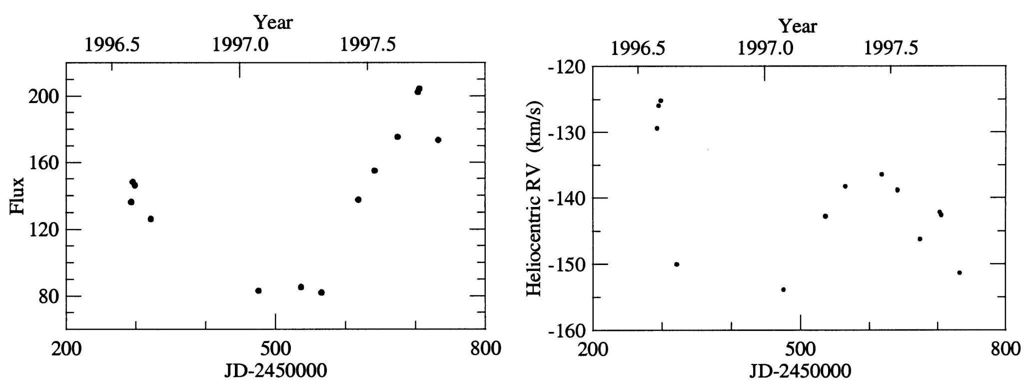

Figure 4.14: Left: H_α flux in units 10^{-12} erg cm^{-2} s^{-1}; Right: H_α radial velocity during the time of observation.

these data can be analysed only when the quiescent orbital behaviour of the line is known.

Table 4.12: The He I 4713 line data

JD 2 450 000+	Phase	RV $\mathrm{km\,s^{-1}}$	$F \times 10^{-12}$ $\mathrm{erg\,cm^{-2}\,s^{-1}}$
293.394	0.082	−134.785	0.926
322.282	0.134	−164.299	0.565
677.283	0.777	−146.807	2.158
703.307	0.824	−150.814	1.561
732.274	0.877	−167.798	0.651

Helium lines

He I *4713 line*

During the time of all observations this line had a nebular profile and a width (FWHM) of about 70 $\mathrm{km\,s^{-1}}$. The data of its flux and radial velocity are listed in Table 4.12. The radial velocity varied with the orbital phase. As in the case of the H_α line we will consider this variation only when result of an analysis of its quiescent data is available.

He II *4686 line*

In July and August 1996 as well as in June – September 1997 the He II 4686 line consisted of two emission components – a central narrow component with width (FWHM) equal to about 90 $\mathrm{km\,s^{-1}}$ and a broad one whose width was much greater (Fig. 4.15). Only the last spectrum, taken in October 1997, revealed one component profile of this line when only a narrow emission component was present. We measured the intensity of the broad component in the following way. The observed spectrum in its region was corrected through removing some weak emission lines of O II and N II as well as the strongest absorption lines of the giant. Then it was analysed by fitting with Gaussian function. The parameters obtained with this procedure are listed in Table 4.13. The equivalent width and the flux of the line were derived with an error ranging from 10 to 26 per cent depending on the error of the local continuum of the individual spectra. The wide of the line at the continuum level (FWZI) was determined from that distance from its center where the fit reaches the level of the noise. The velocity of the stellar wind (see below) of the hot companion υ_{hot} (Table 4.13) is equal to the half of the FWZI of the line. The values of this velocity in the table were determined taking also into account the error of the line width (FWHM). It was not possible to fit

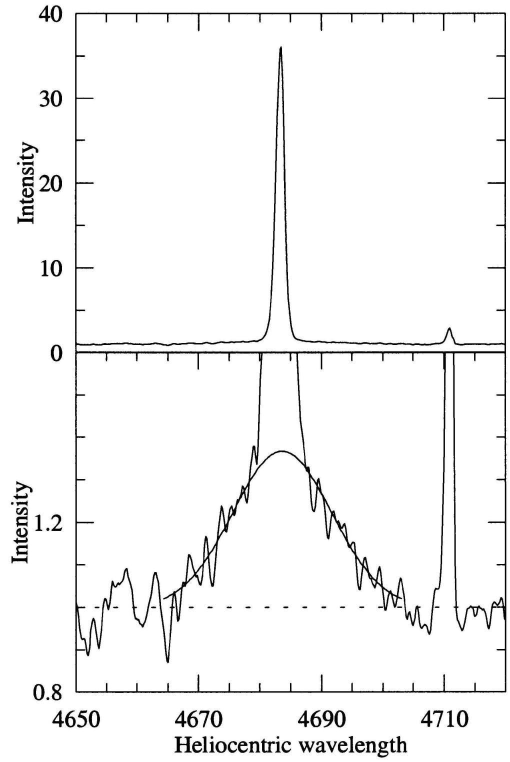

Figure 4.15: Upper panel: the profile of the He II 4686 line, based on a CCD frame on 16.08.97. Lower panel: the area of the wings where the broad component is seen. The level of the local continuum is marked with a dashed line.

the broad component with good accuracy on the spectrum taken on June 19, 1997 (JD 2 450 619) because of cosmic rays on its red wing. However taking into account the data based on the other spectra, we consider that the hot companion of the system has also had a stellar wind with a velocity of about 1000 km s^{-1} and a mass-loss rate of 10^{-7} $M_\odot$ yr^{-1} at that time.

In the previous section we considered different mechanisms of line broadening and came to the conclusion that three processes, namely electron scattering, disc's emission and wind's emission can give rise to the broad component of the lines H_β, H_γ and He II 4686 of AG Dra during its 1995 outburst, but the stellar wind has probably basic contribution. Now we will check if the broad component of the He II 4686 line during the 1996 and 1997 outburst of the system is determined by the same mechanisms.

We first consider the possibility that this component is determined only by electron scattering. The total flux of the line, which is a sum of the fluxes of the two components ranges from 23.218×10^{-12} erg cm^{-2} s^{-1} to 49.548×10^{-12}

Table 4.13: The He II 4686 line data

JD 2 450 000+	Phase	RV(N) km s^{-1}	F(N)$\times10^{-12}$ erg cm^{-2} s^{-1}	FWHM(B) km s^{-1}	FWZI(B) km s^{-1}	$v_{\rm hot}$ km s^{-1}	F(B)$\times10^{-12}$ erg cm^{-2} s^{-1}	$\dot{M}_{\rm hot}$
293.394	0.082	−139.67	28.318	1223 ± 82	2404	1200	3.221	1.18
322.282	0.134	−157.54	20.722	1188 ± 154	2212	1100	2.496	0.96
619.369	0.672	−167.72	33.273					
677.283	0.777	−154.19	42.559	1213 ± 56	2556	1300	6.989	1.89
703.307	0.824	−149.74	42.444	1055 ± 58	2252	1100	5.147	1.38
732.274	0.877	−161.65	25.900					

N – narrow component, B – broad component;

$\dot{M}_{\rm hot}$ is in units of 10^{-7} (d/1.7 kpc)$^{3/2}$ M$_\odot$ yr^{-1}.

erg cm^{-2} s^{-1} (Table 4.13). With the parameters of the nebula adopted in Sect. 4.3.3 this gives emission measures of $(0.59 \div 1.25) \times 10^{59}$ (d/1.7 kpc)^2 cm^{-3}. Assuming a constant electron density of 10^{10} cm^{-3} (Mikolajewska et al. 1995) we obtain a radius of $(5.19 \div 6.69) \times 10^{12}$ (d/1.7 kpc)$^{2/3}$ cm of the spherical emitting volumes. If the broad component was produced only by electron scattering it would appear in regions with optical thickness of about 0.11–0.15. Using these optical thicknesses and an electron density of 10^{10} cm^{-3}, we obtain $(1.71 \div 2.29) \times 10^{13}$ (d/1.7 kpc)$^{2/3}$ cm for the radius of these regions, corresponding to enormous emission measures of $(2.094 \div 5.004) \times 10^{60}$ (d/1.7 kpc)^2 cm^{-3}. Since this result is in disagreement with the previous one, we conclude that the broad component is probably not produced only by electron scattering.

This point will be more clear if we analyze the data of Gonzalez-Riestra et al. (1999) for this line as well. They revealed the presence of two emission components too, which were present at the two stages of the evolution of the system – the quiescent one before 1994 and the active phase after this time. The broad emission component was absent at some epochs during quiescence, for instance on 10 Jan. 1993. On 5 Jan. 1994, however, it was present and if supposed to be due to electron scattering, the optical thickness of its emitting region will be equal to 0.08. In this case the radius and the emission measure are found to have values close to those ones calculated with the total flux of the line and our assumption of electron scattering only can not be rejected. A broad component was observed on 19 Aug. 1995 too and when supposed to be a result of electron scattering the optical thickness is derived to be 0.14. In this case the radius of the emitting region and its emission measure are found to be considerably greater than those determined by the total line flux. This means that the broad component was not due only to electron scattering. Thus, when the intensity of the broad component of the He II 4686 line is low it can be due only to electron scattering. However at the times July–August 1996 and June–September 1997 another process contributes to its appearance.

An emission line similar to the He II 4686 broad component can be radiated by a small accretion disk around the compact object, rotating with Keplerian velocity. Let us consider whether this was the case in July–August 1996 and June–September 1997 when the intensity of this component was high. For the radius of the secondary component of the system we adopt a value of 0.10 $R_\odot$ (see below). The mass of this component was assumed by Mikolajewska et al. (1995) to be about 0.6 $M_\odot$ and by Gonzalez-Riestra et al. (1999) to be about 0.3 $M_\odot$. We supposed it is in the range $0.3 \div 0.6$ $M_\odot$. In this case a Keplerian velocity of $757 \div 1070$ km s^{-1}is obtained, which is comparable to the velocity of about $1100 \div 1300$ km s^{-1}, corresponding to the FWZI of the broad component (Table 4.13). A small disk rotating with this velocity and located close to the hot secondary appears as a result of accretion of a stellar wind.

Another possibility is the broad component to be emitted by a high-velocity stellar wind. We considered this possibility in the last section. Then as in the case of the 1995 outburst we suppose that electron scattering and an optically thin accretion disc have some contribution in the broad component, but this component is formed mainly by emission of a stellar wind. As in the case of the 1995 outburst we will calculate the upper limit of the mass-loss rate of the outbursting object.

To determine the mass-loss rate of the hot compact object of the AG Dra system, as in the case of the 1995 eruption, we applied the nebular approach, described in the work of Vogel & Nussbaumer (1994), based on the relation of this parameter with the line flux.

The particle density in the wind is a function of the distance to the center and is expressed via the continuity equation. The electron temperature was adopted to be $T_e = 20\,000$ K and the state of the helium ionisation was supposed to be He^{++} as in the case of 1995 eruption. We also used a recombination coefficient of 2.689×10^{-13} cm^3 s^{-1} for case B, corresponding to this temperature and a density of 10^{13} cm^{-3} (Storey & Hummer 1995) and a parameter μ of 1.4 (Nussbaumer & Vogel 1987) determining the mean molecular weight μm_H in the hot wind. As the line flux is thought to be emitted by a spherical region, the radii of integration must be determined. Since we treat the wind in the nebular approach, the inner radius is thought to be the radius of the star. We used the same inner and outer radii as in the case of 1995 eruption. The mass-loss rates obtained are listed in Table 4.13.

4.5.3 Discussion

The active 1994–1998 phase of the symbiotic star AG Dra is characterized by several increases of the optical light and the amplitude of the greater of them was more than three magnitudes in the U-band photometric system. Broad emission components indicating high velocity stellar wind from the compact companion are present in the spectrum after the 1995 (Tomova & Tomov 1999), 1996 and 1997 light maxima. According to the evolutionary models of an accreting white dwarf (Shara et al. 1993; Kato & Hachisu 1994; Yungelson et al. 1995) the total mass lost by it is approximately equal to the mass of the accumulated hydrogen envelope. If we suppose that the whole envelope has been lost during the time of an individual outburst, the accretion must be realized at a mean rate close to that of the loss of mass 10^{-8}– 10^{-7} $M_{\odot}\,yr^{-1}$, since these two processes had approximately the same duration. However, when the accretion rate is 10^{-8}– 10^{-7} $M_{\odot}\,yr^{-1}$ a steady burning of hydrogen is realized which excludes the possibility of a thermonuclear runaway (Mikolajewska & Kenyon 1992). Consequently the optical brightenings of AG Dra after 1994 most probably are not determined by thermonuclear runaway at the surface of a white dwarf.

4.6 Mechanism of increase of the light

For an explanation of the X-ray spectrum, Greiner et al. (1997) proposed a model where the accretion rate is increased, leading to an expansion of the compact secondary at constant bolometric luminosity. The growth of the U light, however, is caused by an enhancement of the nebular continuum, which is determined by increase in the number of the recombining ions. During the 1994 and 1995 light maxima the U flux of the circumbinary nebula and its emission measure increased by factors of 36.2 and 12.9 compared to their quiescent maximal values. At 1996, 1997 and 1998 light maxima they increased by factors of 8.3, 14.9 and 6.6 respectively. The intensity of the nebular continuum is proportional to the ion density. There is also a linear dependence between the ion density and the density of the radiation field of the ionizing star. Then if the compact companion is supposed to be this source, which heats the circumbinary nebula, the nebular U flux and the emission measure should increase proportionally to the companion's Lyman photon luminosity. Supposing a black body energy distribution and using a distance to the system of 1.7 kpc, the data of Greiner et al. (1997) for the luminosity and the temperature of the hot component as well as the velocity of its expansion calculated by them, we find that the Lyman photon luminosity of this star increases by a factor of 1.5, which is not greater than the observational error. This result means that the Lyman luminosity does not change during the active phase. According to other authors, however, (Gonzalez-Riestra et al. 1999) the Lyman luminosity increases. Our supposition for a black body was based on the UV data analysis of Gonzalez-Riestra et al. (1999) as well as on the generally accepted view for the continuum energy distribution of the hot stellar components of the symbiotic binaries (Mürset et al. 1991). Then, to explain the growth of the U flux and the emission measure of the nebula additional mechanism of ionization is need.

Let us consider the increase of the amount of the emitting gas following the scenario proposed by Greiner et al. (1997), since an appearance of a stellar wind from the compact companion, such as observed, is supposed in the framework of this scenario. We suppose that the hot companion has a luminosity high enough, which makes it able to ionize the whole circumbinary nebula, except some region behind the giant. In this case the growth of the companion's luminosity by itself will not lead to an increase in the number of ions recombining in the nebula during the active phase. This can be caused by an increase in the mass-loss rate of the giant star. Such a mechanism was initially suggested by Nussbaumer & Vogel (1988) to explain the optical outbursts of symbiotic stars. Moreover the analysis of the radial velocities by Galis et al. (1999) suggests that the cool giant pulsates, which probably leads to changes in its mass-loss rate.

We propose the following sequence when an outburst takes place:

1. The U light begins to increase because of appearance of a shell in the wind of the giant and rises while the hot companion is able to maintain ionization in the same region of the nebula as in quiescence;

2. When the ionized region begins to shrink as a result of the increase of the mass-loss, the light stops its rise and remains constant, while the shell reaches the companion and its accretion rate begins to increase;

3. The increased accretion rate leads to creation of an envelope and gives rise to the Lyman luminosity, the companion ionizes an additional part of the nebula and the light rises for a longer time. It reaches a maximal value together with the Lyman luminosity when a high velocity wind appears. So the time of rise of the light is more than $80^d - 90^d$, the time needed for a particle of the giant's wind to travel the distance between the two stars. The wind velocity is not supposed to change during the active phase and remains approximately the same, $30\,\mathrm{km\,s^{-1}}$ (Mikolajewska et al. 1995). The mass-loss rate of the giant declines to its quiescent value before the epoch of the light maximum;

4. The wind of the companion stops the accretion and contributes to the expansion of the ejected shell. At the same time the accreted envelope burns out and the Lyman luminosity decreases to its quiescent value. The two processes determine the return of the U light to its quiescent level.

This scenario gives a possibility to explain some details of the curve (Fig. 4.6) – for example, that the light after its 1994 maximum dropped to a level considerably higher than its quiescent value. The reason can be an early increase of the mass-loss rate of the giant.

4.7 Conclusion and results

In 1994 – 1998 the symbiotic binary AG Dra underwent an active phase consisting of five optical brightenings. We present results based on multicolour photometric observations and high-resolution spectral data derived in the regions of several optical lines in the quiescent state before the active phase and during activity.

The results of the photometric observations are as follows. The shape of the U quiescent light curve shows that the flux corresponding to the orbital amplitude is emitted by a small high-density region located around the hemisphere of the giant which faces the hot companion and undergoing occultation.

Using the mass-loss rate of the cool giant and the U fluxes of the different components of the system we calculated its distance and the radius of the giant to be in the ranges 1560÷1810 pc and 28÷32 $R_{\odot}$, respectively.

The photometric data give us the possibility to obtain the emission measure of the circumbinary nebula adopting a distance to the system of 1.7 kpc and using the nebular contribution to the observed U flux. Emission measures of $n^2V = 1.59 \times 10^{59}$ $(d/1.7\ kpc)^2$ cm^{-3} and $n^2V = 0.36 \times 10^{59}$ $(d/1.7\ kpc)^2$ cm^{-3} at the orbital photometric maximum and minimum were obtained on the basis of the quiescent U flux. At the times of the five maxima of the U light during the 1994 – 1998 active phase the emission measure was increased by factors of 36, 13, 8, 15 and 7 compared with its quiescent maximal value.

The results of optical spectral observations carried out in the blue region as well as in the region of the line H_{α} of the symbiotic binary AG Dra at quiescence and during its 1994 and 1995 outbursts are as follows. Profiles, fluxes and radial velocity data of a number of emission lines were derived. Their basic characteristic was the comparatively large width (FWHM) especially in June 1994 immediately before the light maximum.

Two kinds of variations of the H_α profile were detected during the quiescent stage. The first were in the area of the wings, determined by variations of the emitting-atoms number. We consider they are due to an occultation of the ionized region(s) of the surrounding nebula, which occultation was supposed to exist in this system by Mikolajewska et al. (1995). The second kind of variations are related to the upper part of the profile, determined by the variations in the optical depth. The wing intensity and the line width increased considerably during outburst.

The He II 4686 line flux was observed to have increased at one time after the light maximum during the 1995 outburst by a factor of 1.6 compared with its quiescent value at a phase close to maximal light.

Radial velocities of the emission lines were close to the system's mass center velocity at most observation phases. No Balmer progression was ascertained. The radial velocity of the cool primary was measured using some absorption lines of the K spectrum in the region of H_α .

After the visual light maximum in 1995, the profile of the lines $H\beta$ and H_γ consisted of two emission components: a central narrow component and a broad component. There is possibility the broad component to be due to scattering by free electrons, emission of Keplerian accretion disc and emission of optically thin stellar wind produced by the compact companion. We suppose that the contribution of the stellar wind predominates. The velocity of this wind was equal to 800 $\mathrm{km\,s^{-1}}$. The upper limit of the mass-loss rate of the companion was estimated of $0.97 \times 10^{-7}(\mathrm{d}/1.7\,\mathrm{kpc})^{3/2}$ $\mathrm{M_\odot\,yr^{-1}}$.

We conclude also that at the time of existence of the broad emission components the symbiotic binary AG Dra has been at a stage of colliding stellar winds. The ratio of their momentum rates allows the possibility the hot wind to reach the close vicinity of the giant. The mechanical energy of the winds is 5 $\mathrm{L_\odot}$, which is an upper limit of the X-ray luminosity of the collision region.

Variations of the width (FWHM), the flux and the intensity of the wings of the line H_α were observed during the time 1996 − 1997 correlating with the light. The behaviour of the wings showed an increase of the number of emitting atoms in the nebula during the outbursts in agreement with the increase of the emission measure. The FWHM showed a more pronounced gas turbulence during the times of activity.

After the visual light maxima in 1996 and 1997 the profile of the He II 4868 line consisted of two emission components: a central narrow component and a broad component indicating mainly stellar wind. This wind had a velocity of 1100–1300 $\mathrm{km\,s^{-1}}$ and was probably produced by the compact companion, which was supposed to lose mass at a rate of about $(1-2)\times10^{-7}(\mathrm{d}/1.7\,\mathrm{kpc})^{3/2}$ $\mathrm{M_\odot\,yr^{-1}}$. Based on these data we concluded that the outbursts of the system during its 1994 – 1998 active phase most probably are not thermonuclear, since the accretion rate in this case should be close to this one of the loss of mass. The mass-loss rate, obtained by observation, has a high value and accretion at a rate close to it falls into the region of a steady-state burning of hydrogen at the surface of a white dwarf.

The growth of the Lyman photon luminosity of the companion is less than the growth of the emission measure of the nebula and is not sufficient to explain the optical outbursts that are caused by variation of the nebular emission. Supposing high luminosity of the companion we suggest that the optical outbursts of the system could be mainly due to a growth of the mass-loss rate of the giant. According to this idea the optical outbursts can result from both an increase in the mass-loss rate of its cool giant and an increase of the Lyman photon luminosity of the hot companion.

Chapter 5

Investigation of the symbiotic prototype Z And during its last active phase in 2000 – 2013

5.1 Introduction

Z And is considered as a prototype of the classical symbiotic stars and of the group of symbiotic stars as a whole. It consists of a normal cool giant of spectral type M4.5 (Mürset & Schmid 1999) and a hot compact object with temperature higher than 10^5 K (Fernandez-Castro et al. 1988; Sokoloski et al. 2006). The third component of the system is an extended nebula formed by the wind of both components and partly photoionized by the hot companion. The orbital period of this binary is $758\overset{\mathrm{d}}{.}8$, which is based on both photometric (Formiggini & Leibowitz 1994) and radial velocity (Mikolajewska & Kenyon 1996) data.

The light curve of Z And is characterized by phases of activity alternating with periods of quiescence. The quiescent optical light displays an orbital modulation with amplitudes of about 0.5 mag in the BV region and 1 mag in U. A 28-minute oscillation of the B light was also detected during quiescence and the small 1997 outburst as well with an amplitude of 2–5 mmag, which is supposed to arise from the rotation of an accreting magnetic white dwarf (Sokoloski & Bildsten 1999). The quiescent spectrum resembles a typical symbiotic star with TiO absorption bands and numerous emission lines of HI, HeI, HeII, NIII, CIII, FeII, [OIII], [NeIII], [NeV] and [FeVII].

The Z And system has spent much of its time in phases of increased activity (after 1915, 1939, 1960, 1984 and 2000) characterized by several brightenings, whose amplitudes reach up to 2–3 mag. During the major outburst in

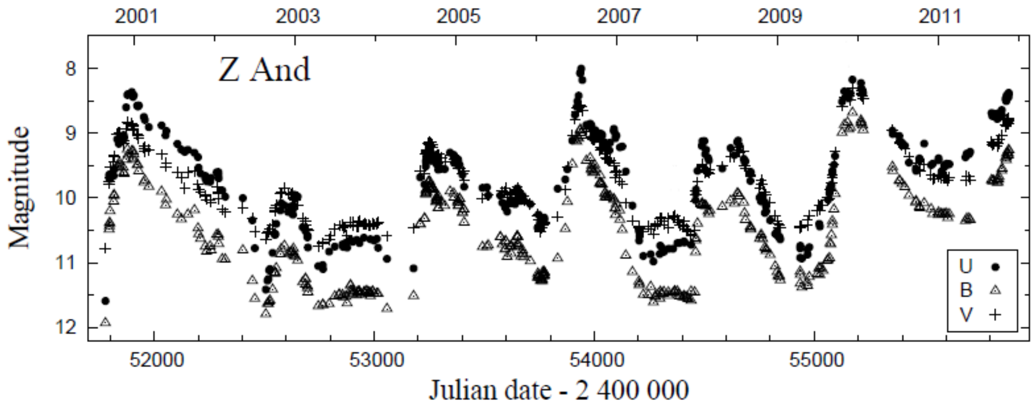

Figure 5.1: Light curve of Z And during the 2000 – 2013 active phase from Skopal et al. (2012).

1939 its visual magnitude reached about 8^m and the only spectrum which was observed was that of the P Cyg type expanding shell with lines corresponding to an A star. The profiles of hydrogen, helium and the ionized metal lines contained blueshifted absorption components, indicating a massflow with a velocity of about 100 $\mathrm{km\,s^{-1}}$. The spectrum of the M giant and the circumbinary nebula were not visible (Swings & Struve 1941). The optical spectrum of Z And during its time of activity after 1960 was observed by Boyarchuk (1967b). The data suggest continuum flux redistribution caused by expansion and cooling of the hot component when the light rises. Fernandez-Castro et al. (1995) analysed radio and UV low and high resolution spectral data of Z And taken during its 1984–1985 active phase. They obtained that the rise in the visual emission coincides closely with a minimum in the UV and radio. The anticorrelation between visual and UV was explained as extinction of the hot star radiation by a false photosphere produced by the ejection of a shell of dense material.

Z And entered its last active phase at the end of August 2000 (Skopal et al. 2000) and reached the first maximum of its optical light in December, when the V magnitude was about $8\overset{\mathrm{m}}{.}9$ (Fig. 5.1). During the time of the light maximum the 28-minute oscillation disappeared, indicating probably a blocking of the flux from the white dwarf by an optically thick shell (Sokoloski et al. 2002).

Based on spectra taken with the *Far Ultraviolet Spectroscopic Explorer (FUSE)* Sokoloski et al. (2002, 2006) reported P Cyg profiles of some UV lines, which evolved on a time-scale of weeks during the rise to maximum light. The first observation revealed such profiles of lines of lower ionization degree (singly and doubly ionized C, Fe and Si) whereas the next observations showed a hotter gas moving at hundreds of km s^{-1}, emitting in the P V λ 1117 line. Some lines evolved from absorption to emission. Skopal et al. (2006) reported the existence of the P Cyg type profile of the UV line O VI λ 1032 throughout the whole active phase. They noted, in addition, the appearance of a P Cyg type profile of the He I λ 5876 line at the time of the maximal light, whose absorption component indicated an outflow velocity of about 100 km s^{-1}. The authors came to the conclusion that the outbursting component has had an optically thick slowly expanding shell with a disc-like structure. The line He II λ 4686 had broad emission component indicating optically thin stellar wind with a velocity of about 500 km s^{-1} (Tomova, Tomov et al. 2008).

In August 2002 the optical light was in a deep minimum (Skopal 2003). After that time it increased again and reached maximum in November, but the UBV amplitudes were not great $\sim 1^m$ (Fig. 5.1). At the same time, however, the IR emission was heavily enhanced – to the level close to that in December 2000. The star underwent an outburst again, but it was different to the first outburst when the visual emission of the hot companion predominated over the other components in its typical energy distribution – a weak UBV emission and relatively strong $JHKLM$ one (Tomov et al. 2004). During the growth of the light in the period September – November 2002 the emission line spectrum of the system had various features. The H_α and H_γ lines had double-peaked profile. The H_α line had broad wings extended to not less than $\pm$2000 km s^{-1} from its center. The lines H_γ and He II λ 4686 had a broad emission component with a low intensity which indicated velocities up to more than 1000 km s^{-1} (Tomov et al. 2010a).

During the historical 2006 eruption optical collimated bipolar outflow was well observed along with other regimes of loss of mass (Burmeister & Leedjärv 2007; Tomov et al. 2007; Skopal et al. 2009a; Tomov et al. 2010b). At that time the line H_α had an absorption component with a high velocity of about 1400 km s^{-1} (Tomov et al. 2007). This component went into emission in the middle of July (Tomov et al. 2007) and thus the main central peak of the line during the period July – December had additional emission satellites with velocities of 1100–1400 km s^{-1}, located on its either side (Burmeister & Leedjärv 2007; Tomov et al. 2007; Skopal et al. 2009a). The appearance of the line H_β was similar (Tomov et al. 2007; Skopal et al. 2009a). Both kinds of the high velocity components – the absorption and emission ones were assumed to appear in bipolar collimated outflow (Tomov et al. 2007).

In the middle of July 2006 the line H_γ and the He I lines had multicomponent P Cyg absorption reaching velocity of up to about 1500 km s^{-1}. After the end of July till the beginning of October 2006 the line H_γ had absorption P Cyg component with low velocity of about 100 km s^{-1} only. The behaviour of the He I lines was similar but their P Cyg absorption was visible till the beginning of December 2006. This behaviour resembles that of the He I triplet lines during the 2000 outburst (Skopal et al. 2006; Tomov et al. 2008).

After the optical maximum the emission profile of the lines H_γ and He II 4686 was two component one consisting of a central narrow component and a broad component with full width at zero intensity of 1000 $km\,s^{-1}$ similar to that during the 2000 outburst (Tomov et al. 2008).

The optical brightenings included in the 2000 − 2013 active phase have different photometric amplitudes. The bolometric luminosity of the outbursting compact component, however, increased during all of the investigated brightenings reaching its typical value of about 10 000 $L_\odot$ (Tomov et al. 2003a, 2004; Sokoloski et al. 2006; Skopal et al. 2006, 2009a).

The basic aims of our research are as follows:

1. To suggest a scenario for explanation of the multistage pattern of the light curve during the first (2000 – 2002) brightening of the system and a mechanism providing a growth of the bolometric luminosity of the outbursting compact object during the first and the other brightenings of the active phase;

2. To investigate the process of loss of mass and to obtain quantitative estimate of the mass-loss rate of the outbursting compact object;

3. To suggest a model for interpretation of the line spectrum of the system during its whole active phase.

For our consideration we used the ephemeris Min(vis) = JD $2\,442\,666^{d} + 758\overset{d}{.}8 \times E$, where the orbital period is based on both photometric and spectral data and the epoch of the orbital photometric minimum coincides with that of the spectral conjunction (Formiggini & Leibowitz 1994; Mikolajewska & Kenyon 1996; Fekel et al. 2000). We adopted also a distance to the system d = 1.12 kpc according to Fernandez-Castro et al. (1988, 1995).

5.2 The optical light during the 2000 – 2002 outburst

5.2.1 The peculiar character of the rise of the light

During the 2000 – 2002 brightening of Z And were obtained detailed optical light curves which clearly show that the rise of the light to its maximum occurs in a multistage mode. The light curves obtained during the previous brightenings were not detailed enough to detect this effect. Moreover, only for the two last active phases observational data in different wavelength regions are available (obtained by instruments on spacecraft).

The UBV light curves for the 2000 – 2002 brightening are shown in Fig. 5.2. The first stage of the rise of the light started in the end of August 2000 and continued for about 60 days. During that time the light increased by 1.9^m. Further it remained constant one and even slightly decreased over about 25–30 days. The light began to rise again after November 13, 2000, and reached a second maximum (in fact, the overall maximum of the outburst) after approximately 25 days (near December 6, 2000). The times of the first and second maxima are marked in Fig. 5.2 with dashed lines.

The most detailed light curve, published by Sokoloski et al. (2006) is shown in Fig. 5.3. According to these data, there is one feature more on the curve – a kink that appears about 2.5 weeks after the onset of the outburst. This led Sokoloski et al. to distinguish three stages of the rise of the light, separated by two plateaus. The rise stages last 2.5, 2.5 – 3, and slightly more than 3 weeks respectively, while the first and the second plateaus last one week and about one month.

The existence of the first maximum is explained in the works of Sokoloski et al. (2005) and Sokoloski et al. (2006) as being due to clearing of the ejected shell and the future rise of the light is related to the revealing the white dwarf. However, the UV and the optical spectral data presented in the works of Sokoloski et al. (2002) and Tomov et al. (2003b) contain P Cyg lines indicating mass outflow from the dwarf at the time of the light maximum. Thus, these observational data cast some doubt on the suggestion made by Sokoloski et al. (2005) and Sokoloski et al. (2006).

In the framework of our investigation we make an attempt to explain the behavior of the light of Z And using the colliding-winds model (Bisikalo et al. 2006).

5.2.2 Mechanism of development of the outburst

Thermonuclear burning at the surface of the accretor is considered to be the most probable origin for the observed features of symbiotic stars (Kenyon 1986; Iben & Tutukov 1996). The burning of hydrogen at the white-dwarf's surface depends substantially on the accretion rate (Paczynski & Rudak 1980). For a narrow range of accretion rates stable hydrogen burning is possible (Paczynski & Zytkow 1978; Fujimoto 1982). For the mass of the white dwarf in Z And $M = 0.6 M_\odot$ this range is $2.1 \times 10^{-8}\ \mathrm{M_\odot\,yr^{-1}} \leq \dot{M}_{acc} \leq 4.7 \times 10^{-8}\ \mathrm{M_\odot\,yr^{-1}}$.

In the commonly accepted picture the outbursts of classical symbiotic

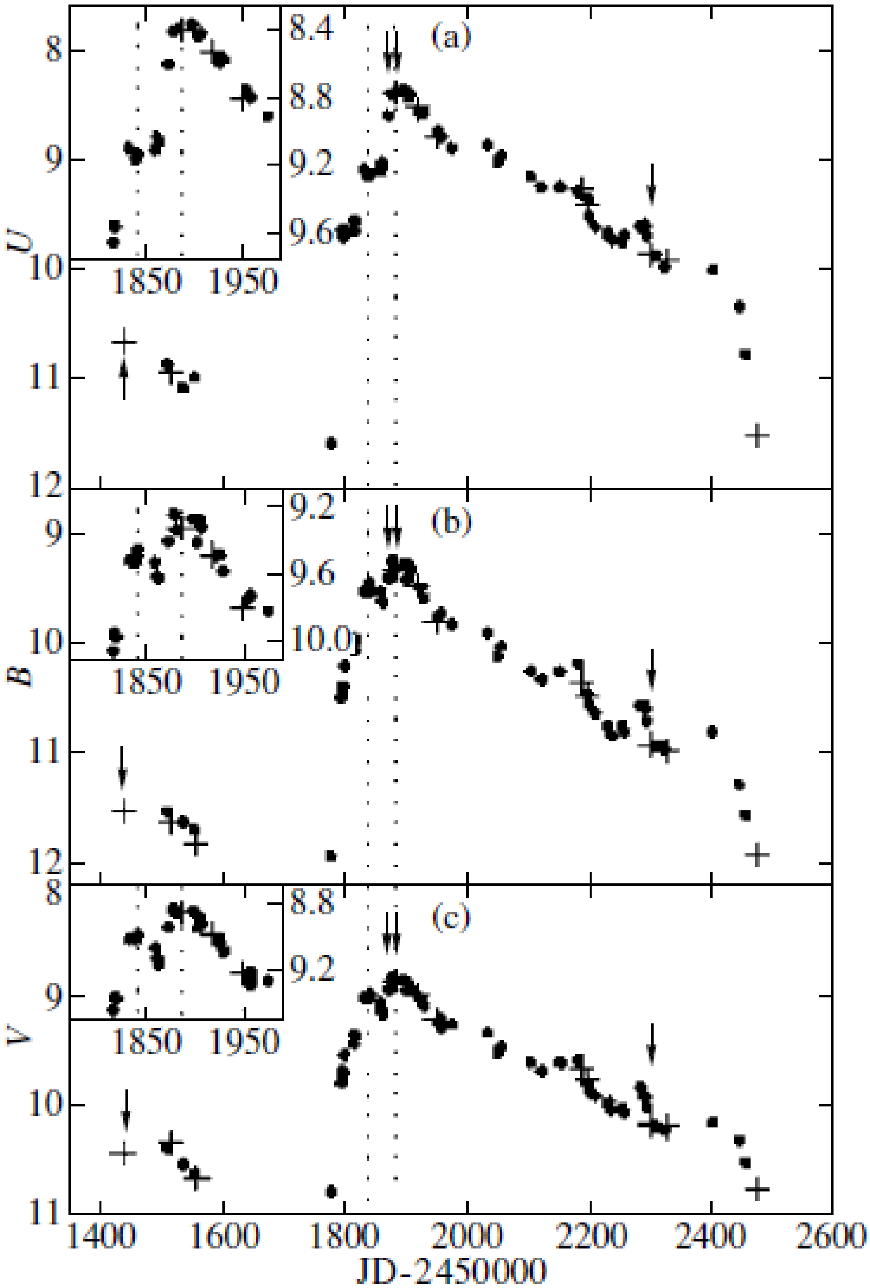

Figure 5.2: UBV light curve of Z And during the 2000 outburst. Data from Skopal et al. (2002, 2004) (points) and our own observations (crosses) are shown. The first and second brightness maxima are marked by dashed lines and the moments for which the ratio of ionizations and recombinations μ were calculated—by arrows. The inserts show the behaviour near the maximum on a larger scale.

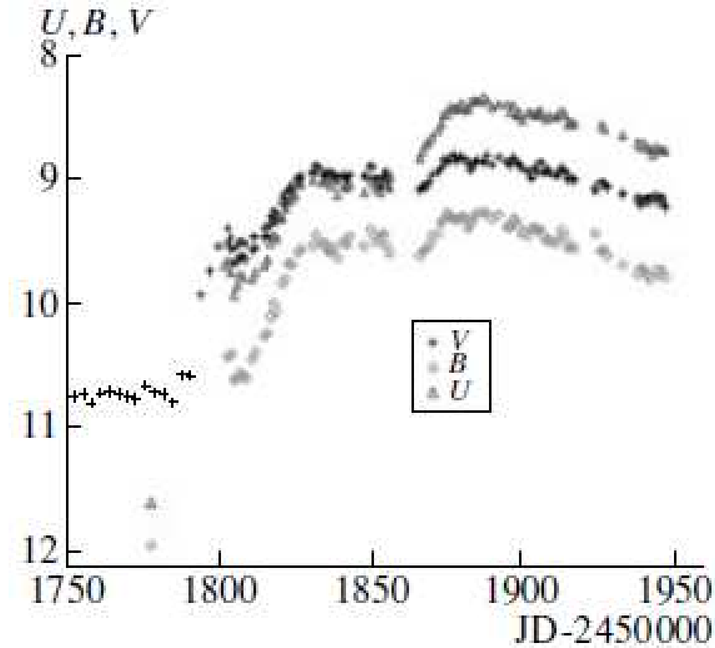

Figure 5.3: Light curve of Z And during the 2000 outburst from Sokoloski et al. (2006).

stars realize when the accretion rate exceeds the upper limit for stable hydrogen burning. If this occurs, the accreted matter accumulates above the hydrogen-burning shell and the star expands to giant dimensions. However, the luminosity scale of some observed outbursts casts doubt on the possibility that they are associated purely with accretion processes. The estimates show that the energetics of the 2000 – 2002 event requires an accretion rate exceeding $10^{-5} M_\odot\,\mathrm{yr}^{-1}$ (Sokoloski et al. 2006), in contradiction with both observations and computational results (Mitsumoto et al. 2005). We considered a “combined” mechanism of the outburst where the increase of the accretion rate due to disruption of the disk results in variations of the burning rate (Tutukov & Yungelson 1976; Bisikalo et al. 2002; Kilpio et al. 2005a,b). In this case the amount of the accreted matter $10^{-8} - 10^{-7} M_\odot\,\mathrm{yr}^{-1}$ (Mitsumoto et al. 2005) is sufficient to explain the observed luminosity variations (according to the estimates given in Sokoloski et al. (2006), it is necessary to accrete $\sim 10^{-7} M_\odot$). A similar model was suggested by Sokoloski et al. (2006), who supposed that the disk instability leads to an increase of the accretion rate, which, from its side, causes an increase of the rate of the nuclear burning.

The transition from quiescence to active phase requires a sufficient increase in the accretion rate. According to the observational data, the mass-loss rate of the donor in Z And is $\sim 2 \times 10^{-7} M_\odot \, \mathrm{yr}^{-1}$. Since the amount of matter accumulated in the disk during the inter outburst period 1997–2000 should not exceed $\sim 5 \times 10^{-7} M_\odot$, the development of the outburst requires the accretion of at least an appreciable part of the mass of the disk even in the framework of the combined model where the increase of the nuclear-burning rate is taking into account. As a rule, accretion-disk instabilities result in the infall of $\sim 10\%$ of the total mass of the disk, which is clearly not enough.

The required increase of the accretion rate can be provided in the framework of the mechanism suggested in Bisikalo et al. (2002), based on the results of two-dimensional gas-dynamical modeling and confirmed by the three dimensional computations of Mitsumoto et al. (2005). According to that mechanism even a small increase of the velocity of the donor's wind is sufficient to change the accretion regime. At the time of the transition from disk acretion regime to wind one, the disk disrupts and the wind with increased velocity causes the infalling its material onto the surface of the accretor. The theoretical considerations, however, show that it is possible the whole mass of the disc not to accrete and some part of it to remain in the disc. The analysis of the results of these computations has shown the following important points:

1. Variation of 5 $\mathrm{km\,s^{-1}}$ of the donor's wind velocity of 25 $\mathrm{km\,s^{-1}}$ (Fernandez-Castro et al. 1988) is sufficient to change significantly the flow pattern as well as the accretion regime – from disk accretion to wind one. When the wind velocity amounts to 30 $\mathrm{km\,s^{-1}}$, a conical shock forms. When it is equal to 20 $\mathrm{km\,s^{-1}}$, an accretion disk appears in the system.

2. In the quiescence the accretion rate is $\sim (4.5 - 5) \times 10^{-8}$ $\mathrm{M_\odot\,yr^{-1}}$ (for a mass-loss rate of the donor of $\sim 2 \times 10^{-7}$ $\mathrm{M_\odot\,yr^{-1}}$ (Fernandez-Castro et al. 1988)) which corresponds to the range of stable hydrogen burning for the adopted mass of the white dwarf in Z And .

3. The disruption of the disk is accompanied by a jump in the accretion rate (Fig. 5.4). A growth of the accretion rate by a factor of $\sim 2.0 - 2.2$ relative to its initial value provides exceeding the upper limit of the region of stable hydrogen burning. According to the computations the disk is disrupted in not more than 0.1 orbital period of Z And and a mass of several units of $10^{-8} - 10^{-7}$ $\mathrm{M_\odot}$ accretes during that time.

This amount of matter turns out to be sufficient to increase the pressure and the temperature providing an increase of the nuclear-burning rate. According to Sokoloski et al. (2006) the typical time scale for the response of

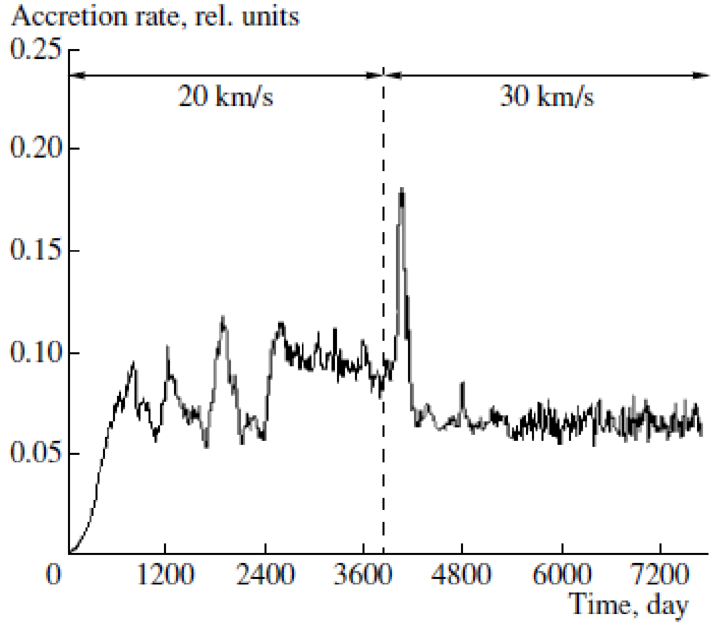

Figure 5.4: Variation of the accretion rate for the solution with an increase of the wind velocity from 20 to 30 $\mathrm{km\,s^{-1}}$. The vertical dashed line marks the moment when the wind velocity changes.

the nuclear-burning shell after the accretion of a sufficient amount of matter is about one month, which is in good agreement with the observed time of the formation of a kink of the light curve. This time is 2.5 weeks after the onset of the outburst. The growth of the luminosity during the time interval before the increase of the burning rate is due to rise of the accretion rate. If we suppose that the amount of matter accreted during that time is sufficient to initiate an enhanced burning rate, the further increase of the luminosity will be due to the enhanced burning rate. According to Sokoloski et al. (2006) after the appearance of the first kink of the light curve associated with the enhancement of the burning rate, an expanding envelope – a pseudophotosphere and/or optically thick wind forms in the system.

It is commonly accepted that the increase of the visual light is due to the energy redistribution towards the longer wavelengths during the expansion of the envelope of the compact component (Sokoloski et al. 2006; Tomov et al. 2003a; Fernandez-Castro et al. 1995). However, an expansion of the envelope on its own is unable to explain the above features of the light curve. Moreover, the presence of the wind in the system should influence its light. If the wind of the white dwarf arises as the outburst progresses (after 2.5 weeks after the beginning of the outburst according to the data in Sokoloski et al. (2006)), it will seem that its influence will begin to manifest itself not at the very beginning of the outburst, but at its later stages.

Since the hot wind arises during the outburst, the shape of the optical curve will be determined from three processes:

1) an increase of the accretor's luminosity causing expansion of its pseudophotosphere;

2) wind propagation in the nebula resulting in the formation of a high-temperature region;

3) formation of shock structure appeared as a result of the winds collision.

If the effects related to the wind are strong enough, they should be visible in the light curve. It is evident that the increase of the luminosity of the hot component and the expansion of its pseudophotosphere have the main contribution in the variation of the visual light (Tomov et al. 2003a). If at some time the component determined by the wind propagation in the nebula is added, followed by the formation of shocks providing further increase, the resulting light curve will have two variations of its slope related to the hot wind.

The shape of the light curve will be more complex if the flux of the expanding photosphere has time variations. It is obviously that, at some time, the expansion of the photosphere can be replaced by a contraction. This time will correspond to a peak in the light curve. Its final shape depends on the time of the hot wind appearance (the second term), the time when the shocks form (the third term) and the position of the peak.

The velocity of the wind is about 50 $\mathrm{km\,s^{-1}}$ (Tomov et al. 2003a). Then, assuming the shock is located between the components of the system (at a distance of $1/3\,A - 2/3\,A$ from the accretor, where A is the component's separation), we can estimate the time that elapses before the contribution of the shock to become substantial. This time turns out to be $26-52$ days after the onset of the wind. The peak determined by the contribution of the shock will be attained after some time in addition.

To estimate the time scale of the shock's development a set of computations with parameters close to the conditions for the Z And outburst were carried out. The results show that after the change of the conditions at the accretor's surface an S-shaped shock structure and contact discontinuity form in the space between the components.

Figure 5.5 shows the development of the events after the change of conditions at the accretor's surface. In the model presented the wind velocity

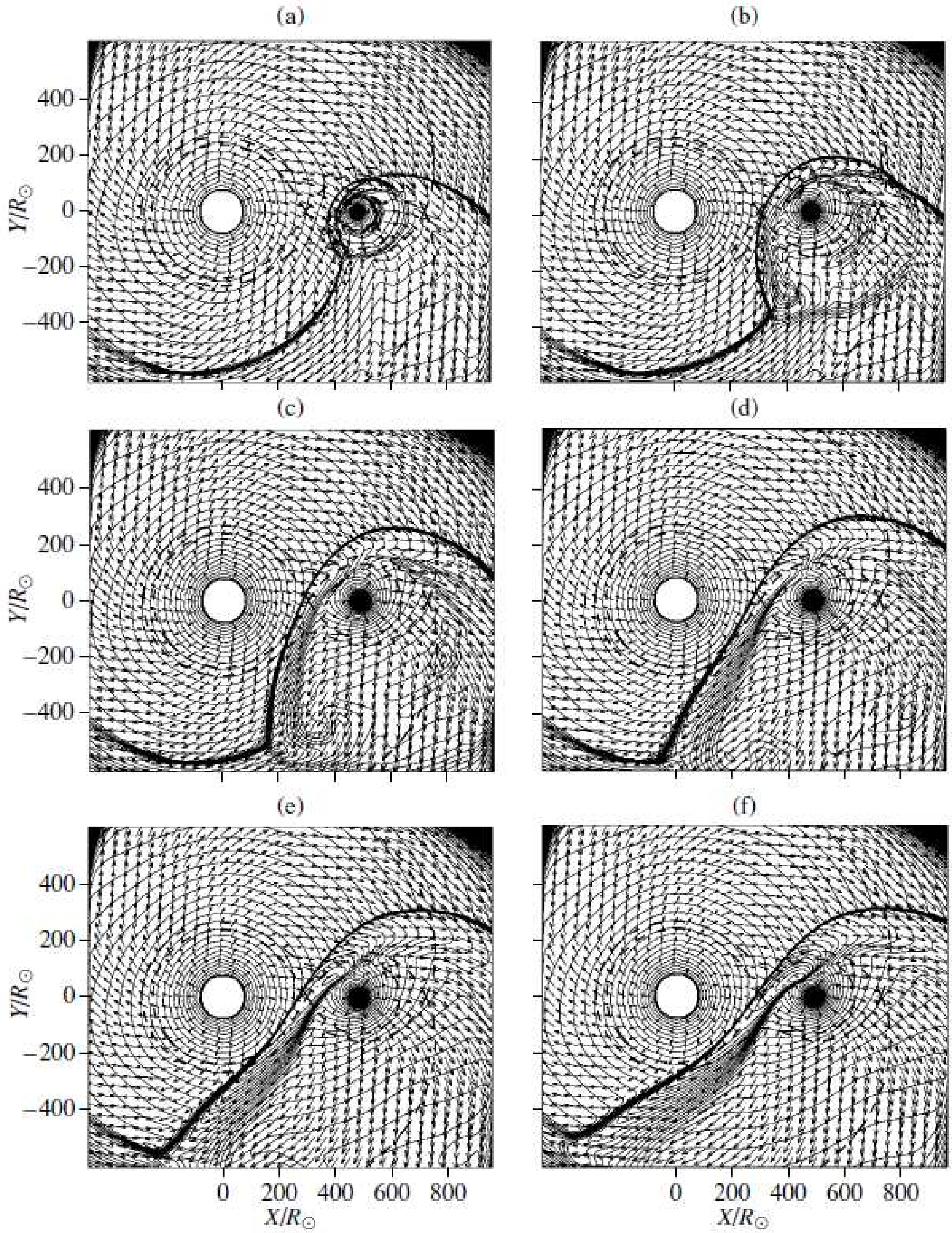

Figure 5.5: Contours of equal density and velocity vectors for six moments during the outburst's development: (a) 12, (b) 42, (c) 70, (d) 103, (e) 125 and (f) 150 days after the start of computations. The hollow circle denotes the donor (the radius corresponds to the donor radius).

at the accretor's surface is 50 $\mathrm{km\,s^{-1}}$. The density distribution and the velocity vectors for the entire computational domain are shown for six times corresponding to 12, 42, 70, 103, 125, and 150 days after the start of the computations (the change of the conditions at the accretor's surface). Shocks are seen as concentrations of the density contours. The orbital motion of the accretor is counterclockwise. The dashed lines show the contours of the standard Roche potential. It is seen that the system of shocks forms fairly quickly – the shock occupies its final location on the X axis between the components already after about 70 days (Fig. 5.5 (c)). The analysis of the results shows that the shock is established first between the components and in the regions above and below the line of their centers it forms 20 – 30 days later (Fig. 5.5 (d)). Further the parameters of the shock do not change substantially (Figs. 5.5 (d)– 5.5 (f)).

Summarizing the results of the numerical modeling it must be expected that the contribution of the wind will begin to be significant on the time scale of tens of days. The third process, formation of shock structures, will begin to manifest in the light of the system 70 days after the wind's appearance. It will reach its maximum after 20 – 30 days in addition.

In our analysis of the light curve of the 2000 – 2002 brightening of Z And we can assume that the first maximum, when the light rose by 1.9^m in ~ 60 days, is determined only by the expansion of the optically thick pseudophotosphere (the first process). It is known from observations (Sokoloski et al. 2006) that the first kink of the light curve appeared close to September 15, 2000, and is related to the onset of the wind of the hot component. Assuming that the time of the wind appearance is close to September 15, 2000, it can be expected , according to the computations, that for a wind velocity of 50 $\mathrm{km\,s^{-1}}$ the shock will begin to form 70 days after the rise of the first kink, i.e. after the appearance of the wind. The analysis of the light curve shows that the second change of its slope realizes on November 13, 2000, i. e. after 60 days. The peak associated with the formation of the shock should be shifted at 20 – 30 days (according to the computations), while the observational data show that it forms after 25 days (December 6, 2000). Thus, the comparison of the results of the computations with the observations shows all main stages of the change of the light are in good agreement with the model.

To be sure that the presence of the wind (the second process) and the shock (the third process) really provide the observed light variations we must estimate their contributions.

The contribution of the hot wind to the light of the system can be estimated assuming that the location of the shock – the boundary of the areas of the two winds, is determined by the condition for equality of the ram pressures: $\rho_1 v_1^2 = \rho_2 v_2^2$. We can estimate the density of the hot wind assuming

Table 5.1: Emission of the hot wind.

Photometric waveband	Flux, 10^{-12} erg·cm^{-2}s^{-1}Å^{-1}	Fraction of the nebula emission on November 22.11.2000
U	0.4646	23%
B	0.1346	19%
V	0.1180	19%

that the boundary is located in the middle of the components' separation (Fig. 5.5). Using the known parameters of the donor's wind (a mass-loss rate of $\sim 2 \times 10^{-7} M_{\odot}\,\mathrm{yr}^{-1}$, a velocity of 30 $\mathrm{km\,s^{-1}}$) and the velocity of the hot wind (50 $\mathrm{km\,s^{-1}}$), we can estimate the mass-loss rate of the hot component. It turned out to be $\sim 1.2 \times 10^{-7} M_{\odot}\,\mathrm{yr}^{-1}$.

Assuming that the hot wind is spherically symmetric we can calculate its UBV fluxes emitted by a spherical layer. The inner boundary of this layer is equal to $2.2\,R_{\odot}$ and is close to the observed radius of the pseudophotosphere on November 22, 2000 and the outer one of $240.5\,R_{\odot}$ is equal to the half of the component separation. The emission of the region beyond the outer edge can be neglected. It was supposed in our calculations that the gas consists of hydrogen and ionized helium (the wind region is hot), the helium abundance is 0.1, and the distance to the system is 1.12 kpc. The contribution of the wind in the UBV bands is shown in Table 5.1. It is seen that it is fairly large being on average $\sim 20\%$ on November 22, 2000. However, as we will see in the Section 6 of this chapter, a model without spherical symmetry of the wind is need to explain the line spectrum of Z And . The emission of such a wind was calculated in the work of Tomova (2014) with use of a mass-loss rate based on high-resolution spectral data from the paper of Tomov et al. (2008). This emission is very close, but greater than that, calculated by us.

In regard to the contribution of the shock, according to the computations we can present the following view. A calculated structure of the wind collision is presented in Fig. 5.6. The notation is similar to that in Fig. 5.5. The region in the vicinity of the shocks is shown in Fig. 5.7 in more detail.

Our analysis shows that the region between the shocks has a considerably higher temperature than the surrounding medium: on the X axis passing through the component centers, it is higher by a factor of 50 than in the surrounding regions of the nebula and reaches 10^6 K. This is in agreement with the results of Nussbaumer & Walder (1993) for their model of a symbiotic binary with colliding winds. It was suggested in their work that just the high-temperature region between these shocks is the source of the X-ray emission observed from some symbiotic stars. Our estimates based on the method described in Girard & Willson (1987) show that for the assumed parameters

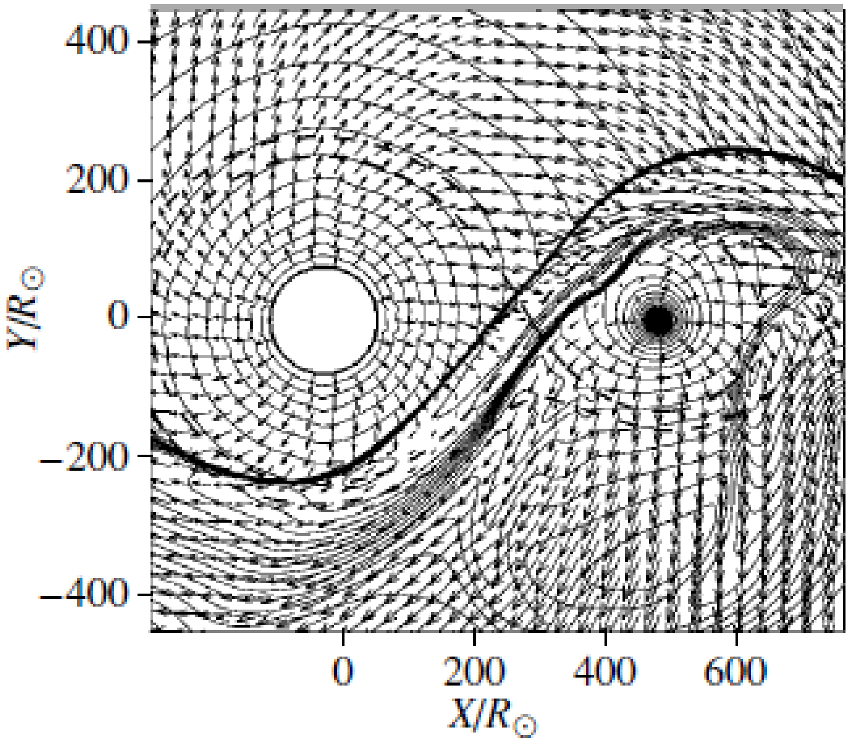

Figure 5.6: Contours of equal density and velocity vectors for the two-dimensional computations. The hollow circle denotes the donor (the radius corresponds to the donor radius). The distances are in solar radii.

of the winds and the computed area of the shock the X-ray luminosity is $10^{31} - 10^{32}$ erg. This result is in very good agreement with the observed X-ray luminosity during the 2000 outburst of Z And (Sokoloski et al. 2006).

Summarizing our results we conclude that both the propagation of the wind (the second process) and the development of shock structure (the third process) can significantly determine the light behaviour of the system. Since the appearance of these phenomena in the framework of the model is at the same time as observed, we suggest that precisely they are responsible for the observed behavior.

During the $2000-2002$ brightening of Z And a very good set of data describing one too detailed curve of the rise of the optical light, which shows its multistage pattern, was obtained (Sokoloski et al. 2006). This set of data provides possibility the light to be interpreted in detail and we proposed a model where a number of mechanisms to explain both the consecutive stages of the rise and the details of the curve are taken into consideration. To explain the

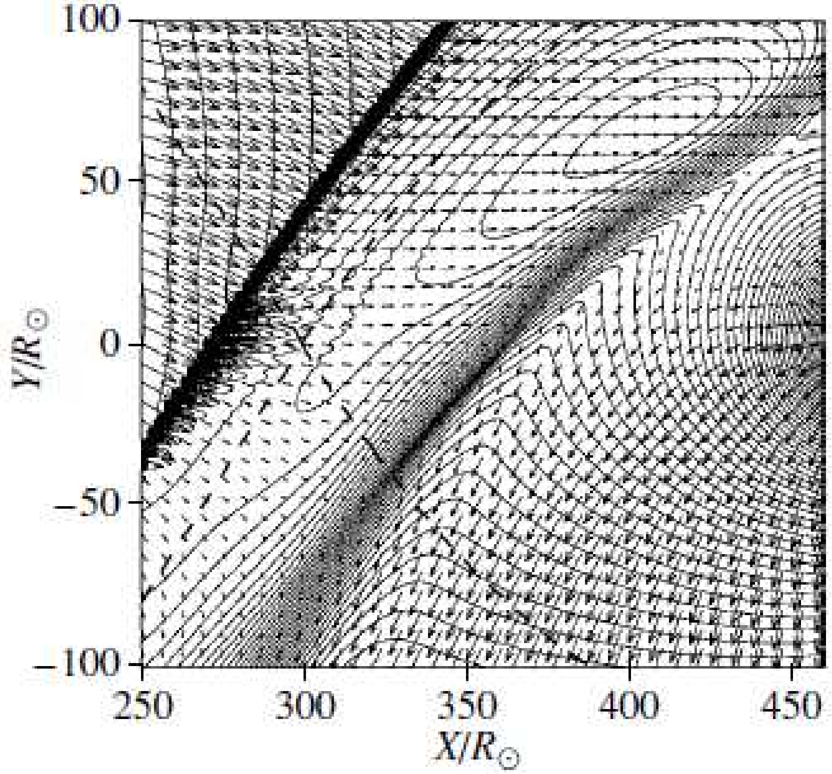

Figure 5.7: Contours of equal density and velocity vectors in the region of the shocks.

increase of the bolometric luminosity we suggested "combined" mechanism of the outburst where the increased accretion rate leads to change of the burning rate. To explain all details of the change of the light an appearance of stellar wind (massoutflow) from the outbursting accretor and development of shock structure was secured in the framework of our model.

The observational data (photometric and spectral ones) obtained during the next brightenings of Z And revealed again both the increase of the bolometric luminosity and the expansion of (massoutflow from) the outbursting accretor. The set of these data, however, was not so full to reveal all details of the change of the optical light. Nevertheless, the "combined" mechanism, proposed by us, including an appearance of stellar wind and system of shock waves should be used for interpretation of the light behaviour during these brightenings too.

5.2.3 Comparison with observations and contribution of the shock to the total light of the system

In the previous section we showed that the proposed scenario of the outburst based on our modeling is in good agreement with the observed temporal behavior of the light. If this model is correct, the presence of the shock will also result in other observed effects, for example, such as existence of shock ionization in the nebula. Let us consider some results of the observations of the Z And brightening.

According to the observational data (Sokoloski et al. 2006; Tomov et al. 2003a), the last stage of the rise of the light started on November 13, 2000 (JD 2 451 862) and lasted for about 25 days. In the proposed scenario this stage is provided by formation of a system of shocks resulting from the collision of the winds. To estimate the influence of these shocks on the light of the system we used the results from the work of Tomov et al. (2003a), where the basic parameters of the system's components (the cool component, the hot component, and the nebula) and their continuum fluxes were estimated from observational data.

The continuum fluxes of the components of Z And for November 22 and December 6, 2000 (Tomov et al. 2003a) are listed in Table 5.2. These data show that the emission of both the nebula and the hot component increased during this time interval. We used the difference between the total (model) and the observed fluxes as a percentage of the observed flux as a criterion for the agreement between the model continuum and the observed one. On the other hand, the UV continuum fluxes at wavelengths 1059 and 1103 Å where only the hot component emits, taken from the work of Sokoloski et al. (2006), show that its emission increased during the period November 16 – November 27, 2000, and was constant after that, till December 15, 2000. The result of the continuum analysis is in qualitative agreement with the UV data, as far as the time interval November 22 – December 6 covers the interval November 22 – 27 when the emission of the hot component was rising. However, since this emission was not changing between November 27 and December 15, we propose a second case of the continuum analysis for December 6 too in Table 5.2, with a smaller growth of the radius of the hot component. When we calculate the emission due to shock ionization we shall consider this second variant too, since it is in better agreement with the observed behavior of the hot component in the UV, although the total and the observed fluxes in the infrared are in better agreement in the first variant.

Table 5.2: The continuum fluxes of the system's components in units 10^{-12} erg cm^{-2} s^{-1} Å^{-1}. The uncertainties of the observed values are in the same units. Adapted from Tomov et al. (2003a).

Date	SC[a]	U	B	V	R	I	J	H	K	L	M
2000 Nov. 22	Cool	0.020	0.160	0.376	0.710	1.755	1.343	0.856	0.439	0.113	0.034
Active	Hot	5.537	2.934	1.336	0.730	0.340	0.063	0.022	0.007		
	Neb.	1.983	0.717	0.631	0.547	0.432	0.147	0.081	0.051	0.020	
	TF	7.540	3.811	2.343	1.987	2.527	1.553	0.959	0.497	0.133	0.034
$R_{\rm hot} = 2.22\,R_{\odot}$	OF	7.205	3.848	2.492			1.591	0.927	0.461	0.117	0.024
EM $= 17.4 \times 10^{59}$ cm^{-3}		±0.054	±0.036	±0.022			±0.002	±0.001	±0.001	±0.001	±0.001
	r	5	−1	−6			−2	3	8	14	42
2000 Dec. 06	Cool	0.020	0.160	0.376	0.710	1.755	1.343	0.856	0.439	0.113	0.034
Active	Hot	6.257	3.315	1.510	0.826	0.384	0.071	0.024	0.008		
	Neb.	2.382	0.861	0.758	0.657	0.519	0.176	0.098	0.061	0.024	
Case 1:	TF	8.659	4.336	2.644	2.192	2.658	1.590	0.978	0.508	0.137	0.034
$R_{\rm hot} = 2.36\,R_{\odot}$	OF	8.662	4.257	2.682			1.635	0.944	0.478	0.120	0.024
EM $= 20.9 \times 10^{59}$ cm^{-3}		±0.064	±0.039	±0.023			±0.001	±0.001	±0.001	±0.001	±0.001
	r	0	2	−1			−4	4	6	14	42
2000 Dec. 06	Cool	0.020	0.160	0.376	0.710	1.755	1.343	0.856	0.439	0.113	0.034
Active	Hot	5.841	3.094	1.410	0.770	0.358	0.066	0.023	0.007		
	Neb.	2.737	0.989	0.871	0.754	0.600	0.202	0.114	0.074	0.030	
Case 2:	TF	8.598	4.243	2.657	2.234	2.713	1.611	0.993	0.520	0.143	0.034
$R_{\rm hot} = 2.28\,R_{\odot}$	OF	8.662	4.257	2.682			1.635	0.944	0.478	0.120	0.024
EM $= 24.0 \times 10^{59}$ cm^{-3}		±0.064	±0.039	±0.023			±0.001	±0.001	±0.001	±0.001	±0.001
	r	−1	0	−1			−1	5	9	19	42

[a] The system's components, TF=Cool+Hot+Nebular – total flux, OF – observed flux, r=(TF−OF)/OF in %.

According to the proposed model three processes contribute to the light curve: the rise of luminosity causing an expansion of the envelope, the rise and development of the high temperature region in the nebula formed by the white dwarf's hot wind, and the shock structure formed by the collision of the winds.

The most correct approach to determine the contribution of the shock is to estimate the shock ionization. Let us consider the ratio of the number of ionizing photons and the number of recombinations in the nebula μ in the quiescence and on November 22 and December 6, 2000. This ratio is estimated as

$$\mu = \frac{L}{n_e n_+ \alpha V} \ , \tag{5.1}$$

where L is the Lyman photon luminosity of the hot component, n_e and n_+ are the number densities of the electrons and ions respectively, α is the total (to all levels) recombination coefficient, and V is the volume of the nebula. The Lyman luminosity is

$$L = 4\pi R^2 H_{\lambda<912} = 8\pi^2 \frac{R^2}{c^2} \left(\frac{kT}{h}\right)^3 G(T) \ , \tag{5.2}$$

where R and T are the radius and effective temperature, $G(T)$ is a function related to the number of the ionizing photons (given in numerical form in the book of Pottasch (1984)), and the remaining quantities have their commonly accepted meaning. The number of recombinations is

$$n_e n_+ \alpha V = [1 + a(\mathrm{He})]\, \alpha n^2 V \ , \tag{5.3}$$

where a(He) is the number abundance of helium relative to hydrogen. If we obtain from observations the radius and the effective temperature of the hot component and the emission measure of the nebula in addition, we will calculate the ratio μ.

In the state of ionization equilibrium when only radiative ionization is realized in the nebula $\mu \geq 1$. The equality is satisfied when all photons are absorbed in the nebula. When $\mu < 1$ the number of recombinations is greater, which means that shock ionization is realized in the nebula along with radiative one. The ratio of the continuum fluxes due to shock and radiative ionization is $(1-\mu)/\mu$ when all photons are absorbed in the nebula. In some cases of the distribution of the circumstellar gas some fraction of the photons can leave the nebula. Then $(1-\mu)/\mu$ is a lower limit of the ratio of the continua corresponding to shock and radiative ionization.

Table 5.3: Ratio of the numbers of ionizing photons and of recombinations at various times.

Date (state of the system)	μ
15.09.1999 (quiescence)	1.12
22.11.2000 (outburst, rise to the second maximum)	$1.00^{+0.25}_{-0.21}$
06.12.2000 (outburst, close to the maximum) – variant 1	$0.94^{+0.24}_{-0.20}$
06.12.2000 (outburst, close to the maximum) – variant 2	$0.76^{+0.24}_{-0.20}$

The ratio μ was calculated with use of the parameters of the system's components determined for different times during the outburst in the work of Tomov et al. (2003a). It was found in this work that the dominant ionization state of helium in the nebula in quiescence is He^{++} and during the outburst – He^{+}. It was assumed that the nebular continuum in quiescence is emitted by hydrogen and ionized helium and during the outburst – by hydrogen and neutral helium. These assumptions were taken into account when computing μ. For this purpose the value of a(He) was doubled for quiescence. The helium abundance was taken to be 0.1, in accordance with the results of Nussbaumer & Vogel (1989). It was assumed that the average number density in the Z And nebula is $10^8 - 10^{10}$ cm^{-3} (Fernandez-Castro et al. 1988; Proga et al. 1994; Mikolajewska & Kenyon 1996; Birriel et al. 1998). The recombination coefficients were taken from Storey & Hummer (1995) for Menzel case B.

The computational results and their rms errors are presented in Table 5.3. The errors were derived from the uncertainties of the parameters of the system given in Tomov et al. (2003a). We did not present the error for the quiescence, since in this case the Lyman luminosity was calculated using the average temperature from the results of other authors, based on UV data. We present both variants for December 6, 2000.

The data in Table 5.3 show that $\mu > 1$ in quiescence (September 15, 1999). It is known that the Z And nebula is partially ionized in quiescence (Fernandez-Castro et al. 1988; Mikolajewska & Kenyon 1996; Schmid & Schild 1997; Birriel et al. 1998) and our result (within the errors) indicates that some fraction of the photons leave the ionized region. The ratio μ is equal to unity for November 22, 2000 (less than in quiescence) and less than unity for December 6, 2000. Thus it decreases with time, which means that the role of the shock ionization increases.

The second case for the time of the light maximum proposes $\mu = 0.76$.

Table 5.4: Fluxes from various regions of the nebula in units of 10^{-12} erg cm^{-2} s^{-1} Å^{-1}.

Source	U	B	V
22.11.2000			
Entire nebula	1.983	0.717	0.631
Hot wind (second term)	0.465	0.135	0.118
Shock (third term)	0	0	0
Cool region of the nebula	1.518	0.582	0.513
06.12.2000 – variant 2			
Entire nebula	2.737	0.989	0.871
Hot wind (second term)	0.465	0.135	0.118
Shock (third term)	0.657	0.237	0.209
Cool region of the nebula	1.615	0.617	0.544

This means there is no doubt that the shock ionization takes place and its contribution to the emission of the nebula is not less than 0.24 (since some fraction of the photons can leave the nebula). This contribution can be as high as 0.44 when we take into account the observational uncertainties. The UBV fluxes determined by the shock ionization in the case of $(1-\mu) = 0.24$ are presented in Table 5.4. The contribution of the wind is presented also in this table. This contribution is the same for the two epochs since the parameters of the wind are considered to be constant and, according to the model (Fig. 5.5), the boundary between the winds does not change after some time. Subtracting the contribution of the hot wind and the shock from the total emission of the nebula, we find that the flux of its cool part changes because of the increase of the radiative ionization during the period November 22 – 27, 2000 resulting from the growth of the hot component's luminosity. This change, however, is insignificant.

Thus, our analysis of the observational data shows that the light variations at the last stage of the outburst's development are well explained by means of the proposed scenario and consequently can be interpreted in the framework of the model of the colliding winds.

5.3 The line spectrum during the 2000 – 2002 outburst

The line spectrum of Z And during its 2000 – 2002 brightening was described and interpreted in the works of Tomov et al. (2003a, 2008, 2010b, 2011a,b); Tomova, Tomov et al. (2008); Kilpio et al. (2011).

Table 5.5: List of the observations in 2000 – 2002.

Date	JD– 2 450 000	Orb. phase	Spectral region
1999 Jan. 7	1186.50	0.228	He II λ 4686, H_γ
1999 Sept. 17	1439.48	0.562	He II λ 4686, H_γ
1999 Nov. 27	1510.24	0.656	He II λ 4686, H_γ
2000 Nov. 17	1866.36	0.125	He II λ 4686, H_γ
2000 Dec. 5	1884.35	0.148	He II λ 4686, H_γ
2000 Dec. 6	1885.38	0.150	He II λ 4686, H_γ
2001 July 8	2098.54	0.432	He II λ 4686, H_γ
2001 Sept. 7	2160.44	0.512	He II λ 4686
2001 Oct. 3	2186.47	0.547	He II λ 4686, H_γ
2002 Jan. 23	2298.25	0.694	He II λ 4686, H_γ

5.3.1 Observations and reduction

The regions of the lines He II λ4686 and H_γ of the spectrum of Z And were observed on ten nights with the Photometrics CCD camera mounted on the Coudé spectrograph of the 2m RCC telescope of the National Astronomical Observatory Rozhen. The spectral resolution was 0.2 Å px^{-1}. Ever when we made more than one exposure per night, the spectra were added with the aim to improve the signal to noise ratio. Three of the nights were in 1999 when the star was at the quiescent state and the other ones – during the time of its 2000 – 2002 outburst (Table 5.5). The IRAF package[1] was used for data reduction as well as for obtaining the dispersion curve and calculating the radial velocities and equivalent widths.

The absolute fluxes of some selected lines in the observed regions were calculated with use of their equivalent widths and the continuum fluxes at their positions based on *BV* photometric data.

The *BV* fluxes were corrected for the strong emission lines of Z And. The quiescent data and those, obtained after February 2001 were corrected in the same way as the quiescent data in the paper of Tomov et al. (2003a). The fluxes, related to the other epochs were not corrected because of the strong increase of the stellar and nebular continua and the relative decrease of the emission lines (Tomov et al. 2003a).

All the fluxes were corrected for an interstellar reddening of $E(B-V) =$

[1] The IRAF package is distributed by the National Optical Astronomy Observatories, which is operated by the Association of Universities for Research in Astronomy, Inc., under contract with the National Science Foundation.

0.30 using the extinction law of Seaton (1979).

5.3.2 Analysis of the spectrum

He I lines

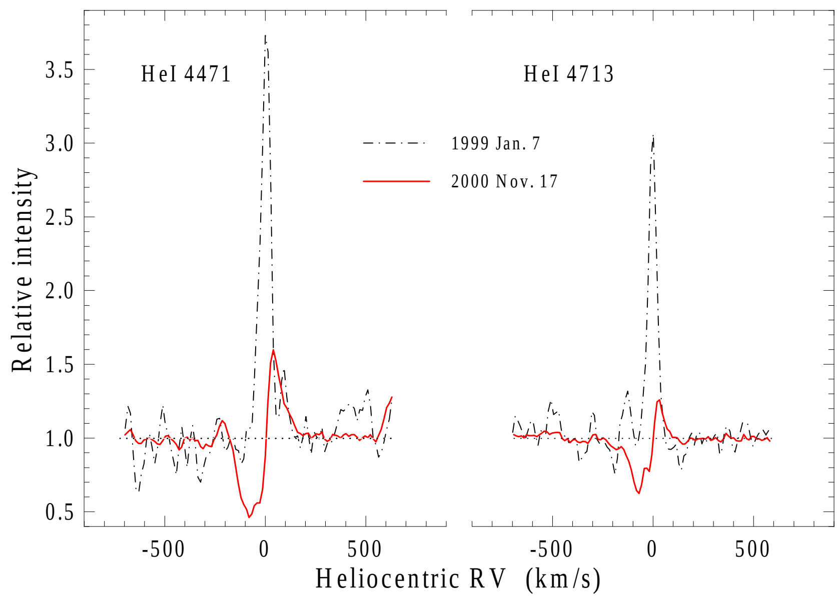

Figure 5.8: The profiles of the He I triplet lines during the quiescent and active phase.

The triplet lines of helium He I $\lambda\,4471$ and He I $\lambda\,4713$ had purely emission profile and FWHM $= 45 \div 50$ km s^{-1} in the quiescent state of the system. A blue-shifted absorption appeared in November and December 2000 during the time of the maximal light (Fig. 5.8). In November this absorption had a two- component structure. The He I $\lambda\,4471$ line reached a residual intensity of 0.46 in November and 0.60 in December. As the cool giant's continuum at the same time amounted to about 0.07 – 0.08 of the total continuum of the system at the wavelengths of these lines (Tomov et al. 2003b), their appearance can be related to the hot companion. We observed the system at orbital phases close to the spectral conjunction, where the radial velocity of the companion is close to 0 km s^{-1} (Mikolajewska & Kenyon 1996). Then the velocity of the absorption components of about -60 km s^{-1} is related to the outflowing material from the companion. In this case, we can only suppose that the companion's photosphere has been expanded and we have observed a P Cyg stellar wind. The fluxes of the helium lines are listed in Table 5.6.

Table 5.6: The fluxes of the He I lines of Z And during its 2000 – 2002 outburst in units 10^{-12} erg cm^{-2} s^{-1}.

Date	Orb. phase	He I λ 4388	He I λ 4471	He I λ 4713
1999 Jan. 7	0.228	0.736	0.861	0.627
1999 Sept. 17	0.562	0.987	2.459	1.050
1999 Nov. 27	0.656	0.772	1.729	0.697
2000 Nov. 17	0.125	2.202		
2000 Dec. 5	0.148	2.308		
2000 Dec. 6	0.150	2.265		
2001 July 8	0.432	2.215	3.160	1.937
2001 Sept. 7	0.512			1.717
2001 Oct. 3	0.547	2.093		1.648
2002 Jan. 23	0.694	1.339	2.156	1.215

He II λ 4686 line

All of our spectra showed the He II λ 4686 line has single-peaked core and extended low intensity variable wings, indicating velocity of several hundreds km s^{-1}. The intensity of the wings reached its maximum at the time of the maximal light, whereas the intensity of the core had a minimal value at that time. Moreover the wings displayed rapid variability on a timescale of about one day and the core did not (see below). These facts gave us a reason to suppose that the core and the wings were two different components of the line. We called these a narrow central component and a broad component with a low intensity.

The behaviour of the radial velocity of the narrow component during the outburst differed greatly from that in the quiescent state. In quiescence, this velocity was close to the velocity of the centre of mass of the system. During the active phase, however, its behaviour resembled the orbital velocity of a secondary stellar component (Fig. 5.9). This behaviour, as well as the increased width of the line, suggests that it was emitted probably in the expanding shell of the companion. The emission region of the line was probably decreased and was related only to the close vicinity of the companion since its flux became smaller.

In the quiescent state the broad component of the He II λ 4686 line was very weak. Its existence was concluded on the basis of the presence in its wavelength region of an emission exceeding the level of the local continuum. This emission is associated with a number of details, which are related neither

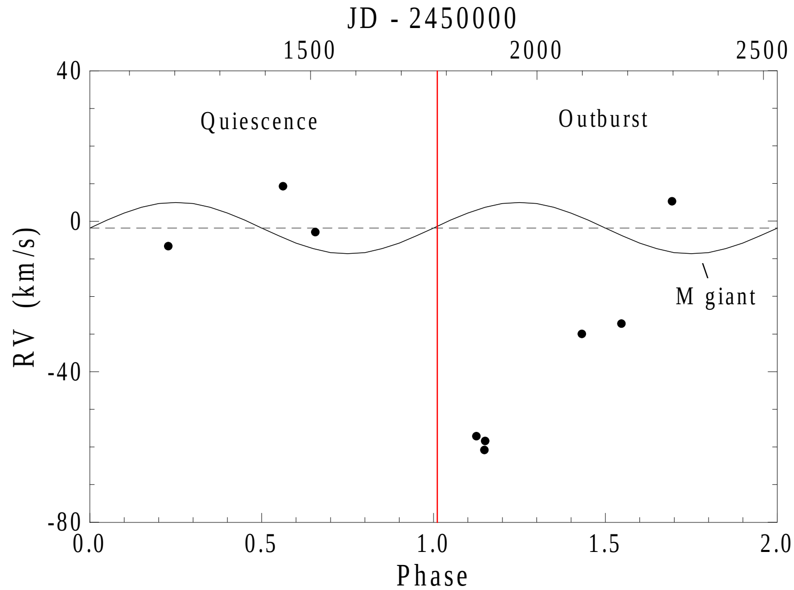

Figure 5.9: The variations of the radial velocity of the He II $\lambda\,4686$ line. The uncertainty of the measurement reaches up to 3 $\mathrm{km\,s^{-1}}$. For comparison the behaviour of the velocity of the cool giant in the system is shown as well, according to the orbital solution of Formiggini & Leibowitz (1994).

to the noise of the detector nor to nebular spectral lines. However, as this emission is too weak, it cannot be measured with adequate accuracy. With regard to its possible origin, we cannot exclude the possibility of electron scattering in the surroundings of the compact companion in so far it is a hot high-luminosity object.

During the active phase the broad emission increased and its height above the level of the local continuum reached up to 0.2. We analyzed this emission by fitting with a Gaussian function (Fig. 5.10). Its FWHM obtained with this procedure is listed in Table 5.7. The equivalent width was obtained with an error reaching up to 25 per cent, which depends mainly on the level of the local continuum. However, as the broad emission is not clearly visible because of blending with the central narrow component and its profile is actually not Gaussian, the error of the equivalent width is greater than this value.

The broad component of the He II $\lambda\,4686$ line indicate a high velocity and, as it is emitted in close vicinity of the hot companion, most probably the high velocity is related to nebular material ejected by the companion. The Gaussian fit shows that the centre of the broad emission is close to the laboratory wavelength and its blue wing is less visible than the red wing

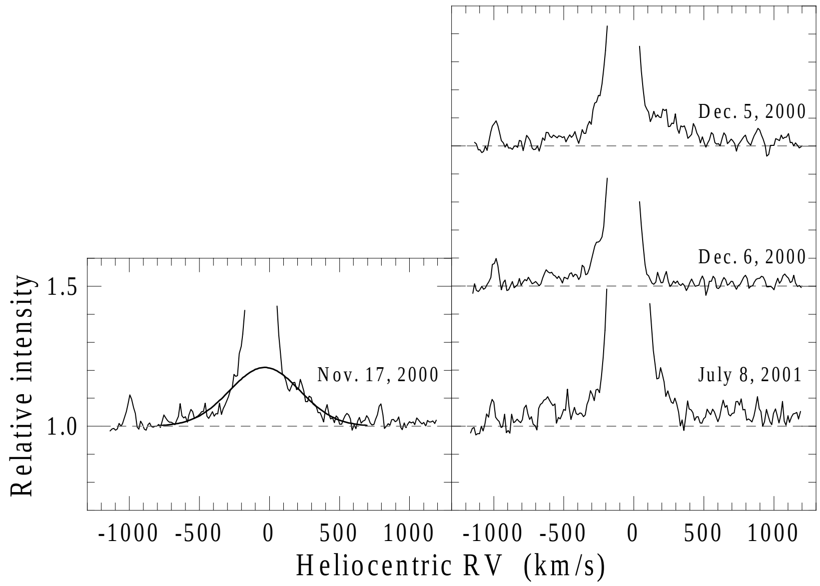

Figure 5.10: The area of the wings of the He II $\lambda4686$ line where the Gaussian fit of its broad component is seen. The spectra show the rapid variability of the broad component. The level of the local continuum is marked with a dashed line.

because of blending with the blueshifted narrow component of the line.

In some cases, the broad component underwent strong variations on a time-scale of about one day. For example, its red wing was much weaker on 2000 December 6 than on 2000 December 5 (Fig. 5.10). That is why we propose that the broad component was a result of a variable stellar wind with a high velocity (Table 5.7). The velocity was obtained on the basis of the FWZI of the line.

5.4 The line spectrum during the outburst at the end of 2002

The line spectrum of Z And during its brightening at the end of 2002 was described and interpreted in the works of Tomov et al. (2005a,b, 2009, 2010a,b).

5.4.1 Observations and reduction

High resolution data in the regions of the lines H_α and H_γ of the spectrum of the Z And system were obtained in 2002 with a Photometrics CCD camera

Table 5.7: The He II λ4686 line data.

Date	Orb. phase	RV ($km\,s^{-1}$)	FWHM(N) ($km\,s^{-1}$)	F(N)	FWHM(B) ($km\,s^{-1}$)	FWZI(B) ($km\,s^{-1}$)	v_{fast} ($km\,s^{-1}$)	F(B)
1999 Jan. 7	0.228	−6.65	71.0	32.84				
1999 Sept. 17	0.562	9.34	64.0	39.35				
1999 Nov. 27	0.656	−2.88	71.0	37.15				
2000 Nov. 17	0.125	−57.13	119.6	14.54	590 ± 40	1240	620	7.198
2000 Dec. 5	0.148	−60.78	132.4	14.93	560 ± 43	1180	590	7.234
2000 Dec. 6	0.150	−58.41	119.6	15.78				
2001 July 8	0.432	−29.94	123.5	30.17	680 ± 150	1340	670	3.489
2001 Sept. 7	0.512		108.8	34.96	500 ± 80	980	490	2.988
2001 Oct. 3	0.547	−27.19	104.9	29.35	500 ± 50	950	480	3.055
2002 Jan. 23	0.694	5.31	83.2	30.31	390 ± 35	730	370	1.394

N – narrow component
B – broad component
F = F $\times$ 10^{-12} $erg\,cm^{-2}\,s^{-1}$

mounted on the Coudé spectrograph of the 2m RCC telescope of the National Astronomical Observatory Rozhen (Table 5.8). The spectral resolution was 0.2 Å px^{-1} on all occasions. The IRAF package was used for data reduction as well as for obtaining the dispersion curve and calculating the radial velocities and equivalent widths.

The absolute fluxes of the observed lines were calculated by using their equivalent widths and the continuum fluxes at their positions (Tomov et al. 2008). The continuum fluxes in range of the line H_γ were obtained using linear interpolation of the B and V photometric fluxes on the same night or close nights. The continuum flux at the wavelength position of the H_α line

Table 5.8: List of the observations in 2002 and the H_α flux in units 10^{-12} $erg\,cm^{-2}\,s^{-1}$.

Date	JD 2 452 000+	Orb. phase	H_α flux
Sept. 25	543.35	0.017	173.494
Oct. 20	568.37	0.050	255.255
Nov. 12	591.20	0.080	292.098

was calculated using linear extrapolation of the V and R photometric fluxes taken also on the same night or close nights. To calculate the fluxes of the spectra from September and October we used photometric data of Skopal et al. (2004). The fluxes of the spectra obtained in November were calculated on the basis of the photometric data for November 12, 2002 from our work Tomov et al. (2004).

The BV fluxes were corrected for the strong emission lines of Z And in the same way as the quiescent data in the work Tomov et al. (2003a) because of the fact that the heights of these lines during the active phase were practically the same as those in the quiescence.

All the fluxes were corrected for the interstellar reddening of $E(B-V) = 0.30$ using the extinction law of Seaton (1979).

5.4.2 Analysis of the spectrum

$\mathbf{H_\alpha}$ line

In the quiescent state of the system the line H_α was of nebular type, but had, in addition, broad wings extended to not less than ± 2000 km s^{-1} from its center. It exceeded the local continuum by a factor of more than 100 at orbital phases close to 0.5 (Tomov et al. 2008). The width (FWHM) of the line was about $100-120$ km s^{-1} and only occasionally went beyond this value. The width remained the same during the 2000 – 2002 optical brightening too (Tomov et al. 2008). The view that the broad wings of the line in the quiescent state of the system are due to Raman scattering of Lyβ photons by atomic hydrogen is widely accepted (Lee 2000; Arrieta & Torres-Peimbert 2003; Tomov et al. 2008). Lee (2000), though, considered an other theoretical possibility for their appearance too. This author noted that Raman scattering and radiation damping depend on the wavelength in the same way, and the latter also cannot be excluded.

During the growth of the light at the end of 2002 the line was double (Fig. 5.11), it exceeded the local continuum by a factor of about 30 and its width increased by a factor of two. The dip between the two peaks had the same radial velocity at all times of observation.

According to the theoretical modeling of the flow structure in a system with parameters close to those of Z And (see Sect. 5.6), after each individual outburst of the active phase an extended disc-like envelope of a nebular nature covering the existing to that time accretion disc forms as a result of accretion of material from the potential well of the compact object. In such a case we can suppose that the double-peaked profile is determined from Keplerian motion in an accretion structure although the Balmer lines of the

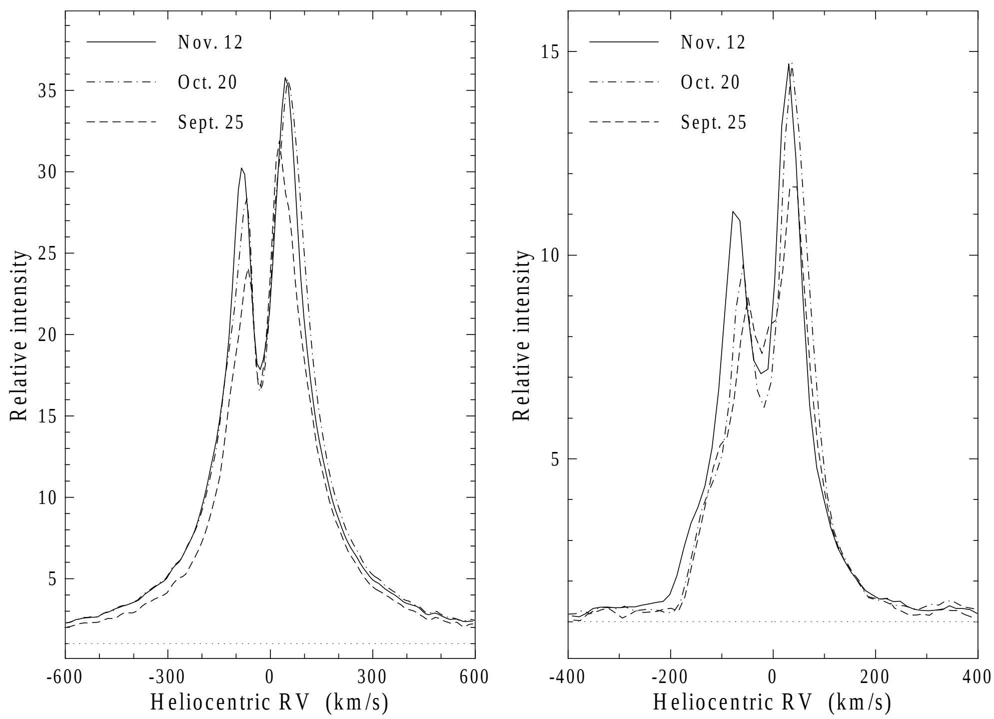

Figure 5.11: The profiles of the H_α (left panel) and H_γ (right panel) lines. The level of the local continuum is marked with a doted line.

symbiotic stars are always influenced by optical depth effects. Let us check this supposition.

If the H_α profile is radiated by an accretion disc, the growth of the emission during the brightening should be mainly due to its formation and this growth should be large. The H_α emission in this case is a sum of the emission of the circum-binary nebula and the disc. The emission of the nebula can increase or at least will not decrease during the brightening. At the same time disc's emission must predominate over that of the nebula to determine the profile. To examine it, we will compare the H_α flux during the brightening with its quiescent value.

The intensity of the Balmer emission lines of Z And varies with the orbital phase (Mikolajewska & Kenyon 1996; Tomov et al. 2008) and their flux during the brightening must be compared with the quiescent one at the same phase. We were not able to find in the literature Balmer fluxes at orbital phase close to 0 in the quiescent state of Z And. Mikolajewska & Kenyon (1996) have obtained the H_α flux at phases 0.16 – 0.34 where it increases from 40 $\times$ 10^{-12} to 103 $\times$ 10^{-12} $\mathrm{erg\,cm^{-2}\,s^{-1}}$. Schwank et al. (1997) have shown that the Balmer emission lines of symbiotic stars in their quiescent state are predominantly formed in the recombination zone which separates the H^{o} from the H^{+} region of the cool giant's wind since the density of this zone is the highest one. These authors have shown also that the Balmer lines are always self-absorbed emission lines. These theoretical considerations show that the absorption will be maximal at phase 0 where the giant is in its inferior conjunction because of the highest density of the absorbing particles. Then the line flux will have minimal value at this phase and in the case of Z And the H$_\alpha$ flux will be probably less than 40 $\times$ 10^{-12} erg cm^{-2} s^{-1}. The comparison of this flux with fluxes (170 $\div$ 290) $\times$ 10^{-12} erg cm^{-2} s^{-1} (Table 5.8) shows that it is strongly increased during the brightening, which can be due to addition of a new component in the line, possibly from an accretion disc. The same conclusion is obtained for the line H$_\gamma$ too. The data of Mikolajewska & Kenyon (1996) show that its flux at the orbital phase 0.0 is less than 2.1 $\times$ 10^{-12} erg cm^{-2} s^{-1} and the flux of the narrow component during the outburst is (16 $\div$ 29) $\times$ 10^{-12} erg cm^{-2} s^{-1} (Table 5.9).

Let us calculate the outer radius of the line emission region in the disc from the separation of the two peaks. The separation was equal to 2.8 $\pm$ 0.2 Å on November 12, 2002 at the time of the maximal light. To calculate the outer radius the orbit inclination is need. We will use the value of 55 deg as an upper limit of the orbit inclination (see the next subsection). At a mass of the hot component of 0.6 M$_\odot$ (Fernandez-Castro et al. 1988; Schmid & Schild 1997) for the upper limit of the outer radius of the emission region we obtain 19 $\pm$ 2 R$_\odot$ for orbit inclination of 55°. This result supports our supposition, as it is in agreement with the theoretical models of discs resulted from accretion of stellar wind (Mitsumoto et al. 2005).

The intensity of the H$_\alpha$ wings increased during the growth of the light at the end of 2002. Skopal (2006) obtained synthetic profiles arising from an optically thin bipolar stellar wind from the hot components of the symbiotic stars and was able to make a fit of the observed H$_\alpha$ wings of a sample of ten symbiotic stars. According to him, however, the profile formed in the stellar wind is approximated by a function of the same type as that arising from Raman scattering. For this reason he concluded that it is not possible to distinguish between these two processes directly. Ikeda et al. (2004) noted that the polarization profile of the H$_\alpha$ line of Z And does not agree with that of its Raman λ 6830 Å line on October 25, 2002, i.e. during the brightening considered by us. Based on the data of Ikeda et al. (2004) we suppose that the extended H$_\alpha$ wings of Z And during this brightening are probably not due to Raman scattered Ly$_\beta$ photons. Attention, however, should be paid to the fact that the FWZI of the H$_\alpha$ wings of Z And does not practically change during the active phase after the year 2000 and keeps its quiescent value of 4000 km s^{-1}. This fact gives us some reason to suppose that during the 2002 brightening the FWZI was determined mainly from radiation damping and the stellar wind can have some contribution in the wings at smaller distances from the centre of the line. The problem about the nature of these wings during active phase needs to be considered further.

H_γ line

The quiescent H_γ line of the system Z And was of nebular type and had an additional blue emission component with low intensity. Its width was about 80–90 $km\,s^{-1}$ and occasionally exceeded this value. The width remained the same during the 2000 – 2002 brightening like the line H_α (Tomov et al. 2008).

During the growth of the light at the end of 2002 an additional broad emission exceeding the local continuum by a factor of 1.3 and with a full width at zero intensity (FWZI) of about 2000 $km\,s^{-1}$ appeared together with the nebular component of the line (Figs. 5.11, 5.12). In this way the H_γ line consisted of a narrow component of a nebular type and a broad component. At the same time the behavior of the narrow component closely followed that of the H_α line. Its profile was double-peaked and the width increased by a factor of two compared with its quiescent value. The dip between two peaks of the line had the same radial velocity at all times of observations, which was close to the velocity of the dip of the H_α line (Fig. 5.13).

Let us calculate the outer radius of the emission region of the line in the disc using the separation between the two peaks. This separation was equal to 1.4 ± 0.1 Å on November 12 and with use of the parameters of the system adopted by us it gives an upper limit of the outer radius of $33 \pm 4\ R_\odot$ for orbit inclination of 55°. This radius is in agreement with the theory of discs formed as a result of wind accretion like the size of the H_α region (Mitsumoto et al. 2005). We obtained that the outer radius of the emission region of the H_γ line is greater than that of H_α but when atoms are excited as a result of recombination and the density decreases with the distance from the star, the region of the H_α line is expected to be located outward from that of H_γ.

The data propose not only greater peaks' separation of H_α, but also greater width of this line. If the emitting region is fully transparent in Balmer lines, their width will be the same. The Balmer lines of symbiotic stars, however, are always self-absorbed emission lines. The reason for the greater width and peaks' separation of H_α of Z And can be its higher optical depth compared to H_γ.

There is, however, an other possibility for the greater separation of the peaks of the line H_α, which follows from the flow structure. This line is possible to be emitted at greater distance from the orbital plane, but more close to the axis of the disc, where the rotational velocity is greater.

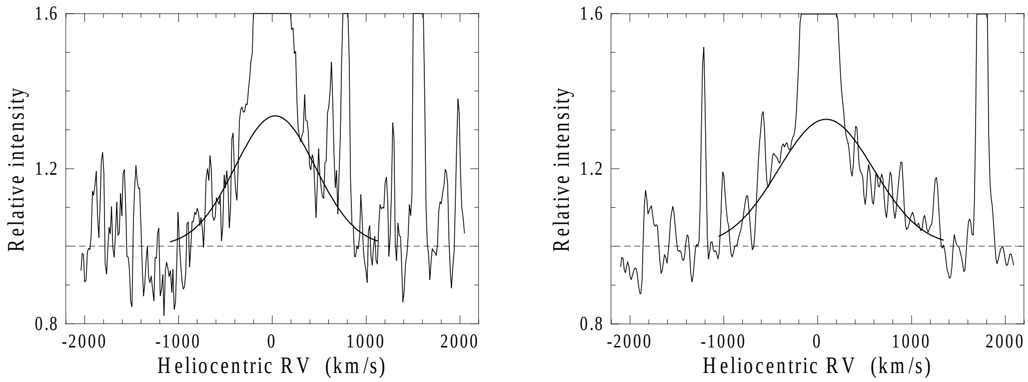

Figure 5.12: The H_γ (left panel) and He II $\lambda\,4686$ (right panel) broad components. The level of the local continuum is marked with a dashed line.

The broad component of the H_γ line was measured in the following way. The observed spectrum was corrected through removing several weak emission lines of Fe II, O II and N III as well as the most intensive absorption lines of the giant. After that it was analyzed by fitting with a Gaussian function (Fig. 5.12) and its parameters obtained with this procedure are listed in Table 5.9. The error of the equivalent width is not greater than 20 per cent depending on the noise of the different spectra.

To conclude about the nature of the gaseous environment where the broad component appeared we will treat different mechanisms of line broadening. One of them is the electron scattering. The total flux of the line, which is a sum of the fluxes of two components, is $(19 - 34) \times 10^{-12}$ erg cm^{-2} s^{-1} (Table 5.9). This gives emission measures of $(1 - 2) \times 10^{59}$ (d/1.12 kpc)^2 cm^{-3}. To calculate the radius of a spherical emitting volume, having this emission measure, the mean electron density is needed. Fernandez-Castro et al. (1988) obtained a mean quiescent electron density of 10^{10} cm^{-3} in the nebula of Z And. We assume that the mean electron density in the close vicinity of the compact object during the brightening is close to the quiescent electron density and will perform our calculations with the value 10^{10} cm^{-3}. We come to the same conclusion, however, if we use lower densities too. We obtain a radius of $(6 - 8) \times 10^{12}$ (d/1.12 kpc)$^{2/3}$ cm of the spherical emitting volume. If the broad component appeared due only to the electron scattering it would be risen in region with optical thickness of $0.17 - 0.19$. Using these values and a density of 10^{10} cm^{-3}, we derive the radius of almost 3×10^{13} (d/1.12 kpc)$^{2/3}$ cm, corresponding to an enormous emission measure of 10^{61} (d/1.12 kpc)^2 cm^{-3}. This result differs from the previous one and we conclude that the broad component is probably not produced by electron scattering.

Table 5.9: The data of the lines H_γ and He II $\lambda\,4686$. N and B denote narrow and broad component respectively. The flux is in units 10^{-12} erg cm^{-2} s^{-1} and the other quantities are in units km s^{-1}.

Date	FWHM(N)		Flux(N)		FWHM(B)		FWZI(B)		υ_h	Flux(B)	
	H_γ	He II	H_γ	He II	H_γ	He II	H_γ	He II	He II	H_γ	He II
Sept. 25	166	87	15.718	46.319	1014 ± 100	1091 ± 92	1900	2113	1050	3.193	3.713
Oct. 20	165	92	22.796	59.782	1073 ± 78	1170 ± 101	2100	2201	1100	4.885	5.234
Nov. 12	171	105	28.800	70.110	1010 ± 70	1192 ± 56	2030	2416	1200	5.236	6.658

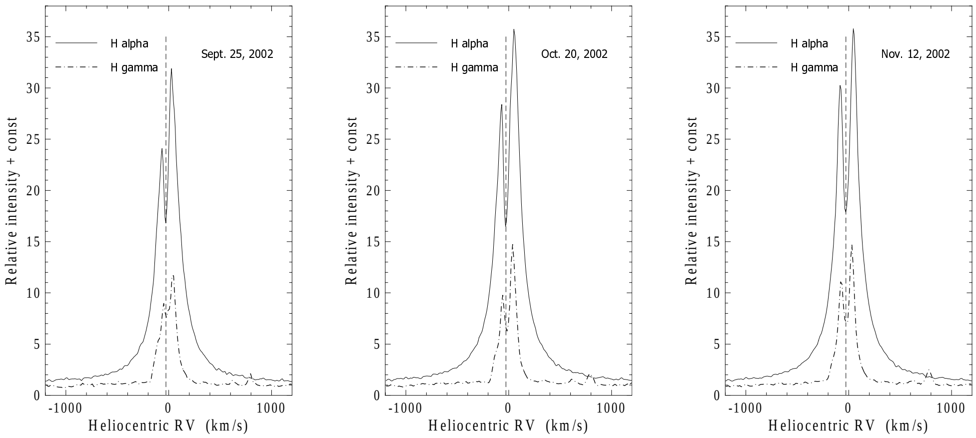

Figure 5.13: The lines H_α and H_γ in each time of observation. The dips of the two lines have close velocity positions.

An other possible mechanism the broad component to appear is to be emitted by an optically thin Keplerian accretion disc. The half width at zero intensity of the broad component on November 12 at the time of the light maximum was about 1020 $\mathrm{km\,s^{-1}}$ (Table 5.9). The velocity, derived from the width at zero intensity of the line, is related to the movement at the inner boundary of the disc. This velocity, however, is on the line of sight. Taking into consideration the orbit inclination of 55°, the obtained velocity at the inner boundary is 1240 $\mathrm{km\,s^{-1}}$. With the mass of the compact object adopted by us $M_{wd} = 0.6 M_\odot$ we obtain an inner radius of the disc of 0.07 $R_\odot$. This estimate is smaller than the upper limit of the radius of this object at the time of the maximal light ($\sim 0.13\,(d/1.12$ kpc) $R_\odot$ evaluated by Tomov et al. (2004)). The estimate of the disc radius, however, has an appreciable uncertainty due to the velocity, which depends from the level of the local continuum. Our data take small range of 200 Å which leads to additional difficulty in determining continuum level. Its uncertainty can reach up to 5 per cent. Variation of 5 per cent can lead to reduction of 20 per cent of the velocity which is based on the FWZI of the line. So, a velocity of 800 $\mathrm{km\,s^{-1}}$ gives us an upper limit of the inner radius of the disc of 0.12 $R_\odot$. Then we can think that the inner radius is about $0.1 \div 0.2$ $R_\odot$ for the range of orbit inclination treated by us and is in satisfactory agreement with the upper limit of the radius of the compact object of 0.13(d/1.12 kpc) $R_\odot$. That is why we will suppose that the emission of an optically thin accretion disc can be possible reason for the broad H_γ component. An other possible origin of the broad component is emission by a high-velocity stellar wind.

5.4.3 Discussion

Gas dynamical modeling shows that a disc from wind accretion with a typical radius of 50 – 60 $R_\odot$ and a mass of 5×10^{-7} $M_\odot$ exists in one binary system with parameters close to those of Z And in its quiescent state (Sect. 5.6; Bisikalo et al. 2002; Tomov et al. 2010b, 2011a)). During each outburst the wind of the compact object "strips" the disc and ejects some part of its mass. After the cessation of the wind some part of the ejected mass accretes again creating an extended disc-like envelope with a mass smaller than the mass of the initial accretion disc.

We will suppose that the increase of the emission measure of the circumbinary nebula during the outburst is entirely on account of a creation of a disc-like envelope located in the Roche-lobe of the compact object. The increase of the emission measure is equal to the residual of its values at the light maximum in November of $11.7{\times}10^{59}(\mathrm{d}/1.12\ \mathrm{kpc})^2\ \mathrm{cm}^{-3}$ and in the quiescent state of the system in August of $2.6{\times}10^{59}(\mathrm{d}/1.12\ \mathrm{kpc})^2\ \mathrm{cm}^{-3}$ (Tomov et al. 2004). These two times are at close phases and the orbital variation of the emission measure due to occultation by the giant component is negligible in this case. The masses of the components of Z And are 2 $M_\odot$ and 0.6 $M_\odot$ (Bisikalo et al. 2002), and the orbital period – $758\overset{\mathrm{d}}{.}8$ (Formiggini & Leibowitz 1994; Mikolajewska & Kenyon 1996). Then the components' separation accounts to 481 $R_\odot$. In a binary system with such a separation, a radius of the cool component of 85 (d/1.12 kpc) $R_\odot$ (Tomov et al. 2003a) and an orbit inclination not higher than 55° (Tomov et al. 2012, 2014), a disc shaped structure located in the Roche lobe of the compact object is not eclipsed. Then we will accept that the residual of the active and quiescent emission measures of $9.1{\times}10^{59}(\mathrm{d}/1.12\ \mathrm{kpc})^2\ \mathrm{cm}^{-3}$ is an upper limit of the emission measure of the disc-like envelope and in such a case all its parameters are also an upper limit. We assume that the shape of the envelope is close to cilinder and its inner radius is equal to 0.2 $R_\odot$, very close to the upper limit of the size of the observed photosphere of the outbursting compact object. We accept a mass of the envelope of $1.3{\times}10^{-8}$ $M_\odot$. Then, a disc-like envelope with an outer radius of about 50–100 $R_\odot$, a height of 53–13 $R_\odot$ and a mean density of $8{\times}10^{10}\ \mathrm{cm}^{-3}$ can appear in the Roche-lobe of the compact object. Its shape is close to torus and it can account for the observed increase of the emission measure during the outburst.

Let we calculate the Keplerian velocity at the lower limit of the outer radius of the disc-like envelope of 50 $R_\odot$ with used by us mass of the compact object of 0.6 $M_\odot$. This velocity is 48 $\mathrm{km\,s^{-1}}$which should be corrected for an orbit inclination of 55°. Taking this inclination, for the doubled value of the velocity we obtain 78 $\mathrm{km\,s^{-1}}$. The observed peaks separation of the line

H_α at the time of the maximal light is 128 ± 9 km s^{-1}, and that of H_γ is 96 ± 7 km s^{-1}, which means that they are broadened more than only from rotation of such an envelope. The greater separation can be due to optical depth effects (self-absorption) and/or an additional line broadening by a gas turbulence caused by collision of the stellar wind of the outbursting component with the envelope.

Concluding this section we can outline that we have no spectral indication of an accretion disc structure in the system Z And during this outburst, but the observational data show that the growth of the nebular emission can be connected with a creation of such a structure in the Roche lobe of the compact object with parameters compatible with the predicted ones by the gas dynamical modeling and the peaks separation of the Balmer lines. The other possibility is that the double-peaked Balmer profiles are determined from self-absorption only.

5.5 The line spectrum during the 2006 – 2007 outburst

The line spectrum of Z And during its 2006 – 2007 brightening was described and interpreted in the works of Tomov & Tomova (2006); Tomov et al. (2007, 2012, 2014).

5.5.1 Observations and reduction

The regions of the H_α, He II 4686 and H_γ lines of the spectrum of Z And was observed on fourteen nights during 2006 July – December covering its major eruption with the Photometrics CCD camera mounted on the Coudé spectrograph of the 2m Ritchey-Chretien-Coudé (RCC) telescope of the National Astronomical Observatory Rozhen. In addition the region of the line Hβ was observed on four nights from September till December 2006 (Table 5.10). The spectral resolution was 0.2 Å/px on all occasions. When more than one exposure was taken per night, the spectra was added with the aim of improving the signal-to-noise ratio. The IRAF package was used for the data reduction as well as for obtaining the dispersion curve, calculating the radial velocities and equivalent widths.

The absolute fluxes of some selected lines in the observed regions were calculated by using their equivalent widths and the continuum fluxes at their positions. The continuum fluxes in the regions of the lines H_β, He II 4686 and H_γ were obtained using linear extrapolation of the B and V photometric fluxes taken on the same, or close, nights from the paper of Skopal et al.

Table 5.10: List of the observations in 2006.

Date	JD− 2 453 000	Orb. phase	Spectral region
Jul 08	924.56	0.837	H_α , He II λ 4686, H_γ
Jul 09	926.45	0.840	H_α , He II λ 4686, H_γ
Jul 14	931.48	0.846	H_α , He II λ 4686, H_γ
Jul 19	935.59	0.852	H_α , He II λ 4686
Jul 20	936.55	0.853	H_γ
Aug 08	956.39	0.879	H_α
Aug 12	960.47	0.885	H_α
Aug 13	960.51	0.885	He II λ 4686, H_γ
Sept 07	985.57	0.918	H_α , He II λ 4686, H_γ
Sept 08	986.54	0.919	H_α , H_β , He II λ 4686, H_γ
Oct 03	1012.47	0.953	H_α , He II λ 4686, H_γ
Oct 04	1013.46	0.954	H_α , H_β , He II λ 4686, H_γ
Oct 31	1040.37	0.990	H_α , He II λ 4686, H_γ
Dec 01	1071.37	0.031	H_α , H_β , He II λ 4686, H_γ
Dec 02	1072.30	0.032	H_α , H_β , He II λ 4686, H_γ
Dec 30	1100.24	0.069	H_α , He II λ 4686, H_γ

(2007). To obtain the fluxes of the lines in the H_α region we used the Cousins R_C photometric band flux from the same paper. According to the continuum analysis of Skopal et al. (2009a) the flux at the positions of the lines Hα and He I 6687 of Z And is practically equal to its R_C flux. The BV fluxes were not corrected for the intensive emission lines of Z And because of the strong increase of the stellar and nebular continua and the relative decrease of the emission lines. The uncertainty of the continuum flux is not more than 10 per cent. All the fluxes were also corrected for the interstellar reddening of $E(B-V) = 0.30$ using the extinction law of Cardelli et al. (1989).

5.5.2 Analysis of the spectrum

Balmer lines

H_α line

The evolution of the H_α profile was considered in the work of Tomov et al. (2012). According to these data the line consisted of strong central narrow emission component (core), located around the reference wavelength, broad wings extended to about 2 000 km s^{-1} and additional absorption and emission

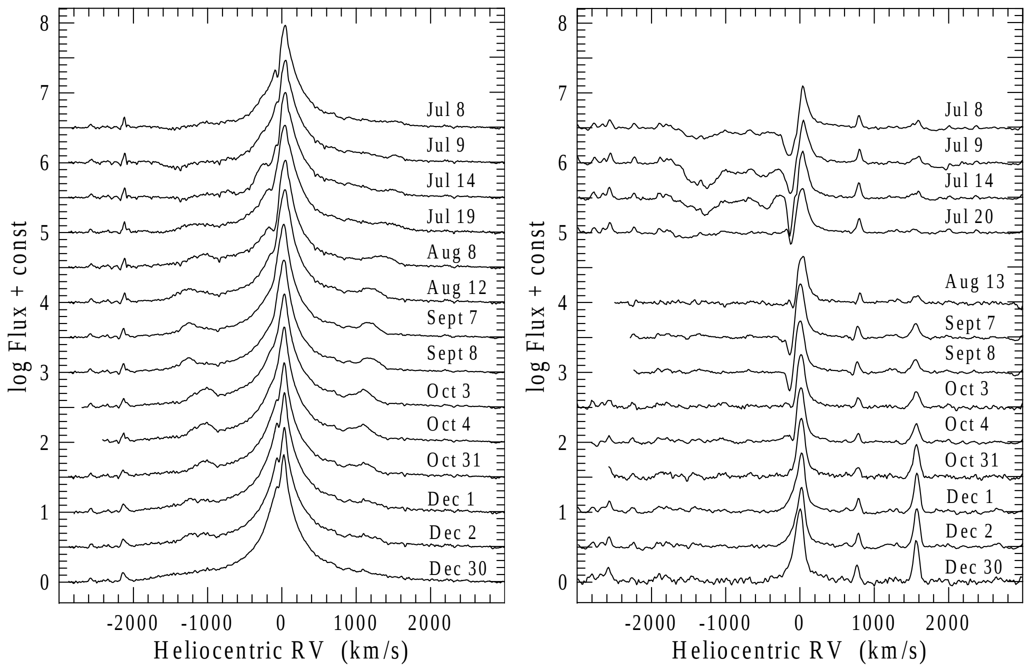

Figure 5.14: Time evolution of the H_α (left panel) and H_γ (right panel) lines.

features on both sides of the central component (Fig. 5.14). The central component presented a weak peak/shoulder(s) on its short-wavelength side, which was not visible only on the spectra taken in September. A weak peak component is seen in the spectrum of August 8 and the dip feature indicates a moderate velocity of about 100 $\mathrm{km\,s^{-1}}$. Very weak peak component was seen again from October 31. The high-velocity satellite emission components were fitted with a Gaussian and the other part of the line (the core together with the wings) – with two or three Lorentzians. The uncertainty of the equivalent width of the satellite emissions was not more than 30 per cent and that of the whole line – about 2 per cent.

High resolution H_α data taken in quiescence before the 2000 – 2013 active phase was analysed in the work of Tomov et al. (2008) and was concluded that the broad wings of the line extending to velocities not smaller than about 2000 $\mathrm{km\,s^{-1}}$ from its centre are formed mainly through Raman scattering of Lyβ photons by atomic hydrogen in the wind of the giant. It was also concluded that radiation damping has probably some contribution in these wings too. In July 2006 the red wing was appreciably more intensive than the blue one. Skopal (2006) suggested that the H_α wings of the symbiotic stars during their active phases form in the high velocity wind of their compact component. Based on this suggestion Skopal et al. (2009a) concluded that

Table 5.11: The H_α and H_β lines data.

Date	Line	$F(t)^a$	Blue RV	Blue F	Blue $\dot{M}$	Red RV	Red F	Red $\dot{M}$	$\dot{M}_{cw}{}^b$
Jul 19	H_α	332.527	−1196	1.675	1.05	1445	1.675	1.05	2.10
Aug 8	H_α	279.490	−1087	2.883	1.24	1346	3.244	1.46	2.70
Aug 12	H_α	...	−1260	4.407	1.69	1201	3.526	1.27	2.96
Sept 7	H_α	262.478	−1245	2.642	0.84	1178	2.936	0.96	1.80
Sept 8	H_α	257.047	−1262	2.496	0.76	1196	3.083	1.07	1.83
	H_β	90.170	−1291	1.198	0.90	1196	1.800	1.38	2.28
Oct 3	H_α	264.773	−1050	4.071	1.37	1112	3.053	0.86	2.23
Oct 4	H_α	270.444	−1070	4.071	1.34	1099	3.053	0.90	2.24
	H_β	91.199	−1074	2.507	1.79	1078	1.393	0.88	2.67
Oct 31	H_α	241.650	−1054	2.295	0.82	1132	1.620	0.66	1.48
Dec 1	H_α	251.334	−1214	1.577	0.89	1174	1.092	0.68	1.57
	H_β	73.248	−1261	0.804	0.73	...	...	...	> 0.73
Dec 2	H_α	250.484	...	...	...	1185	1.092	0.78	> 0.78
	H_β	76.814	−1177	1.408	1.71	...	...	...	> 1.71
Dec 30	H_α	279.816	...	...	...	...	...	...	...

All fluxes are in units of 10^{-12} erg cm^{-2} s^{-1}, the mass-loss rate – in units of $10^{-7}(d/1.12\text{kpc})^{3/2}$ $M_\odot$ yr^{-1} and the radial velocity – in units of km s^{-1}.
[a] $F(t)$ is the total line flux.
[b] $\dot{M}_{cw}$ is a sum of the mass-loss rates based on the satellite components.

the H_α wings of Z And during the 2006 brightening are also determined from stellar wind. However, attention should be paid to the fact that the FWZI of the H_α wings of Z And was the same in both stages of the system, the quiescent and active ones, maintaining its value of about 4 000 km s^{-1}. This fact gives us some reason to suppose that during the 2006 brightening the FWZI of the wings was determined mainly from radiation damping like in the quiescent state of the system and the stellar wind emitted at smaller distance from the centre of the line. Moreover, the region of shock waves produced by the collision of the wind with the accretion disc/envelope can contribute to the wings too (Drake et al. 2009; Ionov et al. 2012). The problem on the nature of the H_α wings needs to be considered further.

Together with the central component and the broad wings the H_α line presented additional satellite components with velocity of more than 1 000 km s^{-1} situated on either side of the central component (Fig. 5.14). The view that they are an indication of bipolar collimated outflow from the compact object

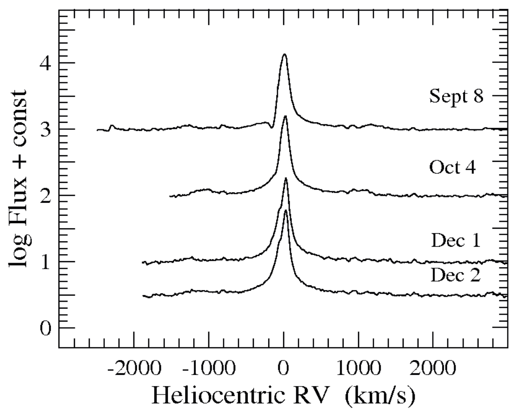

Figure 5.15: Time evolution of the H_β line.

is commonly accepted (Burmeister & Leedjärv 2007; Skopal et al. 2009a; Tomov et al. 2012). We associate these components with a collimated stellar wind.

The first of our spectra, taken in July, show one pronounced absorption with a velocity of 1 400 km s^{-1} on the short-wavelength side of the central component of the line and only weak emission component, irregularly shaped and having velocity of about 1 500 km s^{-1} on its long-wavelength side. The absorption indicates mass outflow which projects on to the observed photosphere of the outbursting compact object (its flat shell) (Tomov et al. 2014). As is seen from the evolution of the spectrum the absorption component disappears and emission appears. Thus two emission components on the two sides of the central peak form after the middle of July and were visible until December. The disappearance of the blueshifted absorption component and the development of emission are most probably due to a decrease of the mass-loss rate of the compact object and/or increase of the number of emitting atoms in that area of the wind which does not project on to the observed photosphere. The evolution of the spectrum (Fig. 5.14, Table 5.11) shows also that the line flux of the satellite components after the beginning of October decreases with time, which is due to decrease of the mass-loss rate of the compact object.

H_β line

Figure 5.15 shows the evolution of the H_β line in one short period of time from September to December 2006. At that time the H_β profile was similar to the profile of H_α and consisted of strong central emission component (core), located around the reference wavelength, broad wings extended to about

$1\,500\ \mathrm{km\,s^{-1}}$ from the center of the line and additional emission features on both sides of the central component. On the spectrum of Sep. 8 the line had one blueshifted absorption dip in its emission profile at a velocity of about $-150\ \mathrm{km\,s^{-1}}$ from its center. In December the central emission presented a weak shoulder on its short-wavelength side at a velocity of 70 $\mathrm{km\,s^{-1}}$ from the line center like the absorption dip in the emission profile of H_α at that time. The high-velocity satellite emission components were fitted with a Gaussian and the other part of the line (the core together with the wings) – with two or three Lorentzians. The uncertainty of the equivalent width of the satellite emissions was not more than 30 per cent and that of the whole line – about 2 per cent. According to the theory the profile of the spectral line determined from radiation damping is approximated with a Lorentzian function. That is why we assume that the broad H_β wings are determined mainly from radiation damping. It is possible, however, the stellar wind of the outbursting object and the region of shock waves produced by the collision of the wind with the accretion disc/envelope to contribute to these wings too.

The line H_β presented additional satellite emission components with a velocity of up to about $1\,300\ \mathrm{km\,s^{-1}}$ situated on either side of the central component indicating bipolar collimated outflow from the system like the line H_α. The evolution of the spectrum shows that their flux decreases with time due to decrease of the mass-loss rate of the compact object (Fig. 5.15, Table 5.11).

H_γ line

The evolution of the H_γ profile was considered in the work of Tomov et al. (2014). According to these data it was a multicomponent one with features related to all the components of the flow in the system. The H_γ line presented a broad emission component with a low intensity and a FWZI of about 1000 $\mathrm{km\,s^{-1}}$ in addition to its central narrow component with a nebular profile like during the 2000 – 2002 outburst (Tomov et al. 2008). The broad component is best seen on the spectra taken after 2006 October 31 (Figs. 5.14 and 5.16). The broad component was analysed by fitting with a Gaussian function (Fig. 5.16, left panel), and its parameters obtained with this procedure are listed in Table 5.12. The error of the equivalent width due to the uncertainty of the continuum level reaches up to 10 per cent. On the spectra taken in July – September the blue wing of the broad component was not seen because of blending with the P Cyg absorption component (see below and Fig. 5.14, right panel). On the spectra taken in October and December the blue wing appeared to be less extended than the red one due to

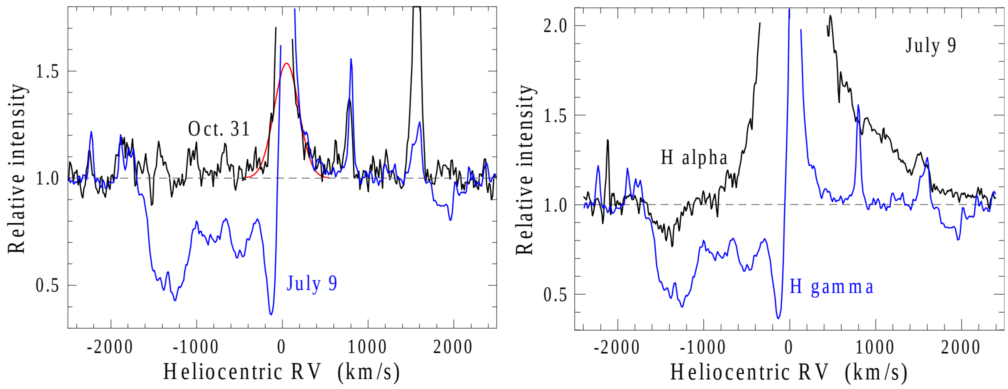

Figure 5.16: *Left panel:* The profile of the H_γ line on July 9 and October 31. The Gaussian fit of the broad component is also shown. The level of the local continuum is marked with a dashed line. *Right panel:* The profile of the H_α and H_γ lines on July 9. The level of the local continuum is marked with a dashed line.

blending with the P Cyg absorption. What is the mechanism of broadening of the line H_γ ? If we suppose that its broad emission component is produced by electron scattering, even at low electron temperature of 10 000 K its wide (FWHM) should be large, accounting to $\sim$ 900 $\mathrm{km\,s^{-1}}$. Since its wide of 340 – 480 $\mathrm{km\,s^{-1}}$ is much smaller, it is probably not produced by electron scattering. An other possibility is emission by an optically thin Keplerian accretion disc. According to (Skopal et al. 2009a) the radius of the observed photosphere of the outbursting compact object is equal to 12 ± 4 $R_\odot$ at a distance to the system of 1.5 kpc. Baring in mind the error of the observations, this radius is reduced to 10 $R_\odot$ at a distance of 1.12 kpc. Using a mass of the compact object of 0.6 $M_\odot$ (Fernandez-Castro et al. 1988; Schmid & Schild 1997) and a radius of 10 $R_\odot$ we obtain Keplerian velocity of 100 $\mathrm{km\,s^{-1}}$ which is too small compared to the half wide at zero intensity of the line of 370 – 510 $\mathrm{km\,s^{-1}}$. Then we suppose that the broad emission component indicates mainly an optically thin stellar wind from the outbursting object. The region of shock waves produced by the collision of the wind with the disc/envelope, however, can contribute to this component too.

On the spectra taken during July – September 2006 the central narrow component of the line had positive radial velocity, which was due to presence of a blueshifted P Cyg absorption (Figs. 5.14 and 5.16). In July this absorption presented multi-component structure and occupied a velocity range from about -100 to about $-1\,500$ $\mathrm{km\,s^{-1}}$. After that it gradually weakened and converted in low velocity absorption presenting in the spectrum until the beginning of October 2006 (Fig. 5.14). On September 8 this absorption was

Table 5.12: The H_γ line data.

Date[a]	FWHM(N) ($km\,s^{-1}$)	F(N)	FWHM(B) ($km\,s^{-1}$)	FWZI(B) ($km\,s^{-1}$)	v_w ($km\,s^{-1}$)	F(B)	$\dot{M}$
Jul 8	92.6	26.697					
Jul 9	111.2	28.791					
Jul 14	106.4	35.054					
Jul 20	126.4	45.003					
Aug 13	111.2	27.873					
Sep 7	103.6	32.064					
Sep 8	102.9	29.453					
Oct 3	99.5	27.676					
Oct 4	96.0	30.550					
Oct 31	85.6	20.174	340±40	746	370	7.834	1.05
Dec 1	82.9	20.003	430±40	981	490	6.209	1.14
Dec 2	82.9	20.074	480±50	1022	510	6.280	1.20
Dec 30	86.3	28.498	490±50	1062	530	10.450	1.53

[a] The data taken in Jul 8 – Oct 4 are for the whole observed emission including the red wing of the broad component.
N denotes narrow component and B – broad component.
F is in units of $10^{-12}\,erg\,cm^{-2}\,s^{-1}$,
$\dot{M}$ is in units of $10^{-7}(d/1.12\ kpc)^{3/2}\ M_\odot\,yr^{-1}$.

at the same velocity position of about $-150\ km\,s^{-1}$ like the absorption dip in the H_β emission profile (Fig. 5.17). The residual intensity of this absorption was minimal in the middle of July at 0.4. As the cool giant's continuum, at the same time, was less than 9 per cent of the total continuum of the system at the wavelength position of the B photometric band (Skopal et al. 2009a) which is close to the H_γ line, the P Cyg profile originates from absorption of the radiation emitted by the mass outflow from the compact object.

The comparison of the spectra taken on July 9 and October 31 shows that the red wing of the broad component on the two spectra coincide (Fig. 5.16), which suggests that the H_γ line has three components, consisting of a central narrow emission, a broad emission with low intensity and multi-component P Cyg absorption occupying broad range of velocities of the outflowing material – from about 100 to 1 500 $km\,s^{-1}$.

The comparison of the H_γ profile with those of H_α and H_β taken on September 8 (Fig. 5.17) shows that the H_γ line displays the same satellite emission components visible in the H_β and H_α profiles. Both H_γ satellite components

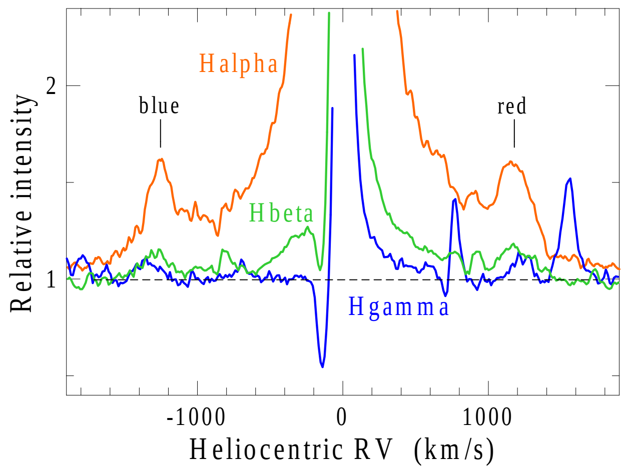

Figure 5.17: The profiles of the H_α, H_β and H_γ lines based on a CCD frame on 2006 September 8. The satellite components are marked with vertical lines. The level of the local continuum is indicated by a dashes line.

were observed only in September when the intensity of the H_α components was maximal. In October only a blueshifted H_γ emission was present in the spectrum. This means that in September the H_γ profile consisted of four groups of components.

The absorption component of the line H_α occupies more narrow velocity range compared with the H_γ absorption (Fig. 5.16). We can suppose that the atoms absorbing the H_α photons are situated probably in more outer part of the area projecting onto the observed photosphere where the radial velocities occupy more narrow range (Fig. 5.25).

Helium lines

The singlet lines of He I with wavelengths 4388 Å and 6678 Å in the period July 8 – 20 had a high velocity absorption component of the type P Cyg with the same position like the absorption component of H_α and the most blueshifted component of H_γ (Fig. 5.18). After that time the absorption of the line He I 4388 converted into narrow feature with much lower velocity, which in September was about 100 km s^{-1}. Since October the profile of this line was purely in emission. The He I 6678 profile was purely in emission after July 20.

The triplet line of He I with wavelength 4713 Å in the period July 8 – 20 had a high velocity P Cyg component with the same position like the absorption components of Balmer lines and the singlet lines (Fig. 5.20). A high velocity component with the same position was observed in the triplet

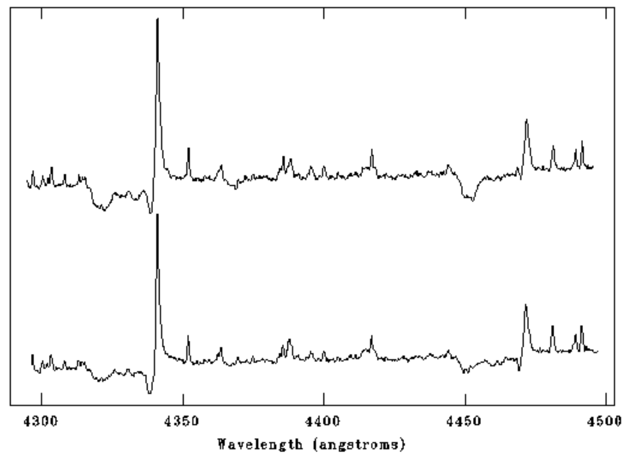

Figure 5.18: The region of the line H_γ based on CCD frames taken on 2006 July 8 (lower spectrum) and July 9 (upper spectrum). The lines of He I 4388 and 4471 are seen. These three lines have a high velocity P Cyg absorption component.

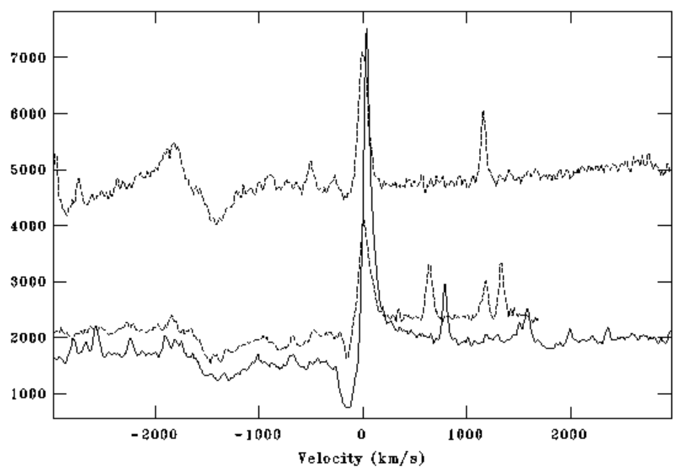

Figure 5.19: The lines H_γ (lower spectrum), He I 4471 and 4713 on CCD frame taken on 2006 July 8.

line He I 4471 too, but this line had also additional absorption components, occupying an interval of lower velocities similar to the line H_γ (Fig. 5.19). After July 20 the P Cyg absorption of the triplet lines converted into narrow component showing a low velocity of the outflowing material of about 100 $\mathrm{km\,s^{-1}}$ like the line H_γ, but this component was observed up to the beginning of December (Fig. 5.20). The line fluxes of the helium lines are listed in Table 5.13.

Table 5.13: The fluxes of the emission lines of Z And during its 2006 outburst in units 10^{-12} erg cm^{-2} s^{-1}.

Date	[O III] λ 4363	He I λ 4388	He I λ 4471	Fe II λ 4629	He I λ 4713
Jul 8	2.047	3.547	7.421	2.828	3.839
Jul 9	2.173	3.311	7.946	2.768	2.846
Jul 14	1.902	3.566	8.098	3.459	3.099
Jul 19				2.898	1.798
Jul 20	1.187	2.477	6.289		
Aug 13	1.574	0.794	3.584	1.781	1.128
Sep 7	3.303	2.293	5.786	2.045	2.543
Sep 8	3.158	2.094	4.911	2.055	2.314
Oct 3	3.497	3.660		1.970	2.825
Oct 4	3.901	3.741	4.662	2.000	2.591
Oct 31	6.714	4.558	3.566	1.977	2.269
Dec 1	7.017	3.914	2.412	1.828	1.276
Dec 2	7.027	4.062	2.344	1.797	1.481
Dec 30	6.943	3.981	3.646	1.883	2.414

In the framework of our model the P Cyg components of the He I lines can be interpreted as absorption by the outflowing material which is projecting onto the observed photosphere of the outbursting compact object (the flat shell) (Fig. 5.25). The absence of high velocity emission components of the He I lines suggests that the emission region of He I was small.

Lines of elements of high degree of ionization

The evolution of the line He II 4686 during the period of our observations is shown in Fig. 5.20. In October – December it was two component one, consisting of a central narrow emission and a low intensity broad component with FWZI of 1200 km s^{-1} like during the previous brightening of Z And in 2000–2002 (Tomov et al. 2008). The two components had different behaviour with the fading of the light: the energy flux of the narrow one increased whereas the flux of the broad component did not (Table 5.14). Before October this component was hardly visible due to the intensive optical continuum of the system, absorption by the high-velocity P Cyg component of the line He I 4713 and its natural variability. At that time it was associated with an emission, exceeding the level of the local continuum, which can not be measured with adequate accuracy, like in the quiescent state of the system (Tomov et

Table 5.14: The He II $\lambda\,4686$ line data. $\dot{M}_{\rm w}$ is based on both lines H_γ and He II $\lambda\,4686$. The other quantities are the same as in Table 5.12.

Date	RV(N) ($\rm km\,s^{-1}$)	FWHM(N) ($\rm km\,s^{-1}$)	F(N)	FWHM(B) ($\rm km\,s^{-1}$)	FWZI(B) ($\rm km\,s^{-1}$)	$v_{\rm w}$ ($\rm km\,s^{-1}$)	F(B)	$\dot{M}$	$\dot{M}_{\rm w}$
Jul 8	< -200	...	5.046						
Jul 9	-84	213	0.986						
Jul 14	< -200	...	5.230						
Jul 19	-100	219	2.549						
Aug 13	-89	197	3.540						
Sep 7	-87	141	9.083						
Sep 8	-132	265	5.867						
Oct 3	-58	208	9.552						
Oct 4	-57	134	7.580	$558\pm\ 40$	1228	600	4.945	1.14	1.14
Oct 31	-24	147	27.424	613 ± 100	1215	600	3.824	0.80	1.05
Dec 1	-25	160	28.249	$682\pm\ 40$	1392	700	5.330	1.02	1.14
Dec 2	-25	160	26.010	$590\pm\ 30$	1240	600	4.776	0.82	1.20
Dec 30	-24	137	42.910	$634\pm\ 50$	1302	650	4.465	0.82	1.53

al. 2008). We analysed the broad component by approximating with a Gaussian function and its parameters obtained with this procedure are listed in Table 5.14. The error of the equivalent width due to the uncertainty of the continuum level is $8-14$ per cent. The broad component showed a velocity close to that of the line H_γ and we supposed that it is emitted by the same regions in the system which give rise to the H_γ broad component, mainly by the stellar wind of the outbursting object.

In July, at the time of the light maximum a weak broad variable emission with an irregular shape at a wavelength position close to that of the line He II 4686 was visible only (Fig. 5.20). On July 9 it was much weaker compared to July 8, undergoing thus strong variation on a time-scale of about one day. At some times its long wavelengths side was partly absorbed by the high-velocity P Cyg component of the line He I 4713. We suppose that both components of the line He II 4686 contributed to this variable emission.

The energy flux of the line He II 4686 was about 3.6×10^{-11} $\rm erg\,cm^{-2}\,s^{-1}$ in quiescence (Tomov et al. 2008) and decreased to about 5×10^{-12} $\rm erg\,cm^{-2}\,s^{-1}$ at the time of the light maximum, which means that its emitting region was probably decreased and was related only to the close vicinity of the hot companion. At the time of the light maximum the line He II 4686 had a high negative velocity of less than $-200\rm km\,s^{-1}$, which increased to about $-20\rm km\,s^{-1}$ in December (Table 5.14). This means that the motion of the emitting gas differs from the motion of the mass center of the system, whose velocity is -2 $\rm km\,s^{-1}$ (Mikolajewska & Kenyon 1996; Fekel et al. 2000). As

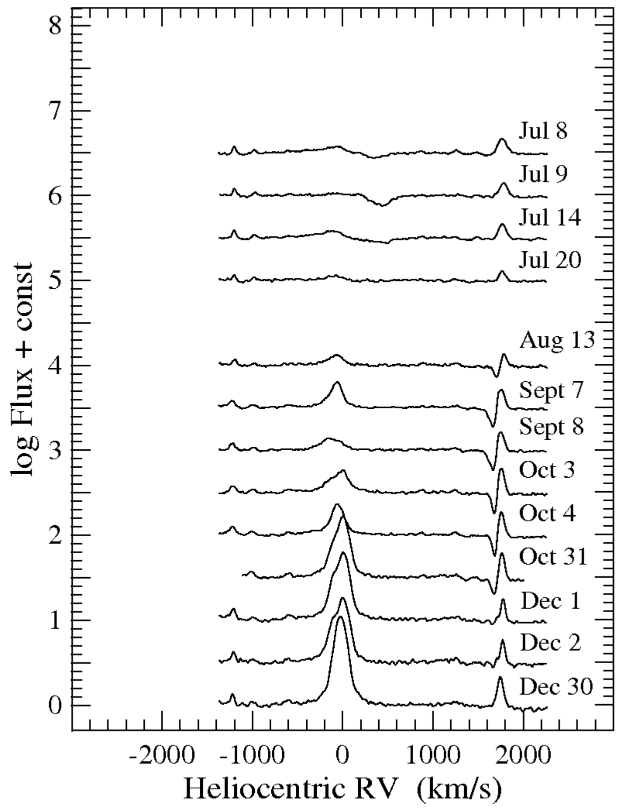

Figure 5.20: The evolution of the profile of the lines He II 4686 and He I 4713

in our previous work (Tomov et al. 2008), we suppose that the narrow component of the line He II 4686 is emitted in a region of a shock ionization where the outflowing material from the outbursting object meets the accretion disc and disc-like envelope. According to the gas dynamical modeling this region is heated mainly by propagation of a shock wave which begins to form about 70^d after the appearance of the companion's wind and reaches its maximal development about 20–30^d later (Bisikalo et al. 2006). This period of about 100 days is close to the typical time of the growth of the optical light during the outbursts of Z And which means that the region of shock wave should form close to the light maximum and exist after it. The temperature of this region is appreciably higher than that of the surrounding medium and can reach 10^6 K. Some part of this region is occulted by the effective photosphere (the flat shell) of the outbursting object (Fig. 5.25). It is possible the gas particles in this region to move radially outwards which, in this case, determines the width of the line.

After the light maximum the mass-loss rate of the compact object de-

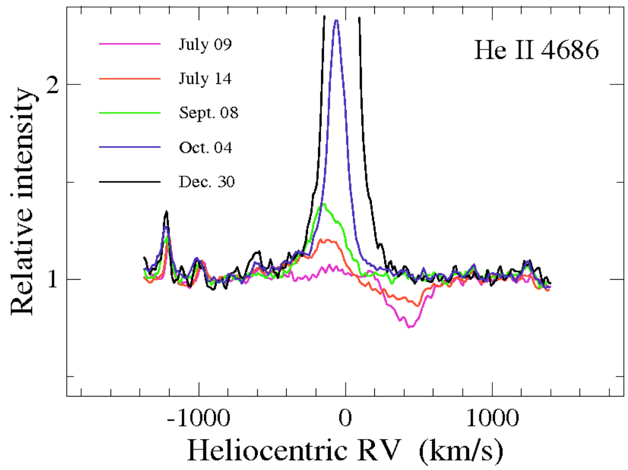

Figure 5.21: The increase of the intensity of the He II 4686 narrow component and its gradually shift to the long wavelengths side with the decrease of the light.

creased (see the next section) which moved the level of the effective photosphere back to the star (Fig. 5.25). The size of this photosphere decreased and it occulted less and less the shock region. This determined both the increase of the intensity of the He II 4686 narrow component and its shift to the long wavelengths side (Fig 5.21) since more particles in the back part of its emitting region, which move away, are seen.

We observed also some lines of elements with high ionization degree – N III 4634, N III 4641 and C III 4647 which are in the region of the He II 4686 line. The width of these lines increased and was well above its quiescent value of about 40 km s^{-1} (Tomov et al. 2008).

The line N III 4634 creates an unresolved blend with the line Cr II 4634. The relative intensity of the lines of high ionization degree strongly decreased at the time of maximal light and in July and August the nitrogen line was weaker than the line of Cr II. That is why in July and August the nitrogen line was not measured (Table 5.15).

During the outburst the line N III 4641 broadened and formed thus an unresolved blend with the lines of O II λ 4639, 4642. The nitrogen lines were undergoing strong variation on a time-scale of about one day being on July 9 much weaker compared to July 8 like the line He II 4686. For this reason the line N III 4641 was very weak and was not measured on July 9. Moreover, it was weak and thus badly blended with the O II lines on July 19, Aug. 13 and Sept. 8 and was not measured too (Table 5.15). Our data show that after the end of October the intensity of the N III lines increased (Table 5.15,

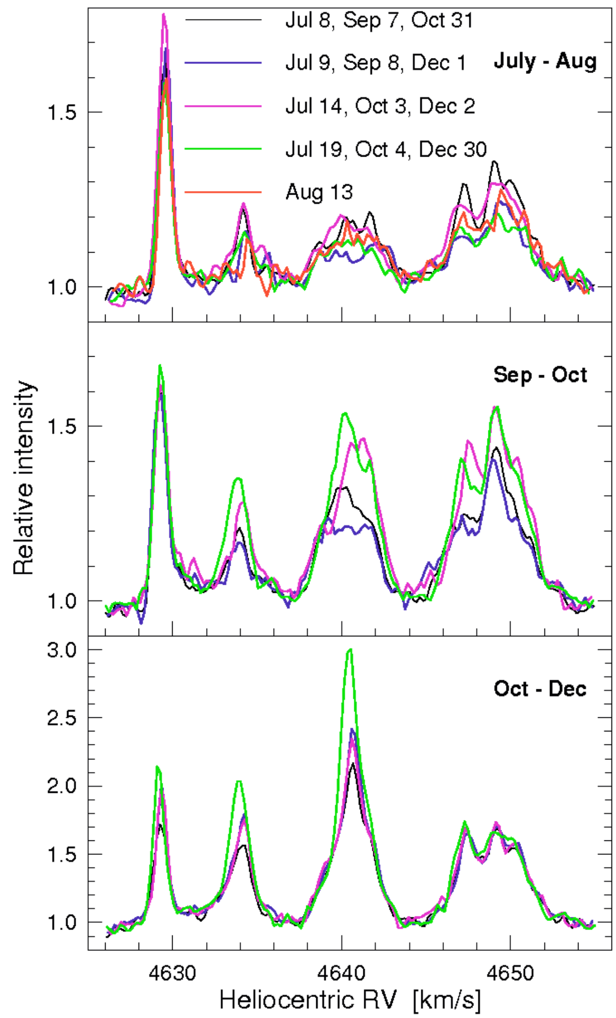

Figure 5.22: The evolution of the profile of N III and C III lines: in July – August (upper panel), September – October (middle panel) and October – December (lower panel)

Fig. 5.22).

During the outburst the line C III 4647 broadened too and blended with the lines Fe II 4649, O II 4649, C III 4650 and O II 4651. For this reason it was not measured on Aug. 13, Sept. 7 and Sept. 8.

The radial velocity of the central narrow component of the line He II 4686 and the other lines of high ionization degree is shown in Fig. 5.23. The velocity of all lines increased. The data in Table 5.15 show that the flux of the nitrogen lines increases after the light maximum like the flux of the narrow He II component. This behaviour can be explained with the supposition the

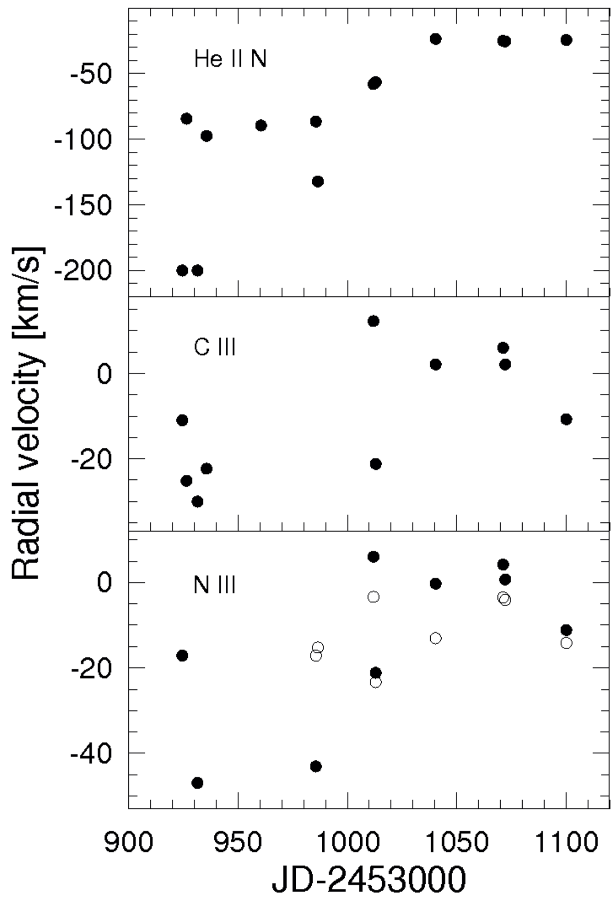

Figure 5.23: The radial velocity of the lines of elements with high ionization degree. On the lower panel open circles mark the line N III 4634 and filled circles – the line N III 4641. The uncertainty of the measurement reaches up to 5 $\mathrm{km\,s^{-1}}$.

nitrogen lines appear in the same region of shock wave whose unocculted part rises with the decrease of the mass-loss rate of the outbursting object.

5.5.3 Mass-loss rate

According to the model we suggested the wind of the outbursting compact object associated with the broad emission components of the lines H_γ and He II 4686 is collimated by the envelope covering the accretion disc and the collimated outflow is observed as the satellite emission components of the lines H_α , H_β and H_γ . These two groups of lines appear in different parts of the outflow but both of them indicate mass-loss. The total mass-loss rate of

Table 5.15: The N III and C III lines data. RV and FWHM are in units $\mathrm{km\,s^{-1}}$ and F – in units $10^{-12}\ \mathrm{erg\,cm^{-2}\,s^{-1}}$.

Date	N III λ 4634			N III λ 4641			C III λ 4647		
	RV	FWHM	F	RV	FWHM	F	RV	FWHM	F
Jul 8				−17	96	1.515	−11	97	2.213
Jul 9							−25	108	1.206
Jul 14				−47	136	2.160	−30	113	2.088
Jul 19							−22	123	1.822
Sep 7	−17	100	1.019	−43	171	3.012			
Sep 8	−15	83	0.769						
Oct 3	−3	107	1.365	6	158	3.465	12	89	2.043
Oct 4	−23	102	1.787	−21	148	3.884	−21	103	1.880
Oct 31	−13	113	2.535	0	107	4.986	2	100	2.701
Dec 1	−4	99	2.534	4	94	4.598	6	95	2.196
Dec 2	−4	94	2.315	1	102	4.648	2	105	2.432
Dec 30	−14	92	2.979	−11	92	5.785	−11	92	2.023

the compact object will be derived as a sum of the mass-loss rates related to each part of the outflow – noncollimated and collimated ones. The mass-loss rate was determined from the energy flux of the lines supposing that the outflow has a constant velocity and using the nebular approach (Vogel & Nussbaumer 1994).

The mass-loss rate based on the broad H_γ emission component was calculated from the spectra obtained since October 31, as in the period prior to it the blue wing of the H_γ line was absorbed by the wind outflow responsible for the P Cyg absorption (Table 5.12). The mass-loss rate based on the broad He II 4686 emission component was calculated from the spectra obtained since October 4 (Table 5.14).

The particle density in the wind is expressed via the continuity equation. In our calculations, we adopted a value of the electron temperature in the wind of 30 000 K like during the first outburst (Tomov et al. 2008). We used a parameter $\mu = 1.4$ (Nussbaumer & Vogel 1987), determining the mean molecular weight μm_{H} in the wind and a helium abundance of 0.1 (Vogel & Nussbaumer 1994). We adopted a distance to the system d=1.12 kpc (Fernandez-Castro et al. 1988, 1995) to compare the results with our previous paper on Z And more easily. It is supposed that the line is emitted by a spherical layer and the radii of integration must be estimated. We assumed optically thin medium and the inner radius in this case is thought to be the photospheric radius. The photospheric radius was estimated from the bolometric luminosity and the effective temperature of the outbursting compact object at the time of each observation. We used a bolometric luminosity of 10^4 $L_\odot$ (Sokoloski et al. 2006) and Zanstra temperature from Burmeister & Leedjärv (2007) and Burmeister (2010). The outer radius of integration was 14 $R_\odot$ (see below). We used a recombination coefficient for case B (Storey & Hummer 1995) corresponding to temperature of 30 000 K and the density at the level of the photosphere at the time of each observation. The results are presented in Tables 5.12 and 5.14.

It is seen that the mass-loss rates based on these two lines are practically equal. Since, however, it is possible the line He II 4686 to be emitted by a smaller region in the wind than H_γ, as a final result we accepted the rate based on H_γ. We used the rate based on He II 4686 only when that obtained from H_γ was not available. The final mass-loss rate $\dot{M}_w$, related to the noncollimated part of the outflow is present in the last column of Table 5.14.

The mass-loss rate based on the H_α and H_β satellite emission components was calculated for each observation. The wind outflow was considered to occupy a spherical sector with opening angle θ and solid angle Ω. The solid angle Ω (Skopal et al. 2009a) is given with

$$\Omega = 2\pi \left(1 - \cos\frac{\theta}{2}\right) \ , \tag{5.4}$$

where θ is the opening angle, which can be approximated as

$$\theta = 2 \arcsin \frac{W}{\upsilon_{\rm obs} \tan i} \ . \tag{5.5}$$

Here W is the half width at zero intensity of the satellite line components, $\upsilon_{\rm obs}$ is their observed velocity and i – the orbital inclination of the system. To calculate θ and Ω the inclination of the orbit is need. Schmid & Schild (1997) propose an inclination angle of $47° \pm 12°$ derived from their polarimetric orbit. Skopal & Shagatova (2012) propose a close value of $59° -2/+3°$ considering the Rayleigh scattering in the system. The appearance of a strong blueshifted absorption feature of all observed by us hydrogen amd helium lines proposes high column density of the outflowing material which is projected onto the stellar photosphere. That is why the inclination angle should not be high. In conformity with these results we will use the value of 55° as an upper limit of the inclination angle. With this limit for the H_α satellite components we obtained average values of the lower limit of the opening angle of the spherical sector of $\theta(f)_\alpha = 18.4° \pm 1.1°$ for the front wind component and $\theta(b)_\alpha = 16.8° \pm 0.7°$ for the back wind component. For the H_β satellite components we obtained close average values of $\theta(f)_\beta = 17.2^\circ \pm 2.8^\circ$ for the front component and $\theta(b)_\beta = 15.0^\circ \pm 1.6^\circ$ for the back component.

The next step is to estimate the radii of integration. The broad components and the satellite components are emitted in regions with different velocity fields. We assume that the satellite H_α and H_β components are emitted in the region of the wind where the velocity is at a maximum. The inner radius of this region was determined in the next way. The absorption satellite component is an indication of mass outflow which is projected on to the observed photosphere of the outbursting compact object (its flat shell). Emission lines appear above the projected part of the outflow. In Sect. 5.5.2 we took a radius of the flat shell of 10 $R_\odot$ at a distance of 1.12 kpc. Then using a diameter of 20 $R_\odot$ and an inclination angle of 55° for the inner radius of the region of the collimated wind we obtained 14 $R_\odot$. We adopted an outer radius of this region of infinity. We used a recombination coefficient for case B (Storey & Hummer 1995) corresponding to a temperature of 30 000 K and density at a distance of 14 $R_\odot$ from the compact object at the time of each observation. The results are presented in Table 5.11. The mass-loss rate with use of the H_γ satellite components was not calculated since both of them were visible only at one time of observation (Sect. 5.5.2). The rates based on H_α and H_β differ with no more than 30 per cent which is really their inner uncertainty. Only in December when one satellite component was measured, giving us the lower limit of the rate, the difference between H_α and H_β reached more than 50 per cent. That is why we accept the rate based on H_α only since it is emitted by a greater area in the collimated outflow and because of its more full set of data.

The mass-loss rate based on the satellite components and related to the collimated part of the outflow decreased with the optical light (Table 5.11). It was about 3×10^{-7} $(\mathrm{d}/1.12\,\mathrm{kpc})^{3/2}$ $M_\odot\,\mathrm{yr}^{-1}$ at the time of the light maximum and decreased to a value close to zero at the end of December when these components were not possible to be measured. The mass-loss rate based on the broad components and related to the noncollimated part of the outflow was close to $1 \times 10^{-7} (\mathrm{d}/1.12\,\mathrm{kpc})^{3/2}$ $M_\odot\,\mathrm{yr}^{-1}$ in October–December (Table 5.14). So we obtained that in October–December the total mass-loss rate has decreased from about 3×10^{-7} $(\mathrm{d}/1.12\,\mathrm{kpc})^{3/2}$ $M_\odot\,\mathrm{yr}^{-1}$ to about 1×10^{-7} $(\mathrm{d}/1.12\,\mathrm{kpc})^{3/2}$ $M_\odot\,\mathrm{yr}^{-1}$. As, however, since the time of the light maximum a noncollimated wind was observed too, we suppose that the total mass-loss rate has been about 4–5 $\times 10^{-7}$ $(\mathrm{d}/1.12\,\mathrm{kpc})^{3/2}$ $M_\odot\,\mathrm{yr}^{-1}$ at the time of the light maximum and has decreased to 1×10^{-7} $(\mathrm{d}/1.12\,\mathrm{kpc})^{3/2}$ $M_\odot\,\mathrm{yr}^{-1}$ at the end of December.

5.6 A model for interpretation of the line spectrum

5.6.1 General characteristics of the line spectrum

The model for interpretation of the line spectrum of Z And during its 2000–2013 active phase was considered in the works of Tomov et al. (2010b, 2011a,b, 2012, 2014). High resolution optical data indicating greatly different physical conditions (velocity, density, temperature) in the emitting regions of the lines were obtained during this active phase (Skopal et al. 2006; Sokoloski et al. 2006; Tomov et al. 2007; Tomova, Tomov et al. 2008; Skopal et al. 2009a; Tomov et al. 2010a).

The main features of the flow structure during the active phase indicated by our data can be summarized as follows:

1. We suppose that an accretion disk is present in the system. Only in this way we can explain the presence of the He II λ4686 line in the spectrum and its behavior during the 2000 – 2002 outburst (Tomov et al. 2008; Tomova, Tomov et al. 2008) as well as the multi-velocity regime of the stellar wind.

2. Stellar wind was observed in the system during all the outbursts. Winds with different velocity and optical thichkness were observed simultaneously (Sokoloski et al. 2006; Skopal et al. 2006; Tomova, Tomov et al. 2008; Tomov et al. 2008, 2012).

3. Bipolar collimated outflow appeared during the 2006 – 2007 outburst. In the beginning of July 2006 the H_α line had an absorption component shifted by -1400 km s^{-1} from its center. It went into emission and later, in July–December 2006, the line H_α had additional emission components on either side of its central peak corresponding to velocities of 1100–1500 km s^{-1} (Burmeister & Leedjärv 2007; Tomov et al. 2007; Skopal et al. 2009a; Tomov et al. 2012). The lines H_β and H_γ had similar features (Tomov et al. 2007; Skopal et al. 2009a). In July the H_γ had a blueshifted P Cyg absorption with a multi-component structure occupying a broad velocity range. The He I lines presented similar high velocity P Cyg absorption. Both the emission and absorption components are assumed to be formed in a bipolar collimated outflow (Tomov et al. 2007, 2012).

During the 2000 – 2002 and 2002 brightenings we detected spectral indications of stellar wind outflow. On the other hand, the spectral features observed during the 2006–2007 brightening indicated both stellar wind and high-velocity bipolar collimated outflow. These indications leads to the idea of presence of some kind of mechanism of collimation related to the accretion disc. The existence of collimated outflow during the 2006 − 2007 brightening and its absence during the previous brightenings hint that this outflow can have its origin in processes occurring during the previous brightenings and show that our idea about the disc-like formation in the system is necessary to be improved and developed further, considering the active phase as a whole rather than each individual brightening separately.

The question about the nature of the collimated outflow is important as its solution can provide concepts about the physical processes in the system during outburst. The nature of the collimated jets is subject of intensive theoretical investigation and the view they represent outflow from an accreting compact object is widely accepted. Theoretical considerations show that the presence of both accretion disc and magnetic field is mandatory condition collimated jets to occur. (Zanni et al. 2007; Livio 2011; and references therein). Following the theory collimated jets in the symbiotic stars should be observed during both of their states, always when an accretion disc and collimating magnetic fields are available in the system. Accretion disc can form in their quiescent state (Bisikalo et al. 2002; Mitsumoto et al. 2005) and can survive during the active state (Tomov et al. 2011a), which proposes possibility jets to exist during both of these states. Moreover, it follows from the theory that there is even better possibility jets to exist in the quiescent state since the stellar wind from the outbursting compact object destroys the disc, moving its inner annulus outward where Keplerian velocities are low and do not contribute to the jet velocity. Observations, however, show that in many of the stars with optical indication of collimated outflow (Z And , Hen 3-1341, StHα 190, BF Cyg), this indication is present in the spectrum only during their active state when non collimated loss of mass by the outbursting white dwarf realises too (Skopal et al. 2009a; Tomov et al. 2012; Tomov T. et al. 2000; Munari et al. 2001, 2005; Skopal, Tomov et al. 2013). That suggests to us the two kinds of outflow are probably connected and the collimated outflow occurs only along with the non collimated one. That is why we suggest an other model to interpret the line spectrum of the symbiotic stars during their active phases where the collimated outflow results from the non collimated. In the framework of this model the collimated ejection could arise due to a stellar wind, if mechanism of collimation is available in the system. Such a mechanism can be related to a disc-like formation surrounding the white dwarf which provides a small opening angle of the outflowing jets. The proposed model gives possibility to explain all features of the observed spectrum without any important contradictions.

The main aim of our study is to suggest a model for the flow structure in the system Z And to explain all spectral features. We believe that it will be helpful in explaining not only the data acquired during the last active phase of Z And , but also all spectroscopic data taken during earlier phases, those following 1939, 1960 and 1984 and possibly the activity of other classical symbiotic stars.

5.6.2 Model

The mass transfer in Z And is from the stellar wind of the giant and the general structure of the flow thus largely depends on the wind parameters. As it was shown by two-dimensional and three-dimensional gas-dynamics modeling accretion can occur either with or without accretion disc depending on the wind parameters (Bisikalo et al. 2002, 2006; Mitsumoto et al. 2005). For the quiescent wind parameters of Z And an accretion disc forms in the system, which is seen in Fig. 5.24 (a). This figure shows that some of the flow lines in the orbital plane close around the accretor which indicates appearance of an accretion disk. The contours of constant density and the velocity vectors in the orbital plane are shown in Fig. 5.24 (b). The density contours also close around the accretor, which shows that an accretion disc forms in the system. The radius of the disk is about 50 $R_{\odot}$ for a wind velocity of $20-25$ $\mathrm{km\,s^{-1}}$and thus the outer part of the disk is optically thin. The mass of the disk is estimated as product of one quarter of the mass-loss rate of the giant $\sim 2 \times 10^{-7}$ $M_{\odot}$ yr^{-1} (Fernandez-Castro et al. 1988), and the typical time interval between the active phases—about 10 years. Based on the size and the mass of the disk of $\sim 5 \times 10^{-7}$ $M_{\odot}$ we can assume that its inner region can be optically thick. So we suppose that a thin accretion disc, located in the orbital plane exists in the quiescent state of the system.

To change the system from quiescent to active state a sufficiently large increase of the accretion rate is needed. Accretion of a considerable fraction of the disk's mass is required in order for an outburst to develop even in the combined model where the increased nuclear burning rate is taken into account (Bisikalo et al. 2006). Maximal increase of the accretion rate is possible in the framework of the mechanism proposed by Bisikalo et al. (2002) and Mitsumoto et al. (2005). According to this mechanism, even a small increase of the velocity of the wind of the donor is sufficient to change the accretion regime. During the transition from disk accretion to accretion from the flow, the disk is partially disrupted and the increased velocity of the wind causes falling of the material of the disk onto the accretor's surface. However, even in this case a considerable amount of mass (up to $50-80$ per cent) stays in the disk. Then massive accretion disk exists in the system

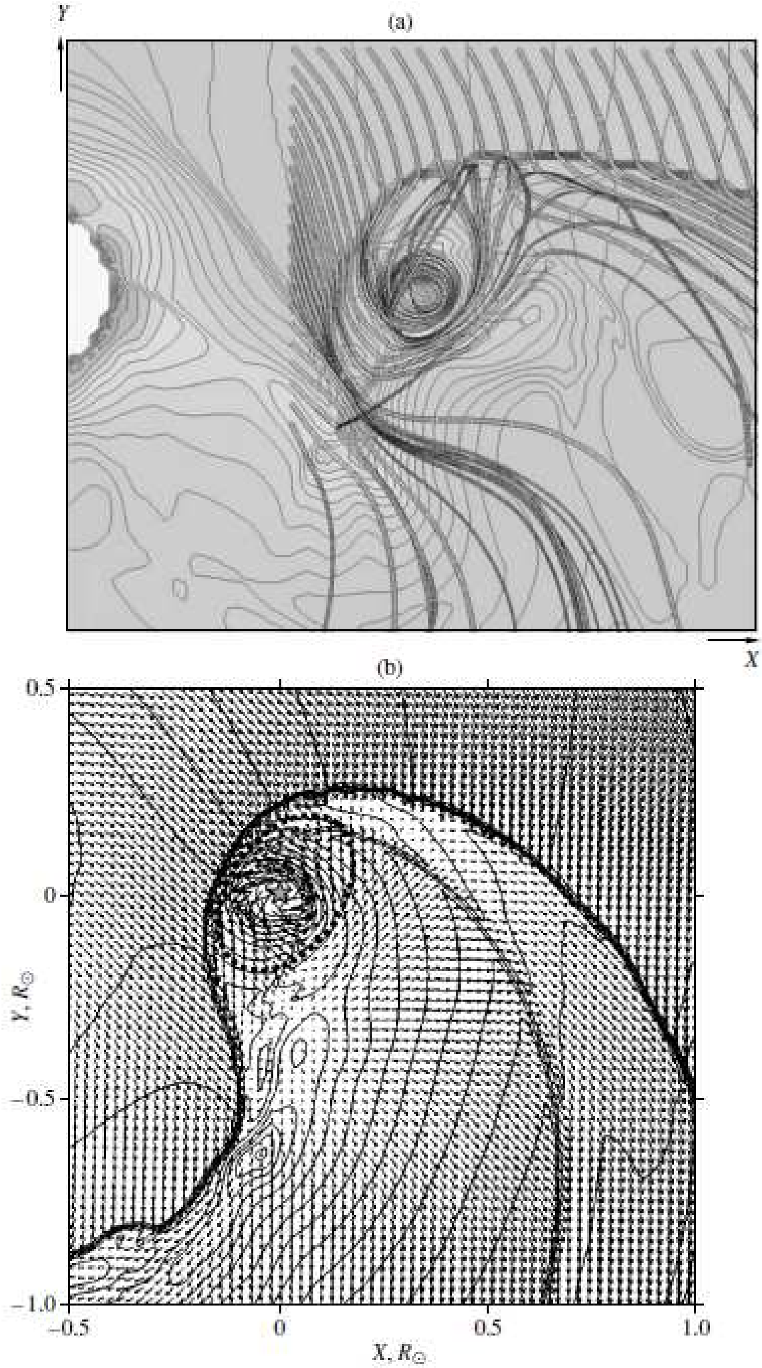

Figure 5.24: (a) Flow lines in the orbital plane of the system. The accretor is in the center. (From the 3D computations presented in Mitsumoto et al. (2005).) (b) Contours of constant density and velocity vectors in the orbital plane of the system. The dashed curve is the edge of the accretion disk.

during the active phase too.

During the first outburst the high velocity wind collides with the accretion disc. As a result of the collision its velocity close to the orbital plane decreases and does not change at higher stellar latitudes. The decrease of the velocity leads to an increase of the density and the level of the observed photosphere resides further away from the star. At higher stellar latitudes the level of the photosphere resides closer to the star. In this way an optically thick disc-like shell forms in the orbital plane, which plays the role of the observed photosphere. This shell occults the hot compact object and since the shell has a lower effective temperature (Tomov et al. 2003a; Skopal et al. 2006, 2009a) it is responsible for redistribution of the continuum energy from shorter wavelengths toward the optical region, resulting in the detection of an outburst. The observed P Cyg absorption is related to this shell. The collision of the wind with the accretion disc is equivalent to collision of two stellar winds and leads to appearance of region of shock waves whose temperature can reach 10^6 K (Nussbaumer & Walder 1993; Bisikalo et al. 2006).

During the active phase the wind of the compact object "strips" the accretion disc and ejects some part of its mass. At the end of each outburst some part of the ejected mass locates in the potential well of the compact object. After the cessation of the wind it begins to accrete again. Because of conservation of the initial angular momentum the accreting material falls into the disc and an envelope covering the disc forms. In this case an inverse P Cyg profile can not be observed since the disc is large compared to the effective photosphere. The envelope is located at a greater distance from the orbital plane than the accretion disc itself. The existence of centrifugal barrier leads to the appearance of two hollow cones with a small opening angle ($15° - 30°$) around the axis of rotation (Fig. 5.25, left panel) (Icke 1981; Blandford & Begelman 2004).

During the first outburst the envelope does not exist[2]. During the following outbursts of the active phase the extended envelope can collimate the wind, which in this case occupies only the two hollow cones and bipolar outflow forms (Fig. 5.25, left panel). This outflow is observed as high velocity satellite components, situated on either side of the main peak of the emission line. Their presence in the spectrum depends on the density of both the envelope (i. e. on the system's activity during its previous phases) and the outflowing material. These components will appear only if the density

[2]We consider the case when the envelope from the previous active phase has already disappeared. If not, we can observe collimated outflow from the very beginning of the active phase.

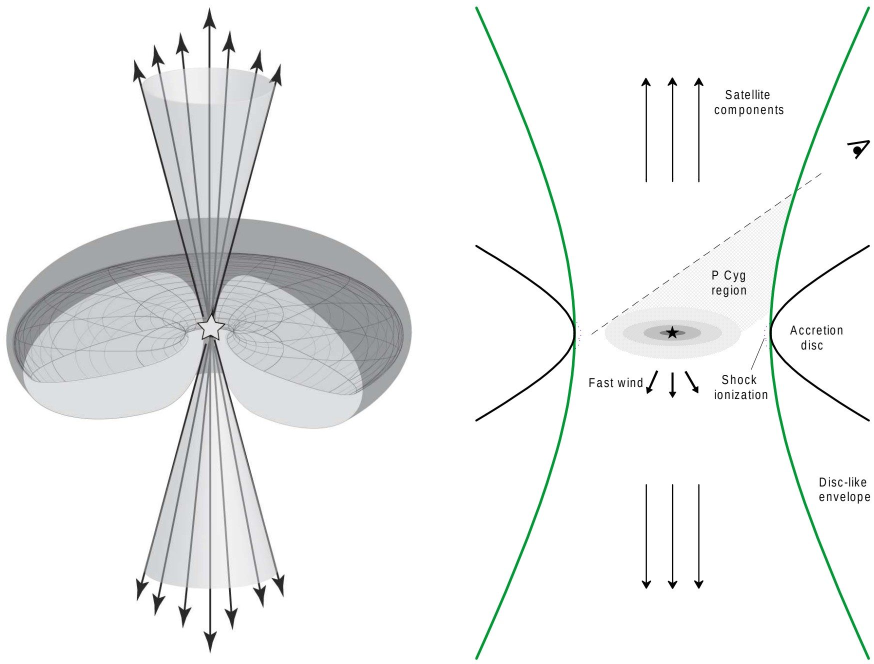

Figure 5.25: *Left panel:* Schematic model of the region around the hot component during recurrent strong outburst. *Right panel:* The same, but in the plane perpendicular to the orbital plane where the emission regions are shown. (From Tomov et al. (2010b, 2011a, 2014).)

of the envelope is high enough to provide collimation and the mass-loss rate of the outbursting component is also high. According to our model they are expected to be observed during outbursts accompanied by mass-loss at high rates and preceded by similar strong outburst.

This model predicts a stellar wind from the outbursting object for every system with spectral indication of collimated outflow during active phase (Tomov et al. 2014). For systems seen at high inclination ($i \sim 90^\circ$, eclipsing systems) it predicts emission wind component at a velocity position at the center of the line with a full width at zero intensity (FWZI) equal to the doublet velocity of the wind if the wind is optically thin. This component should be blended with the emission component of the collimated outflow. If the stellar wind is optically thick, it is expected to form a blueshifted absorption of the type P Cyg. So the systems seen at high inclination can not be distinguished from the systems with stellar wind only (without collimated outflow) and central emission from the nebula.

With decreasing the orbit inclination satellite components on both sides (if the collimated outflow is bipolar one) of the line center appear and reach their maximal velocity position at inclination $i = 0^\circ$ (systems seen pole-on). When $i = 0^\circ$ and the front part of the outflow (wind+stream) is optically thin, a blueshifted emission component should present in the spectrum. It can occupy a broad range of velocities – from the velocity of the wind close to the outbursting object to the terminal velocity. When the front part of the outflow (wind+stream) is optically thick, a blueshifted absorption component should exist, which can occupy a broad range of velocities too. In this case, however, if some part of the outflow does not project on the effective photosphere (depending from the opening angle of the stream) it can give rise to blueshifted emission, whose velocity can be within the velocity range of the absorption. When the outer part of the outflow is optically thin and its inner part - optically thick, a blueshifted emission and less blueshifted absorption should be observed.

When $i = 0^\circ$ a redshifted satellite component can not present in the spectrum due to occultation of the back stream by the effective photosphere, which depends from the opening angle of the stream. If the outer part of the back stream is only seen (center is occulted), the velocity of the redshifted component will be smaller than the (effective) velocity in the stream. The wind particles moving perpendicular to the line of sight should give rise to emission close to the line center which will be blended with the line component from the nebula.

The gas outflowing close to the surface of the cone, whose velocity is lower than that along to the cone axis, can contribute to the broad wind emission components too (Fig. 5.25). Depending on the inclination angle of the orbit and the opening angle of the cone the outflow close to the cone surface can have a radial velocity, which makes it able to emit at wavelengths far away from the center of the satellite emission. According to this model, the profiles of the symbiotic binaries with collimated ejection during their active phases can have complex morphology depending from the inclination of the orbit, the opening angle of the stream and the velocity and optical thickness of the outflows.

As a result of interaction of the stellar wind with the disc/envelope a high-temperature region of collisional ionization emitting X-ray spectrum forms close to the orbital plane. Two-dimensional gas-dynamical model of a system with parameters close to those of Z And shows that when the velocity of the wind of the outbursting compact companion is even as low as 50–100 $\mathrm{km\,s^{-1}}$, a region of shock waves appears as a result of collision with the wind of the giant (Bisikalo et al. 2006). According to these computations shock structure begins to form about 70^d after the onset of the companion's wind and reaches its maximal development about $20-30^d$ later. The temperature of the shock region is appreciably higher than that of the surrounding medium and can reach 10^6 K. With the accepted parameters of the wind the computed area of the shock has a X-ray luminosity of 10^{31} – 10^{32} $\mathrm{erg\,s^{-1}}$. This result is in good agreement with the X-ray luminosity of Z And observed during its 2000 – 2002 eruption (Sokoloski et al. 2006). It allows us to assume that a similar region should arise close to the collision boundary between the companion's wind and the disc/envelope. This region should contribute to the broad lines.

According to this model a geometrically thin accretion disc exists in the system during the first (2000 – 2002) outburst. The wind from the compact companion with a high velocity of about 500 $\mathrm{km\,s^{-1}}$, indicated by the broad emission component of the line He II 4686, appears at early stage of the outburst and is slowed down close to the orbital plane due to the collision with the disc. As a result of the collision the wind acquires low velocity, becomes optically thick and gives rise to the low velocity P Cyg component of the lines of He I. The collision provides possibility a region of shock ionization with a high electron temperature to appear in the system, which gives rise to the narrow component of the line He II 4686. The emitting region of this line thus moves together with the compact companion and its back side is occulted by the flat shell. This conclusion explains the great negative velocity of the line.

An envelope covering the accretion disc, which can collimate the stellar wind is possible to form in the Roche lobe of the compact object during the recurrent outbursts of the active phase. This envelope can determine the behaviour of both the optical light and the profiles of the spectral lines. Its emission measure can be less or equal to the increase of the emission measure of the whole circumbinary nebula. It was shown that the double-peaked Balmer lines H_α and H_γ during the outburst in the end of 2002 can be emitted by such disc-shaped structure.

We suppose that an envelope covering the accretion disc and collimating the stellar wind exists in the system during the 2006 – 2007 outburst. The wind from the compact companion with a high velocity, indicated by the broad emission component of the lines H_γ and He II 4686 collides with the disc and envelope and a collimated outflow forms after the collision. The outer region of the outflow gives rise to the high-velocity satellite emission components, situated on either side of the main peak of the lines H_α, H_β and H_γ. The outflowing gas which is projected onto the observed photosphere of the outbursting compact object (the flat shell) gives rise to the P Cyg absorption components of the lines H_α, H_γ and the He I lines. Due to this absorption the blue wing of the broad emission component of the line H_γ is not seen. The radial velocities in the area of the wind projecting onto the observed photosphere cover an appreciable range – from values close to zero to the maximal observed velocity of the collimated outflow. This provides the possibility for broad absorption components to form. The red wing of the broad emission component of the lines H_γ and He II 4686 is seen since some part of the back wind component and possibly the collision region of the wind with the disc is not occulted by the observed photosphere (the flat shell). As in the case of the first 2000 – 2002 outburst we suppose that a high-temperature region of collisional ionization heated by shock waves appears close to the accretion disc and gives rise to the narrow component of the line He II 4686.

5.6.3 Applicability of the model for other classical symbiotic stars

We suppose that the model suggested by us can be used to explain the behavior of the line spectrum of other classical symbiotic stars during their active phases too since they have the next general characteristics:

1. The mass transfer in the majority of the classical symbiotic stars is realized with the stellar wind of the giant. The theoretical computations of Bisikalo et al. (2002) and Mitsumoto et al. (2005) show that for systems with parameters close to those of Z And an accretion disk from wind accretion forms around the compact object. The accretion disk prevents the outflowing material during the active phase and outflow with two-component velocity regime forms.

2. The systems with parameters close to Z And have close accretion rate of their compact object. The accretion rate determines the regime of hydrogen burning. The view that hydrogen burns in a steady state in the classical symbiotic stars is commonly accepted. When the accretion rate goes above the upper limit of the steady burning range the white dwarf expands which is observed as optical outburst with typical duration of one year. The first outburst opening the active phase can be followed by repeated outbursts. During the repeated outbursts an extended envelope covering the accretion disk can form in the system and can collimate the stellar wind.

5.6.4 Discussion

Widely accepted view is that collimated ejection by interacting binary stars is related to mass outflow from an accretion disc around a compact object driven by magnetic fields. According to this view collimated ejection by the symbiotic stars is expected to be observed in both of their states - quiescent and active ones if there is an accretion disc with collimating field strong enough in the system. Spectroscopic data, however, show that in most cases the collimated outflow by the symbiotic stars is observed only during phase of activity when it is accompanied by an expansion of the outbursting object. During the 2006 brightening of Z And we observed on one hand high velocity satellite components of the line H_α, H_β and H_γ, indicating bipolar collimated outflow and, on the other hand, multi-component blueshifted absorption of the line H_γ and the He I lines indicating P Cyg stellar wind with velocities in a very broad region – from low velocity of about 100 $\mathrm{km\,s^{-1}}$ to very high ones of 1500 $\mathrm{km\,s^{-1}}$. We suggest an idea to interpret this phenomenon, in the framework of which the collimated outflow follows in the train of the stellar wind by the compact object. This idea provides better interpretation of the line components than the traditional model with a magnetic accretion disc.

5.7 Conclusion and results

After the year 2000 the symbiotic prototype Z And underwent its last active phase. We used results of gas-dynamical modeling of the flow structure in one symbiotic binary with parameters close to those of Z And to study the development of its first 2000 – 2002 outburst. This analysis shows that the accretion processes are not able to provide the observed energetics of the event. As a possible mechanism of the outburst we considered a combined case when the increase of the accretion rate as a result of the disruption of the disk leads to variation of the burning rate. In this way the subsequent increase of the luminosity (the development of the outburst) is determined by the increased nuclear-burning rate. An expanding envelope (pseudophotosphere) or optically thick wind forms in the system after the first kink of the light curve, which is associated with an enhancement of the nuclear burning. In this case the curve of the optical light is determined by three processes: (1) a luminosity increase leading to expansion of the pseudophotosphere, (2) wind propagation in the nebula forming a high-temperature region, (3) appearance of shock structures formed as a result of winds collision. As it is seen from the results of the computation of the gas-dynamical structure, the effects associated with the wind are strong enough to contribute to the complex multistage nature of the rise of the optical light during the period when the outburst progresses.

High-resolution observations of selected lines of He I and He II of the binary were performed during this outburst too. The triplet lines of helium He I $\lambda\,4471$ Å and $\lambda\,4713$ Å had P Cyg profile indicating stellar wind from the compact object with a velocity of about 60 $\mathrm{km\,s^{-1}}$ in November and December 2000 at the time of the maximal light. The orbital variation of the radial velocity of the line He II $\lambda\,4686$ resembled that of a secondary stellar component. The line He II $\lambda\,4686$ contained broad emission component with low intensity indicating stellar wind with a velocity of about 500 $\mathrm{km\,s^{-1}}$ from the compact secondary.

The profiles of the Balmer lines H_α and H_γ were double-peaked during the rise of the light and ligt maximum of the small eruption in the end of 2002. It has been shown that they can be emitted mainly by one extended disc-like envelope, covering the initial accretion disc and located in the Roche lobe of the compact object, whose emission measure is not greater than the increase of the emission measure of the circumbinary nebula during the eruption. The parameters of this envelope are compatible with the predicted ones by the gas dynamical modeling. An other possibility is the Balmer profiles observed to be determined from selfabsorption only.

The profile of the Balmer lines at the time of the light maximum during the 2006 eruption was a multi-component one consisting of an intense central narrow emission located around the reference wavelength, broad wings, a blueshifted absorption and high-velocity satellite absorption/emission features on both sides of the central emission at a velocity position of 1200 – 1500 $\mathrm{km\,s^{-1}}$ indicating bipolar collimated ejection from the compact object in the system. The broad emission wings and the satellite emissions were seen until the beginning of December 2006. The width of the wings in the different Balmer members, however, was different. The blueshifted P Cyg absorption was seen until the beginning of October 2006.

At almost all spectra in 2006 the lines of He I consisted of a narrow emission located close to the reference wavelength and a blueshifted absorption. At the time of the maximal light the absorption of the line He I 4471 was multicomponent one occupying a broad velocity range like the line H_γ. The most blueshifted component was at the velocity position of the satellite component. After that the broad absorption went into a low velocity narrow feature, which was visible till the beginning of December 2006.

In October and December 2006 the line He II 4686 was two-component one, consisting of a central narrow emission and a broad emission component with a low intensity, which behaviour with the optical light was the same like that of H_γ.

The mass-loss rate of the compact object was estimated at several epochs of the eruption. The rate was found to decrease, from $(4-5)\times 10^{-7}(d/1.12\ \mathrm{kpc})^{3/2}\ M_\odot\,\mathrm{yr}^{-1}$ at the time of maximum light to about $1\times 10^{-7}(d/1.12\ \mathrm{kpc})^{3/2}\ M_\odot\,\mathrm{yr}^{-1}$ in December 2006.

The widely accepted view is that collimated ejection by interacting binary stars is related to mass outflow from an accretion disc around a compact object driven by magnetic field. According to this view, the collimated ejection by symbiotic stars is expected to be observed in both of their states - quiescent and active – if there is an accretion disc with a collimating field strong enough. Spectroscopic data, however, show that in most cases the collimated outflow of symbiotic stars is observed only during phase of activity when it is accompanied by an expansion of the outbursting object.

We suggested an idea to interpret this phenomenon, in the framework of which, the collimated outflow is a consequence of interaction between the wind emitted by the compact object and its accretion disc. Initially, there is a thin disc formed by accretion of stellar wind matter in the quiescent state of the system. Due to accretion of mass ejected during the first (and every following) outburst of the active phase, an envelope covering the disc forms, which extends to a greater distance from the orbital plane. The material in the envelope has residual angular momentum and rotates around the same axis as the accretion disc. The centrifugal force produces two hollow cones around the axis of rotation. The stellar wind from the compact object propagates only through these hollow cones during the recurrent outbursts, thereby giving rise to a bipolar collimated outflow. Such a flow structure is expected to form line profiles with a complex morphology which is determined by orbit inclination, opening angle of the stream, velocity, and optical thickness. The interaction of the stellar wind with the disc shaped material produces a high temperature region emitting X-ray radiation. This region should contribute to the broad emission lines.

Based on this scenario we supposed that during the first outburst of the active phase the high-velocity wind of the compact object collides with the disc and as a result a mass-outflow in two velocity regime is observed: a P Cyg wind indicated by the He I lines and a high-velocity optically thin stellar wind indicated by the broad emission component of the line He II 4686. The behaviour of the optical lines of Z And during its recurrent outbursts is considered in the framework of the second stage of this scenario (Tomov et al. 2014). It is supposed that the wind of the compact object collides with the accretion disc and disc-like envelope which plays a role of mechanism of collimation. After the collision the wind is observed as high-velocity satellite absorption/emission components of the Balmer and helium lines. The satellite components are expected to be observed if the density of the envelope is high enough to provide collimation and the mass-loss rate of the outbursting object is also high.

Chapter 6

Symbiotic stars with spectral indication of bipolar ejection and stellar wind

6.1 Introduction

The symbiotic binaries having indication of bipolar ejection and stellar wind are considered in the works of Tomov et al. (2013, 2014). Five of all symbiotic systems with collimated outflow have optical indication related to additional satellite emission/absorption components of their spectral lines. These systems are MWC 560 (Tomov T. et al. 1990), Hen 3-1341 (Tomov T. et al. 2000), StHα 190 (Munari et al. 2001), Z And (Burmeister & Leedjärv 2007; Tomov et al. 2007) and BF Cyg (Skopal, Tomov et al. 2013). In four of these systems, excepting MWC 560, bipolar outflow was observed during phases of activity, when an additional P Cyg absorption, indicating stellar wind from the outbursting compact object, was observed along with the satellite line components. The recent theory of the origin of the bipolar collimated outflow (jets) from compact objects does not envisage the possibility of stellar wind to appear (Zanni et al. 2007). We use a scenario suggested originally for interpretation of the behaviour of Z And where presence of stellar wind is provided along with bipolar collimated outflow. The mean goal of this study is to interpret the line profiles of several symbiotic stars in the light of this scenario. An other aim is to interpret the photometric behaviour of the outbursting compact object in the eclipsing binary BF Cyg during its 2006 – 2015 eruption in the framework of the same scenario.

6.2 Hen 3-1341

Hen 3-1341 consists of a cool giant of spectral type M4 (Mürset & Schmid 1999) without circumstellar dust (Munari et al. 1992; Tomov T. et al. 2000), very hot and luminous white dwarf with effective temperature of $\sim 1.2\times10^5$ K and luminosity of 3.8×10^3 $L_\odot$, and a surrounding nebula partly photoionized by the white dwarf (Munari et al. 2005).

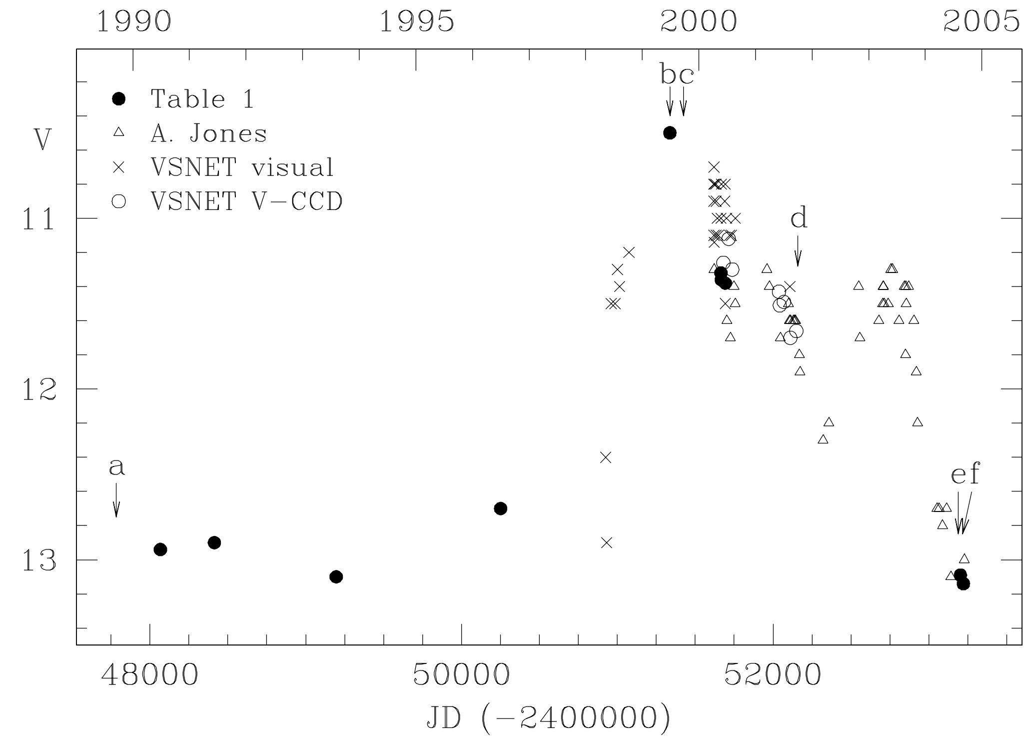

Figure 6.1: The V light curve of Hen 3-1341 over the time 1990–2005 showing the 1998 − 2004 outburst from the paper of Munari et al. (2005).

The system underwent a large outburst lasting from 1998 to 2004 (Fig. 6.1) which was its first outburst ever recorded (Tomov T. et al. 2000; Munari et al. 2005). High-resolution spectral data were obtained by Tomov T. et al. (2000) and Munari et al. (2005) during this outburst. The data of Tomov T. et al. (2000) taken on June 8, 1999 shows that the H_α line had an emission profile consisting of an intensive central singlepeaked component and additional satellite components with velocity of about 800 km s^{-1} on both sides of the central emission. The same appearance had the H_β profile whose satellite components had the same velocity. The profile of the triplet He I λ5876 line was similar to those of the Balmer lines consisting of the same compo-

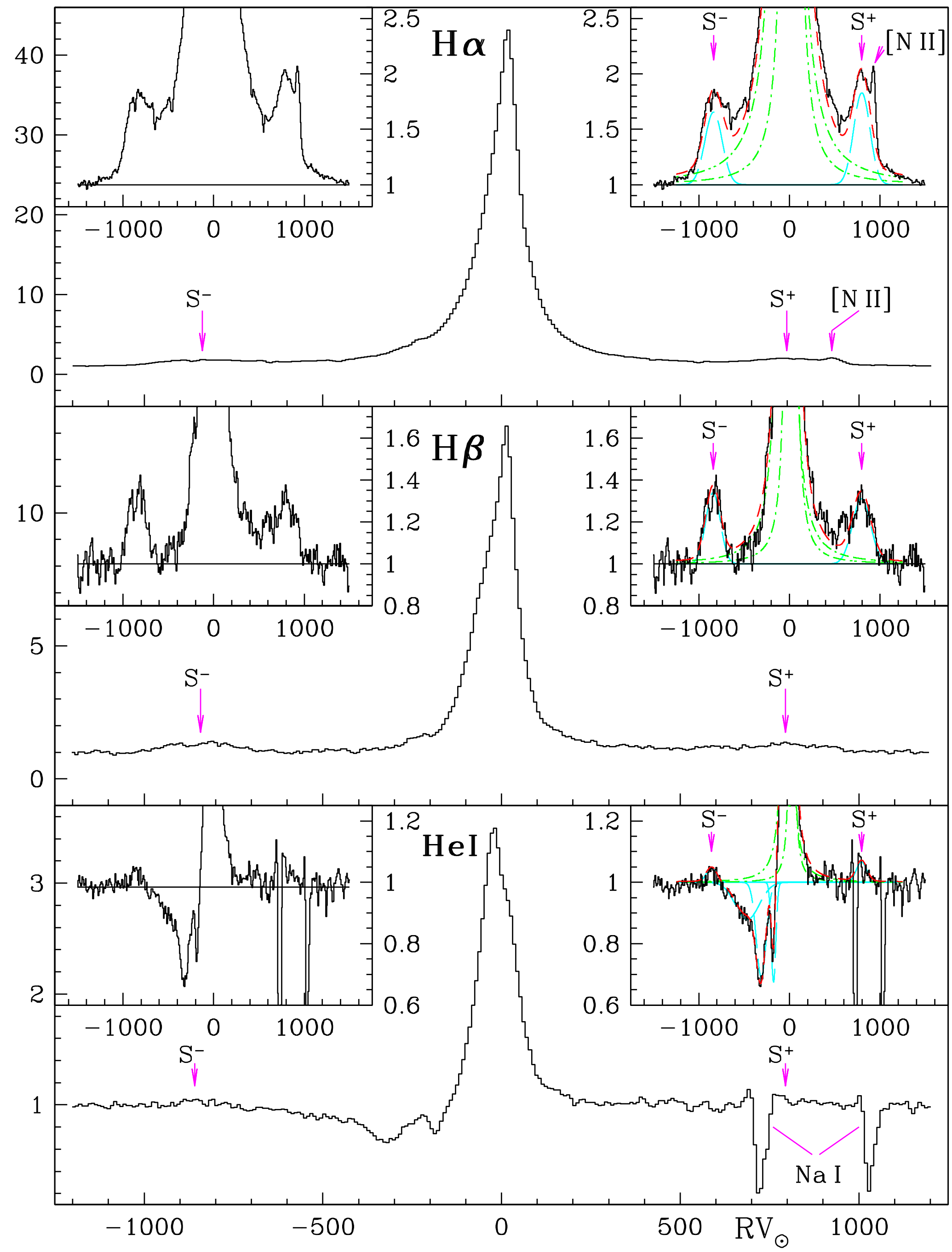

Figure 6.2: The profiles of the H_α, H_β, and He I $\lambda\,5876$ lines of Hen 3-1341 based on CCD frames on June 8, 1999 (From the paper of Tomov T. et al. (2000).)

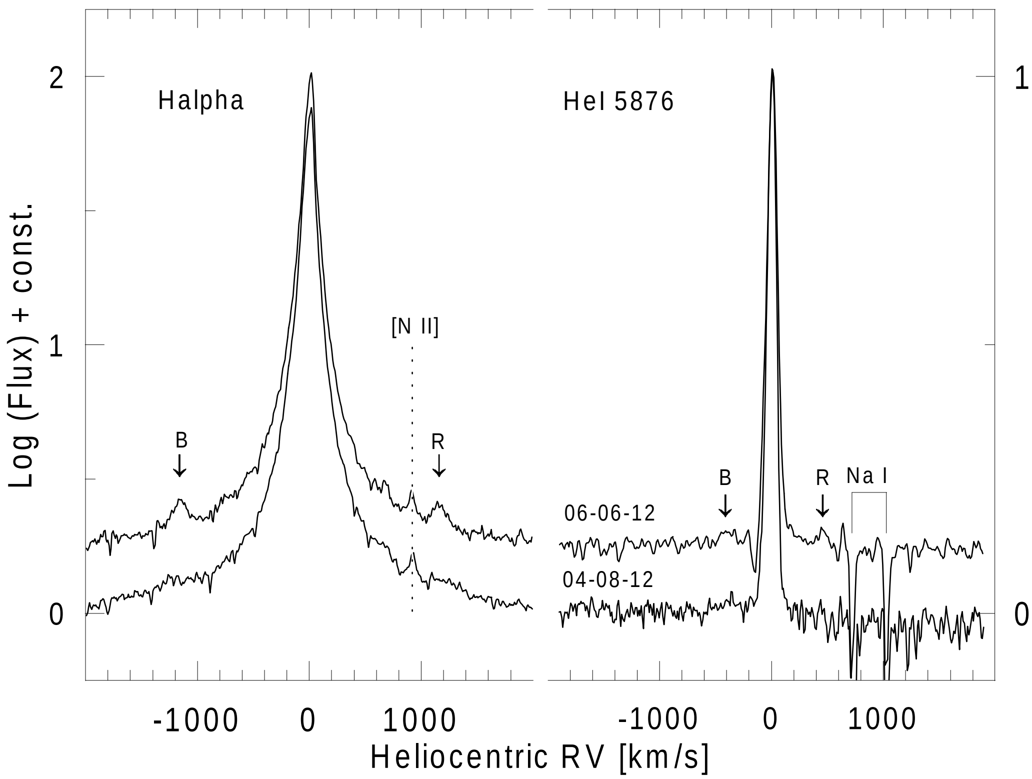

Figure 6.3: The profiles of the H_α and He I $\lambda\,5876$ lines of Hen 3-1341. The spectra are in units of the continuum. The right y-scale is related to the intensity of the helium line.

nents but this line contained two-component P Cyg absorption in addition which occupied broad velocity range—from about 150 to about 700 km s^{-1} (Fig. 6.2). The high-velocity emission satellite components of all lines were attributed by the authors to bipolar jets and the He I P Cyg absorption was recognized as signature of mass outflow (stellar wind) from the outbursting compact object. Munari et al. (2005) paid attention to the tight correlation between the strength of the H_α satellite components and the He I P Cyg absorption. They came to the conclusion that the wind plays a role of feeding mechanism for the bipolar jets.

The system Hen 3-1341 underwent a new outburst in 2012 and in the beginning of March its B light was increased with two magnitudes compared with the quiescent value in July 2011 (Munari et al. 2012a). We observed the regions of its lines H_α and He I $\lambda\,5876$ on 2012 June 6 and August 4 (Tomov & Tomova 2013). On June 6 the profile of the line H_α was multicomponent consisting of a central emission located around the reference wavelength,

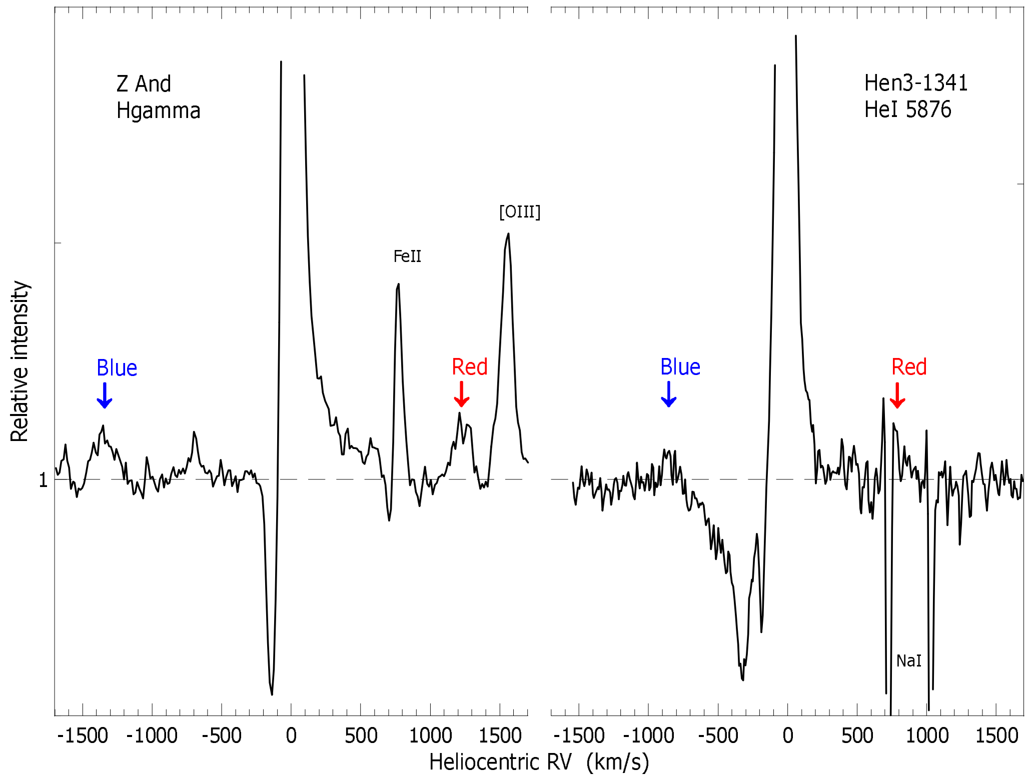

Figure 6.4: The H_γ profile of Z And based on a CCD frame on 2006 September 8 and the He I λ 5876 profile of Hen 3 -1341 based on CCD frame on 1999 June 8 (Tomov T. et al. 2000).

broad wings with low intensity extended to not less than ± 2000 km s^{-1} from the center of the line, and additional satellite emission components with a velocity of 1160 km s^{-1} on both sides of the central emission, indicating bipolar collimated ejection from the system (Fig. 6.3). On August 4 the profile of the line H_α was similar, the satellite emissions were disappearing and only weak remnants were visible at their radial velocity position.

The profile of the He I λ 5876 line (Fig. 6.3) on June 6 consisted of emission component of nebular origin and a P Cyg absorption indicating mass outflow from the system with a velocity of about 150 km s^{-1}. On both sides of the nebular component, however, two very weak emission details were visible pointed with arrows in the figure. Their velocity was much lower than the velocity of the H_α satellite components. The velocity of the blueshifted one was -410 km s^{-1} and the velocity of the redshifted was 460 km s^{-1}. On August 4 the weak emission and the P Cyg absorption disappeared.

In our opinion the correlation between the change of the H_α satellite emissions and the He I absorption as was noted by Munari et al. (2005)Munari et al. (2005) is of primary importance. In the framework of our model the He I λ 5876 line can be interpreted in the following way. The stellar wind from the white dwarf collides with the disc and envelope and a bipolar collimated outflow appears. The radial velocities in the P Cyg area cover an appreciable range—from values close to zero to the terminal wind velocity (Fig. 5.25). This provides the possibility for broad absorption to form. The high-velocity satellite emissions appear in more outer regions of the wind, not projecting onto the effective photosphere.

The He I profile of Hen 3-1341 is compared with the H_γ profile of Z And in Fig. 6.4. The good similarity of the two profiles supports the notion that a similar model could apply to both objects.

6.3 StHα 190

The system StHα 190 has been discovered by Stephenson (1986). It is a yellow symbiotic binary consisting of a G4 III/IV cool giant (Smith et al. 2001) and an O sub-dwarf Munari et al. (2001). Its orbital period is not known. The amplitude of the radial velocity of its cool component, however, is large — of about 30−40 km s^{-1} (Munari et al. 2001; Smith et al. 2001). According to Munari et al. (2001) this amplitude suggests a high orbital inclination, a massive hot component and a short orbital period. The high rotational velocity of the cool component of 105 km s^{-1} (Munari et al. 2001; Smith et al. 2001) also supports the high orbital inclination of the system.

We were not able to find in the literature photometric data, indicating outbursts of the star StHα 190. According to Munari et al. (2001) its photometric $UBV(RI)_{\rm C}$ data do not show presence of eruptive activity since its discovery to mid 2000, just before their observation of line components indicating bipolar jet-like outflow. The broad-band $JHKL$ data of the star taken during the time of this observation (Munari et al. 2001) were not above their mean values in October 1983 – July 1987 from the photometry of Whitelock et al. (1995). Moreover, we did not find any data indicating eruptive activity in all time after the appearance of the 2000 bipolar outflow. The V photometric data of ASAS taken in the time interval JD 2452000 – 2455200 do not show eruptive activity too.

Munari et al. (2001) obtained high resolution spectral data in the ranges of the lines H_α, He I λ 5876, and [O III] λ 4959 in August – December 2000. The H_α profile consisted of main central component with FWHM of 40 – 50 km s^{-1} and additional peaks (shoulders) situated on both sides of the central component, resulted from blending with satellite emission components

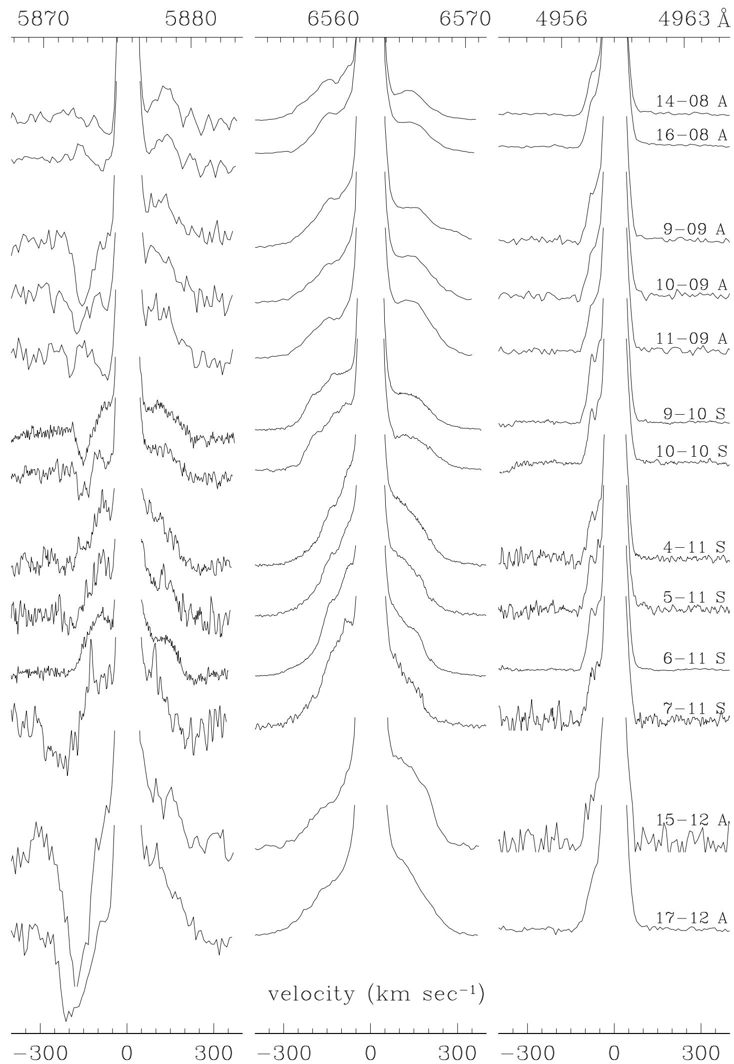

Figure 6.5: Evolution of the H_α, He I λ 5876 and [O III] λ 4959 lines of StHα 190 in August – December 2000. The spectra are in units of the continuum. (From the paper of Munari et al. (2001).)

with FWHM of about 150 – 250 km s^{-1} (Fig. 6.5). Moreover, as the authors wrote, "Weak P Cyg absorptions interfere with the blue jet component, reducing its width and its velocity shift vs. the main H_α component". The radial velocity of the satellite components was about 150 km s^{-1}. Since the orbital inclination is supposed to be high, the real velocity of the outflowing gas emitting the satellite components should be also high and can be about 1000 km s^{-1}. The profile of the triplet line He I λ 5876 was similar to that of H_α consisting of the same components. The P Cyg absorption of He I, however, was highly variable and good visible, occupying velocity range of up to about 200 $\mathrm{km\,s^{-1}}$. At some times it was multicomponent one (Fig. 6.5). The emission satellite components were identified by the authors as spectral signatures of jet-like discrete ejection events and the variable P Cyg absorption was recognized as signature of blobby mass outflow. We do not know how does the intensity of the satellite components change with the change of the P Cyg absorption, but as these data show, a strong P Cyg wind existed together with the collimated ejection during the whole time of observation.

One of the basic features of the system StHα 190 is that eruptive activity is not observed although an indication of variable stellar wind is present in the spectrum. We do not know how the system has come in a state of wind outflow from the compact object. Our main aim is to propose model of the mass ejecting secondary to interpret the profiles of the spectral lines. If as a result of an outburst a stellar wind appears for a long time, and an extended, geometrically thick disc exists which can provide collimation, a stationary flow regime will settle in the system when a part of the ejected material will fall back into the disc. Since the disc is large the infalling material can not project on the observed photosphere of the outbursting object and an inverse P Cyg profile can not be observed. A binary system in such stationary flow regime can not change his light. Then the line profiles of StHα 190 can be considered in the light of the model of Z And.

6.4 BF Cyg

6.4.1 Balmer lines

The symbiotic BF Cyg system is an eclipsing binary (Belczynski et al. 2000) consisting of a late-type cool component classified as an M5 III giant (Kenyon & Fernandez-Castro 1987), a hot compact object with temperature of about 100 000 K and an extended surrounding nebula (Skopal 2005). Its orbital period is about 757^{d}, which is based on both photometric (Mikolajewska 1987) and radial velocity (Fekel et al. 2001) data.

The historical light curve of BF Cyg shows three types of activity. It contains one very prolonged outburst, lasting for decades and similar to that of the symbiotic novae, several eruptions of an other type such as those observed in the classical symbiotic stars and sudden rapid brightenings, lasting a small portion of the orbital period (Skopal et al. 1997). The last major eruption of BF Cyg began in 2006 and at the present time continues (Fig. 6.6).

We observed the regions of the H_α and H_β lines of BF Cyg on seven nights during 2009 June–2012 September (Skopal, Tomov et al. 2013). During the

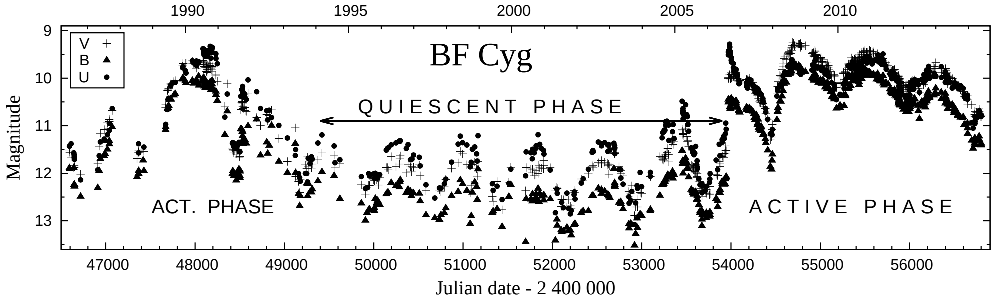

Figure 6.6: The UBV light curves of BF Cyg during its outburst after 1989 and 2006 and the quiescent stage between them from the work of Skopal et al. (2015).

whole time of the observations the H_α line had multicomponent profile. It had central narrow emission which at times was double with a blueshifted central reversal and very broad wings with a low intensity extended to velocity of about ± 2200 km s^{-1} from the center of the line (Fig. 6.7). They were analyzed by fitting with a Gaussian function but their nature was rather unclear. The H_α line had additional peaks/bumps situated on either side of its central component with radial velocity position of ~ 400 km s^{-1}. At the more early stage of the outburst a blue peak was not seen but only an extended wing of the line. Since 2011 Sept. 5, however, a blue peak appeared and was more pronounced than the red one (Fig. 6.8). Comparison with the H_β line (see below) proposes that the absence of the blue peak at the more early stage of the outburst is most probably due to optical depth effect (Fig. 6.8). Based on both comparison with H_β and analysis of the line profiles (Skopal, Tomov et al. 2013) we assume that the H_α peaks/bumps with radial velocity position of $\sim$ 400 km s^{-1} indicate bipolar collimated outflow from the outbursting component of the system.

The H_β line consisted of a narrow core, which at times was double with a blueshifted central reversal similar to H_α , and additional emission/absorption components (Fig. 6.8).

The high-velocity absorption component on the spectrum of 2010 May 25 and the most blueshifted emission peak on the last three spectra have the same position close to -400 km s^{-1}. This gives us a reason to suppose they are related to the same individual line component which appears as absorption at some stage of the outburst and after that goes into emission. The transformation of the absorption into emission is seen on the spectrum of 2011 September 5. The presence of this individual component in the spectrum of 2009 June 5 is indicated by one weak absorption. This absorption does not present in the spectrum of 2009 October 11 taken at orbital phase

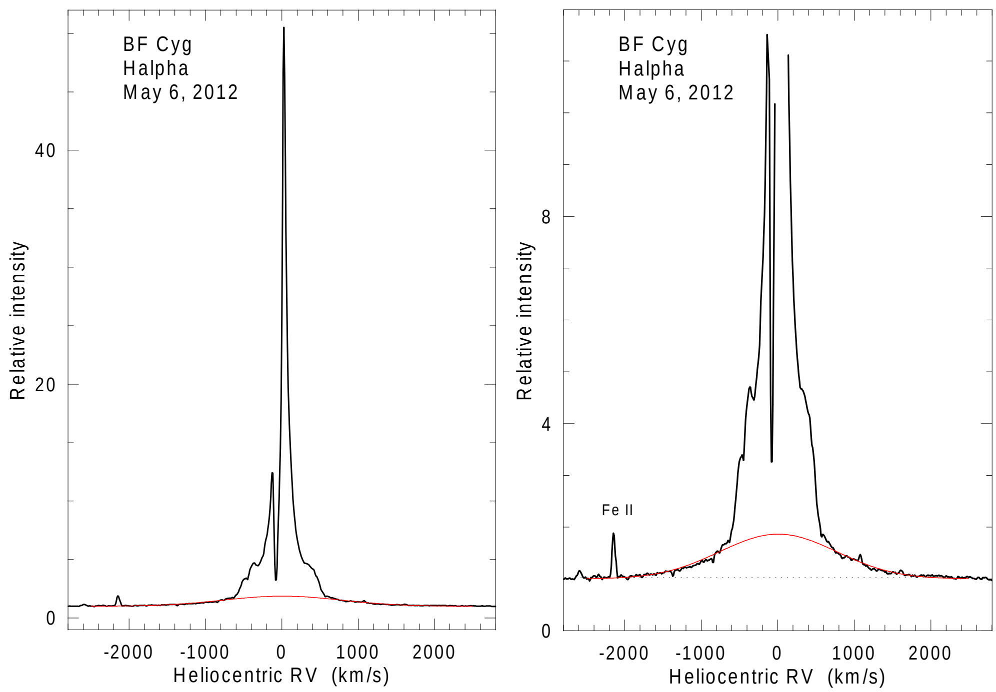

Figure 6.7: *Left panel*: The profile of the H_α line of BF Cyg based on a CCD frame on 2012 May 6. *Right panel*: The area of the wings where the broad component is better seen. The level of the local continuum is marked with a dashed line.

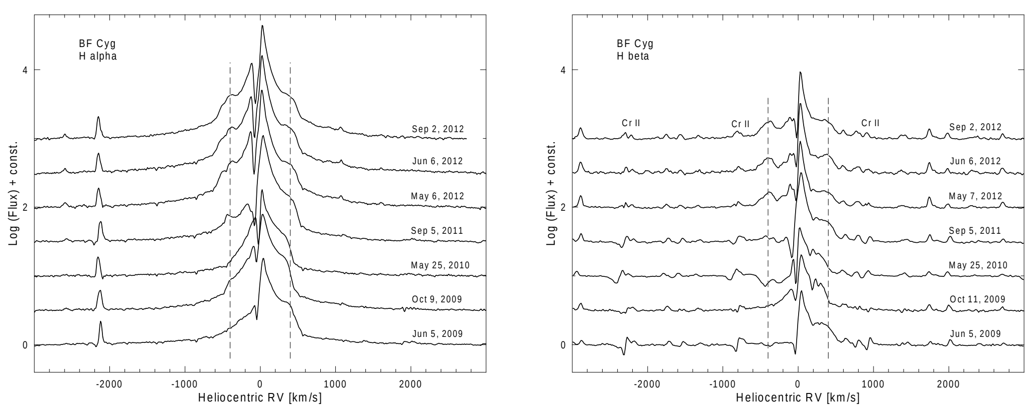

Figure 6.8: Time evolution of the H_α and H_β lines of BF Cyg.

0.914, probably because of eclipse effect of the effective photosphere (pseudophotosphere) of the expanding compact object.

We assume the individual component at a position of $-400\ \mathrm{km\,s^{-1}}$ probably indicates collimated ejection from the expanding compact object which

Table 6.1: Parameters of Gaussian fits to the satellite emissions in H_α and H_β lines: Radial velocity RV_S [$km\,s^{-1}$], $FWHM_S$ [$km\,s^{-1}$], opening angle θ_0 [°], flux F_S [$10^{-12}\,erg\,cm^{-2}\,s^{-1}$] and emission measure EM_{jet} [$10^{58}\,cm^{-3}$].

Date	Line	RV_S		$FWHM_S$		θ_0		F_S		EM_{jet}	
dd/mm/yyyy		S^-	S^+	S^-	S^+	S^-	S^+	S^-	S^+	S^-	S^+
05/06/2009	H_α	–	+298	–	270	–	18.4	–	18.0	–	17
	H_β	–	+295	–	302	–	20.8	–	10.1	–	25
09/10/2009	H_α	-334	+308	215	161	13.0	10.6	7.5	11.7	7.1	11
11/10/2009	H_β	–	+221	–	249	–	22.9	–	8.2	–	21
25/05/2010	H_α	–	+332	–	203	–	12.4	–	12.1	–	11
	H_β	–	+291	–	192	–	13.4	–	6.9	–	17
05/09/2011	H_α	–	+317	–	274	–	17.5	–	16.7	–	16
	H_β	–	+301	–	261	–	17.6	–	7.7	–	20
06/05/2012	H_α	-361	+375	248	258	13.9	13.9	13.8	13.8	13	13
07/05/2012	H_β	-378	+334	167	302	8.9	18.3	2.2	4.0	5.6	10
06/06/2012	H_α	-368	+377	248	258	13.6	13.9	12.1	13.8	11	13
	H_β	-376	+333	167	319	9.0	19.4	2.1	4.4	5.3	11
02/09/2012	H_α	-363	+381	247	247	13.8	13.1	13.5	14.1	13	13
	H_β	-370	+307	214	344	11.7	22.7	2.6	5.5	6.6	14

ejection is optically thick at the more early stage of the outburst. On the spectra taken after 2012 May one redshifted emission peak at the same velocity of 400 $km\,s^{-1}$ is seen. Then we assume that it is emitted by the back component of the collimated ejection, i.e. the ejection is bipolar one. This bipolar ejection probably gives rise to the peaks/shoulders at the same velocity of $\sim$ 400 $km\,s^{-1}$ on the other H_β spectra and to the peaks/shoulders in the emission profile of the H_α line. The satellite H_α and H_β emission components with a velocity of about ± 400 $km\,s^{-1}$ are analyzed with a Gaussian function to determine their exact wavelength position and equivalent width in our paper (Skopal, Tomov et al. 2013). Their fluxes were obtained with the aid of simultaneous broad–band $UBVR_CI_C$ photometry, corrected for the emission lines. The profile of the satellite emissions is shown in Fig. 6.9 and their parameters are listed in Table 6.1. The opening angle of the cone was calculated as in the case of Z And (Sect. 5.5.3, Eq. 5.5). The uncertainty in the RVs is $10-20$ $km\,s^{-1}$, in the FWHMs – 0.4 Å and in the line flux is about $10-20$ per cent. The average value of the opening angle is $\theta_0 = 15.2° \pm 1.5°$. During the 2006 – 2015 outburst of BF Cyg satellite line components indicating collimated ejection were observed for the first time in this system.

One absorption component of the line H_β at a radial velocity position of

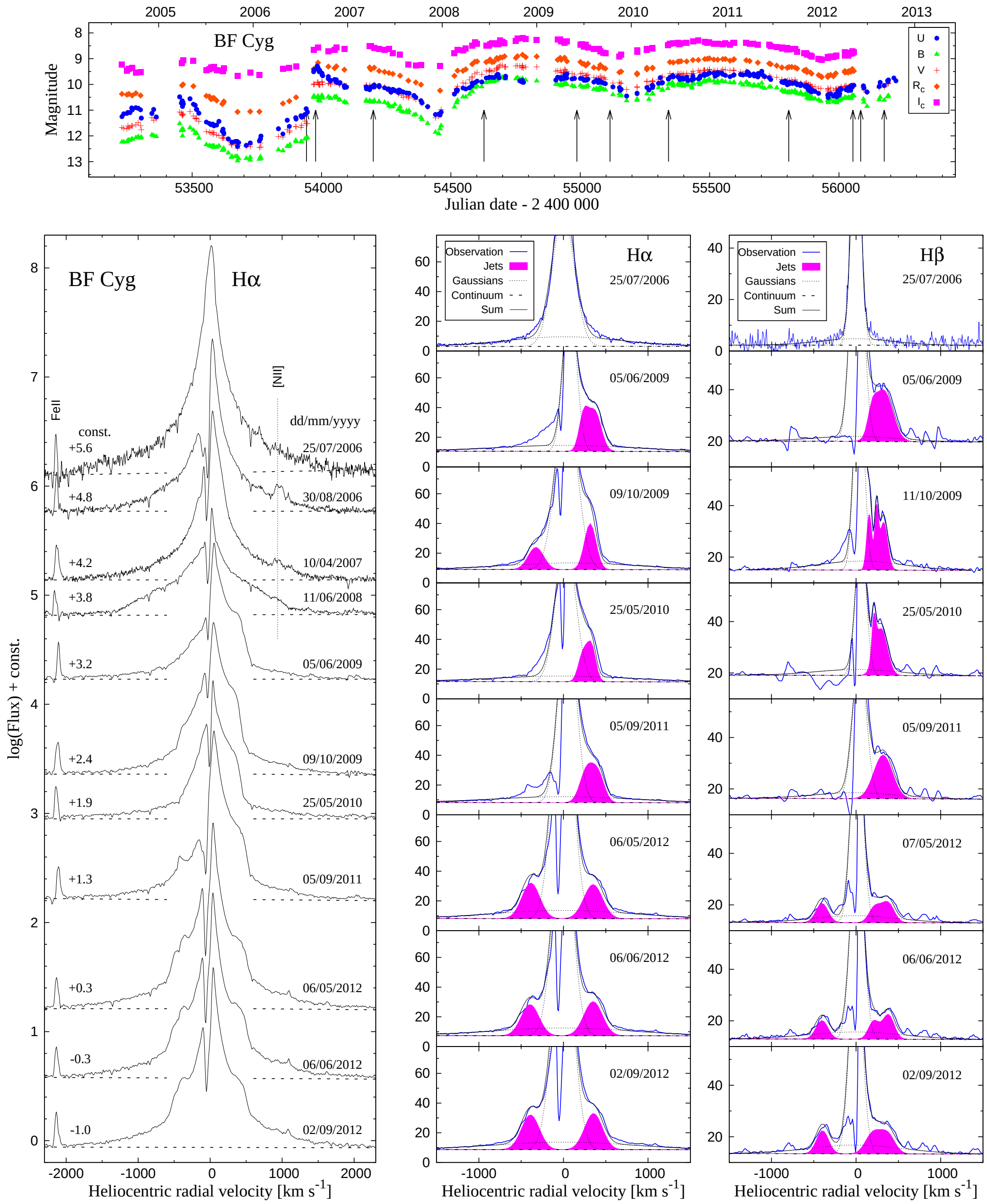

Figure 6.9: The upper panel shows the $UBVR_{\mathrm{C}}I_{\mathrm{C}}$ light curves of BF Cyg covering its current active phase (Skopal et al. 2007, 2012). The arrows indicate times of our spectroscopic observations. The lower panels display evolution of the H_α and H_β line profiles along the outburst. The filled curves represent the satellite emission components. Fluxes are in $10^{-13}\,\mathrm{erg\,cm^{-2}\,s^{-1}\,\AA^{-1}}$.

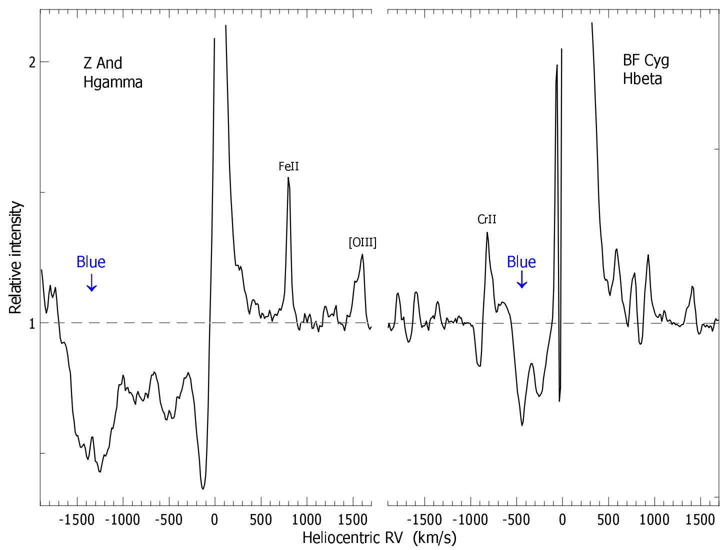

Figure 6.10: The H_γ profile of Z And based on a CCD frame on 2006 July 9 and the H_β profile of BF Cyg based on a CCD frame on 2010 May 25.

-250 km s^{-1} indicating P Cyg wind is seen on the spectrum of 2010 May 25. After that time it weakened and was not present in the spectrum of 2012 May 7 (Fig. 6.8). Another P Cyg absorption component with lower velocity of -30 to -90 km s^{-1} was seen in the spectra till 2011 September 5 and after that disappeared too. This indicates fading of the P Cyg wind together with the decrease of the optical thickness of the collimated outflow.

The H_β profile of BF Cyg is compared with the H_γ profile of Z And in Fig. 6.10. Both systems have an absorption satellite component and additional P Cyg absorption.

The H_β profile of BF Cyg is considered in the light of the scenario of Z And.

6.4.2 Transient accretion disc-like envelope during the 2006 – 2015 optical outburst

The interpretation of the light curve(s) of BF Cyg during its last 2006 – 2015 optical eruption is considered in the works of Tomov et al. (2015a,b).

Behaviour of the optical light

The eclipse of the compact object in BF Cyg is at the time of the inferior conjunction of the giant according to the ephemeris of Fekel et al. (2001)

$$\mathrm{Min} = 2\,451\,395\overset{\mathrm{d}}{.}2 + 757\overset{\mathrm{d}}{.}2 \times \mathrm{E}\,.$$

The system shows periodic wave-like orbital variation in its quiescent state similar to those of AG Peg (Skopal et al. 2012). The analysis of the spectral energy distribution by Skopal (2005) shows that in quiescence the UBV continuum fluxes of the circumbinary nebula are comparable to the continuum fluxes of the hot compact object. Then the decrease of the brightness at the phase of the orbital minimum is determined from both an eclipse of the compact object and an occultation of a part of the circumbinary nebula. At other orbital phases the nebula is partially occulted too.

Eclipses are observed in the BF Cyg system during its outbursts as well (Skopal et al. 2012). Its last outburst began in July – August 2006 and continues up to the present time when several orbital minima were detected caused by eclipses (Fig. 6.6). The first minimum is deeper than the following ones. After the first maximum the light decreases in different way compared to the next maxima. Initially the U light falls steeply at about one magnitude. In our view it is most probably due to decrease of the mass-loss rate of the outbursting component which moves the level of the observed photosphere back to the star and redistributes the continuum emission from longer wavelengths towards the UV region. After the initial steeply fall the light begins to decrease more slowly and the basic reason for this decrease is the occultation of the circumbinary nebula. Assuming a decrease of the mass-loss rate, a part of the ejected material can remain within the gravitational potential of the compact object and begin to accrete (Tomov et al. 2014). Observational indication of the increase of the mass-loss rate can be an appearance of absorption component of the spectral lines. During the rise of the light to the second maximum the mass-loss rate was probably increased again as proposed by the spectral data of Siviero et al. (2012). Strong P Cyg components of some Balmer and metal lines appeared after February 10, 2008. The light reached its second maximum at the end of 2008. Some time after that the Balmer lines acquired satellite components indicating bipolar collimated outflow (Skopal, Tomov et al. 2013).

Interpretation

The decrease of the depth of the orbital minimum implies an increase of the emission of the uneclipsed geometrical structure of the compact object. We suppose that a thin accretion disc from wind accretion has initially existed in the system BF Cyg and an extended disc-like envelope has formed after that as a result of decrease of the mass-loss rate and accretion of material from the potential well of the compact object in the period between the two orbital minima. We suppose that this envelope has collimated the stellar wind later. Some part of it is not eclipsed during the second and following minima determining their smaller depth. The continuum flux determined by recombinations and free-free transitions of a wind with a constant velocity υ is $F_{\lambda}^{\rm cont} \sim 1/\upsilon^2$. Then the emission of the jets is negligible because of the high velocity of the outflow. Our aim is to calculate the $UBVR_{\rm C}I_{\rm C}$ emission of such a model structure and to compare it with the observed residual of the depths of the first and second minima. If the model emission (the uneclipsed part of the envelope) is close to the observed residual, we can conclude that the formation of a disc-like envelope collimating the stellar wind of the compact object is a possible reason for both the appearance of the satellite components of the spectral lines and decrease of the depth of the orbital minimum of BF Cyg . After the third minimum the system's brightness fades and the depth of the orbital minimum increases again. We suppose that former is probably due to decrease of the optical flux of the outbursting object and destruction of the envelope and the latter – to destruction of the envelope only.

Calculation

Gas dynamical modeling shows that a disc from wind accretion with a typical radius of 50 – 60 $R_{\odot}$ and a mass of 5×10^{-7} $M_{\odot}$ exists in one binary system with parameters close to those of Z And in its quiescent state (Bisikalo et al. 2002; Tomov et al. 2010b, 2011a). During the outburst the wind of the compact object "strips" the disc and ejects some part of its mass. At the end of the outburst some part of the ejected mass locates in the potential well of the compact object. After the cessation of the wind it begins to accrete again creating an extended disc-like envelope with a mass smaller than the mass of the initial accretion disc.

The system BF Cyg has parameters very close to those of Z And – orbital period, masses of the components and mass-loss rate of the cool giant (Fekel et al. 2001). Then we suppose that a disc from accretion of a stellar wind with a size and a mass close to that in the system Z And exists in BF Cyg in its quiescent state. During the outburst the newly appeared disc-like envelope should have smaller mass. We accept an inner radius of the envelope of 25 $R_{\odot}$, equal to the radius of the pseudophotosphere of the outbursting compact object on October 23, 2008 according to Skopal et al. (2015), an

Table 6.2: Dereddened fluxes of BF Cyg in units of 10^{-12} erg cm^{-2} s^{-1} Å^{-1} with their inner uncertainties at the times of the orbital minima under consideration.

Date	JD 2 450 000+	F_U	F_B	F_V	F_{R_C}	F_{I_C}
Dec. 16, 2007	4451.220	0.720	0.533	0.367	0.330	0.291
		±0.037	±0.015	±0.011	±0.009	±0.009
Dec. 13, 2009	5179.202	1.375	1.522	0.883	0.613	0.511
		±0.065	±0.044	±0.025	±0.017	±0.015

outer radius of ~ 150 R$_\odot$ very close to the mean size of the Roche lobe of the compact object, a height of the envelope of ~ 170 R$_\odot$ and a mass of $\sim 3.5 \times 10^{-7}$ M$_\odot$. Its mean density is thus 7.5×10^{10} cm^{-3}. In reality the shape of this envelope differs from cylinder. With use of the orbital period and masses of the components of BF Cyg of Fekel et al. (2001) for the binary separation we obtain 492 R$_\odot$. Fekel et al. (2001) propose a radius of the cool giant of 70 ± 32 R$_\odot$ at a distance to the system of 2 kpc, and Skopal (2005) – ~ 150 R$_\odot$ at a distance of 3.8 kpc. Fekel et al. (2001) propose an orbit inclination of 75°, and Skopal et al. (1997) – $70 \div 90°$. We accept an inclination of 75°. In this case the radius of the giant should be large to provide eclipse and we accept a radius of 150 R$_\odot$ according to Skopal (2005). With this radius about a half of the volume of the disc-like envelope will be visible during the eclipse at orbital phase 0.0.

To calculate the residual of the depths of the first and second orbital minima we used photoelectric and CCD data from the work of Skopal et al. (2012). The data of Dec. 16, 2007 at the time of the first minimum are an arithmetical mean of several estimates taken in December 2007. At the time of the second minimum we used the UBV data of Dec. 13, 2009 and $R_C I_C$ data of Jan. 23, 2010 since there was no infrared data in December. The stellar magnitudes were converted into continuum fluxes using the calibration from the book of Mihailov (1973). The U flux was not corrected for the energy distribution of BF Cyg in the region of the Balmer jump since we were not provided with spectral data in this region. The UBV fluxes were not corrected for the emission lines for the same reason – absence of spectral data in the UBV region. All fluxes were corrected for the interstellar reddening $E(B-V) = 0.35$ (Skopal 2005) with use of the approach of Cardelli et al. (1989) and are listed in Table 6.2.

We will calculate the emission of the uneclipsed part of the disc-like envelope at orbital phase 0.0 and will compare it with the observed residual of the depths of the first and second orbital minima in the photometric bands $UBVR_{\rm C}I_{\rm C}$. Our unpublished high resolution data taken at that time do not show presence of the line He II 4686 in the spectrum of BF Cyg. Then we will assume that helium in the nebula of BF Cyg is ionized and the nebular continuum is emitted by hydrogen and neutral helium. The continuum flux determined by recombinations and free-free transitions is given with

$$F_{\lambda} = \frac{1 + a({\rm He})}{4\pi d^2} \left[\gamma_{\nu}({\rm H^o}, T_{\rm e}) + a({\rm He}) \gamma_{\nu}({\rm He^o}, T_{\rm e}) \right] n_{\rm e}^2 V \times \frac{c}{\lambda^2} 10^{-8} \,, \qquad (6.1)$$

where a(He) is helium abundance relative to hydrogen, d is a distance to the system, $\gamma_{\nu}({\rm H^o}, T_{\rm e})$ and $\gamma_{\nu}({\rm He^o}, T_{\rm e})$ are continuum emission coefficients of hydrogen and helium, $n_{\rm e}$ – electron density and V – volume of the emitting region.

We accept an electron temperature in emitting region $T_{\rm e} = 30\,000$ K equal to the mean temperature in the nebula according to Skopal et al. (2015). In such a case we used continuum emission coefficients at the positions of the $UBVR_{\rm C}I_{\rm C}$ photometric bands for this temperature from the paper of Ferland (1980) and the book of Pottasch (1984). We took the arithmetical mean of the values of the hydrogen coefficient on both sides of the Balmer limit at the position of the U band and accepted helium abundance of 0.1 (Vogel & Nussbaumer 1994). The fluxes and emission measure of the whole circumbinary nebula, our model envelope and its uneclipsed part at orbital phase 0.0 are presented in Table 6.3. The emission measure of the nebula was taken from Skopal et al. (2015) and its fluxes were calculated by us. The residual of the depths of the first and second orbital minima, obtained as residual of the fluxes in Table 6.2, is presented at the last row in Table 6.3. The model fluxes of the uneclipsed part are compared with this residual. It is seen that all fluxes of the uneclipsed part excepting only that in B band are close to the residual. The reason for the greater difference in the B band is rather unclear. The quiescent emission measure of BF Cyg at phase very close to the orbital photometric maximum is 3.1×10^{60} cm^{-3} (Skopal 2005) and on October 23, 2008 – 2.6×10^{61} cm^{-3} (Skopal et al. 2015). Its increase is thus 2.3×10^{61} cm^{-3}. Then it appears that the emission measure of the envelope of 2.2×10^{61} cm^{-3} is almost equal to this increase.

About Balmer lines again

The evolution of the H_{α} profile of BF Cyg during its outburst after 2006 was considered in the works of Skopal, Tomov et al. (2013); Skopal et al. (2015).

Table 6.3: $UBVR_CI_C$ continuum fluxes and emission measure of the different regions in the circumbinary nebula. The fluxes are in units 10^{-12} erg cm^{-2} s^{-1} Å^{-1} and emission measure – in 10^{61} cm^{-3}.

Emitting region	F_U	F_B	F_V	F_{R_C}	F_{I_C}	n_e^2V
Whole nebula	2.184	0.913	0.768	0.647	0.491	2.60[a]
Disc-like envelope	1.856	0.776	0.653	0.550	0.417	2.21
Uneclipsed part	0.928	0.388	0.327	0.275	0.208	1.10
Residual	0.655	0.989	0.516	0.283	0.220	
of the depths	±0.075	±0.046	±0.027	±0.019	±0.017	
r[b]	42	−61	−37	−3	−5	

[a] The data are for Oct. 23, 2008 in the work of Skopal et al. (2015).

[b] r =(U−R)/R in per cent; U – Uneclipsed part, R – Residual of the depths.

The observational data were taken in the period July 2006 – April 2013. We interpreted the decrease of the depth of the orbital minimum with an appearance of a disc-like envelope whose emission measure is the greatest part of the emission measure of the whole circumbinary nebula. In such a case the Balmer lines should be emitted mainly by this envelope. The Keplerian velocity at its inner radius is 68 km s^{-1} and at the outer radius – 27 km s^{-1} with use of the mass of the compact object of 0.6 $M_\odot$ according to Fekel et al. (2001). Taking into consideration the orbit inclination, the radial velocities resulted from the rotation of the envelope should be 66 – 26 km s^{-1}. If the H_α profile was determined only by this rotation, it should be double-peaked with a peak separation of 52 km s^{-1} and a full width at zero intensity (FWZI) of 132 km s^{-1}. The observed peaks separation of the line during the time of the collimated outflow, however, ranged from 100 km s^{-1} to 150 km s^{-1}, which means that it was broadened more than only from the rotation of the envelope. The inner uncertainty of the measurement is not more than 5 km s^{-1}. A possible additional mechanism of line broadening is a gas turbulence caused by collision of the stellar wind of the outbursting component with the envelope.

The structure of the central emission of the H_α line, however, was double-peaked before the first orbital minimum too (Skopal, Tomov et al. 2013; Skopal et al. 2015), and the velocity of the dip between the two peaks was always of about −100 km s^{-1}. A P Cyg absorption with a velocity of about

$-30\ \mathrm{km\,s^{-1}}$ was present in the H_β line from June 2009 till May 2010. The velocity of this absorption was $-90\ \mathrm{km\,s^{-1}}$ in September 2011 and after that it went into an absorption dip in the emission profile with a velocity of about $-30\ \mathrm{km\,s^{-1}}$ again. It was concluded that it indicates a stellar wind which exists together with the collimated ejection. We suppose that this wind produces the absorption dip with a velocity of about $-100\ \mathrm{km\,s^{-1}}$ in the emission profile of H_α.

6.5 Conclusions

We considered profiles of selected lines of several symbiotic systems which contain high-velocity satellite components indicating bipolar collimated ejection from the outbursting compact object in these systems along with blueshifted absorption indicating P Cyg wind.

The profile of the H_α and H_β lines of the Hen 3-1341 system during its 1998 – 2004 outburst had high velocity satellite emission components on both sides of the central peak of the line with a velocity of $\sim 800\ \mathrm{km\,s^{-1}}$, indicating bipolar collimated outflow from the outbursting compact object. The same components presented in the profile of the helium triplet line with wavelength $\lambda\,5876$, but this line contained broad two-component P Cyg absorption in addition (Tomov T. et al. 2000; Munari et al. 2005). The line H_α during the 2012 outburst had satellite emission components with a velocity of 1160 $\mathrm{km\,s^{-1}}$ indicating bipolar collimated ejection and the line He I $\lambda\,5876$ had P Cyg absorption with a velocity of 150 $\mathrm{km\,s^{-1}}$ (Tomov & Tomova 2013).

The profile of the H_α and He I $\lambda\,5876$ lines of StHα 190 in 2000 had satellite emission components of both sides of the central emission with a velocity of $\sim 150\ \mathrm{km\,s^{-1}}$ indicating bipolar collimated outflow from the system with a high velocity, probably of not less than 1000 $\mathrm{km\,s^{-1}}$. Moreover, these lines had an additional absorption of type P Cyg. The P Cyg component of the helium line was multicomponent and highly variable and at some times absorbed completely the emission in the blueshifted satellite component (Munari et al. 2001).

The profile of the H_β line of the BF Cyg system during its 2006 – 2015 outburst contained satellite components with a velocity of $\sim 400\ \mathrm{km\,s^{-1}}$ situated on both sides of the line center indicating bipolar collimated outflow from the outbursting compact object. The blueshifted satellite component was an absorption one at the more early stage of the outburst which after that went into emission. At the time when the blueshifted component appeared as absorption, an other absorption of P Cyg type at a velocity position of

-250 km s^{-1} presented in the spectrum. A second P Cyg absorption with lower velocity of -30 to -90 km s^{-1} was seen at the same time. The H$_\alpha$ line had emission peaks/shoulders with the same velocity of ~ 400 km s^{-1} situated on both sides of the central emission like the H$_\beta$ satellite components.

We interpreted these profiles in the framework of the scenario of Z And (Tomov et al. 2011a, 2012, 2014).

Moreover, we considered the behaviour of the optical light of the eclipsing binary BF Cyg during its 2006 – 2015 eruption.

We concluded that the decrease of the depth of its orbital photometric minimum and the appearance of satellite components of the Balmer lines, indicating bipolar collimated outflow at one time between the first and second orbital minima, is probably due to formation of an extended disc-like envelope covering the accretion disc of the compact object and collimating its stellar wind. The uneclipsed part of the envelope is responsible for the decrease of the depth of the orbital minimum. We assumed that the envelope results from diminution of the mass-loss rate of the compact object after the first light maximum and accretion of material from its potential well in the time between the first and second orbital minima.

We supposed that the shape of the envelope is close to torus with an inner radius of 25 $R_\odot$, equal to the radius of the pseudophotosphere of the outbursting object, an outer radius of ~ 150 $R_\odot$ very close to the mean size of its Roche lobe and a height of ~ 170 $R_\odot$. The mass of the envelope is accepted of $\sim 3.5 \times 10^{-7}$ $M_\odot$, its mean density thus amounts to 7.5×10^{10} cm^{-3} and the emission measure – to 2.21×10^{61} cm^{-3}. This emission measure is almost equal to the increase of the emission measure during the outburst.

In accordance with these parameters the central emission of the H$_\alpha$ line should be produced mainly by this envelope but the analysis of its profile shows that it is additionally broadened by a gas turbulence due to collision of the stellar wind with the envelope and its double-peaked structure is determined mostly from an optically thick outflow producing an absorption dip in the emission profile.

With use of a binary separation of 492 $R_\odot$ and inclination of the orbit of 75° (Fekel et al. 2001) and a radius of the cool giant in the system of 150 $R_\odot$ (Skopal 2005) about a half of the volume of the disc-like envelope will be visible during the eclipse at orbital phase 0.0. We calculated the emitted by this volume $UBVR_\mathrm{C}I_\mathrm{C}$ fluxes and compared them with the observed residual of the depths of the first and second orbital minima. It turned out that the model fluxes are in agreement with the observed ones.

We concluded that the increase of the depth of the orbital minimum with fading of the light during the outburst, on its side, is probably due to destruction of the disc-like envelope, which thus indicates its transient nature.

Chapter 7

Conclusions and results

This Chapter contains the mean results of the study.

The main result of the investigation of the symbiotic binary EG And is as follows:

1. The orbital radial velocity variations of the H_α emission line of the symbiotic binary EG And are not in phase with those of its giant component, implying that the motion of the emitting gas differs from the stellar orbital motion. The minimal intensity of the line is at phases when the giant is closer to the observer. The minimal and maximal intensity are not at the phases of the spectral conjunction but at later phases. At the phases of minimal intensity the profile of the line is doublepeaked, with a deep absorption going below the continuum. At the phases of maximal intensity the line is singlepeaked (Smith 1980; Oliversen et al. 1985; Tomov & Tomova 1995a,b; Burmeister 2010).

   The resonance lines C IV $\lambda 1548 - 1550$ Å of the symbiotic binary EG And have P Cyg absorption components indicating wind outflow from the hot compact secondary in the system with a velocity of about 100 km s^{-1} (Oliversen et al. 1985; Pesce et al. 1987; Sion & Ready 1992; Vogel 1993).

   The behaviour of the lines is interpreted in the framework of a model of colliding winds. A nebular region with a shape of a cone occurs on the collision boundary between the two winds. As the compact secondary has lower mass-loss rate and the velocity of its wind is low, the momentum of this wind is smaller and the conical surface surrounds the area behind the compact secondary. As a result of the orbital motion the cone distorts in a direction opposite to the motion. Besides the conical region, the hot compact secondary ionizes a portion of the giant's wind too. The H_α line is supposed to appear in the conical region and ionized portion of the giant's wind. In this case it is selfabsorbed because of the increasing density in the giant's wind. The H_α flux has been calculated with the parameters of this wind, accounting to about 10^{-10} erg cm^{-2} s^{-1}, which is in agreement with the observed flux of 5×10^{-11} erg cm^{-2} s^{-1}. The difference is due mainly to self-absorption (Tomov 1995).

The prototype of the symbiotic novae AG Peg has undergone a single outburst – the most prolonged one among outbursts of symbiotics. The main results of our investigation of the star at the final stage of its outburst are as follows:

1. The mass-loss rate of the outbursted compact object in the binary system AG Peg based on the flux of the broad emission component of the lines H_β, H_γ and He II 4686 derived from intermediate resolution optical data taken in 1995 was obtained being in a good agreement with the mass-loss rate derived from UV data. It is compared with an earlier value based on both optical and UV data, obtained nine years ago, and turns out to have decreased by a factor of 1.8. The decrease of the rate changes the geometry of the collision region of the winds. This proposes explanation of the changed radial velocity of the lines of some elements in 1995. The energy fluxes of 24 optical lines have been calculated. They have decreased by a mean factor of about 2 compared with their values in 1986. It is concluded this decrease is mainly due to decrease of the Lyman photon luminosity of the outbursted compact object whose decrease factor is the same (Tomov et al. 1998). The nebular continuum of AG Peg decreases too due to decrease of the Lyman luminosity. The ratio of the U fluxes at the time of photometric maximum in 1986 and 1995 is equal to the ratio of the Lyman luminosity (Tomov & Tomova 1998).

2. The photometric orbital U variations as well as the fading of the U light on a long timescale of decades of the symbiotic binary AG Peg are explained in the framework of a model of colliding winds. The orbital variations, caused by occultation of a dense bright region by the M giant in the system, are used to determine the geometry and the mean density in this region. The region is supposed to appear close to the giant on its side facing the hot companion as a result of winds collision being ionized by the companion. Its mean density and emission decrease with the time causing fading of the U light on a long timescale. One value of the mean density of the region of $(2-4)\times 10^{10}$

cm^{-3} at one particular time has been derived. It is supposed that the irregular variations of the U light of AG Peg in its orbital minima and maxima are determined by occultation of the dynamically unstable interaction zone of the winds, whose density changes. It is supposed that when the decreasing mass-loss rate of the hot companion drops below about $5{\times}10^{-10}$ $M_{\odot}\,yr^{-1}$ only the wind of the giant will exist in the system. Then the bright region resulted from the winds collision will disappear (Tomov & Tomova 2001).

The symbiotic binary AG Dra experienced an active phase in the period 1994 – 1998 consisting of five optical outbursts. The main results of our investigation of the system in the quiescent period prior to this active phase and during activity are as follows:

1. The quiescent U fluxes of the components of the symbiotic binary AG Dra at the time of its orbital photometric maximum were determined. Based on the fluxes of the cool giant and the circumbinary nebula the radius of the cool giant of $28 \div 32$ $R_{\odot}$ and the distance to the system of $1560{\div}1810$ pc have been obtained assuming spherical symmetry and constant expansion velocity of the giant's wind. The mass and bolometric luminosity of the giant of $1.1 \div 1.5$ $M_{\odot}$ and $242 \div 316$ $L_{\odot}$ were calculated. The bolometric luminosity and accretion rate of the hot compact companion of $967{\div}1302$ $L_{\odot}$ and $1.2{\div}1.7\times10^{-8}$ $M_{\odot}\,yr^{-1}$ were calculated for the distance to the system obtained by us. With use of the core mass-luminosity relation of accreting compact objects (Yungelson et al. 1996) the mass of the compact companion of 0.3 $M_{\odot}$ was obtained. It turns out that the accretion rate is in the range of steady hydrogen burning at the surface of a white dwarf with a mass of 0.3 $M_{\odot}$.

   It was concluded that the shape of the orbital U light curve is determined by occultation of a bright gaseous region located close to the hemisphere of the giant facing the hot compact companion. The U flux of this region is by a factor of about 3 greater than the flux of the unocculted part of the circumbinary nebula (Tomov et al. 2000).

2. A mass-loss rate of $(1-2)\times10^{-7}$ $(d/1.7\ kpc)^{3/2}$ $M_{\odot}\,yr^{-1}$ of the outbursting compact object in the symbiotic binary AG Dra based on the energy flux in the broad emission component of its lines H_{γ} and He II 4686 has been obtained during three consequtive outbursts of the system in 1995, 1996 and 1997. The loss of mass by the compact object during each outburst has a typical time of several months. Since the

time of loss of mass in this case is close to the time of accretion, according to the evolutionary models of an accreting white dwarf (Shara et al. 1993; Kato & Hachisu 1994; Yungelson et al. 1995) the accretion rate should be close to the mass-loss rate being of about 1×10^{-7} M$_\odot$ yr^{-1} too. However, when the accretion rate is $10^{-8} - 10^{-7}$ M$_\odot$ yr^{-1} a steady burning of hydrogen is realized, instead of thermonuclear event (Mikolajewska & Kenyon 1992). Consequently the compact object in the symbiotic binary AG Dra during the 1995, 1996 and 1997 optical outbursts of the system has been rather in a state of steady burning of hydrogen at its surface and has not underwent thermonuclear outburst (Tomova & Tomov 1999; Tomov & Tomova 2002).

3. A scenario for interpretation of the growth of the optical light of AG Dra during active phases is suggested. The increase of the emission measure of the circumbinary nebula of this system during active phase is much greater than the increase of the Lyman photon luminosity of the outbursting compact companion. That is why the companion is supposed to be very luminous which makes it able to ionize the whole nebula, except some region behind the cool giant and the increase of the emission measure in this case is supposed to be due to increase of the mass-loss rate of the giant. The light changes at two stages: in the beginning its growth results from an increase of the mass-loss rate of the giant and after the accretion of some amount of gas – from increase of the Lyman luminosity of the companion giving rise to an additional ionization. The decline of the giant's mass-loss rate to its initial value and the burning out of the accreted envelope of the companion determine the return of the light to its quiescent level (Tomov & Tomova 2002).

The prototype of the classical symbiotic stars Z And experienced new active phase in the period 2000 – 2013 consisting of seven individual outbursts. The main results of our investigation of the star during this active phase are as follows:

1. A detailed optical light curve acquired during the 2000 – 2002 brightening of the star Z And was analysed with use of the results of gas-dynamical modeling of the flow structure in this system to study the development of the outburst. The analysis shows that the accretion processes cannot provide the observed energetics of the event. As a possible mechanism of the outburst a "combined" model is considered where the increase of the accretion rate as a result of disruption of the accretion disc in the system leads to increase of the burning rate. The multistage pattern of the rise of the optical light is explained in

the framework of the model of the colliding winds. It is shown that the shape of the light curve is determined from three processes: an increase of the accretor's luminosity causing expansion of its pseudophotosphere, wind propagation in the nebula resulting in the formation of a high-temperature region and formation of shock structures appeared as a result of the winds collision.

The theoretical scenario is in a good agreement with the observational data – it is in accordance with both the observed temporal characteristics of the individual stages of the rise of the light and their amplitudes as well as with the scale of the shock ionization. During the outburst a stellar wind in two component velocity regime was observed – optically thin high-velocity wind and P Cyg wind with a low velocity. The appearance of shock structures was observationally confirmed by detection of collisional ionization in the nebula. The ratio of the nebular continuum fluxes due to collisional and radiative ionization is approximately 1/3.

The observational data obtained during the next brightenings of the 2000 – 2013 active phase of Z And revealed again both a growth of the bolometric luminosity and an expansion of the outbursting accretor. That is why the "combined" model proposed can be used for interpretation of the light behaviour of the system during these brightenings too and possibly for the brightenings of other classical symbiotic stars (Bisikalo et al. 2006).

2. The profiles of the Balmer lines H_α and H_γ were double-peaked during the rise of the light and ligt maximum of the small eruption in the end of 2002. It has been shown they can be emitted mainly by one extended disc-like envelope, located in the Roche lobe of the compact object, whose emission measure is not greater than the increase of the emission measure of the circumbinary nebula during the eruption. The parameters of this envelope are compatible with the predicted ones by the gas dynamical modeling. The greater observed peaks separation of the lines can be due to optical depth effects (selfabsorption) and/or an additional broadening by a gas turbulence. An other possibility is the double-peaked Balmer profiles to be determined from selfabsorption only.

   The H_α line has broad wings extending to not less than 2000 $\mathrm{km\,s^{-1}}$ from its center. They were supposed to be determined mainly from radiation damping but stellar wind could contribute to their emission at smaller distance from the centre of the line.

3. The most prominent one among the outbursts belonging to the 2000 – 2013 active phase of Z And was developed in 2006. The profile of the Balmer lines at the time of the light maximum was a multi-component one consisting of an intense central narrow emission located around the reference wavelength, broad wings, a blueshifted absorption and high-velocity satellite absorption/emission features on both sides of the central emission at a velocity position of 1200 – 1500 km s^{-1} indicating bipolar collimated ejection from the compact object in the system. The broad emission wings and the satellite emissions were seen until the end of December 2006. The width of the wings in the different Balmer members, however, was different. The blueshifted P Cyg absorption was seen until the beginning of October 2006.

   In 2006 the lines of He I consisted of a narrow emission located close to the reference wavelength and a blueshifted absorption. At the time of the maximal light the absorption of the line He I 4471 was multi-component one occupying a broad velocity range like the line H_{γ}. The most blueshifted component was at the velocity position of the satellite component. After that the broad absorption went into a low velocity narrow feature, which was visible till the beginning of December 2006.

   In October and December 2006 the line He II 4686 was two-component one, consisting of a central narrow emission and a broad emission component with a low intensity.

   The mass-loss rate of the compact object was estimated at several epochs of the eruption. The rate was found to decrease, from (4 – 5) $\times$ 10^{-7} (d/1.12 kpc)$^{3/2}$ $M_{\odot}$ yr^{-1} at the time of maximum light to about 1 $\times$ 10^{-7} (d/1.12 kpc)$^{3/2}$ $M_{\odot}$ yr^{-1} in December 2006.

   The behaviour of the line spectrum is interpreted in the light of the model of collimated stellar wind (Tomov et al. 2012, 2014).

4. Comparison of high resolution optical spectra with results of gas-dynamical modeling provides possibility to propose a scenario to explain the spectral behavior of the symbiotic prototype Z And during its last 2000 – 2013 active phase as well as the differences in its observed properties during the different outbursts of the active phase. The basic points of this scenario are the following ones:

   - An accretion disk from wind accretion exists in the system.
   - During the outburst the gas leaving the surface of the compact component at high velocity collides with the accretion disk. As a

result its velocity decreases near the orbital plane, but remains unchanged at higher stellar latitudes. Hence, two wind components with different velocities are observed.

- During the outburst the wind from the compact component partially disrupts the disk. Some part of its mass does not leave the potential well and after the wind ceases, it begins to accrete again. Because of conservation of the initial angular momentum an envelope covering the disc and extending to larger distance from the orbital plane forms.
- The existence of a centrifugal barrier creates two hollow cones around the axis of rotation which leads to appearance of collimated outflow during the recurrent outbursts. This outflow can be observed as high-velocity components on either side of the main peak of the line.
- Collimated outflow will appear when the density of the disk-like envelope is high enough to provide collimation and the mass-loss rate of the compact component is also high. High-velocity satellite line components thus can be observed during outbursts accompanied by loss of mass at high rate, preceded by a similar strong outburst.

This scenario provides possibility to explain all spectral features of Z And observed during active phase. Its general character permits to suppose that similar scenario is possible for other classical symbiotic stars too (Tomov et al. 2010b, 2011a, 2014).

Main results of investigation of other symbiotic binaries:

1. Four out of a total of five symbiotic systems whose optical spectral lines contain satellite components indicating collimated ejection have an additional absorption of type P Cyg at different velocity. These systems are Z And, Hen 3-1341, StHα 190 and BF Cyg. It is shown that the line profiles of every of the systems Hen 3-1341, StHα 190 and BF Cyg can be interpreted in the framework of the scenario of collimated stellar wind, which provides a better interpretation of the line components than the traditional model with a magnetic accretion disc (Tomov et al. 2014).
2. The optical light curve of the eclipsing symbiotic binary BF Cyg during its last 2006 – 2015 outburst is interpreted in the framework of the model of collimated stellar wind. It is supposed that the variations

of the depth of the orbital photometric minimum are due to appearance of an extended disc-like envelope covering the accretion disc of the outbursting compact object and collimating its stellar wind. This disc-like shaped envelope gives rise to a bipolar collimated outflow which is observed as satellite components of the Balmer lines. The uneclipsed part of the envelope is responsible for the decrease of the depth of the orbital minimum. The calculated $UBVR_{\mathrm{C}}I_{\mathrm{C}}$ fluxes of this uneclipsed part are in agreement with the observed residual of the depths of the first and second orbital minima. The parameters of the envelope require that it is the main emitting region of the line H_α but the H_α profile is less determined from its rotation and mostly from other mechanisms. It is concluded that the envelope is a transient nebular region and its destruction determines the increase of the depth of the orbital minimum with fading of the optical light (Tomov et al. 2015a,b).

List of publications

A. Journals with IF

1. Tomov N. A. "A colliding winds interpretation for the spectral variability of EG And", 1995, MNRAS, v. 272, p. 189

2. Tomov, N., Tomova, M. "Hα and U light variability of EG And during 1991-1994", 1995, C. R. Acad. Bulg. Sci. 48, No. 11-12, 11-14

3. Tomov N., Tomova M., Raikova D. "The visual line spectrum of AG Peg in 1995", 1998, A&AS 129, 479-488

4. Tomova M., Tomov N. "Spectral observations of AG Draconis during quiescence and outburst (1993-1995)", 1999, A&A 347, 151-163

5. Tomov N., Tomova M., Ivanova A. "Analysis of the U-band orbital variation of the symbiotic binary AG Draconis during quiescence", 2000, A&A 364, 557-562

6. Tomov N., Tomova M. "A colliding-winds interpretation of the U orbital variation of the symbiotic binary AG Pegasi", 2001, Ap&SS 278, 311

7. Tomov N., Tomova M. "Hydrogen and helium emission of the symbiotic binary AG Draconis during an active phase (1996 - 1997)", 2002, A&A 388, 202-212

8. Tomov, N., Taranova, O., Tomova, M. "Mass ejection by the symbiotic binary Z And during its 2000-2002 outburst", 2003, A&A 401, 669-676

9. Tomov N., Tomova M., Zamanov R. "Spectral observations of Z Andromedae during quiescence and its 2000 active phase", 2003, in "Symbiotic stars probing stellar evolution", eds. R. L. M. Corradi, J. Mikolajewska, and T. J. Mahoney, ASPC 303, 254-257

10. Taranova O.G., Tomov N., Tomova M., Shenavrin V.I. "The Symbiotic System Z Andromedae during the Flare of 2000-2002", 2004, Astr. Rep. 48, 742-750

11. Tomov, N., Tomova, M., Taranova, O. "Broad-band multicolour observations of the symbiotic binary Z And during quiescence and its activity at the end of 2002", 2004, A&A 428, 985-992

12. Tomov, N., Tomova, M., Taranova, O. "The HeII 4686 line of the symbiotic binary Z And during its outburst at the end of 2002", 2005 in The Astrophysics of Cataclysmic Variables and Related Objects, eds. J. M. Hameury, & J. P. Lasota, ASP Conf. Ser. 330, 465-466

13. Bisikalo D.V., Boyarchuk A.A., Kilpio E.Yu., Tomov N.A., Tomova M.T. "A Study of an Outburst in the Classical Symbiotic Star Z And in a Colliding-Wind Model", 2006, Astr. Rep. 50, 722-732

14. Tomov N.A., Tomova M.T., Bisikalo D.V. "Bipolar ejection by the symbiotic binary system Z And during its 2006 outburst", 2007, MNRAS 376, L16-L19

15. Tomov, N.A., Tomova, M.T., Bisikalo, D.V. "Spectral indications of ejection of mass by the symbiotic binary Z And during its 2000–2002 outburst", 2008, MNRAS 389, 829-838

16. Tomov N.A., Tomova M.T., Bisikalo D.V. "The Hydrogen and Helium Lines of the Symbiotic Binary Z And during Its Brightening at the End of 2002", 2010, Astr. Rep. 54, 528-536

17. Tomov N.A., Bisikalo D.V., Tomova M.T., Kilpio, E. "A Study of Outburst Activity of Z And in 2000-2010", 2010, Astr. Rep. 54, 628-644

18. Kilpio, E.Yu., Bisikalo D.V., Tomov N.A., Tomova M.T. "Classical symbiotic star Z And During the Recent Activity Period", 2011, Ap&SS 335, 155-160

19. Tomov, N.A., Tomova, M.T., Bisikalo, D.V. "Mass ejection by the symbiotic prototype Z And during its 2006 outburst 2012", 2012, Baltic Astronomy 21, 112-122

20. Skopal, A., Tomov, N.A., Tomova, M.T. "Discovery of collimated ejection from the symbiotic binary BF Cygni", 2013, A&A 551, L10

21. Tomov N.A., Tomova M.T., Bisikalo D.V. "Symbiotic Stars with Spectral Indication of Bipolar Ejection and Stellar Wind", 2014, AN 335, 178-188

22. Tomov N.A., Tomova M.T., Bisikalo D.V. "Transient accretion disclike envelope in the symbiotic binary BF Cygni during its 2006 – 2015 optical outburst", 2015, AN accepted

B. International meetings

1. Tomov N., Tomova M. “Hα observations of AG Dra during quiescence and the 1994 outburst”, 1997, in ”Physical Processes in Symbiotic Binaries and Related Systems“, ed. Mikolajewska J., Copernicus Foundation for Polish Astronomy, Warsaw, p. 185

2. Tomov N. “General observational characteristics of symbiotic binaries”, 2001, in Proceedings of the Balkan meeting of young astronomers, eds. A. Antov, R. Konstantinova-Antova, R. Bogdanovski and M. Tsvetkov, p. 97 - 106

3. Tomov N., Tomova M., Taranova O. “The Activity of the Symbiotic Binary Z And at the End of 2002”, 2005, Aerospace Research in Bulgaria, v. 20, Proceedings of the Balkan Astronomical Meeting (BAM 2004), Rozhen - June 2004, 252-257

4. Taranova O., Tomov N., Tomova M., Shenavrin V. “The Symbiotic System Z Andromedae during the Flare of 2000–2002”, 2007, in Proc. of the memorial D.Ya. Martynov regional conference, held 22-24 May 2006, GAISH

5. Tomov N.A., Tomova M.T., Bisikalo D.V. “Evidences for an Accretion Disc in the Spectrum of the Symbiotic Binary Z And during its Outburst at the end of 2002”, 2009, AIP Conf. Proc., SPACE PLASMA PHYSICS: School of Space Plasma Physics, ed. I. Zhelyazkov, 1121, 22-27

6. Tomov N.A., Bisikalo D.V., Tomova M.T., Kilpio, E. “Interpretation of the line spectrum of classical symbiotic stars in the scenario for their prototype Z And”, 2011, AIP Conf. Proc., 3RD SCHOOL AND WORKSHOP ON SPACE PLASMA PHYSICS, eds. I. Zhelyazkov and T. Mishonov, 1356, 35-44

7. Tomov, N.A., Tomova, M.T., Bisikalo, D.V. “Symbiotic Stars with Similar Line Profiles during Activity”, 2013, AIP Conf. Proc., 4TH SCHOOL AND WORKSHOP ON SPACE PLASMA PHYSICS, eds. I. Zhelyazkov and T. Mishonov, 1551, 30-45

8. Skopal, A., Sekeras, M., Tomov, N., Tomova, M., Tarasova, T., Wolf, M. “What powers the 2006 outburst of the symbiotic star BF Cygni?”, 2015, in the Proceedings of the Palermo Workshop THE GOLDEN AGE OF CATACLYSMIC VARIABLES AND RELATED OBJECTS

- II, eds. F. Giovannelli and L. Sabau-Graziati, Acta Polytechnica, in press

9. Tomov N.A., Tomova M.T., Bisikalo D.V. “Interpretation of the UBVRcIc light variations of the symbiotic binary BF Cyg during its 2006 - 2014 optical outburst”, 2015, AIP Conf. Proc., 5TH SCHOOL AND WORKSHOP ON SPACE PLASMA PHYSICS, eds. I. Zhelyazkov and T. Mishonov, accepted

C. Other publications

1. Tomov, N., Tomova, M. “Hα and U light variability of EG And during 1991–1994 – a support of the colliding winds interpretation”, 1995, in 100 yr Astronomical Observatory of Sofia University, eds. K. Maslev, and R. Kurtev, Naturela, Sofia, p. 103

2. Montagni, F., Maesano, M., Viotti, R., Altamore, A., Tomova, M., Tomov, N. “Photometry of the 1994–1995 active phase of AG Dra”, 1996, IBVS 4336

3. Tomov, N., Tomova, M. “Photoelectric UBV observations of EG Andromedae” 1996, IBVS 4341

4. Tomova, M., Tomov, N. “UBV observations of AG Dra in 1996 and 1997 during active phase”, 1998, IBVS 4561

5. Tomov, N., Tomova, M. “Photometric investigation of the nebula in the AG Peg system”, 1998, IBVS 4574

6. Tomov, N., Tomova, M. “UBV observations of AG Dra in the end of the last active phase and after it”, 2000, IBVS 4953

7. Tomov, N., Tomova, M. “Hα observations of the symbiotic binary system Z And during its 2006 outburst”, 2006, BlgAJ 8, 76

8. Tomova, M., Tomov, N., Bisikalo, D. “Two-velocity type mass outflow from the symbiotic binary Z And during its 2000 – 2002 outburst”, 2008, BlgAJ 10, 39

9. Tomov, N., Bisikalo, D., Tomova, M., Kilpio, E. “Eruptive activity of Z And in 2000–2010”, 2011, BlgAJ 15, 35

10. Tomov, N., Tomova, M., Bisikalo, D. “Balmer lines of the symbiotic binary Z Andromedae during its 2006 outburst”, 2011, BlgAJ 17, 70

11. Tomov, N., Tomova, M. “Bipolar ejection from the symbiotic binary Hen 3-1341 during its 2012 outburst”, 2013, IBVS 6055

Acknowledgements

I am grateful to Dmitry Bisikalo for the fruitful collaboration in the framework of which the best results of this research were obtained.

I am grateful also to Radoslav Zamanov, Nevena Markova and Donka Raikova for the helpful discussions and good advices.

I would like to thank all colleagues from IA and NAO, whose field is stellar spectroscopy, for their help and constructive comments.

I am indebted to Vasil Popov for his help in my first steps in observational astronomy.

This research was partly supported by the grants DO 02-85 and BSTC 01/14 Bulgaria – Slovakia of Bulgarian Scientific Research Fund.

Bibliography

Abramowicz, M., Chen, X., Kato, S., et al. 1995, ApJ 438, L37

Altamore, A., & Cassatella, A. 1997, A&A 317, 712

Allen, D.A. 1979, in Changing Trends in Variable Star Researh, ed. Bateson F. et al., IAU Coll. 46, Hamilton N.Z.; U. Waikato Press, p. 125

Allen, D.A. 1980, MNRAS 192, 521

Arrieta, A., & Torres-Peimbert, S. 2003, ApJS 147, 97

Bastian, U. 1998, A&A 329, L61

Belczynski, K., Mikolajewska, J., Munari, U., Ivison, R. J., & Friedjung, M. 2000, A&AS 146, 407

Belyakina, T.S. 1991, Izv. Krym. Astrofz. Obs. 83, 118

Belyakina, T.S. 1992, Izv. Krym. Astrofiz. Obs. 84, 49

Belyakina, T.S., & Prokofieva, V.V. 1992, Izv. Krym. Astrofiz. Obs. 86, 46

Birriel, J.J., Espey, B.R., & Schulte-Ladbeck, R.E. 1998, ApJ 507, L75

Bisikalo, D.V., Boyarchuk, A.A., Kilpio, E.Yu., Kuznetsov, O.A. 2002, ARep 46, 1022

Bisikalo, D.V., Boyarchuk, A.A., Kilpio, E.Yu., Tomov, N.A., Tomova, M.T. 2006, ARep 50, 722

Blandford, R.D., Begelman, M.C. 2004, MNRAS 349, 68

Bode, M.F. 2010, AN 331, 160

Borkowsky, J. 1988, REWIA: Instrukcija Obslugi, Torun Astronomical Observatory, Internal Report

Boyarchuk, A.A. 1966, AZh 43, 976

Boyarchuk, A.A. 1967a, AZh 44, 12

Boyarchuk, A.A. 1967b, AZh 44, 1016

Boyarchuk, A.A. 1969, in Non-Periodic Phenomena in Variable Stars, ed. Detre L. (Academic Press, Budapest), p. 395

Boyarchuk, A.A. 1985, in Workshop on Recent Results on Cataclysmic Variables, ed. Burke W.R., ESA, ESTEC, Noordwijk, p. 97

Boyarchuk, A.A., Belyakina, T.S., Tarasov, A.E., Glagolevski, Yu.V. 1987, Ap&SS 131, 775

Burgarella, D., & Paresce, F. 1992, ApJ 389, L29

Burmeister, M. 2010, Ph.D. Thesis (Tartu University Press, Tartu)

Burmeister, M., & Leedjärv, L. 2007, A&A 461, 5L

Cardelli, J.A., Clayton, G.C., Mathis, G.C. 1989, AJ 345, 245

Cassatella, A., Fernandez-Castro, T., Gonzalez-Riestra, R., Fuensalida, J. 1992, A&A 258, 368

Contini, M. 1997, ApJ 483, 887

Drake, J., Laming, J., & Ness, J.-U. 2009, ApJ, 691, 418

Duschl, W. 1986a, A&A 163, 56

Duschl, W. 1986b, A&A 163, 61

Fekel, F.C., Hinkle, K.H., Joyce, R.R., Skrutskie, M.F. 2000, AJ, 120, 3255

Fekel, F.C., Hinkle, K.H., Joyce, R.R., Skrutskie, M.F. 2001, AJ 121, 2219

Ferland, G.J. 1980, PASP 92, 596

Fernandez-Castro, T., Cassatella, A., Gimenez, A., & Viotti, R. 1988, ApJ 324, 1016

Fernandez-Castro, T., Gonzalez-Riestra, R., Cassatella, A., Taylor, A., & Seaquist, E. R. 1995, ApJ, 442, 366

Fernie, J.D. 1985, PASP 97, 653

Formiggini, L., & Leibowitz, E. M. 1994, A&A, 292, 534

Friedjung M., 1997, in Physical Processes in Symbiotic Binaries and Related Systems, ed. Mikolajewska J., Proc. of the International Conf., Copernicus Foundation for Polish Astronomy, Warsaw, p. 105

Friedjung, M., Hric, L., Petrik, K., Galis, R. 1998, A&A 335, 545

Fujimoto, M. Y. 1982, ApJ 257, 767

Galis, R., Hric, L., Friedjung, M., Petrik, K. 1999, A&A 348, 533

Garcia, M.R., & Kenyon, S.J. 1988, in The Symbiotic Phenomenon, ed. Mikolajewska J. et al., IAU Coll. 103, Kluwer, p. 27

Girard, T., & Willson, L.A. 1987, A&A, 183, 247

Gonzalez-Riestra, R., Viotti, R., Iijima, T., & Greiner, J. 1999, A&A 347, 478

Greiner, J., Bickert, K., Luthardt, R. et al., 1997, A&A 322, 576

Griffin, R.E.M., & Lynas-Gray, A.E. 1999, AJ 117, 2998

Hachisu, I., & Kato, M. 1999, ApJ 517, L47

Hachisu, I., & Kato, M. 2000, ApJ 536, 93

Hagen, W. 1978, ApJS 38, 1

Hatchings, J.B., & Redman, R.O. 1972, PASP 84, 240

Hatchings, J.B., Cowley, A.P., Redman, R.O. 1975, ApJ 201, 404

Hernanz, M., & José, J. 2000, AIP Conf. Ser. 522, 339

Hofleit, D. 1968, Irish Astr. J. 8, 149

Hric, L., Skopal, A. 1989, IBVS 3364

Hric, L., Skopal, A., Urban, Z., et al. 1991, Contr. Astr. Obs. Skalnaté Pleso 21, 303

Hric, L., Skopal, A., Urban, Z., et al. 1993, Contr. Astr. Obs. Skalnaté Pleso 23, 73

Hric, L., Skopal, A., Chochol, D., et al. 1994, Contr. Astr. Obs. Skalnaté Pleso 24, 31

Hric, L., Skopal, A., Urban, Z., et al. 1996, Contr. Astr. Obs. Skalnaté Pleso 26 46

Huang, C.C., Friedjung, M., Zhou, Z.X. 1994, A&AS 106, 413

Hutchings, J.B., & Redman, R.O. 1972, PASP 84, 240

Hutchings, J.B., Cowley, A.P., Redman, R.O. 1975, ApJ 201, 404

Iben, I. 1982, ApJ 259, 244

Iben, I., & Tutukov, A. 1996, ApJS 105, 145

Icke, V. 1981, ApJ 247, 152

Iijima, T. 2006, CBET 633

Ikeda, Y., Akitaya, H., Matsuda, K., et al. 2004, ApJ 604, 357

Ilmas, M. 1987, in Observations and Interpretation of Stellar Spectra, Dushanbe, p. 81

Ionov, D., Bisikalo, D., Kaygorodov, P., & Shematovich, V. 2012, in ASP Conf. Ser. 282, From Interacting Binaries to Exoplanets: Essential Modeling Tools, ed. M. T. Richards, & I. Hubeny, 545

Ivison, R.J., Bode, M.F., Meaburn, J. 1994, A&AS 103, 201

Kato, M. & Hachisu, I. 1994, ApJ 437, 802

Kenyon, S.J. 1983, PhD thesis, University of Illinois

Kenyon, S.J. 1986, The Symbiotic Stars, Cambridge University, Cambridge

Kenyon, S.J. 1988, in The Symbiotic phenomenon, ed. Mikolajewska et al., Kluwer, 161

Kenyon, S., & Fernandez-Castro, T. 1987, AJ 93, 938

Kenyon, S.J., & Gallagher, J.S. 1983, AJ 88, 666

Kenyon, S., & Truran, J. 1983, ApJ 273, 280

Kenyon, S.J., Fernandez-Castro, T., & Stencel, R.E. 1988, AJ 95, 1817

Kenyon, S., Mikolajewska, J., Mikolajewski, M., Polidan, R., Slovak, M. 1993, AJ 106, 1573

Kilpio, E., Bisikalo, D.V., Boyarchuk, A. A., and Kuznetsov, O.A., 2005, in *The Astrophysics of Cataclysmic Variables and Related Objects*, eds. J.-M. Hameury and J.-P. Lasota, ASP Conf. Ser. 330, p. 457.

Kilpio, E., Bisikalo, D.V., Boyarchuk, A. A., and Kuznetsov, O.A., 2005, in *Interacting Binaries: Accretion, Evolution, and Outcomes*, eds. L.A. Antonelli, L. Burderi, F. D'Antona, T. Di Salvo, G.L. Israel, L. Piersanti, O. Straniero, A. Tornambe, AIP Conf. Proc. 797, p. 573

Kilpio, E., Bisikalo, D.V., Tomov, N.A., Tomova, M.T. 2011, Ap&SS 335, 155

Kovetz, A., & Prialnik, D. 1994, ApJ 424, 319

Landolt, A.U. 1992, AJ 104, 340

Lee, H. 2000, ApJ 541, L25

Leedjarv, L. 2004, BaltA 13, 109

Leibowitz, E.M., & Formiggini, L. 1992, A&A 265, 605

Leibowitz, E.M., & Formiggini, L. 2006, MNRAS 366, 675

Livio, M. 2011, in AIP Conf. Proc. 1358, Gamma Ray Bursts 2010, ed. J. E. McEnery, J. L. Racusin, & N. Gehrels, 329

Lundmark, K. 1921, Astron. Nachrichten 213, Nr. 5094, 93

Luo, D., McCray, R., Mac Low, M.-M. 1990, ApJ, 362, 267

Luthardt, R. 1990, Contrib. Astron. Obs. Skalnate Pleso 20, 83

Mattei, J.A., 1995, AAVSO Observations

Mayall, M.W. 1937, Ann. Harv. Coll. Obs. 105, 491

Mc Keever, J., Lutz, J., Wallerstein, G., Munari, U., Siviero, A. 2011, PASP 123, 1062

Meinunger, L. 1979, IBVS 1612

Mihailov, A.A. 1973, Kurs astrofiziki i zvezdnoj astronomii (Nauka, Moscow), in russian

Mikolajewska, J. 1987, Ap&SS 131, 713

Mikolajewska, J. 1997, in Physical Processes in Symbiotic Binaries and Related Systems, ed. Mikolajewska J., Proc. of the International Conf., Copernicus Foundation for Polish Astronomy, Warsaw, p. 3

Mikolajewska, J., & Kenyon, S.J. 1992, MNRAS 256, 177

Mikolajewska, J., & Kenyon, S.J. 1996, AJ, 112, 1659

Mikolajewska, J., Kenyon, S.J., Mikolajewski, M., Garsia, M.R., Polidan, R.S. 1995, AJ 109, 1289

Mitsumoto, M., Jahanara, B., Matsuda, T., et al. 2005 ARep 49, 884

Montagni, F., Maesano, M., Viotti, R., et al. 1996, IBVS 4336

Munari, U. 1997, in Physical Processes in Symbiotic Binaries and Related Systems, ed. Mikolajewska J., Proc. of the International Conf., Copernicus Foundation for Polish Astronomy, Warsaw, p. 37

Munari, U., Margoni, R., Iijima, T., Mammano, A. 1988, A&A 198, 173

Munari, U., Yudin, B.F., Taranova, O.G., et al. 1992, A&ASS 93, 383

Munari, U., Siviero, A., Henden, A. 2005, MNRAS 360, 1257

Munari, U., Tomov, T., Yudin, B.F., et al. 2001, A&A, 369, L1

Munari, U., Siviero, A., Moretti, S., Graziani, M. , Tomaselli, S., Baldinelli, L., Maitan, A.: 2006, CBET 596, 1

Munari, U., Milani, A., Siviero, A., et al. 2012a, ATel 3946

Munari, U., Valisa, P., Dallaporta, S., Siviero, A. 2012b, ATel 3952

Mürset, U., & Schmid, H. M. 1999, A&AS, 137, 473

Mürset, U., Nussbaumer, H., Schmid, H. M., & Vogel, M. 1991, A&A, 248, 458

Mürset, U., Jordan, S., Walder, R. 1995, A&A 297, L87

Nussbaumer, H., 1982, In Friedjung M., Viotti R. (eds.) The Nature of Symbiotic Stars, IAU Coll. 70, Dordreht: Reidel, p. 85

Nussbaumer, H., & Vogel, M. 1987, A&A 182, 51

Nussbaumer, H., & Vogel, M. 1988, in The Symbiotic phenomenon, ed. Mikolajewska et al., Kluwer, 169

Nussbaumer, H., & Vogel, M. 1989, A&A, 213, 137

Nussbaumer, H., & Walder, R. 1993, A&A 278, 209

Oliversen, N.A., & Anderson, Ch.M. 1982, in The Nature of Symbiotic Stars, eds. Friedjung M. & Viotti R., IAU Coll. 70, Reidel, p. 71

Oliversen, N.A., Anderson, C.M., Stencel, R.E., Slovak, M.H. 1985, ApJ 295, 620

Osterbrock, D. E. 1974, Astrophysics of Gaseous Nebulae. W.H. Freeman and Company, San Francisco, p. 73, 74

Paczynski, B. 1970, Acta Astr. 21, 417

Paczynski, B., & Rudak, B. 1980, Acta Astr. 82, 349

Paczynski, B., & Zytkow, A. 1978, ApJ 222, 604

Penston, M.V., & Allen, D.A. 1985, MNRAS 212, 939

Pesce, J.E., Stencel, R.E., Oliversen, N.A 1987, PASP 99, 1l78

Petrik, K., Hric. L., Galis, R., Friedjung, M., Dobrotka, A. 1998, IBVS 4588

Pottasch, S.R. 1984, Planetary nebulae (Reidel, Dordrecht)

Proga, D., Mikolajewska, J., and Kenyon, S.J. 1994, MNRAS 268, 213

Proga, D., Kenyon, S.J., Raymond, J.C. 1998, ApJ 501, 339

Robinson, K., Bode, M.F., Skopal, A., Ivinson, R.J., Meaburn, J. 1994, MNRAS 269, 1

Schild, H., & Schmid, H.M. 1996, A&A 310, 211

Schmid, H.M. 1997 in Physical Processes in Symbiotic Binaries, ed. Mikolajewska J., Copernicus Foundation for Polish Astronomy, Warsaw, p. 21

Schmid, H.M. 2000, in Thermal and Ionization Aspects of Flows from Hot Stars: Observations and Theory, ed. Henny Lamers & Arved Sapar, ASP Conf. Ser. 204, 303

Schmid, H.M., & Schild, H. 1997, A&A, 327, 219

Schmutz, W., Hamann, W.-R., Wessolowski, U. 1989, A&A 210, 236

Schwank, M., Schmutz, W., Nussbaumer, H. 1997, A&A 319, 166

Seaquist, E.R., & Taylor, A.R. 1990, ApJ 348, 313

Seaton, M. J. 1979, MNRAS, 187, 73p

Shara, M., Prialnik, D., Kovetz, A. 1993, 406, 220

Sion, E.M., & Ready, C.J. 1992, PASP 104, 87

Sitko, M., Lynch, D. , Russell, R., & Venturini, C. 2006, IAUC 8746

Siviero, A., Tamajo, E., Lutz, J., Wallerstein, G., ANS Collaboration: 2012, BaltA 21, 188

Skopal, A. 1994, IBVS 4096

Skopal, A. 1995, Ap&SS 224, 557

Skopal A., 1996, in CCD Techniques in Stellar Photometry, ed. Balazs G. et al., Proc. of the IAPPP Symp. 1995, Arculat Press, Baja, p.129

Skopal, A. 1998, Contrib. Astron. Obs. Skalnate Pleso 28, 87

Skopal, A. 2001, Contrib. Astron. Obs. Skalnate Pleso 31, 119

Skopal, A. 2003, A&A, 401, 17L

Skopal, A. 2005, A&A 440, 995

Skopal A. 2006, A&A, 457, 1003

Skopal A., Chochol D., 1994, IBVS 4080

Skopal, A., & Pribulla, T. 2006, ATel, 882, 1

Skopal, A., & Shagatova, N. 2012, A&A, 547, 45

Skopal, A., Hric, L., Chochol, D., et al. 1995, Contrib. Astron. Obs. Skalnaté Pleso 25, 53

Skopal, A., Vittone, A.A., Errico, L., et al. 1997, MNRAS 292, 703

Skopal, A., Chochol, D., Pribulla, T., & Vanko, M. 2000, IBVS, 5005

Skopal, A., Vanko, M., Pribulla, T., et al. 2002, Contrib. Astron. Obs. Skalnate Pleso 32, 62

Skopal, A., Pribulla, T., Vanko, M., et al. 2004, Contrib. Astron. Obs. Skalnate Pleso 34, 45

Skopal, A., Vittone, A.A., Errico, L., Otsuka, M., Tamura, S., Wolf, M., Elkin, V.G. 2006, A&A, 453, 279

Skopal, A., Vaňko, M., Pribulla, T., et al. 2007, AN 328, 909

Skopal, A., Pribulla, T., Budaj, J., et al. 2009a, ApJ 690, 1222

Skopal, A., Sekaras, M., Gonzalez-Riestra, R., Viotti, R. 2009b, A&A 507, 1531

Skopal, A., Shugarov, S., Vanco, M., et al. 2012, AN 333, 242

Skopal, A., Tomov, N.A., Tomova, M.T. 2013, A&A 551, L10

Skopal, A., Sekerás, M., Tomov, N.A., Tomova, M.T., Tarasova, T.N., Wolf, M. 2015, AcPol, in press

Smirnov, O.M., Piskunov, N.E., Afanasyev, V.P., Morozov, A.I. 1992, in Astronomical Data Analysis Software and Systems. I, ed. Worrall et al., ASP Conf. Ser. 26, 344

Smith, S.E. 1980, ApJ 237, 831

Smith, V.V., Cunha, K., Jorissen, A., Boffin, H.M.J. 1996, A&A 315, 179

Smith, V.V., Pereira, C.B., Cunha, K. 2001, ApJ 556, L55

Sobolev, V.V. 1975, Theoretical Astrophysics. Nauka, Moscow, p.293 (in Russian)

Sokoloski, J.L., & Bildsten, L. 1999, ApJ, 517, 919

Sokoloski, J.L., Kenyon, S.J., Kong, A.K.H., et al. 2002, in The Physics of Cataclysmic Variables and Related Objects, ed. B. T. Gänsicke, K. Beuermann, K. Reinsch, ASP Conf. Ser. 261, 667

Sokoloski, J.L., Kenyon, S.J., et al. 2005 in The Astrophysics of Cataclysmic Variables and Related Objects, ed. J.-M. Hameury and J.-P. Lasota, ASP Conf. Ser. 330, 293

Sokoloski, J. L., et al. 2006, ApJ 636, 1002

Sokoloski, J. L., Rupen, M.P., Mioduszewski, A.J. 2008, ApJ 685, L137

Southwell, K.A., Livio, M., & Pringle, J.E. 1997, ApJ 478, 29

Starrfield, S., Timmes, F. X., Iliadis, C., et al. 2012, BaltA 21, 76

Stencel, R.E. 1984, ApJ 281, L75

Stencel, R.E., & Sahade, J. 1980, ApJ 238, 929

Storey, P.J., & Hummer, D.G. 1995, MNRAS, 272, 41

Swings, P., & Struve, O. 1941, ApJ, 93, 356

Taylor, A.R., & Seaquist, E.R. 1984, ApJ 286, 263

Taylor, A.R., Seaquist, E.R., Mattei, J.A. 1986, Nature 319, 38

Taylor, A.R., Davis, R.J., Porcas, R.W. 1989, MNRAS 237, 81

Tomov, N.A. 1993a, Izv. Krym. Astrofiz. Obs. 88, 11

Tomov, N.A. 1993b, Izv. Krym. Astrofiz. Obs. 88, 22

Tomov, N.A. 1995, MNRAS 272, 189

Tomov, N.A., & Tomova, M.T. 1992, Izv. Krym. Astrofiz. Obs. 86, 19

Tomov, N.A., & Tomova, M.T. 1995a, in "100 yr Astronomical Observatory of Sofia University" eds. K. Maslev, and R. Kurtev, Naturela, Sofia, p. 103

Tomov, N.A., & Tomova, M.T. 1995b, C. R. Acad. Bulg. Sci. 48, 11

Tomov, N.A., & Tomova, M.T. 1996, IBVS 4341

Tomov, N.A., & Tomova, M.T. 1997, in Physical Processes in Symbiotic Binaries, ed. Mikolajewska J., Copernicus Foundation for Polish Astronomy, Warsaw, p. 185

Tomov, N.A., & Tomova, M.T. 1998, IBVS 4574

Tomov, N.A., & Tomova, M.T. 2000, IBVS 4953

Tomov, N.A., & Tomova, M.T. 2001, Ap&SS 278, 311

Tomov, N.A., & Tomova, M.T. 2002, A&A 388, 202

Tomov, N.A., & Tomova, M.T. 2006, BlgAJ 8, 76

Tomov, N.A., & Tomova, M.T. 2013, IBVS 6055

Tomov, N., Tomova, M., Ivanova, A. 2000, A&A 364, 557

Tomov, N.A., Taranova, O.G., Tomova, M.T. 2003a, A&A, 401, 669

Tomov, N.A., Tomova, M.T., Raikova, D.V. 1998, A&AS 129, 479

Tomov, N.A., Tomova, M.T., & Zamanov, R.K. 2003b, in Symbiotic Stars Probing Stellar Evolution, ed. R. L. M. Corradi, J. Mikolajewska, & T. J. Mahoney, ASP Conf. Ser. 303, 254

Tomov, N.A., Tomova, M.T., Taranova, O.G. 2004, A&A 428, 985

Tomov, N.A., Tomova, M.T., Taranova, O.G. 2005a, ARBI 20, 252

Tomov, N.A., Tomova, M.T., Taranova, O.G. 2005b, in The Astrophysics of Cataclysmic Variables and Related Objects, ed. J.-M. Hameury and J.-P. Lasota, ASP Conf. Ser. 330, 465

Tomov, N.A., Tomova, M.T., Bisikalo, D.V. 2007, MNRAS 376, 16L

Tomov, N., Tomova, M., & Bisikalo, D. 2008, MNRAS 389, 829

Tomov, N.A., Bisikalo, D.V., Tomova, M.T. 2009, in Space Plasma Physics: School of Space Plasma Physics, ed. I. Zhelyazkov, AIP Conf. Proc. 1121, 22

Tomov, N.A., Tomova, M.T., Bisikalo, D.V. 2010a, ARep 54, 528

Tomov, N.A., Bisikalo, D.V., Tomova, M.T., Kilpio, E.Yu. 2010b, ARep 54, 628

Tomov, N.A., Bisikalo, D.V., Tomova, M.T., Kilpio, E.Yu. 2011a, in 3rd School and Workshop on Space Plasma Physics, ed. I. Zhelyazkov & T. Mishonov, AIP Conf. Proc. 1356, 35

Tomov, N.A., Bisikalo, D.V., Tomova, M.T., Kilpio, E.Yu. 2011b, BlgAJ 15, 35

Tomov, N.A., Tomova, M.T. & Bisikalo, D.V. 2012, BaltA 21, 112

Tomov, N., Tomova, M., & Bisikalo, D. 2013, in 4th School and Workshop on Space Plasma Physics, ed. I. Zhelyazkov & T. Mishonov, AIP Conf. Proc. 1551, 30

Tomov, N.A., Tomova, M.T., and Bisikalo, D.V. 2014, AN 335, 178

Tomov, N.A., Tomova, M.T., and Bisikalo, D.V. 2015, in 5th School and Workshop on Space Plasma Physics, ed. I. Zhelyazkov & T. Mishonov, AIP Conf. Proc. accepted

Tomov, N.A., Tomova, M.T., and Bisikalo, D.V. 2015, AN accepted

Tomov, T., Kolev, D., Georgiev, L., Zamanov, R., Antov, A., Bellas, Y. 1990, Nature 346, 637

Tomov, T., Munari, U., Marrese, P.M. 2000, A&A 354, L25

Tomova, M. 2014, BlgAJ 21, 66

Tomova, M.T., & Tomov, N.A. 1998, IBVS 4561

Tomova, M.T., & Tomov, N.A. 1999, A&A 347, 151

Tomova, M., Tomov, N., & Bisikalo, D. 2008, BlgAJ 10, 39

Tutukov, A.V., & Yungelson, L.R. 1976, Astrofizika 12, 521

Üüs, U. 1970, Nauch. Infor. 17, 32

Van Winckel, H., Duerbeck, H.W., Schwarz, H.E. 1993, A&AS 102, 401

Viotti, R., Badiali, M., Cardini, D., Emanuele, A., Iijima, T. 1997, ESA SP-402, 405

Viotti, R., Rossi, C., Muratorio, G. 1998, A&AS 128, 447

Viotti, R., Friedjung, M.; Gonzalez-Riestra, R.; Iijima, T.; Montagni, F.; Rossi, C. et al. 2007, BaltA 16, 20

Vogel, M. 1991, A&A 249, 173

Vogel, M. 1993, A&A 274, L21

Vogel, M., & Nussbaumer, H. 1994, A&A 284, 145

Walder, R., Folini, D. 2000, in Thermal and Ionization Aspects of Flows from Hot Stars: Observations and Theory, ed. Henny J.G.L.M. Lamers & Avred Sapar, ASP Conf. Ser. 204, 267

Webster, B., & Allen, D. 1975, MNRAS 171, 171

Whitelock, P. 1987, PASP 99, 573

Whitelock, P.A., Menzies, J., Feast, M.W., et al. 1995, MNRAS 276, 219

Wilson, L.A., Wallerstein, G., Brugel, E.W., Stencel, R.E. 1984, A&A 133, 154

Yungelson, L., Livio, M.; Tutukov, A.; Kenyon, S. J. 1995 ApJ 447, 656

Yungelson, L., Livio, M., Truran, J.W., Tutukov, A., Federova, A. 1996, ApJ 466, 890

Zamanov, R.K. 1993, Observatory 113, 260

Zamanov, R.K., & Tomov, N.A. 1995, Observatory 115, 185

Zanni, C., Ferrari, A., Rosner, R., Bodo, G., & Massaglia, S. 2007, A&A, 469, 811